ZIPK mediates pre-mRNA processing in chronic lymphocytic leukaemia via histone H3 threonine 6 and threonine 11 phosphorylation

Fraser Thomas

Submitted in accordance with the requirements for the degree of
Doctor of Philosophy

The University of Leeds
School of Medicine
Leeds Institute of Medical Research

January 2020

The candidate confirms that the work submitted is his own, except where work has been included and identified as being from another. The contribution of the candidate and the other authors to this work has been explicitly indicated. The candidate confirms that appropriate credit has been given within the thesis where reference has been made to the work of others. Reference to 'Kreuz unpublished' refers to work carried out by Dr. Sarah Kreuz, which formed the basis for the hypothesis of this body of work, and is fully and explicitly indicated as such on all appropriate figures. Dr. Sarah Kreuz's work is exclusively included in the introduction and as identified as 'preliminary data'. Any and all other data/text/figure not explicitly attributed to Dr. Sarah Kreuz comes from the candidate. Part of this work also forms a jointly-authored publication which is under review as of January 2020.

Experiments within this study using primary CLL cells were performed under ethical approval granted by the Leeds Teaching Hospital NHS Trust REC: 14/WS/0098.

Acknowledgements

This research has been carried out with the support and guidance of a small but excellent team made up of Dr. Pascal Lefevre & Dr. Katherine Holmes with insights from Prof. Peter Hillmen. I would like to thank each of them for their support, technical and scientific advice and discussions throughout the project.

In addition, I would like to recognise the staff, students and academics on level 6 in the Wellcome Trust Brenner Building at St James's University Hospital for continued support both in and out of the lab and, in particular, pointed discussions in the level 6 meeting room. I would also like to acknowledge the WTBB IAs, without which none of our experiments would be possible.

I would like to thank the staff and coordinators from the St James's University Hospital (Leeds) Haematological Malignancy Diagnostic Service (HMDS) for assistance in sample acquisition, tissue culture training and clinical discussions in CLL meetings.

Finally, I wish to express my gratitude towards all the patients and their families.

Abstract

Cross-linking of the B cell receptor (BCR) induces transcriptional activation of immediate early genes (IEGs) including *EGR1* and *DUSP2* in chronic lymphocytic leukaemia (CLL). In this work, we have shown that this transcriptional activation correlated with histone H3 threonine 6 and 11 phosphorylation. We have identified Zipper-Interacting Protein Kinase (ZIPK/DAPK3) as the kinase mediating these histone phosphorylation marks in response to activation of the BCR signalling pathway. We show that this kinase is recruited to RNA polymerase II in an anti-IgM-dependent manner where it appears to be involved in pre-mRNA processing. Both IEG transcription and histone post-translational modifications are repressed by ibrutinib, a small molecule inhibitor used in CLL treatment. DAPK inhibition mimics Ibrutinib-induced repression of both IEG mRNA and histone H3 phosphorylation, and has anti-proliferative effects comparable to ibrutinib on CLL cells *in vitro*. DAPK inhibitor (DAPKi) has a broader anti-tumour effect than ibrutinib in that it can repress both anti-IgM- and CD40L- (NF-kB) dependent activation. We suggest that the broader effect of DAPKi is a result of ZIPK functioning as one of the final downstream enzymes in the transcription cascade. This is also beneficial in a clinical sense concerning disease resistance, in that ZIPK seems to function far downstream of both *BTK* and *PLCγ2* – both of which can be mutated in ibrutinib-resistant CLL. Our data suggests that ZIPK inhibition could be an alternative to ibrutinib treatment in CLL and other DAPK1-silenced malignancies.

Table of Contents

List of Figures

List of Tables

List of Equations

Abbreviations

AA – amino acid

Ab – antibody

Ac – acetylation

AID – activation induced deaminase

AMPK – adenosine monophosphate-activated protein kinase

APE1 – apurinic/apyrimidinic endonuclease 1

AR – androgen receptor

ATF/CREB – activating transcription factor/cyclic AMP-responsive element protein family

ATF4 – activating transcription factor 4

ATM – ataxia telangiectasia mutated

BCL – B cell lymphoma (genes)

BCR – B cell receptor

BH3 – BCL-2 homology 3

BM – bone marrow

BTK – bruton's tyrosine kinase

BTKi – BTK inhibitor

C region – constant region (referring to VDJ)

CaM – calmodulin

CD – cluster of differentiation

cDNA – complementary DNA

CDR – complementary determining region

C_H – constant heavy domain

ChIP – chromatin immunoprecipitation

CIT – chemoimmunotherapy

C_L – constant light domain

CLL – chronic lymphocytic leukaemia

CLP – common lymphoid progenitor

CML – chronic myeloid leukaemia

Co-IP – co-immunoprecipitation

COR – C-terminal of ROC

CR – complete remission

CSR – class switch recombination

CTD – C terminal domain of RNA polymerase

D region – diversity gene segment

DAPK – death associated protein kinase protein family

DAPK1 – death associated protein kinase 1

DAPK2/DRP-1 – death associated protein kinase 2/DAPK-related protein 1

DAPK3 – death associated protein kinase 3

DAPKi/ZIPKi – death associated protein kinase inhibitor

DLBCL – diffuse large B cell lymphoma

DNA – deoxyribonucleic acid

DNA DSB – DNA double strand break

DNMT – DNA methyltransferase

DRAK1 – DAPK-related apoptosis inducing kinase 1

DRAK2 – DAPK-related apoptosis inducing kinase 2

DUSP2 – dual specificity phosphatase 2

E2A - E box binding protein 2A

EBF – early B cell factor

EGR1/2 – early growth response protein 1/2

EMT – epithelial to mesenchymal transition

F_{ab} – fragment antibody binding segment

FC – fludarabine cyclophosphamide

F_c – fragment crystallisable segment

FC-R regiment – fludarabine plus cyclophosphamide with rituximab

FDC – follicular dendritic cell

FN1 – fibronectin

GAIT – gamma activated inhibitor of translation complex

GC (reaction) – germinal centre (reaction)

GEF – guanine nucleotide exchange factor

GTP – guanosine triphosphate

H2BS14P – histone H2B serine 14 phosphorylation

H2BS36P – histone H2B serine 36 phosphorylation

H3 – histone H3

H3.3S31P – histone variant H3.3 serine 31 phosphorylation

H3K14ac – histone H3 lysine 14 acetylation

H3K27ac – histone H3 lysine 27 acetylation

H3K4me3 – histone H3 lysine 4 trimethylation

H3S10P – histone H3 serine 10 phosphorylation

H3S28P – histone H3 serine 28 phosphorylation

H3T11P – histone H3 threonine 11 phosphorylation

H3T3P – histone H3 threonine 3 phosphorylation

H3T45P – histone H3 threonine 45 phosphorylation

H3T6P – histone H3 threonine 6 phosphorylation

H3Y41P – histone H3 tyrosine 41 phosphorylation

HAT – histone acetyltransferase

HDAC – histone deacetylases

HMT – histone methyltransferase

HP1γ – heterochromatin protein 1 gamma

HRPT - hypoxanthine phosphoribosyltransferase

HSC – haematopoietic stem cell

IEG – immediate early gene

IFNγ – interferon-gamma

IgH – immunoglobulin heavy chain

IgL – immunoglobulin light chain

IgM/D/G/A/E – immunoglobulin M/D/G/A/E

IgV_H – immunoglobulin heavy chain variable region

IKKα – IkB kinase α

IL-1 – interleukin 1

IL-6 – interleukin-6

ITAM – immunoreceptor tyrosine-based activation motif

J region – joining gene segment

JAK – Janus kinase

JMJD2C – jumonji C-domain-containing demethylase 2C

KDM – lysine demethylase

LGL – large granular lymphocytic leukaemia

LN – lymph node

LPS – lipopolysaccharide

LSD1 - lysine-specific demethylase 1

M-CLL – mutated CLL

MAPK – mitogen activated protein kinase

MBC – memory B cell

Me – methylation

MHC – major histocompatibility complex

MLC – myosin light chain

MPP – multipotent progenitors

NF-κB – nuclear factor-kB

NIK – NF-kB inducing kinase

NK cell – natural killer cell

NLC – nurse like cell

NLS – nuclear localisation sequence

OS – overall survival

P-TEFb – positive transcription elongation factor b

Pax5 – paired box protein 5

PB – peripheral blood

PC – plasma cell/plasmablast

PFS – progression free survival

PI3K – phosphatidylinositol 3-kinase

PKCß-I - protein kinase C beta I

PLCγ2 – phospholipase Cγ2

POD – PML oncogenic domains

PRC – polycomb repressive complex

Pre-BCR – pre B cell receptor

PRK1 – protein kinase-C related kinase 1

PTB – polypyrimidine tract-binding protein

qPCR – quantitative polymerase chain reaction

R – rituximab (when referring to FCR chemotherapy)

RAG (complex) – recombination activating gene (complex)

RNA – ribonucleic acid

RNA Pol II – RNA polymerase II

RNA Pol II-S2P – RNA polymerase II serine 2 phosphorylation

RNA Pol II-S5P – RNA polymerase II serine 5 phosphorylation

ROC – ras-of-complex

ROS – reactive oxygen species

RR – relapsed/refractory CLL

RSS – recombination signal sequence

S region – switch region (referring to CSR)

S727P – serine 727 phosphorylation

SHM – somatic hypermutation

sIg – surface immunoglobulin

STAT3 – signal transducer and activator of transcription 3

SYK – spleen tyrosine kinase

T180P – threonine 180 phosphorylation

T225P – threonine 225 phosphorylation

T265P – threonine 265 phosphorylation

T299P – threonine 299 phosphorylation

TCR – T cell receptor

TdT – terminal deoxynucleotidyl transferase

TES – transcription end site

T_{FH} – T follicular helper cell

TLK1 – tousled-like kinase 1

TLR – toll like receptor

TNF – tumour necrosis factor

TSS – transcription start site

UM-CLL – unmutated CLL

UNG – uracil-DNA glycosylase

USTAT3 – unphosphorylated STAT3

V region – variable region/variable gene segment (referring to VDJ)

VDJ recombination – variable, diversity, joining gene recombination

V_H – variable heavy domain

V_L – variable light domain

ZAP70 – zeta-chain-associated kinase 70

ZIPK – zipper interacting protein kinase

Chapter 1 Introduction

1.1 B Cell Development

A B cell is a white blood cell which is produced in the bone marrow and circulates in the blood and lymphatic systems. B cells participate in our immune system to combat foreign antigens and infectious agents in our bodies e.g. pathogens and viruses. This immune function is mediated by a B cells ability to produce antibodies specific to particular antigens [1]. Immune responses are classified as cellular or humoral. Cellular responses are mediated by T cells which recognize and attack their targets directly or indirectly by enlisting the help of other immune cells, while humoral responses are characterized by the production of antibodies by B cells [2].

1.1.1 Antibody and antigen receptor structure

Lymphocytes express highly diverse antigen receptors which are capable of recognising a near limitless range of foreign substances. This diversity is generated during the development of mature B and T lymphocytes from committed progenitor cells in the bone marrow and thymus respectively. Committed progenitor cells are driven by B cell specific gene expression programmes to rapidly proliferate and undergo highly ordered antigen receptor gene rearrangements [3]. These gene rearrangements not only fully commit a developing lymphocyte to a B cell fate, but create a vast array of antigen receptor proteins with different antigen specificity from a relatively limited amount of germline DNA. Further, selection events act as checkpoints to ensure the preservation of B cells with functional antigen receptors in the reactivity ‘goldilocks zone’: that being receptors which are they are not strongly auto-reactive, but reactive enough to be beneficial to the organism [4]. This section will focus on the maturation and development of B lymphocytes, including their structure, function and the generation of their antigen receptors.

1.1.1.1 Immunoglobulin structure

With regard to B cells, antibodies or immunoglobulins (Ig) are the major antigen receptors in the lymphoid system (with the TCR present on T cells) [5]. Igs are glycoproteins that are either secreted from mature B cells to combat pathogens or remain bound to the cell surface as receptor molecules e.g. the B cell receptor

(BCR). Igs are ‘Y’ shaped molecules composed of four polypeptide chains where each Ig is comprised of two paired heavy (H) and two light chains (L) [6, 7]. Of note, there are two types of L chain – the Ig κ L chain and the Ig λ L chain. Any given Ig will have either κ or λ L chains, but never a mixture of each.

For descriptive purposes, taking the Ig to be a 3-segment structure comprised of a base and two arms, the ends of each arm are termed variable (V) regions and interact with antigen. There are three areas in the V regions of both H and L chains which are highly variable and known as the complementary determining regions (CDR1, CDR2 and CDR3) [8]. These regions form distinct loops in the Ig protein structure and are also termed hypervariable regions. In both variable H and variable L chains, CDR3 possesses the greatest variability because it is generated as a result of recombination events (discussed below) [8]. The ‘tail’ of the Ig, termed the constant region (C), is less variable and instead interacts with effector cells and other molecules. The term constant region is slightly misleading as the five different classes of Ig (IgM, IgD, IgG, IgA and IgE) are distinguished by their C-region H chains [9].

Per a single Ig, each L chain is made up of one variable (VL) and one constant (CL) domain. The H chains are comprised of one variable domain (VH) and three constant domains (CH1, CH2 and CH3). Disulphide bonds link the H and L chains as well as H chains in the hinge region of the C region. In any given Ig molecule, the two H and two L chains are identical – giving an Ig two identical antigen-binding sites [9] (summarised in Figure 1.1).

1.1.1.2 Antigen receptor generation and the immunoglobulin gene loci structure

The V region of an Ig molecule allows a lymphocyte to recognise the vast and ever-expanding array of antigens that exist in the environment. The capacity for our immune system to generate millions of different antibodies from a relatively limited amount of coding DNA baffled scientists for decades and the elucidation of this mechanism is considered a hallmark in modern immunology. This receptor-diversity is achieved through a process of gene rearrangement termed V(D)J recombination, where the Ig germline DNA is recombined to form exons unique to each antigen receptor.

V(D)J recombination fuses different variable (V) gene segments with diversity (D) and joining (J) segments which give rise to functional Ig proteins with considerably different N-terminal chains in their Ig V regions [10]. At the level of germline DNA, the genes that encode B cell Igs are present in a non-functional state, separated by vast amounts of non-coding DNA, and require effective V(D)J recombination to generate functional protein products. Three separate loci encode the Ig H chains, the Ig κ L chain and the Ig λ L chain on chromosomes 14 [11], 2 [12] and 22 [13] respectively. The 5' portion of each of these genes consists of arrays of V, D (H chain only) and J segments separated by non-coding sequences [14] (the Ig heavy and light chain loci are summarised in Figure 1.2).

At the 5' most end of each gene is the V gene promoter sequence for transcription initiation. Next, there is a leader sequence (or signal sequence) exon that encodes the first 20-30 N-terminal residues of the translated protein. This sequence is responsible for guiding the nascent polypeptides, which are undergoing translation on membrane-bound ribosomes, to the endoplasmic reticulum. Here, the leader sequence is rapidly cleaved and is therefore not present in the mature, functional Ig protein. 3' of the leader sequence are the ~300 base pair V gene segment clusters [15]. The number of V segments varies not only between species but also between the H chains and the κ L and λ L chain loci. For example, there are approximately 100 V gene segments in the human H chain locus, 35 in the κ L chain locus and 30 in the λ L chain locus [14, 16].

Upstream of the V gene segments in the H chain locus only are D segments which are not present in either L chain loci. At varying distances 3' of the V gene in the loci of both the H and L chains are numerous J segments. Similar to the V gene segments, the number of D and J gene segments vary between Ig locus and between species [15].

The 3' end of each Ig locus holds the C region genes. In humans the κ L chain locus has just one C gene (C_κ) while the λ L chain locus has four (C_λ) – these regions are composed of a single exon which encodes the entire constant region of each L chain [17]. In contrast, the H chain locus contains nine C genes (C_H) of five different classes (μ, γ, δ, ε, α). The greater diversity of C_H genes allows for these genes to encode each and every Ig isotype and subtype e.g. C_μ H genes are responsible for the translation of IgM H chains. Typically, the C region of a functional Ig H chain will consist of three to four of the available nine exons, with

two smaller exons coding for the carboxyl-terminal ends of the membrane bound Ig H chains [15, 17]. Of the five Ig isotypes, IgG is the most common in human serum and has four subclasses: IgG1, IgG2, IgG2 and IgG4 which differ in their constant region, at their hinges and upper CH2 domains [18]. These differences alter the binding affinity of IgG to the FcγR receptor (a receptor family for the Fc region of IgG of which there are three classes: FcγRI, II and III) and ultimately allow different IgG subtypes to respond to a variety of antigen and stimulate the appropriate immune response. For example, IgG1 is the most abundant subclass (to the extent that a lack of IgG1 in serum is seen in a variety of antibody deficiencies) and is typically activated in response to soluble protein antigens and membrane proteins [18].

To summarise, the V region of an Ig L chain (κ or λ) is composed of V and J gene segments only and accordingly the process of its rearrangement is termed VJ recombination. The V region of the Ig H chain is comprised of V, D and J segments and is therefore constructed via VDJ recombination. In the latter process two distinct rearrangement processes must occur whereby initially a D segment is joined to a J segment before a V segment is fused to the DJ segment. In all cases, the rearrangement of these gene segments forms a single V(D)J exon that will code for the variable region of an Ig protein.

1.1.1.3 Antibody fragmentation

An antibodies antigen-binding region, or variable region, can also be referred to as the F_{ab} segment (fragment antigen binding segment). These segments therefore consist of the aforementioned VL, CL, VH and CH1 domains [19]. The two identical F_{ab} segments are connected via a hinge region to the paired CH2/CH3 domains of the constant region, or F_c segment (fragment crystallisable segment – named for the original observation that they crystallised well [20]), thus forming the Y-shaped Ig configuration.

Cleavage with specific agents can fragment an antibody into its component sections for research, study or therapeutic applications. Two identical F_{ab} segments which retain their antigen binding capabilities can be cleaved from the Ig structure via protein digestion with papain, leaving the F_c fragment [21]. Alternatively, Ig digestion with pepsin results in the formation of a $F(ab')_2$ fragment. Unlike Fab fragments, the $F(ab')_2$ fragment contains both ‘arms’ of the Ig joined at the hinge via disulphide bonds and similarly retains its antigen-binding

capabilities. The $F(ab')_2$ fragment is written with a prime signification as it contains extra amino acids, including cysteine, as a result of the pepsin digestion. Both Fab and $F(ab')_2$ fragments have therapeutic applications [22].

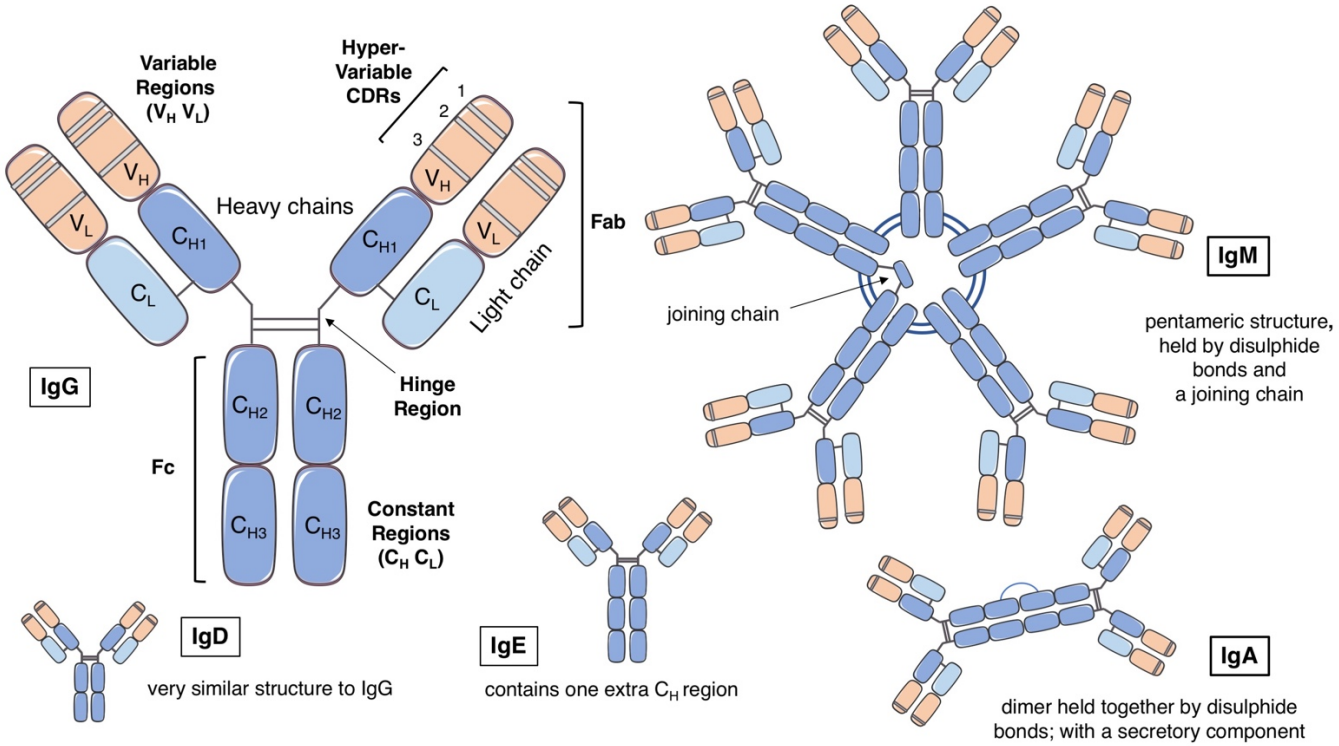

Figure 1.1: Antibody structure. Igs are 'Y' shaped molecules composed of four polypeptide chains where each Ig is comprised of two paired heavy (H) and two light chains (L). For descriptive purposes, taking the Ig to be a 3-segment structure comprised of a base and two arms, the ends of each arm are termed variable (V) regions and interact with antigen. There are three areas in the V regions of both H and L chains which are highly variable and known as the complementary determining regions (CDR1, CDR2 and CDR3) The 'tail' of the Ig, termed the constant region (C), is less variable and instead interacts with effector cells and other molecules. Per a single Ig, each L chain is made up of one variable (VL) and one constant (CL) domain. The H chains are comprised of one variable domain (VH) and three constant domains (CH1, CH2 and CH3). Disulphide bonds link the H and L chains as well as H chains in the hinge region of the C region. In any given Ig molecule, the two H and two L chains are identical – giving an Ig two identical antigen-binding sites. This figure was created using Servier Medical Art templates, which are licensed under a Creative Commons Attribution 3.0 Unported License; https://smart.servier.com.

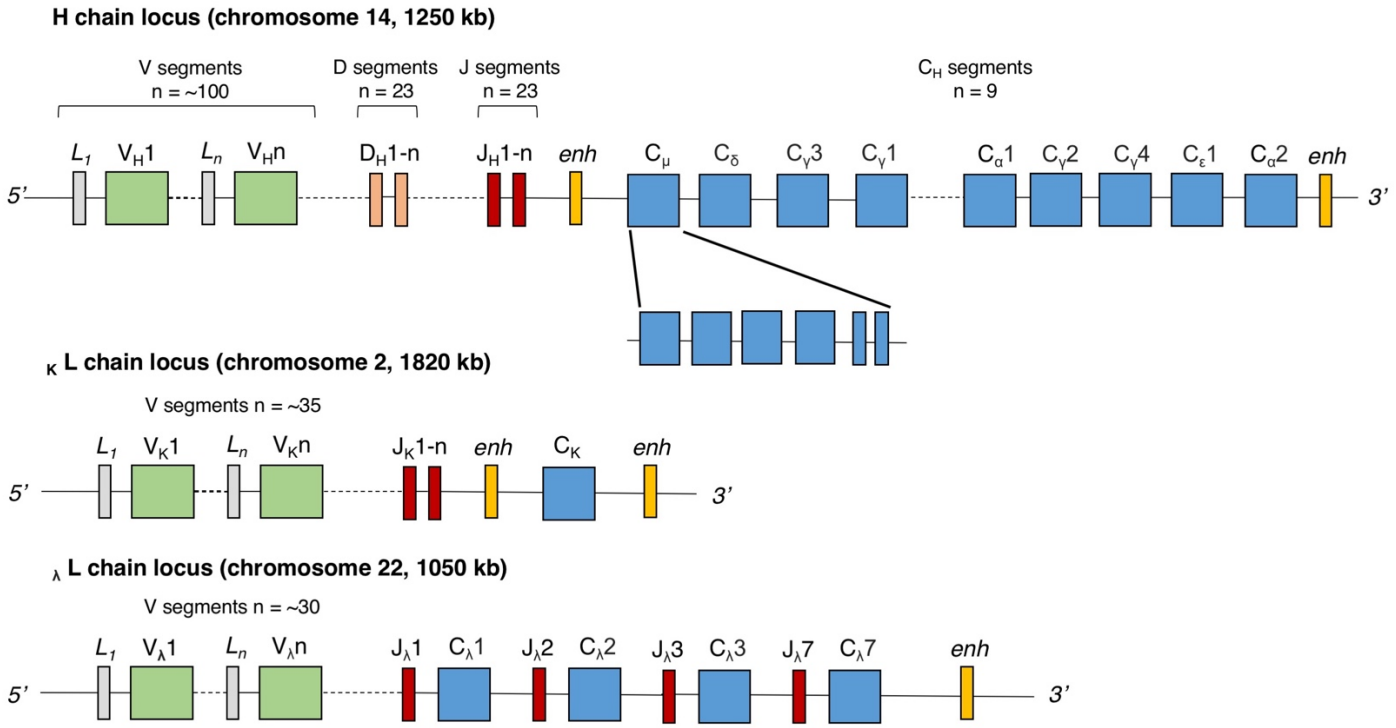

Figure 1.2: Immunoglobulin heavy and light chain organisation. At the level of germline DNA, the genes that encode B cell Igs are present in a non-functional state, separated by vast amounts of non-coding DNA, and require effective V(D)J recombination to generate functional protein products. Three separate loci encode the Ig H chains, the Ig κ L chain and the Ig λ L chain on chromosomes 14, 2 and 22 respectively. The 5' portion of each of these genes consists of arrays of V, D (H chain only) and J segments separated by non-coding sequences. At the 5' end of each gene is leader sequence ($L_{1\text{-}n}$) exon that encodes the first 20-30 N-terminal residues of the translated protein. 3' of the leader sequence are the ~300 base pair V gene segment clusters. There are approximately 100 V gene segments in the H chain locus, 35 in the κ L chain locus and 30 in the λ L chain locus. Upstream of the V gene segments in the H chain locus only are D segments. At varying distances 3' of the V gene in the loci of both the H and L chains are numerous J segments. Similar to the V gene segments, the number of D and J gene segments vary between Ig locus and between species. The 3' end of each Ig locus holds the C region genes. In humans the κ L chain locus has just one C gene (C_κ) while the λ L chain locus has four ($C_{\lambda 1,2,3,7}$). In contrast, the H chain locus contains nine C genes (C_H) of five different classes (μ, γ, δ, ε, α).

1.1.2 The stages of B cell development

1.1.2.1 Haematopoietic stem cells & commitment to the B cell lineage

All lineages of blood cells are derived from pluripotent stem cells in the bone marrow, referred to as haematopoietic stem cells (HSCs), which through a process of successive fate-decision programmes undergo a progressive loss of differentiation potential and self-renewal capacity [23]. Initially, HSCs mature into common lymphoid progenitors (CLPs) which can differentiate further into B cells, T cells and natural killer (NK) cells [24].

CLP commitment to the B cell lineage is ultimately guided by signals from cell-surface receptors to activate or repress transcriptional regulators specific to the B cell program. This transcriptomic activity encompasses one of the earliest definable stages of B cell development. Transcription factors that control early B cell development include Early B cell factor (EBF), E2A (E12/E47), Ets family member PU.1, Ikaros and Paired Box 5 (Pax 5) [25]. These proteins cooperate in a hierarchical regulatory network to direct a HSC towards a mature B cell [26].

Such key transcription factors upregulate distinct gene networks to drive CLPs towards a B cell fate. These proteins are tasked with beginning the process of V(D)J antigen receptor gene rearrangement, promoting display of the pre-B cell receptor (pre-BCR), as well as further altering chromatin structure to allow access to particular antigen receptor gene loci [27]. The different stages of B cell development are characterised by changing cellular characteristics including specific bouts of proliferation, distinct cell surface markers, rearrangement of Ig genes and their subsequent expression (summarised in Figure 1.3).

1.1.2.2 The stages of B cell development: Pro and Pre-B cells

CLPs which have activated transcriptional programmes to commit to the B cell lineage undergo extensive proliferation to generate a large number of progenitor cells. This ensures an eventual large population of diverse lymphocytes with varying antigen-specificity. The earliest definable and committed B cell is the pro-B cell – a progenitor cell which does not express Ig but presents with B-lineage specific surface molecules such as CD19 and CD10, thus differentiating itself from those HCSs driven towards the T cell lineage [28]. The cluster of differentiation (CD) proteins are cell-surface markers which are dynamically

expressed throughout the lifetime of any given B cell which can be used to differentiate cellular life stages [29]. Some CD proteins may be tightly restricted to a specific cell type or development stage (e.g. CD^{+}/CD^{-}) while others may vary in relative expression between several such stages (e.g. CD^{+++}/CD^{---}). These proteins have diverse functions, serving as receptors for growth factors, adhesion molecules and a variety of signal transduction enzymes [30].

At this stage the process of V(D)J recombination occurs in the developing B lymphocyte, now termed an early pro-B cell. This process can only occur in cells which are committed to the B cell lineage, and is one of the earliest characterisable stages of pro-B cells [31]. V(D)J occurs in a series of controlled steps. First, recombination events mediated by chromatin remodelling bring together one D segment with one J segment, deleting the intronic DNA, to form a H chain DJ gene segment [32]. DNA double strand breaks (DSBs) are carefully introduced in a tightly regulated mechanism by the RAG recombinase protein complex at specific recombination signal sequences (RSSs) flanking the coding regions of each V, (D) (and J) gene segments. Recombination activating gene 1 and 2 (RAG1 and RAG2) code for a series of proteins which make up the RAG complex and are first expressed at the pro-B cell stage [15]. Following this, as a late pro-B cell, one of the many 5' V region genes is rearranged and brought into close proximity with the DJ exon to form the complete H chain VDJ exon (V(D)J recombination of the Ig H chain locus is summarised in Figure 1.4). Transcription and subsequent expression of the VDJ exon with a C region exon as a completed Ig H chain is a hallmark of committed B cell lineage precursors.

Expression of terminal deoxynucleotidyl transferase (TdT) is increased during the early pro-B and late pro-B cell stages to promote junctional diversity at the genomic region which codes for the hypervariable CDR3 region [33]. V(D)J gene segment joining is often imprecise and nucleotides can be lost during asymmetrical RAG/Artemis-cleavage at RSSs. TdT catalyses the addition of templated P nucleotides to the asymmetrically cleaved DNA ends present at VD, VJ or DJ junctions. After the addition of P nucleotides, TdT then also adds between 2-20 non-templated base pairs, termed N nucleotides, at the now symmetrical DNA ends [34]. The action of TdT at gene segment junctions changes the amino acid sequences in the CDR3 region and vastly increases its diversity [8]. The addition of P and N nucleotides generates new DNA sequences for V, D and J gene sequences that are not even present in the germline DNA allowing TdT to promote further diversity in antigen receptor proteins [35, 36]. Of note, TdT expression decreases as B cells develop to the pre-B cell stage where

the L chains are recombined. Thus, junctional diversity linked to the addition of N nucleotides is greater in rearranged H chains than in rearranged L chains [37]. Repair is initiated by a large group of proteins composed of many of the classic non-homologous end joining (NHEJ) repair pathway enzymes [31]. The ligated product forms the functional mRNA encoding the V region of an Ig gene.

In order to complete the H chain rearrangement, the C region exons need to be joined with the rearranged VDJ exon. The joining of the C region exons with the V(D)J exon does not occur through a DSB-mediated mechanism but instead takes place at the RNA level through more traditional RNA splicing [10]. The C regions are downstream towards the 3' end of the loci, separated by a J-C intron. In pro-B cells, the rearranged Ig H chain gene is transcribed post VDJ with the J-C intron and remaining J segments still present in the rearranged DNA. Through splicing, the RNA primary transcript is processed via the removal of intronic DNA between the leader exon and the VDJ exon, between the VDJ exon and the first exon of the C_μ locus, and between the individual C_μ exons [38]. The C_μ gene region (the C_H gene responsible for IgM expression) is brought alongside the rearranged VDJ exon as a complete mRNA transcript for the μ Ig H chain [38]. If the VDJ recombination event was productive i.e. bases were added at junctions during recombination in the correct reading frame ensuring the rearranged DNA will encode a functional protein, the μ Ig H chain mRNA is translated into one of the Ig H chains [27, 31, 39].

Typically, half of all committed pro-B cells will rearrange and synthesise a productive μ H chain protein and differentiate further, those cells which make unproductive rearrangements are prompted to apoptose [40]. Productive Ig H chain locus rearrangements leading to Ig μ protein expression progress the developing B cell to the pre-B cell stage, presenting with a pre-BCR, but still needing to rearrange its Ig L chain locus [41].

1.1.2.3 The stages of B cell development: Pre-B cell receptor

Successful formation of the pre-BCR acts as the first major checkpoint of B cell development [42]. The pre-B cell will express rearranged Ig μ H chain protein with surrogate L chains – these are L chains made up of the VpreB and λ5 proteins, which act as surrogates for the V and C regions of a L chain respectively [43]. The surrogate L chain is structurally homologous to a typical κ or λ L chain, but is un-rearranged and identical in all pre-B cells [43]. The pre-BCR is also

complexed with signal-transducing proteins named Igα and Igβ. Signals from the pre-BCR are responsible for an enormous proliferative burst and the greatest expansion of committed B cell progenitors in the bone marrow [44]. Signalling from the pre-BCR activates a pivotal kinase in B cell development in Bruton's tyrosine kinase (BTK), an enzyme responsible for proliferation, survival and maturation. It has been suggested that the pre-BCR is assembled in a tonic state i.e. it functions in a ligand-independent manner and is permanently switched on to promote the requisite proliferative signalling [45].

The pre-BCR also regulates the next stage in B cell development by promoting κ L chain rearrangement. Interestingly, formation of the pre-BCR regulates the rearrangement of Ig genes in another way. If a productive Ig μ H chain is produced through VDJ recombination on one chromosome, the formation of the pre-BCR signals to permanently inhibit further rearrangements on the other chromosome. Similarly, if the first rearrangement is non-productive, the H chain allele on the other chromosome is given a chance to complete productive VDJ recombination. Therefore, in any given B cell one H chain locus is productively rearranged while the other is retained as either germline DNA or in a non-productive rearrangement. This process is known as allelic exclusion and ensures each B cell will not have two differentially rearranged H chains and instead will maintain clonal specificity by expressing a single receptor [46].

1.1.2.4 The stages of B cell development: Immature B cells

Pre-B cells quickly mature to immature B cells following expression of the pre-BCR. Here, developing B cells rearrange their κ L chain locus through VJ recombination [47]. VJ recombination is similar to V(D)J recombination, but L chain loci lack D gene segments. Recombination in the κ L chain locus involves rearranging the germline DNA to bring one V segment into close proximity with a J segment [48]. The ensuing VJ exon is transcribed with a 3' intron separating it from the C region exons. Primary transcript processing removes the VJ-C intron and creates the completed κ or λ L chain mRNA. The κ L chain locus has only one C_κ region exon, but alternative splicing in the λ L chain locus can lead to functional mRNA containing one of four possible C_λ region exons. Despite this, there are no known functional differences between λ L chains using any of the four possible C_λ exons [48].

The synthesised L chain protein associates with the Ig μ H chain, replacing the surrogate L chains, to produce a completed IgM protein [49]. If the κ L chain locus in un-productively rearranged, the cell has a second chance and can rearrange its λ L chain locus to produce a functional IgM. It is the expression of IgM that denotes the immature B cell stage [50]. If a productive κ L chain is synthesised, functional IgM prevents rearrangement of any further λ L chain, and λ L chain rearrangement is only attempted if κ L chain rearrangement results in a non-productive L chain. Therefore, through a process called light chain isotype exclusion, any given B cell clone will only express one of the two types of L chain [51]. Similar to the H chain, expression of the κ or λ L chain is allelically excluded – with expression of each L chain driven from only one chromosome at a time [40]. If both κ and λ L chain rearrangement fails and the gene products are non-functional, the developing B cell will fail to receive the requisite survival signals from the BCR and the cell will apoptose.

The newly assembled IgM molecules are expressed on the cell surface and function as antigen receptors. Accordingly, RAG gene expression is systematically shut-off to prevent further rearrangement of Ig genes [52]. There are three broad outcomes for these immature B cells. First, if their receptors are not strongly self-reactive they may function in a ligand-independent manner similar to the pre-BCR. Second, strongly self-reactive B cells that recognise antigens in the bone marrow with high avidity may undergo cell death in a form of negative selection [53]. Additionally, some B cells with strong autoreactive receptors have a chance to escape negative selection through a secondary rearrangement process termed receptor editing which modifies the already functional gene. Receptor editing allows the B cell to alter the specificity of its BCR and is mediated by the same enzymes (RAG) which coordinate the initial V(D)J recombination. Finally, those immature B cells which are not strongly self-reactive (or are receptor edited to this state) will leave the bone marrow to complete maturation.

1.1.2.5 The stages of B cell development: Mature B cells and IgM^+IgD^+ co-expression

Bone marrow derived mature B cells can be termed B-2 B cells and will either commit to continue developing into a marginal zone B-2 B cell or a follicular B-2 B cell with the majority of B cells committing to the latter [54]. Follicular B cells produce IgD in addition to IgM through RNA splicing. As described previously, in the early stages of B cell development, immature B cells express C_μ region genes

only (IgM expression). For a singular B cell to express both IgM and IgD with the same rearranged VDJ exon, a particularly long primary RNA transcript is produced containing the rearranged VDJ exon as well as the C_μ and C_δ genes. Specific polyadenylation sites guide splicing to occur either between the C_μ and C_δ genes (resulting in a typical μ mRNA for IgM) or 3' of the C_δ gene, removing the intervening C_μ gene (resulting in an δ gene for IgD) [50]. Co-expression of IgM and IgD is a hallmark of a mature B cell – this cell now has the capacity to recirculate and considered functionally competent, but in many respects, it is still a precursor or naïve-B cell. These cells can however effectively respond to antigen, and in doing so can undergo further antigen-induced B cell differentiation in a germinal centre reaction.

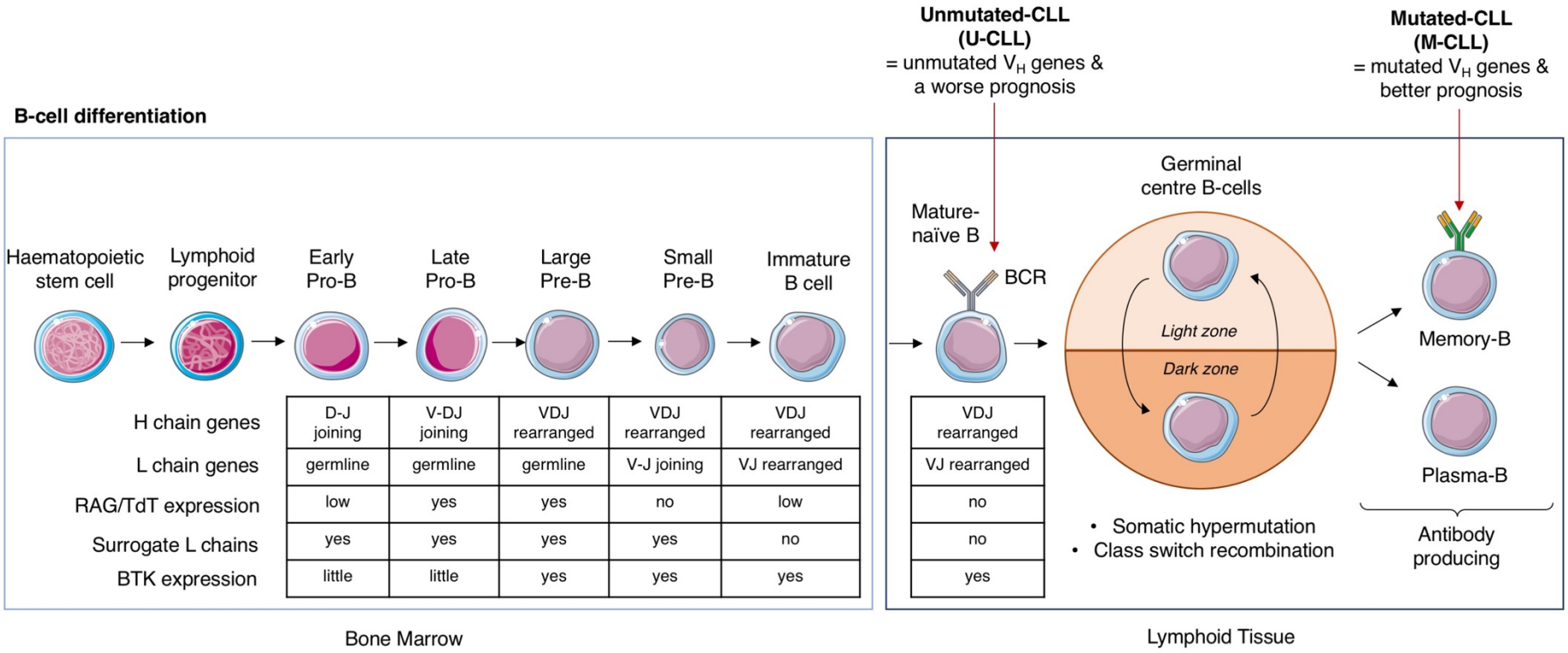

Figure 1.3: B cell development. As HSCs undergo a series of successive fate-decision programmes and commit to the lymphoid lineage, they progress through the stages of B cell development from a Pro-B, Pre-B and immature-B cell to a mature, naïve B cell. As B cells reach this stage they develop and express their B cell receptors. We categorise CLL into two subtypes depending on the nature of the BCR, which refers to the stage in B cell development from which they originate. U-CLL refers to naïve B-cells whose BCRs have not been somatically hypermutated in the germinal centre. When these naïve B cells are exposed to antigen they enter the germinal centre and undergo affinity maturation – they purposefully mutate the variable genes which make up the BCR to generate the best possible receptor for a specific antigen. When these cells exit the germinal centre, they have a more specific, less promiscuous BCR and these cells give rise to M-CLL. The U-CLL cells have a BCR which is less specific and more likely to react with a wide array of antigen lending to a worse prognosis. This figure was created using Servier Medical Art templates, which are licensed under a Creative Commons Attribution 3.0 Unported License; https://smart.servier.com.

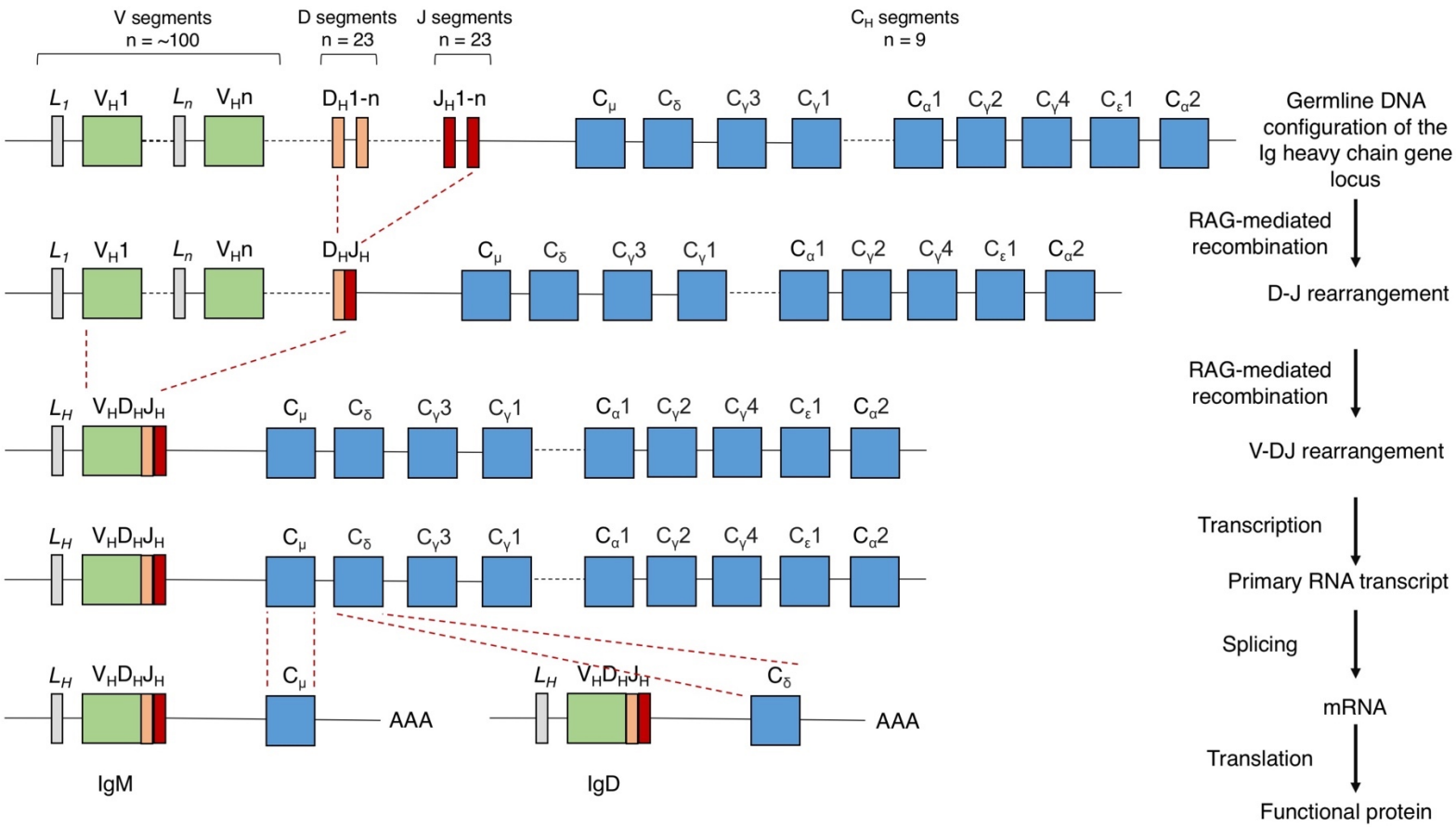

Figure 1.4: Immunoglobulin heavy chain rearrangement. V(D)J occurs in a series of controlled steps. First, recombination events mediated by chromatin remodelling bring together one D segment with one J segment, deleting the intronic DNA, to form a H chain DJ gene segment. DNA double strand breaks (DSBs) are carefully introduced in a tightly regulated mechanism by the RAG recombinase protein complex at specific recombination signal sequences (RSSs) flanking the coding regions of each V, (D) (and J) gene segments. Following this, as a late pro-B cell, one of the many 5' V region genes is rearranged and brought into close proximity with the DJ exon to form the complete H chain VDJ exon. Transcription and subsequent expression of the VDJ exon with a C region exon as a completed Ig H chain is a hallmark of committed B cell lineage precursors.

1.1.3 The germinal centre reaction

1.1.3.1 The germinal centre reaction: initiation

While V(D)J recombination creates a large number of varied antibodies, the repertoire is still not great enough to combat the millions of possible antigens in our environment. The low-affinity (for the antigen to the Ig binding site) IgM expressing antibodies generated in the bone marrow are deemed a first line of defence but are not the end of the story. When these B cells bind antigen, they undergo rapid proliferation within secondary lymphoid organs in transient structures termed germinal centres (GCs) to generate high-affinity antibodies [55].

This process can begin in the lymph node (LN) where naïve IgM^+IgD^+ B cells are present in follicles (regions of the LN) separated by interfollicular regions. T cell rich areas border these follicles and GCs form within the centre of the follicles themselves. Upon antigen-activation, the naïve, mature B cells migrate to the border of the T cell zone and B cell zone where they interact with antigen-specific T cells, become activated and begin to proliferate [56]. For any given antigen, only the subset of B cells with the highest affinity antibodies proceed to the GC reaction as to prevent competition for T cell signals with those B cells with a low-affinity for said specific antigen [57].

The T cells responsible for the above interaction will then commit to become T follicular helper cells (T_{FH} cells) and migrate from the interfollicular region into the follicle which is initially comprised of resident IgM^+IgD^+ follicular B cells and follicular dendritic cells (FDCs). There, through priming by dendritic cells, they upregulate expression of the master regulator of the GC reaction, B cell lymphoma 6 (BCL-6) [58]. B cells also migrate into the follicle and begin to proliferate rapidly, expelling the resident IgM^+IgD^+ follicular B cells, and leading to the formation of dark and light zones as a mature GC. The dark zone is characterized be densely packed B cells, whereas the light zone is comprised of far less B cells and is populated with T_{FH} cells and FDCs.

1.1.3.2 The germinal centre reaction: somatic hypermutation & GC positive selection

Within the dark zone of GC reactions, a process known as somatic hypermutation (SHM) takes place to induce further diversity to the Ig V region genes. SHM produces a large number of B cell clones that will have a varying range of affinities for the immunizing antigen [55]. The process involves the incorporation of single nucleotide substitutions per 1,000 bases into the rearranged V genes to promote antibody affinity maturation via affinity-enhancing mutations [59]. SHM is mediated by the enzyme activation-induced deaminase (AID) which can convert deoxycytidines to deoxyuracils causing both transition (purine-purine substitution) and transversion (purine-pyrimidine substitution) mutations in V region genes [60]. Affinity maturation ensures that the B cells where these mutations result in increased antigen binding affinity undergo selective expansion, and those inferior antibody mutants with low antigen affinity or autoreactivity are outcompeted and/or encouraged to apoptose [55].

Post-SHM, B cells transit into the light zone of the GC reaction to 'test' their newly mutated BCR against antigen presented on FDCs. Here, those B cells with high-affinity antigen receptors undergo T_{FH}-mediated positive selection. It is these high-affinity B cells which are preferentially recirculated between the two zones for further rounds of SHM and selection. It has only recently been shown that T_{FH} cells promote selection within the light zone and that these cells are in fact the driving force behind selecting high-affinity B cells [61]. This process occurs via B cells presenting processed antigen on major histocompatibility complexes (MHC) to the T cell receptor (TCR) of T_{FH}-cells. There is a direct correlation between greater antigen capture and peptide-MHC presentation resulting in more TFH-cell assistance for those B cells with the highest affinity BCRs [61]. Novel techniques allowing cell division within the GC to be tracked have shown that when such high-affinity B cells, which have received the most T_{FH}-cell assistance, recirculate into the dark zone they are programmed to divide, undergo further SHM, and proliferate more than their lower-affinity counterparts in a form of selective expansion [62].

By encouraging those B cells with the highest antigen-affinity to undergo further rounds of proliferation and successive SHM, while selectively removing low-affinity B cell clones via apoptosis, the GC reaction is quickly dominated by a population of the 'strongest' B cells in an elegant example of Darwinian evolution

in fast-forward. This iterative process of selection results in memory B cells and plasma cells with the capacity to produce high-affinity antibodies to combat invading pathogens.

1.1.3.3 The germinal centre reaction: class-switch recombination

A subset of B cells taking part in the GC reaction also undergo class-switch recombination (CSR). CSR, like SHM, is mediated by AID and is a process which targets the Ig H chain locus for a further recombination event [63]. Each C_H gene (except C_δ/IgD) is preceded by a unique DNA region known as a switch (S) region and the CSR recombination event occurs between two S-regions, deleting the intervening C_H genes, including C_μ. This phenomenon brings the VDJ exon closer to the more 3' Ig H chain C_H genes (C_γ, C_ε, C_α) and allows a switch from IgM to IgG, IgA or IgE [64].

Studies have implicated transcription through S-regions as a mechanism for the initiation of CSR, and that the S-regions themselves are not the primary recognition site. These groups suggest that single-stranded DNA is stabilised by transcription-dependent higher order structures, and these structures are the primary substrate for CSR [65, 66]. An example of such a structure is the R-loop, whereby when S-regions were observed to be transcribed, the primary transcripts stably associated with the template DNA strand to form an RNA-DNA hybrid [67, 68]. These R-loops provide a substrate for AID, whose catalytic activity induces mutations in the exposed single-stranded DNA. Enzymes which target the AID-induced mismatched base pairs (uracil-DNA glycosylase (UNG) and apurinic/apyrimidinic endonuclease 1 (APE1)) induce a series in nicks on the non-template stand which together with nicks on the opposite strand induce DSBs in the S-region [64]. Similar to V(D)J, the breaks are processed via synapsis before fusion of two S-region DSBs, likely via the NHEJ pathway [69, 70]. Productive CSR results in a recombined Ig H locus with the VDJ exon aligned with a new C_H gene.

Cytokines are responsible for directing the initial transcription through the H chain locus and determining which Ig isotype the B cell will switch to e.g. lipopolysaccharide (LPS) is thought to drive the switch to IgG while a combination of LPS, transforming growth factor-β (TGF- β) and interleukin-5 (IL-5) are required to switch to IgA [64].

1.1.3.4 The germinal centre reaction: outcomes

B cells harbouring newly developed, high-affinity antigen receptors generated from repeated selection in GC reactions will ultimately differentiate into memory B cells (MBCs) and plasma cells/plasmablasts (PCs), leaving the GC and

entering circulation to combat pathogens and confer long-lived antibody mediated (humoral) immunity [71].The decision to commit to a PC or MBC fate is driven by contrasting signals and gene expression programmes in the light zone of the GC, allowing cells with particular BCRs to be selected for and halt dark zone re-circulation [72]. MBC differentiation is predominantly restricted to low-affinity B cells while maturing PCs require high-affinity BCRs and assistance from T_{FH} cells [72]. In brief, short-lived PCs produce antibody to tackle infection, while repeated encounter with the same antigen (secondary infection) triggers the reactivation of long-lived MBCs to differentiate into PCs [73]. The process of MBC reactivation is thought to involve a new GC reaction as during secondary infection the PC response is often dominated by IgG^+ IgA^+ PCs which have previously undergone CSR [74].

1.2 Chronic Lymphocytic Leukaemia Pathogenesis

Chronic lymphocytic leukaemia (CLL) is the most common leukaemia in the Western world, with an estimated incidence of ~6 cases per 100,000 annually and a median diagnosis age of 72 years. Yet despite its prevalence the complete picture of its pathogenesis and genetic landscape remain unclear. This is in part due to the heterogeneity observed between patients whereby some present with stable disease and do not require therapy while others have a more aggressive disease course and require early treatment [75] [76]. The well-established Rai [77] and Binet [78] CLL staging systems help categorise patients and define their treatment needs by considering lymphocyte count, LN enlargement and how many nodes are affected, spleen size, anaemia and platelet count.

1.2.1 CLL biological and genetic features

CLL is a malignancy of $CD5^{+}CD19^{+}$ B cells characterised by the accumulation and clonal expansion of functionally abnormal B cells in the blood, bone marrow and lymphoid tissues [79]. CLL cells typically present with high levels of cell surface markers which are upregulated after antigen exposure (e.g. CD23, CD25, CD69) and low levels of those which are downregulated after cellular activation (e.g. CD22, CD79b). The level of soluble CD23 found in the serum of a patient is considered one of the most important prognostic markers for the disease [80]. CLL cells also express the memory B cell marker, CD27, and often have gene expression profiles similar to memory B cells [81].

CD38 [82] and ZAP70 [83] are two further important prognostic markers in CLL. CD38 is important for B cell differentiation through an interaction with CD31, a cell surface marker found on NLCs and T cells in the microenvironment. Patients overexpressing CD38 are considered to have a more aggressive disease and a shorter life expectancy. ZAP70 enhances BCR signalling and is an important signalling molecule in B, T and NK cells. Similarly, patients with high levels of ZAP70 have a worse prognosis.

Cytogenetic abnormalities play a large and important role in the pathogenesis of CLL and in disease prognosis. The most frequent abnormalities are deletions of chromosomal material, with the most common found in band 13q, followed by deletions in 11q and 17p. Gain of chromosomal material in the form of chromosome 12 trisomy is also common. 13q deletions are typically considered to be predictive of low risk disease, while the 17p and 11q deletions effect the

critical *TP53* and ataxia telangiectasia mutated (*ATM*) genes respectively, and predict much poorer disease outcome [84]. *TP53* deletion or mutation remains the strongest marker of reduced progression free survival (PFS) and overall survival (OS) in CLL.

The mutational landscape of CLL has been elucidated somewhat through advents in next-generation sequencing. While there are less mutations globally in CLL than in most solid tumours, recurrent mutations have been detected effecting the NOTCH and Wnt signalling pathways, RNA splicing and processing machinery (SF3B1), DNA damage response proteins and chromatin modifiers [85, 86]. More recently, the MYC suppressor, MGA, and proteins in the MAPK-ERK pathway including NRAS, KRAS and BRAF have been identified as drivers in CLL [86].

The CLL epigenome has been extensively studied in recent years with aberrant patterns discovered in DNA methylation, chromatin accessibility and histone modifications [87-89]. Often, epigenetic alterations in CLL are linked to other prognostic factors e.g. U-CLL patients have been observed to harbour more active, open chromatin than M-CLL [87]. The epigenetic background of a CLL cell is also thought to provide a glimpse at its cell of origin with recent work suggesting CLL-specific differences in methylation reflect the stage of B cell development from which they arise [90]. Of note, silencing of the pro-apoptotic Death Associated Protein Kinase 1 (DAPK1) via hypermethylation of its promoter has been suggested to influence tumour progression and metastasis in cancers such as CLL [91] and DLBCL [92] and is a marker of poor survival.

1.2.2 CLL microenvironment

In the bone marrow, CLL cell survival is highly dependent on cellular and molecular interactions with stromal cells and the matrix, collectively referred to as the tissue microenvironment (or sometimes a ‘pseudofollicle’ or proliferation centre) [93]. To expand, nurselike cells (NLCs), mesenchymal stromal cells, T cells and NK cells are critical components of the microenvironment and communicate with CLL cells through a complex network of adhesion molecules, chemokine receptors, tumour necrosis factor (TNF) family members, and soluble factors [94]. These signals regulate specific gene expression profiles, different from those observed in circulating CLL cells, to promote survival and proliferation and are often associated with strong BCR and NF-κB pathway activation [95].

The importance of the CLL microenvironment is reinforced by the efficacy of CLL therapeutics which target this dependency, such as ibrutinib, a small molecule inhibitor which impacts BCR signalling and disrupts CLL cell trafficking to the LN [96].

1.2.3 CLL subtypes

CLL is often divided into two main subtypes defined by the mutational status of their Ig H chain V region gene which reflects the stage of normal B cell development from which the CLL cell has originated [97]. Unmutated CLL (U-CLL) cells originate from a B cell that has not undergone differentiation and SHM in GCs and patients typically present with a more aggressive disease. U-CLL cells are thought to be CD5+ B cells that are readily expressing IgM and/or IgD prior to any potential CSR in the GC.

Mutated CLL (M-CLL) cells arise from post-GC parental B cells (e.g. MBCs) with Ig V regions that have undergone SHM and/or CSR and these cases have a more indolent disease course. These cells may therefore also be found expressing IgA and IgG. There are some exceptions to this division linked to particular BCR V(D)J recombination events which do not abide by the M-CLL/U-CLL prognoses. A paradigm example are those Igs which have undergone V(D)J recombination of the Ig H chain and selected the V3-21 gene for their V region gene segment. These patients suffer from a shorter overall survival (OS) regardless of SHM status and their disease is more alike to U-CLL [98].

Interestingly, despite the enormous potential for variation that is associated with V(D)J recombination, the repertoire of potential Ig molecules of CLL patients are significantly more limited than in healthy B cells and patients often present with nearly identical or highly homologous CDR3 regions. This phenomenon is termed Ig stereotypy and is so extreme that around one third of CLL patients have virtually identical Ig molecules arising from shared sequence motifs in the CDR3 region, reflecting the bias for specific Ig genes [99]. This limited diversity seems to stem from the binding activity of the surface Ig and supports the idea that the recurrent binding of a restricted set of antigens drives the CLL pathogenic process [100]. In many cases, stereotyped CLL BCRs can recognise various autoantigens as well as environmental or microbial antigens including cytoskeletal components, the Fc-tail of IgG, single stranded or double stranded DNA and apoptotic cells [101, 102]. These stereotyped BCRs are grouped into

different subsets, where subset 2 expresses a BCR with the aforementioned IgHV3-21in combination with IgLV3-21. Recent work has highlighted that the subset 2 light chain carries a single point mutation at R110 at the junction between the variable and constant LC regions (termed IgLV3-21^{R110}) and that these patients represent a new, distinct subset with a particularly poor prognosis as the mutation promotes constitutive BCR-signalling [103]. This group provides another example of patients which can be high risk regardless of IgHV status.

1.2.4 NF-κB signalling in CLL

The nuclear factor-κB (NF-κB) pathway plays an essential role in the regulation of cellular processes vital to healthy development including proliferation, inflammation and cell survival – processes closely linked to cancer progression. It is therefore unsurprising that NF-κB is also constitutively active in most CLL, playing a major role in the development of the disease.

The NF-κB family comprises five members: p105/p50, p100/p52, p65 (RelA), RelB and c-Rel encoded by NFKB1, NFKB2, RELA, RELB, and REL respectively. Only p65, c-Rel and RelB are transcriptionally active [104]. Without activatory stimuli, NF-κB proteins remain sequestered in the cytoplasm by inhibitory IκB family members such as IκBα. In addition, p50 and p52 are inhibited by way of their precursor proteins, p105 and p100, from which the active subunits are post-translationally cleaved [105]. NF-κB signalling is classified as either canonical or non-canonical/alternative. Canonical NF-κB signalling is activated via inducible degradation of IκBα by a multi-subunit IκB kinase (IKK) complex resulting in nuclear translocation of p50/p65 and p50/c-Rel dimers. Non-canonical NF-κB signalling is activated via the processing of the p52 precursor protein, p100, by the NF-κB-inducing kinase (NIK) and typically results in the nuclear translocation of p52/RelB dimers [106].

In CLL, NF-κB proteins can be activated downstream of many cell surface receptors promoting CLL proliferation and survival in the microenvironment including the BCR, CD40 and toll-like receptors (TLR) [107]. A handful of low-frequency mutations in the NF-κB pathway have been detected in CLL including MYD88, NKFBIE [108] and BIRC3 but the majority of aberrant NF-κB activation is thought to arise through external stimuli activating the aforementioned signalling cascades [109]. Aberrant epigenetic regulation of NF-κB has also been reported in CLL whereby genes enhancing NF-κB signalling were observed to be differentially methylated in different IgHV subgroups e.g. these genes (including *ADORA3* and *CARD15*) remained unmethylated and overexpressed in poor prognosis U-CLL patients but remained methylated in M-CLL [110]. Further studies have indicated that NF-κB and STAT3, another transcription overexpressed in the disease, are both activated by BCR signalling in CLL. NF-κB and STAT3 can cooperate to inhibit CLL cell apoptosis whereby the strongest cooperation predicts a poor response to therapy [111, 112].

1.2.5 BCR signalling in CLL

As discussed previously, the BCR is formed during B cell development from an Ig molecule (IgA, IgD, IgE, IgG or IgM) which is presented on the cell surface of mature B cells. Like mature B cells, CLL cells will typically co-express IgD and IgM, although at much lower levels than normal B cells [113]. As a functional BCR is of utmost importance to healthy B cell survival, it is of no surprise that B cell malignancies such as CLL often co-opt this pathway for their own aberrant proliferation. It has been suggested that CLL cells harbour constitutively active BCR signalling through either antigen-dependent or antigen-independent signalling (BCR is engaged by autoantigen), or through mutations in one of many of the downstream enzymes involved in the signalling cascade [114] (pathways summarised in Figure 1.5).

In CLL cells, STAT3 is activated downstream of the BCR, whose activation promotes JAK2/STAT3 signalling, induction of STAT3 phosphorylation and its subsequent nuclear shuttling to transcribe pro-proliferative genes [115]. Constitutive STAT3 tyrosine phosphorylation is common in many malignancies, yet in CLL STAT3 is uniquely and constitutively, phosphorylated at serine 727 (STAT3 S727-P) regardless of cell count, disease stage or treatment status. STAT3 S727-P has been shown to translocate to the nucleus and bind DNA, promoting the transcription of genes for CLL cell survival and proliferation [116].

The importance of the BCR signalling pathway is highlighted by the efficacy of small molecule inhibitors that block BCR signalling and which have seen success in the clinic. These include the BTK inhibitor, ibrutinib and the phosphoinositide-3 kinase (PI3K) inhibitor, idelalisib [117]. Typically, U-CLL cells are more sensitive to inhibitors of BCR-signalling than M-CLL cells [118]. This may be linked to the fact that U-CLL cells tend to respond to BCR signalling through enhancing B cell activation, while anergy is the dominant response for most M-CLL cells. Anergy is a state of cellular lethargy caused by chronic activation of the BCR and may explain the more indolent disease course observed in M-CLL patients [119]. The anergic cells in these patients are less likely to proliferate in response to BCR signalling than the more aggressive and proliferative U-CLL cells. It has been suggested that the outcome of BCR-activation (proliferation versus anergy) may be linked to the CLL cell of origin [113].

1.2.6 CLL treatment & resistance to therapy

As stated previously, CLL disease progression is particularly heterogeneous and while some patients present with indolent disease, others require rapid treatment and therapy. Often, patients are diagnosed with completely asymptomatic disease and clinicians may opt to 'watch and wait' for further disease progression before beginning treatment [120]. As the median age of CLL diagnosis is in the early 70s and the disease is considered incurable (aside from allogeneic stem cell transplants), the decision not to treat indolent, asymptomatic CLL patients at diagnosis is understandable. Many patients will die with their disease long before their CLL becomes problematic. However, those that do suffer from more aggressive disease will typically die from CLL-driven causes such as bone marrow failure, infection, or transformation to a high-grade lymphoma [109]. Treatment options range from chemoimmunotherapy (CIT) with chlorambucil or FCR [121] (fludarabine, cyclophosphamide (FC) supplemented with the CD20 antibody rituximab (R)) to targeted, small molecule therapies including the BTK inhibitors (BTKi) ibrutinib and acalabrutinib, idelalisib [122] (phosphatidylinositol 3-kinase (PI3Kδ) inhibitor), venetoclax [123] (BCL-2 inhibitor) or the more novel CD20 inhibitor, obinutuzumab [124]. Combinations of these inhibitors are being considered worldwide in numerous clinical trials, typically comparing their efficacy to CIT, including combinations of ibrutinib with obinutuzumab [125] (iLLuminate trial), acalabrutinib with obinutuzumab [126] (ELEVATE TN trial) and venetoclax with obinutuzumab [127] (CLL 14 trial).

Choosing the correct frontline therapy is an important decision and clinicians must consider patient fitness and history as well as their genetic and cytogenetic profiles such as 17p deletion, *TP53* mutational status and their IgHV subtype classification. Clinicians treating patients with CLL are in the enviable position of having several, very effective frontline therapy options available. Choosing between the variety of targeted therapies is not cut and dry and the choice can depend on both patient characteristics and the clinician's discretion. Generally, a patient diagnosed with CLL under the age of 65 who is considered fit, with mutated IgHV status and favourable cytogenetics, can enjoy long remission with all available regiments, including CIT (this being one of the only scenarios where CIT is comparable to targeted therapies). CIT (both FCR and chlorambucil) is often compared to targeted agents in clinical trials with both the RESONATE 2 [128] and E1912 [129] trials demonstrating the superiority of single-agent ibrutinib compared to chlorambucil. CIT is, of course, associated with high levels of toxicity and a majority of patients face relapse concerns [130].

It is no surprise then that novel targeted agents are consistently shown to be superior to CIT in the context of patients with high risk factors such as 17p deletion or unmutated IgHV status. These patients are notoriously hard to treat and U-CLL represents a major challenge in CLL therapy, even for the newer targeted therapies using venetoclax and obinutuzumab. There are differing opinions on how to treat such high-risk patients and many clinicians prefer to either enrol their patients on clinical trials or opt for BTKi single-agent therapy which has seen success in this patient type in clinical trials [131]. This can be attributed to the fact that there is more long-term safety data for ibrutinib and there is some uncertainty about the benefit of venetoclax/obinutuzumab combination therapy for this subgroup of high-risk patients, although trials are ongoing [127].

1.2.6.1 Ibrutinib in CLL

Ibrutinib has been approved for treatment of all subtypes of CLL and for patients of all ages regardless of any previous treatment with a particular focus on those patients presenting with adverse cytogenetics. A BTK inhibitor which irreversibly binds the cysteine-481 residue in BTKs ATP binding pocket, ibrutinib takes advantage of CLL cell dependency on BCR signalling.

Ibrutinib monotherapy is effective to treat CLL and promotes a rapid reduction in LN enlargement with associated lymphocytosis redistributing the CLL cells from the LN into the peripheral blood (PB) [128]. There are extremely promising results from ibrutinib treatment in front-line therapy as well as in relapsed/refractory (RR) CLL [128, 132]. However, eradication of detectable CLL with ibrutinib monotherapy is rare and patients usually remain on ibrutinib indefinitely or until disease progression. In addition, side effects cause ~10% of patients on ibrutinib to discontinue the drug: these include diarrhea, fatigue, bruising and haemorrhage, hypertension, and atrial fibrillation [133]. Acalabrutinib is a novel, second generation BTK inhibitor currently under assessment in clinical trials. It is hoped this inhibitor will have less side effects, owing to an increased specificity for BTK and less off-target effects [134].

At a transcriptional level, ibrutinib treatment has been shown to induce a rapid down-regulation of inflammatory markers and alter the transcription of genes known to promote CLL [135]. Studies have shown massive alterations to transcriptional networks after just two days of treatment with ibrutinib with the expected strong impact on BCR pathway target genes but also genes

downstream of NF-κB and MYC and additional transcription factors known to promote CLL pathogenesis e.g. (EGR2, EGR3 and IRF5). Similarly, ibrutinib has been shown to downregulate NOTCH1 activity and its downstream target genes in CLL cells [136].

From an epigenetic standpoint, ibrutinib has recently been reported to induce reorganisation of the chromatin landscape in CLL cells [137]. After prolonged ibrutinib treatment a loss of both trimethylation and acetylation of histone H3 lysine 27 (H3K27me3 and H3K27ac) was observed in the cells from CLL patients. These alterations in response to treatment suggested a global reorganisation of chromatin structure which may serve to poise the cell for acquired resistance in the future.

Ibrutinib presents a breakthrough in CLL treatment, but resistance is an emerging concern. Some patients whose disease progresses while on ibrutinib were found to have an acquired mutation of BTK at cysteine-481 (C481S) or gain of function mutations in PLCγ2, an enzyme downstream of BTK, both of which reactivated BCR signalling [138]. Further, there are cases of resistance which cannot be explained by genetic alterations [139-141]. Recent studies indicate that alternative, pro-proliferative signalling pathways can be activated to bypass BTK inhibition, particularly NF-κB, and are only partially blocked by ibrutinib and this may play a role in the development of resistance to ibrutinib molecule [142, 143]. For example, TLR signalling in the lymph node is only partially repressed by ibrutinib [142].

In an effort to combat resistance and expand on the success of ibrutinib monotherapy, combination therapies of ibrutinib with rituximab [144], obinutuzumab [125] and venetoclax [145] are being evaluated and each combination has already seen success as a treatment option in CLL. Yet even in the context of combination therapy resistance can still be a difficulty. For example, while ibrutinib and venetoclax are an effective treatment option, resistance can still arise from strong activation of the NF-κB pathway via microenvironmental agonists such as CD40L and CpG-oligodeoxynucleotides [143]. The connection between BCR and CD40 has also been further demonstrated via experiments showing that CD40L treatment of B cells (healthy or malignant) circumvents the need for BTK in BCR-induced NF-κB activation. Further, CD40-mediated activation of the BCR signalling pathway operates without the need for PI3K or

PLCγ2, and thus bypasses both early (BTK and PI3K) as well as late (PLCγ2) BCR signalosome elements [146, 147].

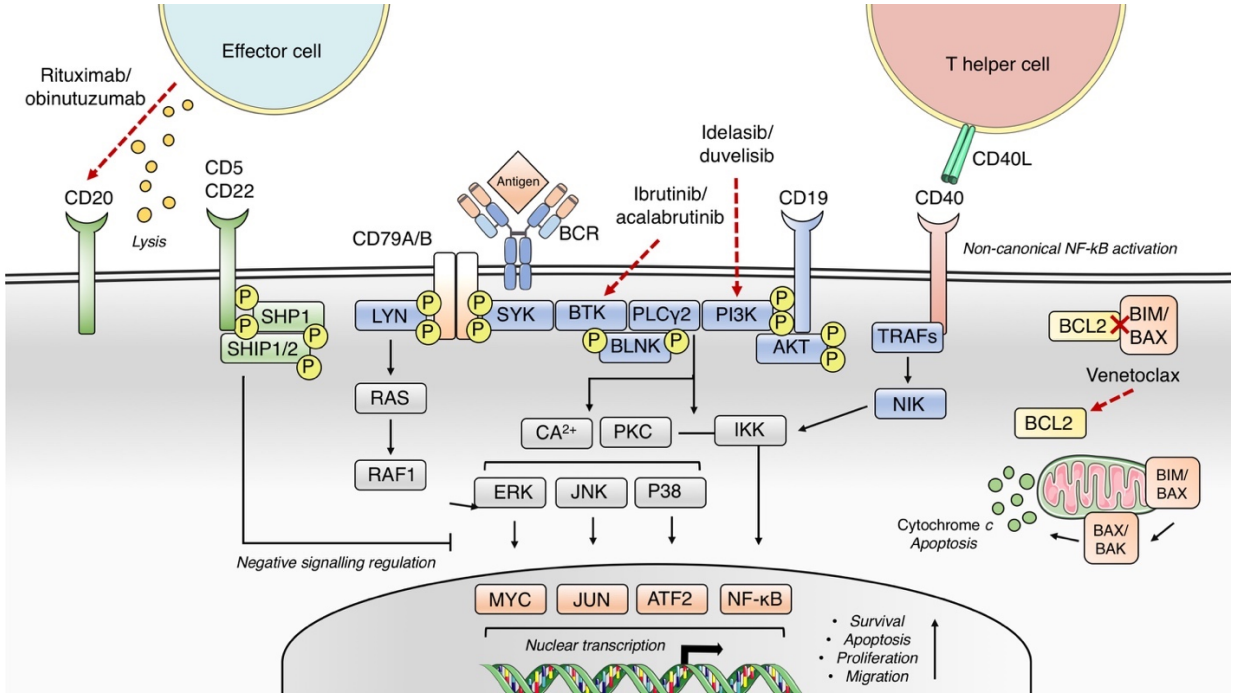

Figure 1.5: Chronic lymphocytic leukaemia (CLL) signalling pathways. The BCR and the BCR signalling pathway play a very important role in normal B cell development/growth but also in CLL progression where the pathway is very often overactive, providing constitutive growth and proliferation signals. Antigen-mediated triggering of the BCR induces activation of early kinases (blue), including LYN and SYK. LYN can activate ERK via RAF1 and RAS, and both LYN and SYK can transduce the signal to other early effectors of the signalling response, including BTK. Through the BLNK adaptor, BTK activates PLCγ2, and subsequent downstream responders (grey), including calcium signalling (Ca^{2+}), PKC, NF-κB, ERK and P38 while ultimately promoting activation of nuclear transcription factors (orange). T cell mediated CD40 activation can also activate the NF-κB pathway and its transcription factors. The positive co-receptor, CD19, contributes to the activation of the PI3K–AKT pathway and to survival induction. The signalling response is tightly modulated by negative coreceptors (green) (e.g. CD22, CD5) and phosphatases, including SHP1 and SHIP1/2. Recently, CLL treatments are focusing the use of targeted therapies which impact on several members of the BCR pathway – e.g. ibrutinib and idelalisib but also include the CD20 antibodies rituximab and obinutuzumab and the BCL2 inhibitor venetoclax. This figure is NOT to scale. This figure was created using Servier Medical Art templates, which are licensed under a Creative Commons Attribution 3.0 Unported License; https://smart.servier.com.

1.3 Signalling to transcription via chromatin remodelling

Having discussed the importance of the BCR and NF-κB signalling pathways in the pathogenesis, development and treatment of CLL we must consider the downstream processes which follow stimulation and activation of these pathways. Reorganisation and remodelling of the chromatin structure is necessary in order for BCR and NF-κB-driven gene expression programmes to be activated and promote CLL disease progression. Further, an understanding of how the processes which precede transcription are regulated can help us to fully understand the ibrutinib mechanism of action. As an inhibitor responsible for switching off a signalling pathway, it is important to understand what impact this may have on the regulation of downstream gene expression at the chromatin level.

1.3.1 Chromatin structure

The information necessary for supporting all of life's processes is encoded in our genome on both a genetic and epigenetic level. While the genetic code provides a blueprint for each and every protein building block, additional regulation at an epigenetic level provides instructions on how, when and where this code should be used by the cell [148].

In order to fit the entirety of the eukaryotic genome into the nucleus of a cell it is required to be both tightly packaged but also highly flexible to allow the plethora of DNA-regulatory factors access to the DNA when and where they are required [149]. This is achieved through the formation of chromatin; a higher-order structure defined as the complex of DNA wrapped around histone proteins to create nucleosomes, the basic units of chromatin [150]. An individual nucleosome is composed of eight histones proteins; two each of the core histones H2A, H2B, H3 and H4 with approximately 146 nucleotides of DNA wrapped ~1.65 times around the histone complex [151]. The tails of histone proteins can be covalently modified to fundamentally alter and reorganize the structure of chromatin to control DNA-based processes such as DNA repair, transcription and DNA replication [152] (summarised in figure 4)

Histone tail modifications are initially laid down by a series of proteins termed epigenetic writers – these include protein kinases, histone methyltransferases (HMTs) [153] and histone acetyltransferases (HATs) [154]. In order for

transcription factors to bind at gene control regions, ATP-dependent chromatin modifying complexes recognise histone tail modifications and through ATP hydrolysis, mobilise, shuffle or unwrap nucleosomes to expose the sites necessary for transcription activation. Chromatin remodelling enzymes are an example of epigenetic readers which are recruited to and interact with these modifications via specific domains to reorganise the chromatin, often to make way for further proteins, including transcription factors [155]. Chromatin readers possess particular domains which allow them to recognise modified histones. For example, the bromodomains of HATs allow for recognition of acetylated histones in chromatin such as the double bromodomain of TAF1 [156]. Further domains include the chromodomain and Tudor domains which can recognises methylated lysine [157]. The most well studied histone readers include the closely related SWI/SNF [158] and RSC (Remodelling the Structure of Chromatin) families and the ISWI family [159].

Epigenetic editors work to remove epigenetic marks from histone tails and include phosphatases, lysine demethylases (KDMs) and histone deacetylases (HDACs) [155]. The placement of reversible histone modifications by epigenetic writers, subsequent interaction via readers and then removal by erasers allows for a complex layer of epigenetic regulation in modulating gene expression, amongst other processes.

1.3.2 Histone modifications and transcription

As discussed, histone protein tails can be post-translationally modified (histone PTMs) by histone-binding proteins to functionally alter the landscape and organisation of chromatin. Chromatin fundamentally controls gene expression as typically the presence of nucleosomes physically prevents the transcription machinery from accessing DNA. Aside from physical impediment, specific histone PTMs can be inhibitory or permissive to the proteins required for transcription.

Histone tail lysine methylation can impact a number of transcriptional processes [160]. Lysine methylation is interesting in that it can be either inhibitory or activatory depending on the level of methylation of specific lysine residues (me1, me2 or me3). Generally, H3K4, H3K36 and H3K79 methylation marks active transcription and H3K9, H3K27 and H4K20 methylation marks silenced or inactive chromatin [161]. These modifications can also interact with one another

to promote or inhibit transcription. For example, chromatin marked simultaneously by methylation of H3K4 and H3K27 plays an important role in shifting gene expression from a poised to active or inactive state in embryonic stem cells [162].

Histone tail lysine acetylation is generally thought to be activatory for transcription in that the addition of an acetyl group by HATs neutralises lysine's positive charge and weakens the histone-DNA electrostatic interaction [163]. For example, the chromatin remodelling enzyme, RSC, can interact with acetylated lysine 14 of histone H3 (H3K14ac) to promote nucleosome remodelling and the eventual recruitment of RNA polymerase II (RNA Pol II) to DNA to promote gene transcription [164].

Histone tail phosphorylation occurs predominantly at a series of serines, threonines and tyrosines found on histone tails. Addition of a phosphate group adds a significant negative charge to the histone tail and can drastically alter chromatin structure. Phosphorylation of histone H3 at serine 10 (H3S10-P), threonine 11 (T11-P) and serine 28 (S28-P) has been clearly associated with H3 acetylation, strongly implicating these modifications in transcriptional activation [165]. H3S28-P works in combination with H3K27ac to displace Polycomb repressive complexes (PRC) from chromatin. This antagonistic relationship induces a methyl-acetyl switch of the adjacent K27 residue at these loci, thereby activating transcription [166].

1.3.3 Signalling kinases as chromatin remodelling enzymes

Among the types of enzyme which modify chromatin, histone kinases typically require activation via upstream signalling cascade and the upstream kinases are not thought to directly phosphorylate histones. However, some histone kinases have been implicated in being able to directly regulate gene expression through specific kinase dependent histone phosphorylation. Interestingly, studies have also shown that these type of histone kinases can even modify additional non-histone substrates including other types of chromatin remodelling enzymes and transcription factors to mediate both up- and downregulation of gene expression.

A recent review [167] highlights the functions of such signalling-histone kinases. This class of kinase has been shown to phosphorylate histone H3 at threonines 3, 6, 11 and 45 (H3T3-P, H3T6-P, H3T11-P and H3T45-P), serines 10 and 28

(H3S10-P and H3S28-P) and tyrosine 41 (H3Y41-P) and histone H2B at serines 14 and 36 (H2BS14-P and H2BS36-P). Regarding serine phosphorylation of histone H3, one example is IκB kinase α (IKKα), a part of the cytoplasmic IKK complex responsible for regulating NF-κB activation. It has been shown that IKKα can be recruited directly to the promoters of NF-κB target genes to phosphorylate H3S10 and initiate transcription [168]. Interestingly, IKKα was shown to travel with elongating RNA pol II S2-P and heterochromatin protein 1 gamma (HP1γ) at NF-κB dependent genes in macrophages [168]. In this co-dependent relationship, IKKα binds to and phosphorylates non-histone substrate HP1γ, which in turn guides IKKα to phosphorylate histone variant H3.3 at serine 31 (H3.3S31-P) within gene bodies.

IKKα also phosphorylates another non-histone substrate, CREB binding protein (CBP), at serine 1382 and 1386. CBP and its homolog p300 are transcriptional co-activators that mediate communication between transcription factors and the transcriptional machinery to regulate gene expression [169]. Phosphorylation of CBP by IKKα is responsible for accelerating cell growth by switching the binding preference of CBP from p53 to NF-κB. This switch activates pro-proliferative NF-κB gene expression programmes while suppressing p53-mediated gene expression.

Additionally, the serine/threonine kinase PIM1 which cooperates with MYC in cell cycle progression and tumorigenesis, has been shown to phosphorylate H3S10 [170]. In this relationship, MYC recruits PIM1 to its target genes to phosphorylate H3S10 and activate their transcription. It is estimated that PIM1 is implicated in the transcription of ~20% of MYC target genes. H3S10-P in this context was specifically related to elongation of MYC through the genes in question. For tyrosine kinases, H3Y41 phosphorylation was shown to be catalysed by JAK2 – a kinase responsible for activation a diverse range of cellular processes through its modulation of various signalling cascades [171]. The presence of H3Y41-P was shown to exclude HP1α from chromatin and lead to the transcriptional activation of various JAK2-mediated genes.

Adenosine monophosphate–activated protein kinase (AMPK) has been shown to directly activate transcription through an interaction with chromatin where it catalyses phosphorylation of H2B at S36. AMPK and H2BS36-P are found colocalised at the promoters of, and within, AMPK-dependent pathway genes, many of which are functionally pro-survival. The activation of AMPK and its

subsequent placement of H2BS36-P is therefore strongly linked to the activation of proliferative transcription programmes [172].

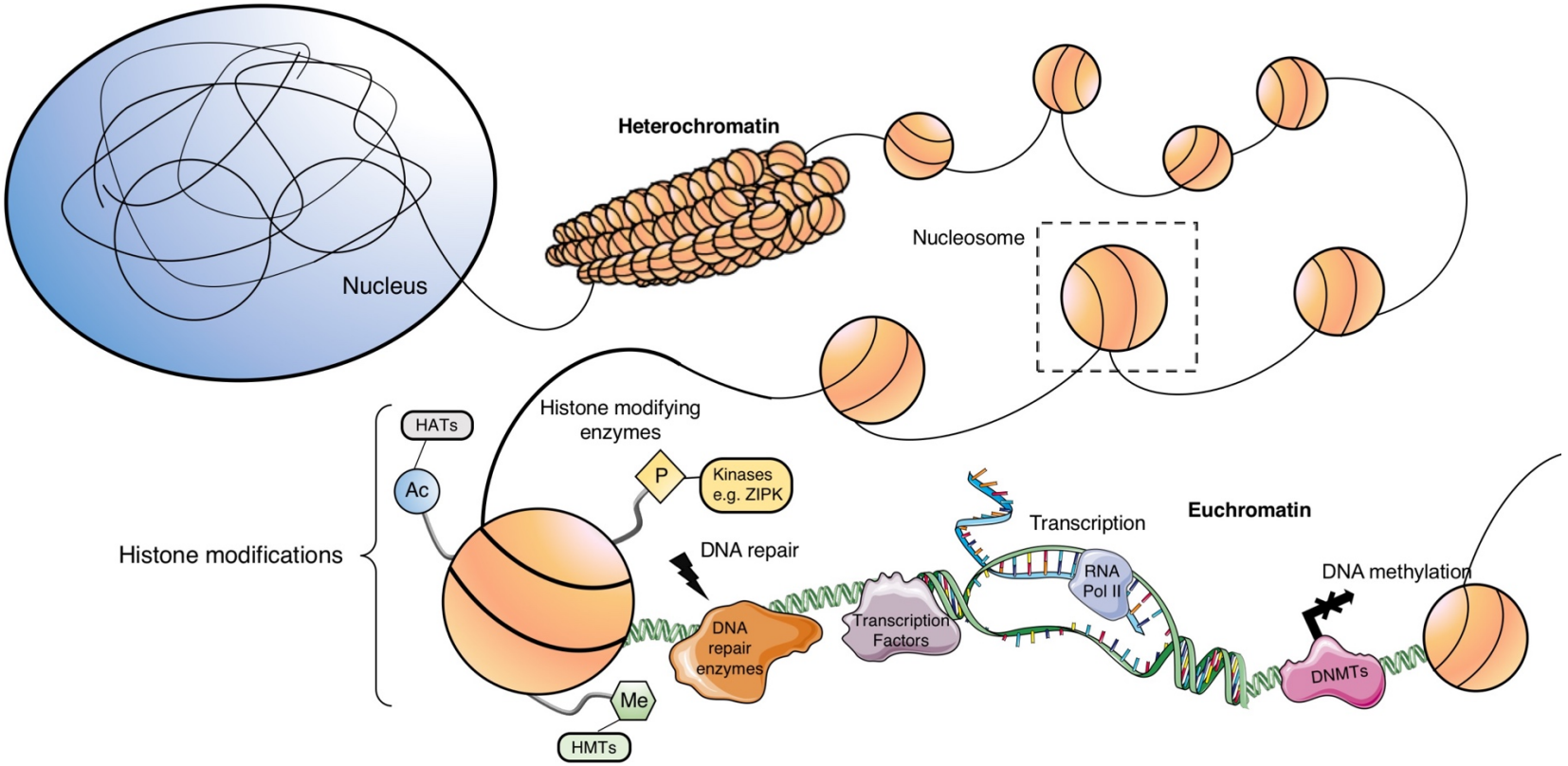

Figure 1.6: Epigenetics & histone modifications. For DNA to be stored in the nucleus of cells it is packaged into structures known as nucleosomes which consist of histone proteins with DNA spooled around them. When they are arranged in close proximity in a compacted form which represses transcription of the DNA the resulting alignment is known as heterochromatin. The tails of histones can be modified e.g. methylated (Me), acetylated (Ac) or phosphorylated (P) by histone modifying enzymes (HATs; histone acetyltransferases, HMTs, histone methyltransferases, kinases) – these modifications can cause conformational changes in the chromatin compaction and structure. The state of chromatin structure can either allow or prevent the access of DNA-binding proteins for a variety of tasks including DNA repair, DNA methylation via DNA methyltransferases (DNMTs) or transcription. For transcription, this provides an epigenetic mechanism of controlling gene expression. This figure was partly created using Servier Medical Art templates, which are licensed under a Creative Commons Attribution 3.0 Unported License; https://smart.servier.com.

1.4 Signalling outcome in CLL

We have now discussed how the BCR and NF-κB pathways are activated in CLL and considered how downstream chromatin reorganisation is both necessary for activation of gene transcription and also how changes to the chromatin landscape can play a role in CLL progression. The next step in the signalling cascade, transcription of the target genes, is similarly important. Immediate early gene activation is the first wave of gene expression upregulated in response to pathway activation and will be discussed below as a model for transcriptional output following BCR and NF-κB signalling.

1.4.1 Immediate early gene expression

Many cell types, including lymphocytes, express a specific class of gene known as the immediate early genes (IEG). IEGs can be rapidly activated and transcribed in response to stimulation by antigen, cytokines and growth factors without the need for *de novo* protein synthesis. Regulation of IEG expression in the B cell response is critical for the rapid proliferation and differentiation required by this cell type in response to infection. Examples of well-known IEGs include the early growth response factor (EGR) and dual specificity phosphatase (DUSP) families, as well as the pro-proliferative partner proteins, FOS and JUN [173]. As the name suggests, IEGs are induced quickly (sometimes within minutes) and transiently and possess particular characteristics at the genomic and epigenomic level to facilitate this process. The transient nature of these genes means their expression can peak just 15-60 minutes post stimulation, often returning to basal levels after as few as 90 minutes [174] [Thomas et al., forthcoming 2020].

To support their transient nature, IEG protein products are often unstable and can be targeted for degradation by the proteasome without prior ubiquitylation [175]. To aid their immediate expression the proteins required for their synthesis (including the transcription factors) are already present in the cell and are not translated in response to the activation process. This is demonstrated by the fact that IEG mRNA can be transcribed in the presence of protein synthesis inhibitors [176].

In addition, by genomic standards IEGs are relatively short (19 kb vs 58 kb) and contain far fewer exons than their delayed primary response and secondary response counterparts. Further, the promoter regions of IEGs tend to be over-

enriched with binding sites for a variety of transcription binding including motifs for serum-response factor (SRF), NF-κB and cyclic AMP response element binding protein (CREB) binding sites, suggesting a predictable and redundant mechanism whereby various TFs can initiate IEG transcription [177]. For example, *EGR1* and *DUSP2* (the IEGs focussed on in the result chapter) are as short as 3.9 and 2.4 kb with 2 and 4 exons respectively, promoting their rapid transcription in response to BCR crosslinking.

1.4.2 Immediate early gene – *EGR1* in B cells

Early growth response gene-1 is an IEG which encodes a transcription factor containing a zinc-finger motif and is widely dysregulated in haematological malignancies. *EGR1* is expressed ubiquitously in many cell types and has specific roles in B cells where it is activated downstream of the BCR, but not CD40 or TLR signalling [178] [179]. Antigen-mediated crosslinking and activation of the BCR upregulates the levels of *EGR1* to promote both B cell survival and proliferation/expansion of B cells. Once activated, *EGR1* which has been shown to regulate the transcriptional activity of genes including TNF-alpha, IL-2 and the cell adhesion molecules CD44 and ICAM-1, which are important for B cell trafficking [180]. The level of *EGR1* induced by BCR activation seems to depend on the stage of B cell development with the highest levels observed in mature B cells and more modest levels in immature B cells [181] and in pre-B cells, where it promotes development [182].

EGR1 expression has been shown to be upregulated in CLL [183] and high levels of *EGR1* were shown to form part of a gene signature post BCR activation indicative of cell cycle entry and CLL cell proliferation [184]. EGR1 shares 90% homology with its family members EGR2 and EGR3 and they share some functional redundancy in B cell development while also having their own unique roles [185]. This is interesting when considering that recent clinical trial data has demonstrated that CLL patients carrying *EGR2* mutations present a new clinically aggressive subgroup, with a poor prognosis similar to those patients with *TP53* mutations [186].

1.4.3 Immediate early gene – *DUSP2* in B cells

In order to combat infectious agents, mitogen activated protein kinase (MAPK) family members, ERK, JNK and p38 are all activated in immune cells in response

to CpG or LPS-mediated TLR signalling. In order to regulate, modulate and inactivate MAPK proteins, various members of the dual specificity phosphatase family can dephosphorylate the threonine and tyrosine residues of the conserved TxY motif found on most all MAPK members. [187].

The expression of DUSP family member, *DUSP2*, is limited to haematopoietic lineages in non-transformed cells and *DUSP2*$^{-/-}$ mice have a considerably disturbed inflammatory response [188]. *DUSP2* is an interesting case and it differs from most DUSP family members in that it can regulate MAPKs in both a positive and negative manner. Loss of DUSP2 function has been shown to increase JNK activity, as expected, but also lead to a reduction in ERK and p38 activity [188], highlighting the complex interactions between MAPKs and their phosphatases. Similar to *EGR1*, *DUSP2* is upregulated in CLL [184] and large B cell lymphomas [189] specifically in response to activation of the BCR signalling pathway [179]. In the context of CLL, *DUSP2* appears to function in its more traditional role as a negative regulator of MAPKs where it has been demonstrated to downregulate ERK activity [184].

In summary, both *EGR1* and *DUSP2* are examples of immediate early genes which are linked to the proliferation and survival of both healthy B cells and malignant CLL cells.

1.4.4 Transcription of IEGs – RNA polymerase II

RNA polymerase II (RNA pol II) is the main eukaryotic polymerase responsible for the transcription of messenger RNAs (mRNA). It is recruited to transcription start sites (TSS) in response to the binding of transcription factors to cis-regulatory elements and begins the process of unwinding the DNA duplex for the transcription of mRNA [190]. The process of mRNA transcription is strictly regulated at multiple stages through polymerase recruitment, initiation, elongation and termination with release of both the polymerase and the primary transcript. One way in which these steps are regulated is through differential phosphorylation of the C-terminal domain (CTD) of the largest RNA pol II subunit, RPB1. Progression of the RNA pol II molecule through a gene relies on balancing phosphorylation of the CTD at serine 5 (S5-P) around the transcription start site and at serine 2 (S2-P) throughout the gene body and towards the termination site. RNA pol II S5-P is typically associated with a poised polymerase and S2-P denotes active transcription [190].

The relationship between IEGs and RNA pol II is critical for their rapid transcription in response to stimuli and they tend to have an abundance of poised RNA pol II S5-P at their promoter regions compared to secondary response genes [191]. This suggests that IEG transcription elongation may begin from a paused polymerase already poised at the TSS, rather than by recruitment of RNA pol II following cellular stimulation, to provide a rapid 'jump-start' of IEG transcription. Indeed, studies have shown paused or stalled polymerases near the TSS of the IEGs FOS, MYC [192] and ARC [193], prior to cellular stimulation, ensuring a kinetic advantage for IEG transcription.

1.4.4.1 Chromatin organisation – regulation of immediate early gene transcription

In addition to the many characteristics of IEGs which promote their rapid and transient expression, there has long been suggestions that they possess distinct chromatin architecture and epigenetic traits key to their expression kinetics. Early literature demonstrated that the nucleosomal response associated with IEG transcription was mediated by a distinct MAPK signalling cascade, alternate to delayed or secondary response genes, and implicated MSK1, a histone H3 kinase, as being activated specifically to modify the chromatin around IEGs [194].

Further examples have demonstrated the distinct modifications responsible for the chromatin remodelling of inflammatory IEGs and how they differ to secondary response genes. A rapid and transient increase in the acetylation of histone H3 at lysine 14 and 27 (H3K14ac and H3K27ac) and histone H4 at lysine 5 (H4K5ac) occurs just 1 hour post cellular stimulation at IEG TSSs. Conversely, late and secondary response genes displayed marked increase in H3K14ac and H3 tri-methylated at lysine 4 (H3K4me3) at 6 hours post stimulation [195]. Histone H3 phosphorylated at serine 10 and serine 28 (H3S10-P and H3S28-P) has also been implicated in IEG-promoter chromatin remodelling to result in the induction of MAPK-specific IEGs, including JUN.

Bivalent phosphorylation and acetylation of the same histone H3 tail may also be indicative of IEG transcription. One study demonstrated that the highly targeted induction of doubly-modified histone H3 associated with the IEGs FOS and JUN. Such phosphoacetylation was only observed on nucleosomes associated with active FOS and JUN [196].

Additionally, the chromatin remodelling associated with NF-κB signalling in the immediate response has been extensively studied [197]. It has been suggested that NF-κB target gene activation occurs in two waves and is largely determined by promoter accessibility [198]. A subset of immediate NF-κB target genes possess an open chromatin structure which is immediately accessible after stimulation and NF-κB nuclear entry. For those secondary and late response genes, a distinct second wave of NF-κB transcription occurs only after significant hyperacetylation of these promoters which were inaccessible in the immediate-early response. It has been suggested that the presence of such open, readily available, chromatin structures could be mediated by atypical activation of the well-known SWI/SNF chromatin remodelling complexes. IEG-specific activation of SWI/SNF saw no need for enzymatic activity of the typical catalytic subunits, BRG1/BRM, which are absolutely required for chromatin remodelling associated with delayed or secondary response genes [199].

These types of data suggest several epigenetic mechanisms are capable of regulating IEG transcription. Distinct patterns of chromatin modifications or alternative signalling pathways may be necessary or activated to stimulate the recruitment of specific chromatin remodelling enzymes and transcription factors which are used specifically for rapid IEG transcription.

1.4.4.2 Chromatin organisation – regulation of pre-mRNA processing

Pre-mRNA processing of primary, nascent RNA transcripts occurs simultaneously with their transcription by RNA pol II and in the vicinity of chromatin. Epigenetic modifiers working to modify chromatin structure in concert with RNA processing enzymes carrying out capping, splicing and end processing duties is important to ensure the accuracy and efficiency of these processes [200].

Nucleosomes can impact pre-mRNA splicing through physical means and several studies have highlighted how nucleosome positioning can contribute to exon selection. For example, differential nucleosome occupancy has been observed in introns compared to exons [201], constitutive exons compared to alternative exons and in exons flanked by long introns and weak splice sites compared to exons with strong splice sites [202]. Nucleosome density and position also strongly impacts RNA pol II elongation rates and splicing defects

have been attributed to increased elongation rates caused by dysfunctional chromatin organisation [203], highlighting the interconnectivity of co-transcriptional pre-mRNA processing.

Aside from nucleosomes acting as physical barriers, histone tail modifications can also promote, impact and guide pre-mRNA processing. Histone H3 tri-methylated at lysine 36 and di-methylated at lysine 27 (H3K36me3 and H3K27me2) are both implicated in pre-mRNA alternative splicing. H3K36me3 is typically low around promoter regions and enriched in the gene body and it has been suggested that its presence can modulate exon choice by slowing RNA pol II transcript elongation rates [204]. Accordingly, both of these histone marks are enriched in exons, with H3K36me3 displaying the most intron-to-exon difference [201]. The majority of excluded exons, i.e. exons which are alternatively spliced, show very low levels of H3K36me3, while included exons tended to have higher levels. This difference suggests that the presence of this histone modification can guide exon-inclusion and alternative splicing. In addition, H3K36me3 seemed to be precluded from particularly short exons (less than 50 bp), controlling their exclusion from the transcript.

The activatory H3K4me3 modification has been implicated in mediating the interaction between chromatin and the splicing machinery, specifically U2 snRNP, one of five small ribonucleoprotein particles that binds 3' splice sites and forms a key part of the spliceosome machinery [205]. A further splicing regulator, polypyrimidine tract–binding protein (PTB), associates with chromatin to modulate alternative splicing [206]. PTB-mediated regulation of alternative splicing implicates both H3K4me3 and H3K36me3, where the levels of H3K36me3 at a particular gene correlates with PTB recruitment to the pre-mRNAs of that gene.

Finally, histone H3 methylated at lysine 9 (H3K9me) can also play a role in alternative splicing with PTB and other splicing factors known to recognise H3K9me3 [207]. H3K9 is typically a silencing mark associated with heterochromatin [208], but it can also be detected at actively transcribed genes [209]. In the case of CD44, a gene with many alternatively spliced isoforms, H3K9me3 marks in the gene body are recognised by the heterochromatin 1 protein (HP1γ). This recognition reduces local transcript elongation rates allowing for the inclusion of variable exons into the pre-mRNA [210]. A similar phenomenon is observed for fibronectin (FN1), with H3K9me3-mediated

recruitment of HP1α resulting in increased alternative splicing and inclusion of variable exons [211].

In summary, it is clear that nucleosomes, both physically and through histone tail modifications, control and mediate a vast number of processes involved in co-transcriptional pre-mRNA processing, particularly alternative splicing. The importance of histone methylation marks in identifying splice sites amongst large numbers of exons is clearly evident.

1.4.5 Preliminary data: immediate early gene expression is inhibited by ibrutinib in CLL

The Lefevre group has previously assessed immediate early gene expression in CLL (Figure 1.7A-B). The genes *EGR1* and *DUSP2* were selected after an initial screening for genes responding to anti-IgM stimulation in primary CLL, and for which the response was repressed by addition of ibrutinib. For this screen, U-CLL cells were pre-treated with ibrutinib for 1 hour before stimulation with anti-IgM to crosslink the BCR and activate BCR signalling with RNA samples taken at 0-24 hours for qPCR analysis. The genes assessed included *EGR1, DUSP2, MYC, DUSP4, CCND2, BCL2A1, PRDX1, NCL, CDC25B, TLR10, PIM1, CXCR4, CXCR5, CCR6* and *CCR7*. From these genes, only the first 5 were convincingly stimulated by anti-IgM activation of the BCR. *EGR1* and *DUSP2* mRNA level rapidly and transiently increased, peaking at 30 minutes post anti-IgM stimulation whereas *MYC*, *DUSP4* and *CCND2* showed peak expression between 2 and 4 hours post stimulation. Expression of both *EGR1* and *DUSP2* could be inhibited by the BTK inhibitor, ibrutinib.

1.4.6 Preliminary data: H3T6-P and H3T11-P occupancy correlates with immediate early gene expression kinetics in CLL

Additionally, the Lefevre group examined alterations to the chromatin landscape in CLL cells treated with ibrutinib, looking specifically at the IEGs which were seen to be upregulated in response to BCR signalling (*EGR1* and *DUSP2*). The group screened for histone modifications which changed after treatment with ibrutinib through a series of ChIP experiments. For these experiments, U-CLL cells were pre-treated with ibrutinib for 1 hour before stimulation with anti-IgM for 30 minutes to activate BCR signalling. Of the numerous histone modifications which were examined, histone H3 was seen to be consistently phosphorylated at threonine 6

and threonine 11 (H3T6-P and H3T11-P) across IEG loci in response to anti-IgM stimulation (Figure 1.7C-D). The histone marks were primarily located in around the IEG TSSs and in the gene bodies (see *EGR1* -0.1, +2.2 and +3.8 kb and *DUSP2* -0.3 and +2.4 kb). Consistently, the placement of these histone marks could be prevented by pre-treating CLL cells with ibrutinib (Figure 1.7C-D).

To summarise, the mRNA expression kinetics of *EGR1* and *DUSP2* correlate with the appearance of H3T6-P and H3T11-P across the loci of both genes. Ibrutinib can prevent both gene expression and the deposition of both histone marks.

1.4.7 H3T6-P and H3T11-P histone modifications

Our preliminary data highlighted phosphorylation of histone H3 at threonine 6 and 11 (H3T6-P and H3T11-P) as potential epigenetic markers for activation of the immediate early genes *EGR1* and *DUSP2* (Figure 1.7 and Thomas et al., forthcoming 2020). Phosphorylation of histone H3 is a diverse histone modification that can be associated with both open chromatin during gene activation and tightly compacted chromatin during mitosis [212]. These histone marks have not previously been implicated in CLL, but have a selection of other functions as described below. Of note, these constitute examples of signalling kinases which also function as chromatin remodelling enzymes (see 1.3.3).

Phosphorylation of H3T6 by protein kinase C beta I (PKCß-I) has been reported to control demethylation at histone H3 lysine 4 (H3K4) by directly preventing lysine-specific demethylase 1 (LSD1) from demethylating H3K4 during androgen-receptor (AR) dependent gene activation [213]. Following AR-induced gene expression, PKCß-I co-localised with AR and LSD1 on target gene promoters to mediate H3T6-P and prevent removal of the active H3K4 methyl mark. Notably, increased levels of PKCß-I and H3T6-P correlate with poor prognosis in prostate carcinomas, and inhibiting PKCß-I can block AR-induced tumour cell proliferation. These findings indicate H3T6-P can be associated with gene activation and a tumorigenic phenotype.

H3T11-P has also been implicated as an activatory histone mark which can promote gene transcription. Protein kinase-C related kinase 1 (PRK1) has been shown to catalyse H3T11-P at AR target genes [214]. Inhibition of PRK1 diminished H3T11-P, reduced androgen-induced demethylation of histone H3 by the Jumonji C-domain-containing demethylase, JMJD2C, and removed RNA pol

II S5-P from AR target gene promoters. In addition, WDR5, a subunit of the SET1/MLL complex, is able to interact with H3T11-P marked regions of chromatin to recruit the MLL1 complex for subsequent placement of the activatory histone mark: H3K4me3 [215].

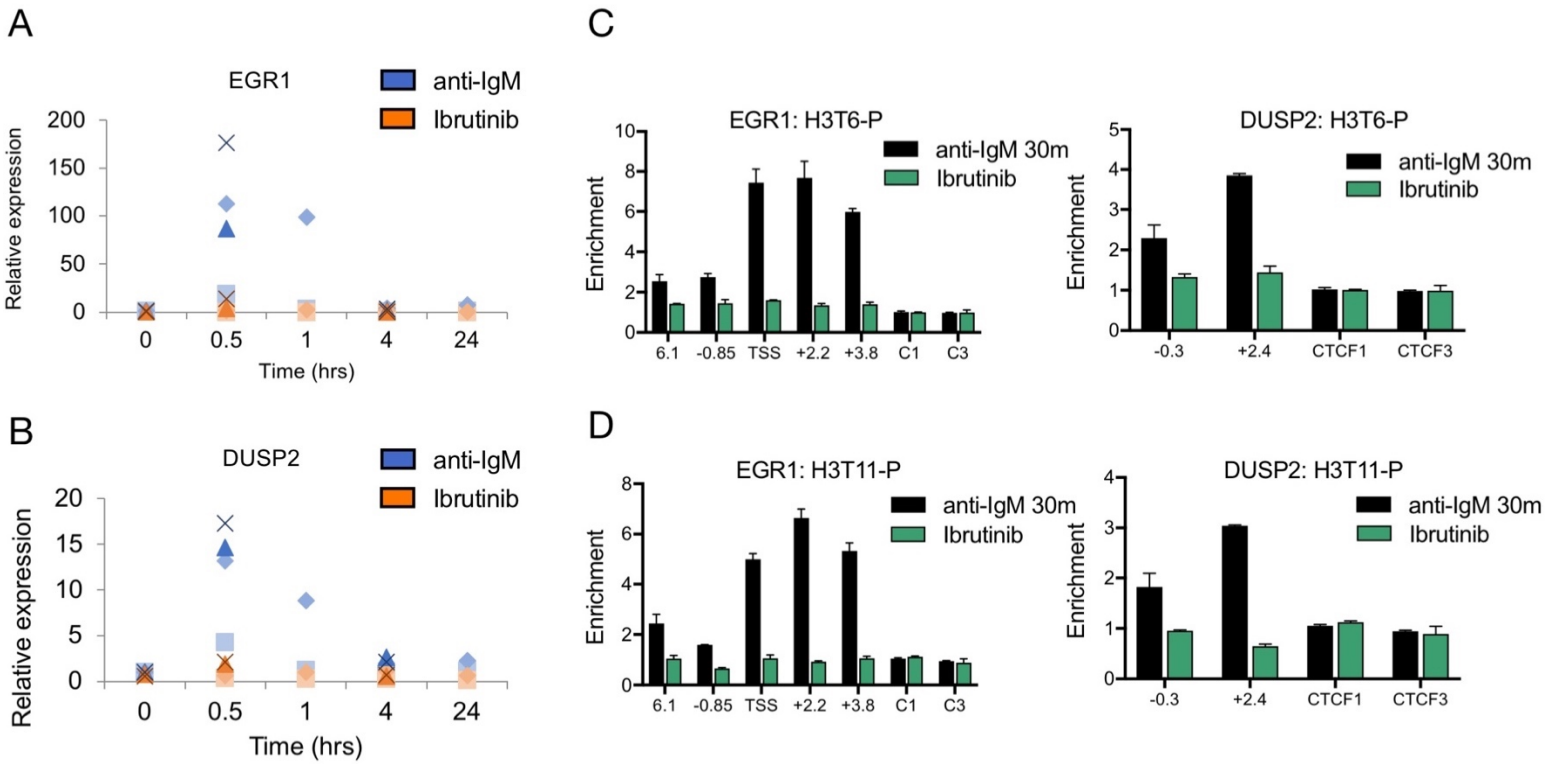

Figure 1.7: Preliminary data linking critical CLL IEG expression with H3-T6 and H3-T11 phosphorylation. (A) (B) qPCR data showing the rapid nature of IEG mRNA kinetics post anti-IgM stimulation. The CLL cells from 4 patients, indicated by the 4 different symbols (cross, diamond, triangle and square), were pre-treated with ibrutinib for 1 hour and then stimulated with anti-IgM with samples taken at the indicated timepoints from 0-24 hrs. These kinetics correlate with H3T6-P and H3T11-P deposition at the *EGR1* and *DUSP2* loci. **(C) (D)** ChIP-qPCR data 30 minutes after anti-IgM-mediated activation of the BCR resulting in an increase of H3T6-P and H3T11-P at the loci of the immediate early genes *EGR1* and *DUSP2*. This histone deposition can be inhibited by ibrutinib. Data provided by S Kreuz (unpublished).

A

H3T6-P

Kinase	Score
MEK2	4
PKCa	5.284
PKCb	4.125
PKCg	2.2
PKCd	2.435
PKCt	5.25
PKCz	3.462
RSK2	4.111
ZIPK	**4.056**

H3T11-P

Kinase	Score
PKCa	2.873
PKCg	2.8
RSK1	3
RSK2	3.222
ZIPK	**6.889**

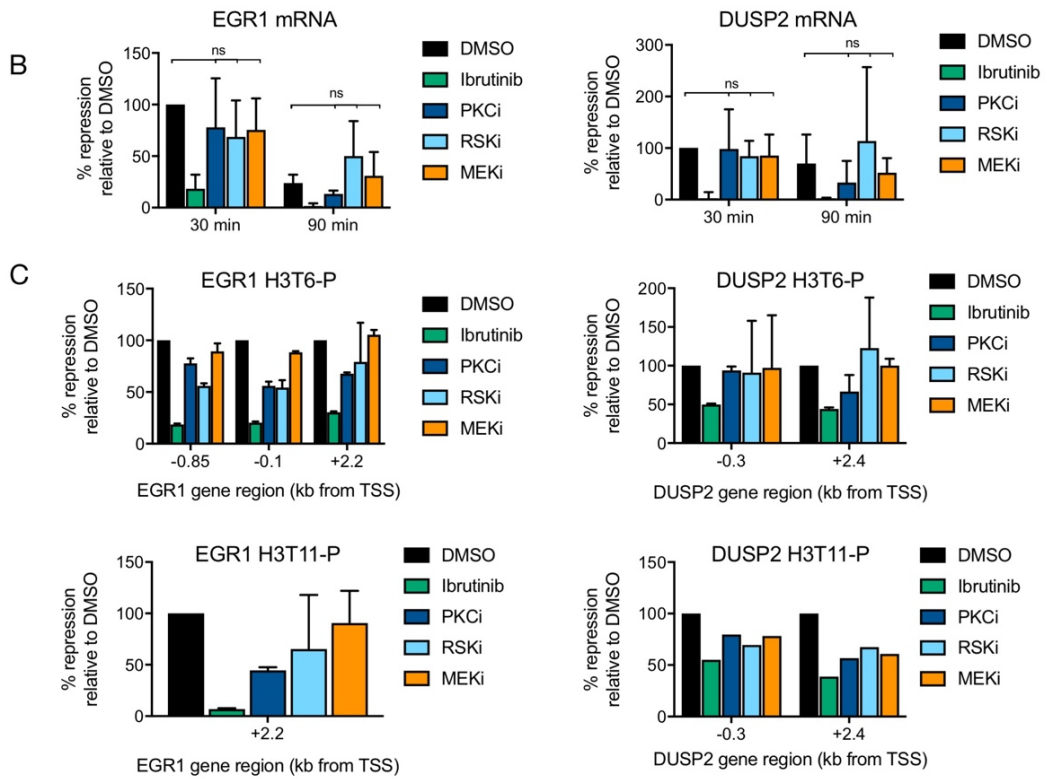

Figure 1.8: Preliminary data identifying ZIPK as a candidate kinase for H3-T6/H3-T11 phosphorylation and expression/histone PTM data demonstrating the inefficacy of other kinase inhibitors. (A) *In silico* kinase prediction software highlighted Zipper-Interacting Protein Kinase (ZIPK) as a candidate kinase for H3T6 and H3T11 phosphorylation. **(B) (C)** Primary CLL cells were cultured for 48 h and then treated with DMSO, 1 µM Ibrutinib, 1 µM Gö6983,10 µM RSK inhibitor II or 10 µM U0126 for 2 h, before the BCR was cross-linked. **(B)** Expression of *EGR1* and *DUSP2* was assessed and the means and SD of at least three independent experiments from different patients are shown normalised to *TBP* and to the induction of *EGR1* or *DUSP2* mRNA expression in DMSO-treated cells after 30 min (ns > 0.05 in Student's t test). **(C)** ChIP was performed before and after 30 min anti-IgM stimulation using primers along the *EGR1* and *DUSP2* genes and antibodies against H3 and H3T6/T11-P. ChIP results after 30 min anti-IgM stimulation are plotted. Results of one representative patient are shown normalised to H3 and the average of the CTCF1 and CTCF3 control regions and, then, versus, unstimulated DMSO-treated cells. Data provided by S Kreuz (unpublished).

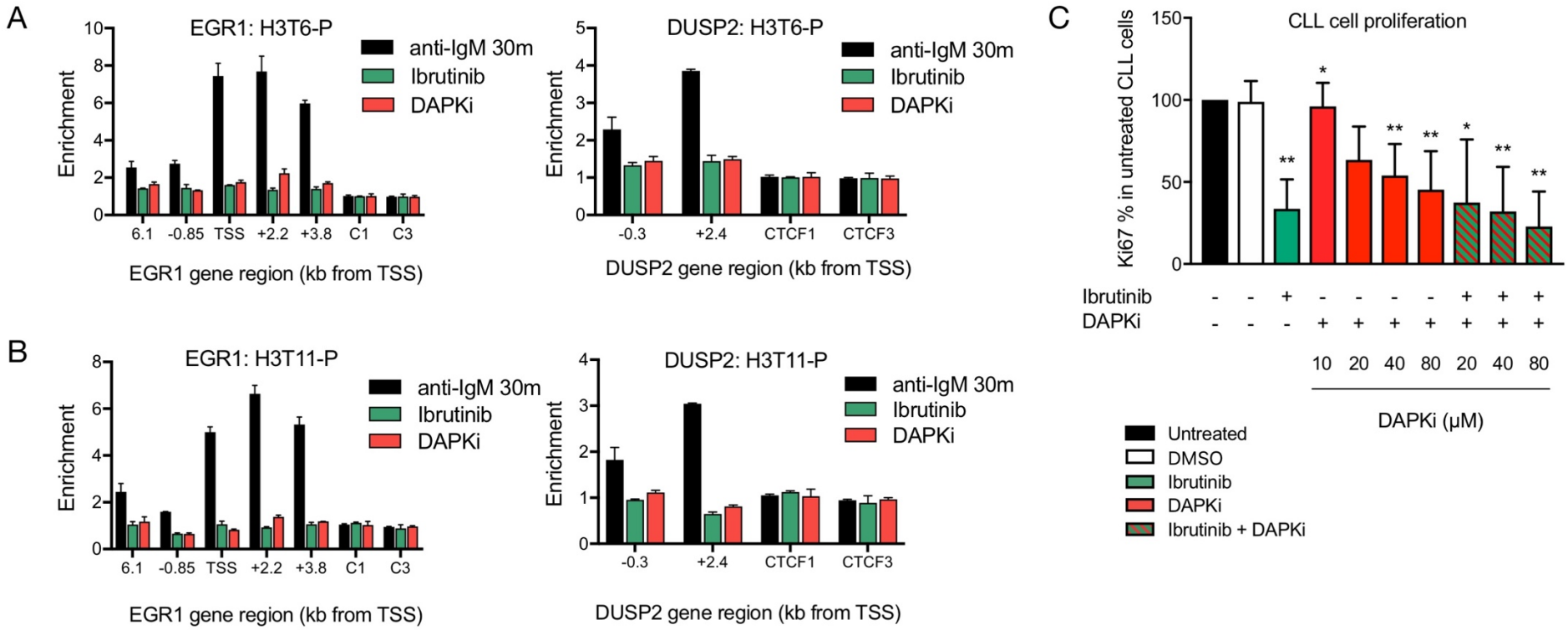

Figure 1.9: Preliminary data demonstrating that ibrutinib and DAPKi prevent H3T6 and H3T11 phosphorylation of the *EGR1* and *DUSP2* loci and the effects of DAPK3 inhibition on CLL cell proliferation. (A) (B) ChIP-qPCR data 30 minutes after anti-IgM-mediated activation of the BCR resulting in an increase of H3T6-P and H3T11-P at the loci of the immediate early genes *EGR1* and *DUSP2*. This histone deposition can be inhibited by both ibrutinib and a ZIPK inhibitor. Data provided by S Kreuz (unpublished). **(C)** Flow cytometric analysis of CLL cells cultured on a CD40L-expressing cell feeder layer. CLL cells were pre-treated with either ibrutinib, increasing concentrations (10-80 μM) of DAPKi, both inhibitors, or DMSO for 1 hour as indicated. Proliferation was assessed via the percentage of cells positive for Ki-67 (** < 0.01, * < 0.05, ns > 0.05 in Student's t test).

1.5 Zipper-interacting protein kinase

1.5.1 Preliminary data: kinase prediction software highlights ZIPK as the potential writer for H3T6-P and H3T11-P

Having observed a link between *EGR1* and *DUSP2* gene expression and the appearance of H3T6-P and H3T11-P, the group wanted to understand which kinase may be responsible for the catalysis of these histone modifications.

In silico kinase predication software highlighted a series of kinases (Figure 1.8A) which have already been observed to phosphorylate H3T6 or H3T11. Among the kinases identified, MEK2, RSK1/2 and PKCs are known downstream elements of the BCR signalling pathway. In order to examine which kinase was functioning at IEGs in CLL, inhibitors for all the predicated kinases were tested to see which could impact on *EGR1* and *DUSP2* gene expression and corresponding H3T6/T11 phosphorylation. In these experiments, U-CLL cells were pre-treated with the inhibitors ibrutinib, Gö6983, a pan-PKC inhibitor, RSK inhibitor II, a pan-RSK inhibitor, and U0126, a MEK1/2 inhibitor before anti-IgM stimulation for 30-90 minutes before qPCR and ChIP analysis. Apart from ibrutinib, none of the other three inhibitors significantly inhibited the induction of *EGR1* or *DUSP2* expression or prevented histone H3 phosphorylation after 30 and 90 min anti-IgM stimulation (Figure 1.8B-C). The data were varied with some PKC and RSK inhibitors able to prevent IEG expression and/or histone modifications to some degree while most could only impact one or the other.

However, both ibrutinib (Figure 1.8) and DAPKi treatment completely abrogated deposition of H3T6-P and H3T11-P occupancy (Figure 1.9) and reduced CLL cell proliferation to comparable levels for 20 μM DAPKi and beyond. Moreover, combining both drugs had a synergistic effect on cell proliferation (Figure 1.9C). Despite the same outcome, it was hypothesised that the impact of ibrutinib and the DAPKi on histone phosphorylation most likely arose through differing mechanisms e.g. prevention of ZIPK activation via BTK inhibition (ibrutinib) vs the direct inhibition of ZIPK kinase activity (DAPKi). Based on these data, we were able to hypothesise ZIPK was the histone kinase functioning to activate IEG expression in CLL via H3T6-P and H3T11-P, but more data was needed to confirm this.

1.5.2 ZIPK structure & family

ZIPK is a serine/threonine kinase originally cloned in 1998 when it was identified as an interacting partner of ATF4, a member of the activating transcription factor/cyclic AMP-responsive element-binding protein family (ATF/CREB), and as a mediator of apoptosis [216]. ZIPK, also known as DAPK3, is a member of the death associated protein kinase family (DAPK) whose members include DAPK1 and DAPK2/DRP-1 (DAPK-related protein 1) and the more divergent DAPK-related apoptosis inducing kinases 1 and 2 (DRAK1, DRAK2) [217]. ZIPK is ubiquitously expressed throughout mammalian tissues and is highly conserved between human, rat and mouse genomes. ZIPK interacts with family member DAPK1 via their catalytic domains. This interaction was shown to improve DAPK1-ZIPK cell death promoting activity [218]. DAPK1 phosphorylates ZIPK at six specific residues in its catalytic domain and these modifications effect both the localisation and oligomerisation of ZIPK (summarised in Figure 1.10).

While these molecules differ in size and subcellular locations, DAPK1, DAPK2 and ZIPK share significant homology at the N-terminus catalytic domain (80% and 83% respectively) whereas DRAK1 and DRAK2 have only ~50% homology with DAPK1 [219]. The C-terminal extra-catalytic domains of the DAPK family members are substantially different however. The ZIPK C-terminal domain comprises several nuclear localisation signal (NLS) sequences and a leucine zipper domain [216]. Such domains are required for homo-oligomerisation and ZIPKs interaction with other leucine zipper containing proteins [220] as well as being critical for its pro-apoptotic effects [221]. Phosphorylation of threonine 180, 225 and 265 are required for full ZIPK kinase activity and phosphorylation of threonine 299 regulates its cytoplasmic localisation [222], with threonine-265 (ZIPK T265-P) highlighted as the major autophosphorylation site critical for ZIPK kinase activity [223].

1.5.3 ZIPK function

All members of the DAPK family have roles associated with cell death signalling. ZIPK has been shown to be a pro-apoptotic mediator of mitochondrial-dependent cell death [224], as well as play a role in autophagy [225]. DAPK1, DAPK2 and ZIPK are found throughout various tissues in mammals yet ZIPK is unique in that it possesses nuclear localisation signals [226].

There is ongoing debate over the intracellular localisation of ZIPK. Indications of a predominant cytoplasmic localisation come from reports that over-expression of active human ZIPK can induce cell death as evidenced by the characteristic membrane blebbing and cell rounding [227]. In the cytoplasm, ZIPK has been reported to regulate smooth muscle contraction by promoting Ca^{2+} independent contraction of smooth muscle cells via phosphorylation of the myosin light chain (MLC) and inhibiting smooth muscle myosin phosphatases [222]. To this end, by enhancing smooth muscle cell contractility ZIPK has been implicated in the development of some hypertensive cardiovascular diseases [38].

Conversely, other studies propose a different picture for ZIPK subcellular localisation suggesting the protein is predominantly nuclear. For example, ZIPK has been identified in PML oncogenic domains (PODs). PODs are nuclear bodies that exist in all nucleated mammalian cells and ZIPK was shown to co-localise with the pro-apoptotic protein Daxx to regulate its recruitment to PODs to promote apoptosis [216]. Further, ZIPK has been shown to interact with and directly bind two transcription factors in the nucleus, ATF4 [216] and STAT3 [228].

1.5.4 ZIPK as a histone kinase

Our preliminary data in combination with current literature suggest that ZIPK that may function as a chromatin modifying enzyme whose kinase activity can regulate transcription. One of the earliest observations of ZIPK was its interaction with chromatin and ability to phosphorylate the core histones H2A, H3 and H4 [229]. Specifically, ZIPK was identified as capable of phosphorylating histone H3 at threonine 11 (H3T11-P) in a mitosis-specific context [230]. H3 phosphorylated at serine 10 (H3S10-P) is typical of a mitotic chromosome, while ZIPK-mediated H3T11-P was enriched specifically at centromeres. In this unique case, ZIPK acts as a centromere-specific histone kinase that plays a role in depositing H3T11-P modifications during mitosis at specific regions of centromeric chromatin. ZIPKs histone kinase functions have yet to be implicated in disease.

Figure 5: DAPK protein family structure

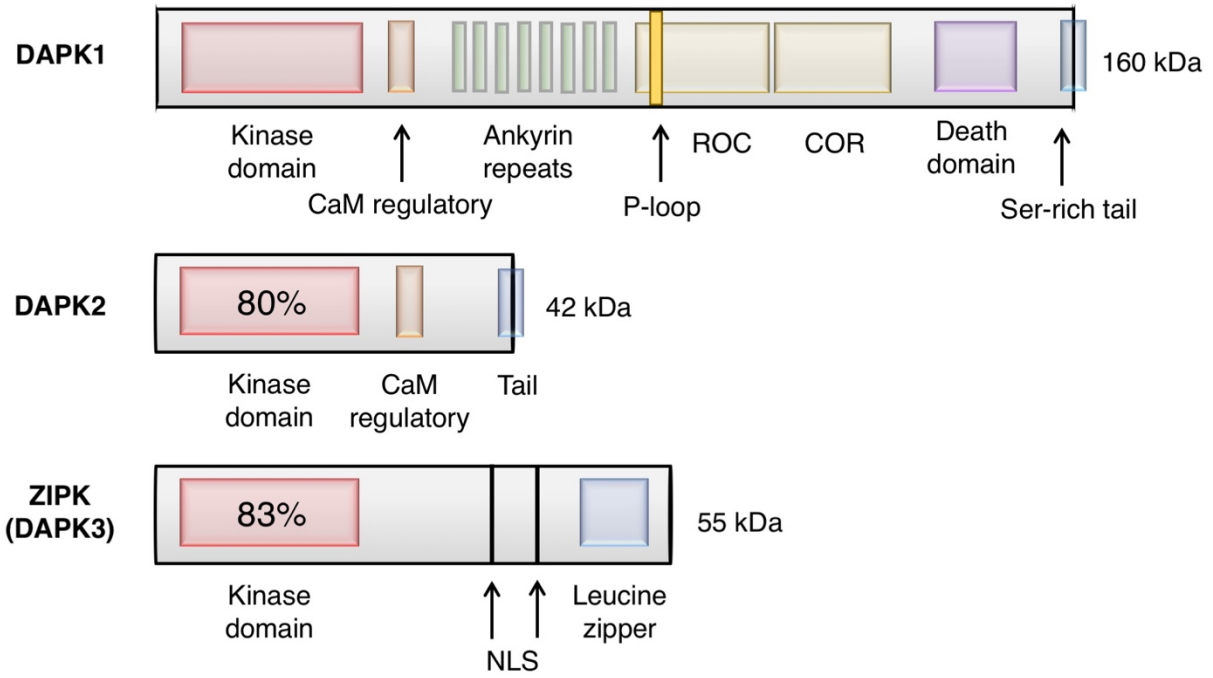

Figure 1.10: DAPK protein family structures. A schematic representation of the domain organization of the main DAPK family members. The percentage in the red boxes, representing the kinase domains, indicates the extent of identity of each catalytic domain to that of DAPK. DAPK is the largest protein in the family, at 160 kDa, and it contains a Ca2+/CaM autoregulatory domain, eight ankyrin repeats, ROC-COR (Ras of complex proteins, C-terminal of ROC) domains, which overlap with a cytoskeletal-binding region, a death domain and a serine-rich C-terminal tail. ZIPK, at 55 kDa, lacks the Ca2+/CaM autoregulatory domain, and thus its regulation differs substantially from that of DAPK and DRP-1. Instead, it contains a nuclear localization signal (NLS) and a leucine zipper.

1.5.5 ZIPK in disease

ZIPK has been demonstrated to have both pro- and anti-tumorigenic functions that vary by context, cell type and intracellular location. Some evidence suggests that ZIPK functions primarily as a tumour suppressor. For example, decreased ZIPK expression corresponding with a reduction in apoptosis has been demonstrated in squamous cell carcinoma [231]. Similarly, loss of ZIPK expression was associated with tumour invasion, metastasis and poor prognosis in gastric cancer [232]. Additionally, loss-of-function point mutations identified in colon, lung and ovarian cancers have been observed to decrease or abolish ZIPK kinase activity with a correlated increase in cell survival, proliferation and resistance to chemotherapy [233].

Conversely, ZIPK can also display anti-apoptotic activity and functions which promote tumorigenesis. For example, in gastric cancer ZIPK has been reported to promote epithelial-mesenchymal transition (EMT) and metastasis through activation of AKT and NF-κB signalling [234]. ZIPK has also been observed as a novel transcriptional co-activator of the androgen receptor (AR) and it has been reported that ZIPK may provide a growth advantage to prostate cancer cells through regulation of AR anti-apoptotic proliferative functions [220]. Studies in gastric cancer highlights the diversity of ZIPK function where it may act as both a tumour suppressor gene at the primary tumour and an oncogene at distant sites after promoting EMT; underlining that its function is context and location dependent.

For CLL, ZIPK was shown to be overexpressed in the sera of CLL patients who had been given allogeneic stem cell transplants was highlighted as an attractive target for CLL therapies outside of transplantation [235]. In addition, ZIPK expression was shown to be closely correlated with the apoptotic trio of prostate apoptosis response protein-4 (PAR-4), DAXX and BCL-2 [236]. In summary, the role of ZIPK in disease has been closely linked to its apoptotic functions and, to date, ZIPK has not been implicated as a histone kinase in CLL or otherwise.

1.5.6 ZIPK-STAT3 relationship

STAT3 is a cytoplasmic transcription factor of the STAT protein family which regulates expression of anti-apoptotic and pro-proliferative genes [237]. STAT family proteins are activated upon their phosphorylation by Janus kinases (JAKs)

which induce their nuclear translocation through the JAK-STAT signalling pathway [238]. Constitutive and aberrant tyrosine phosphorylation of STAT3 has been reported in many solid tumours [239] and haematological malignancies including acute myeloid leukaemia (AML) [240], chronic myeloid leukaemia (CML) [241], large granular lymphocytic leukaemia (LGL) [242] and CLL [115, 116, 243].

ZIPK has been shown to specifically interact with and phosphorylate STAT3 at S727 in the nucleus to enhance STAT3 transcriptional activity (ZIPK does not bind other STAT family proteins or STAT tyrosine residues) [228]. Further, reduced ZIPK expression or mutation of the important ZIPK T265 autophosphorylation residue results in a decrease in interleukin 6 (IL-6) induced STAT3-mediated transcription.

1.6 Aims and Objectives

Based on the initial observations outlined in our preliminary data (Figure 1.7-Figure 1.9), we have highlighted ZIPK as the histone kinase potentially responsible for the phosphorylation of histone H3 at threonines 6 and 11. We have shown that ZIPK inhibition by DAPKi prevents the phosphorylation of these histone marks with a corresponding decrease in the mRNA expression of two IEGs, *EGR1* and *DUSP2*. Of the other candidate kinases identified in our initial screen such as MEK2, RSK1/2 and PKCs, their inhibition did not significantly inhibit *EGR1* and *DUSP2* gene expression or prevent histone H3 phosphorylation after anti-IgM stimulation. These data suggested a link between IEG and expression and histone H3T6 and H3T11 phosphorylation in CLL. Further, we have shown that DAPKi treatment of CLL cells inhibits their proliferation, similarly to ibrutinib, and that combining these two drugs had a synergistic effect on CLL cell proliferation.

With these data in mind, at the outset, this project aimed to examine the following:

- Determine ZIPK function in CLL and the potential benefits of its inhibition in the treatment of the disease compared to ibrutinib, especially in cases of BTKi-resistance.
- Assess IEG response in CLL and the role of ZIPK in mediating IEG expression.
- Examine the dynamics of the transcription factors responsible for CLL IEG expression, particularly STAT3, due to its previously described associations with ZIPK.

Chapter 2 Materials & Methods

2.1 Materials

2.1.1 List of antibodies

Table 1: Table of antibodies

Antibody	Manufacturer	Application
anti-Rat IgG	e-Bioscience/Thermo; 18- 4818-12	Co-IP
B-actin	ThermoFisher; PA1-183	WB
EGR1	CST; #4153	WB
H3T11-P	Abcam; ab5168R	KA, WB, ChIP
H3T6-P	Diagenode; C15410282	KA, WB, ChIP
HDAC2	Santa Cruz Biotech; C-19: sc-6296	WB
Histone H3	Abcam; ab1791	WB, Co-IP, ChIP
HRP-secondary anti-mouse	Jackson-ImmunoResearch; 315-035-003	WB
HRP-secondary anti-rabbit	Jackson-ImmunoResearch; 111-035-003	WB
p65	Santa Cruz Biotech; C-20: sc-482 CST; #8242	WB, Co-IP, ChIP WB, Co-IP, ChIP
RNA pol II	Abcam; ab817	Co-IP, ChIP
RNA pol II S2-P	Abcam; ab5095	WB, Co-IP, ChIP
STAT3	Santa Cruz Biotech; C-20: sc-482 CST; #9139	WB, Co-IP, ChIP WB, Co-IP, ChIP
STAT3-S727-P	Abcam; ab30647 CST; #9134	WB, Co-IP, ChIP WB, Co-IP, ChIP
STAT3-Y705-P	CST; #9131	WB, Co-IP, ChIP
Vinculin	CST; #4650	WB
ZIPK	Bethyl; A304-221A-1	WB

	Bethyl; A304-222A-1	Co-IP, ChIP
ZIPK-T265-P	Abcam; ab63395	WB, Co-IP
	ThermoFisher; PA5-40234	WB, Co-IP, ChIP

KA, kinase assay. WB, western blot. Co-IP, co-immunoprecipitation. ChIP, chromatin immunoprecipitation. RT-PCR, reverse-transcription polymerase chain reaction. qPCR, quantitative polymerase chain reaction.

2.1.2 List of primers

Primers were designed online using Primer3Plus and the NCBI Primer-BLAST tool in conjunction with the *in-silico* PCR function of the UCSC genome browser. The number following a primer indicates the distance from the transcription start site (TSS) in kilobases (kb) of the corresponding gene where negative values are upstream of the TSS and positive values are downstream of the TSS.

Table 2: Table of primers

Primer	Sequence	Application
CTCF1 F	GGCCCAGGACTCCACGTTCAGA	ChIP
CTCF1 R	GCCCTCTGGTGTTTGGCAGCAA	ChIP
CTCF3 F	CACCCAGCAGAGGGCCCAGATA	ChIP
CTCF3 R	CCCTTCGCCTTCTCTCCAGCCA	ChIP
DUSP2 -0.3 F	CTAAAGGGGGACCTGCATCTG	ChIP
DUSP2 -0.3 R	GACTAAGGGAAGGGAAGGTGTT	ChIP
DUSP2 -0.6 F	AGGTCTTGAAATCCCCGCAG	ChIP
DUSP2 -0.6 R	CCAGGCCCCAGAGAGAAGTA	ChIP
DUSP2 -11.0 F	CCTTGACTCCCTGCTGAAGG	ChIP
DUSP2 -11.0 R	CCCATCACAGCCCAAGTCTT	ChIP
DUSP2 +0.5 F	GCTGGTTTTGTCCCCTGTTG	qPCR/RT-PCR
DUSP2 +0.5 R	CTGATCGTGCTCTTCCCCTC	qPCR/RT-PCR
DUSP2 +0.8 F	CCAGTCCTCCTGACCTGAGA	qPCR/RT-PCR
DUSP2 +0.8 R	GTGCCTGTATGGGTCTGTGT	qPCR/RT-PCR
DUSP2 +1.1 F	GGTGCCCCCTTACCAATGAA	qPCR/RT-PCR
DUSP2 +1.1 R	GGGCCTTTTCCGCTACAAGA	qPCR/RT-PCR

DUSP2 +2.4 F	GGAAGTGATGGGTGTGTCATGT	ChIP
DUSP2 +2.4 R	AAATAATTTTCCAGCGCCAGCA	ChIP
DUSP2 +3.1 F	CATTTGGAGTGTCATCCAGCCA	ChIP
DUSP2 +3.1 R	ACAGACCACGGACAGATCCTTA	ChIP
DUSP2 +4.2 F	AGGAGTGAGGTTGATCTGATGT	ChIP
DUSP2 +4.2 R	CCAGCCGTTATGAGTGTCCAT	ChIP
DUSP2 F	TACTTCCTGCGAGGAGGCTT	qPCR/RT-PCR
DUSP2 R	GGCTGGTTTTGTCCCCTGTT	qPCR/RT-PCR
EGR1 -0.1 F	GCCATATTAGGGCTTCCTGCTT	ChIP
EGR1 -0.1 R	GATCCGCCTCTATTTGAAGGGT	ChIP
EGR1 -0.4 F	TCTGGGAGGAGGGAAGAAGG	ChIP
EGR1 -0.4 R	TTCGGGGAAGCCTAGAGC	ChIP
EGR1 -0.85 F	TACAGTGTCCCAAGAACCAAGT	ChIP
EGR1 -0.85 R	CGATCTATGGCACGGTGTCTTT	ChIP
EGR1 -1.0 F	CCCTCCACCTGGACTGGATA	ChIP
EGR1 -1.0 R	CCGAAGTGGGGAAGCTGATT	ChIP
EGR1 -6.1 F	CCTGGGGTAGGAGCAGAACT	ChIP
EGR1 -6.1 R	TGTCACACTTTCCGACTGACTT	ChIP
EGR1 +0.55 F	CAGCACCTTCAACCCTCAGG	qPCR/RT-PCR
EGR1 +0.55 R	ATGGTGGCGAAAGGGTTCC	qPCR/RT-PCR
EGR1 +1.0 F	TCCGTATTTGCGTCAGCTGT	qPCR/RT-PCR
EGR1 +1.0 R	GCTACCATTGACTCCCGAGG	qPCR/RT-PCR
EGR1 +2.2 F	CTGCGACATCTGTGGAAGAAAG	ChIP
EGR1 +2.2 F	GCCGCAAGTGGATCTTGGTAT	ChIP
EGR1 +3.8 F	GCTGCGATTGGGTATGTGTTTC	ChIP
EGR1 +3.8 R	AGAAAACCTCACAGCCCTCAAT	ChIP
EGR1 +4.2 F	GGGCCTGTTCCTCTTCAGTC	ChIP
EGR1 +4.2 F	CACACATGTCCCAGCCCTAA	ChIP
EGR1 F	ACAAAAGTGTTGTGGCCTCTTC	qPCR/RT-PCR

EGR1 R	GTGGCCGGGGATGGATAAGA	qPCR/RT-PCR
EGR1 TSS F	GCCATATTAGGGCTTCCTGCTT	ChIP
EGR1 TSS R	GATCCGCCTCTATTTGAAGGGT	ChIP
GAPDH F	ACAGTCAGCCGCATCTTCTT	qPCR
GAPDH R	ACGACCAAATCCGTTGACTC	qPCR
PPP6C F	TGGAAATGCTAATGCCTGGAGA	qPCR
PPP6C R	TTCCTGATTCCGTTCGATGGTT	qPCR
TBP F	TGCTCACCCACCAACAATTTAG	qPCR
TBP R	TCTGGGTTTGATCATTCTGTAGATTAA	qPCR

ChIP, chromatin immunoprecipitation. RT-PCR, reverse-transcription polymerase chain reaction. qPCR, quantitative polymerase chain reaction.

2.2 Cell culture

2.2.1 Primary CLL cells and cell line maintenance

CLL cells were obtained from the St James's University Hospital (Leeds) Haematological Malignancy Diagnostic Service (HMDS) from patients with no previous treatment for their disease. The experiments using these cells were undertaken with the understanding and written consent of each patient and the study methodologies conformed to the standards set by the Declaration of Helsinki. These experiments were performed under ethical approval granted by the Leeds Teaching Hospital NHS Trust REC: 14/WS/0098. CLL, raji, ramos and HBL1 cells were grown in Roswell Park Memorial Institute (RPMI-1640; Sigma-Aldrich) medium with 10% foetal calf serum (PAA Laboratories Inc.), L-glutamine (ThermoFisher; Gibco™) and penicillin- streptomycin (ThermoFisher; Gibco™). All cells were cultured at 37°C and 5% CO_2. Raji, ramos and HBL1 cells were cultured at 0.1-1.0 x 10^6 cells/ml and CLL cells at 0.1-0.5 x 10^7 cells/ml aiming for ~80% cell density.

2.2.2 Isolation of PBMCs

CLL peripheral blood mononuclear cells were isolated by density centrifugation from whole blood using Lymphoprep™ (Stemcell Technologies). In brief, blood was diluted 1:2 in phosphate-buffered saline (PBS) and carefully layered over an equal amount of Lymphoprep™. After centrifugation at 2000 rpm for 20 min

(acceleration reduced to 60% and with the brake off), PBMCs were carefully recovered with a Pasteur pipette. PBMCs were transferred into a new tube and washed twice with PBS. No specific B cell enrichment step was performed as PBMCs from CLL patients are mostly B-CLL cells. Cells were counted and plated into T25 flasks at appropriate densities or frozen, as required.

2.2.3 Cell counting

For cell survival assays and cell counting in preparation for experiments, cells were stained with trypan blue (ThermoFisher) and counted manually using a standard haemocytometer with a cover slip. Depending on the observed density of cells in culture medium, they were diluted in the range of 1:5 – 1:50 with trypan blue, aiming to achieve a count of ~100 cells. Cell number per ml was determined using the following equation:

$$cell\ number\ per\ ml\ \frac{average\ cell\ count}{number\ of\ squares\ counted} \times 10^4 \times dilution\ factor$$

Equation 1: formula for counting cells *in vitro* using a haemocytometer.

2.2.4 Cell freezing & thawing

Exponentially growing cells were collected by centrifugation and resuspended in ice-cold freezing mix (90% FCS and 10% DMSO) at a density of 10^6 cells/ml for all cell lines and 10^7 cells/ml for CLL cells. 1 ml of the suspension was transferred into a cryotube and stored into a freezing container at -80°C for at least 24 h. The tubes were then transferred into the liquid nitrogen storage tank for long-term storage. For thawing, cells were removed from either -80°C or liquid nitrogen storage and warmed by gently swirling in a water bath set to 37°C until only a small amount of ice remained. The cells were then quickly added to fresh media and pelleted by centrifugation to remove the DMSO-containing freezing mix.

2.2.5 Cellular stimulation and inhibition

Cells were stimulated with F(ab')2 fragment goat anti-human IgM at 10 µg/ml (Jackson-ImmunoResearch; 109-006-129-JR) or recombinant human sCD40 ligand (Peprotech; 310-02) at 5 µg/ml as required and where indicated. Cells were pre-treated with ibrutinib (Pharmacyclics, Sunnyvale, CA, US) at 1 µM or a

DAPK inhibitor (DAPKi) (Calbiochem; 324788-10MG) at 10-120 μM as required and where indicated.

2.2.6 Transfection of lymphoid cell lines with siRNA

ZIPK knockdown was achieved in HBL1 cells with a GenePulser® II electroporation system (BioRad) using siRNAs against ZIPK (ThermoFisher; siRNA ID #557 and #559) complete with a non-targeting negative control siRNA (ThermoFisher; 4390843). Post-electroporation, cells were transferred to flasks of pre-warmed media and left overnight. siRNA transfected cells were incubated for 3-5 days, with addition of fresh RPMI on day 1 and 3, and counted to check cell viability. Cells were subsequently harvested by centrifugation and prepared for western blot analysis to confirm ZIPK knock down.

2.3 Kinase assays

0.1 μg recombinant protein DAPK3-GST (Abcam; ab152327) and 1 μg recombinant protein histone H3-HIS (Abcam; ab198757) were added to kinase buffer (KB) (1 mg/ml BSA, 25 mM HEPES pH 7.9, 10 mM $MgCl_2$, 50 mM NaCl, 1 mM DTT, 10 mM KCl and 10% glycerol) complete with 1x protease inhibitor cocktail (NEB; 5871S) (added fresh). ATP was added where indicated to 200 μM final concentration. Ibrutinib (Pharmacyclics, Sunnyvale, CA, US) was added where indicated to 1 μM final concentration. A DAPK inhibitor (DAPKi) (Calbiochem; 324788-10MG) was added where indicated to 50 μM final concentration. Samples were warmed to 16°C to start the reaction. Aliquots were removed at the indicated time points and immediately heat inactivated for 5 minutes at 65°C to halt the reaction. Reaction samples were spotted onto nitrocellulose membranes and air dried before blocking in 5% BSA at room temperature for 1 hour. Membranes were incubated at 4°C overnight with primary antibodies against H3T11-P (Abcam; ab5168) and H3T6-P (Diagenode; C15410282). HRP-conjugated secondary antibodies against rabbit (Jackson-ImmunoResearch; 111-035-003) and mouse (Jackson-ImmunoResearch; 315-035-003) were used at 1:10,000. Membranes were analysed using ECL (ThermoFisher; Pierce™) and a ChemiDoc system.

2.4 Protein extraction & analysis

2.4.1 SDS lysis

For western blotting, prior to lysis, cells were washed twice with ice cold PBS, centrifuging at 1,200 rpm for 5 minutes. Samples were then lysed with SDS lysis buffer (10% SDS, 0.5 M Tris pH 6.8) supplemented with 1x protease inhibitor cocktail (NEB; 5871S), PMSF (1 µl/ml), NaF (1 µl/ml) and Na_3VO_4 (2 µl/ml) for 5 minutes at 90°C. Lysates were stored at -20°C or used immediately. Protein concentrations of all samples were determined using the BCA Protein Assay (Pierce™, 23227) and a Mithras Plate Reader (Berthold Technologies).

2.4.2 Nuclear-cytoplasmic extraction

Nuclear and cytoplasmic fractionation was carried out using the NE-PER Nuclear and Cytoplasmic Extraction Reagents kit (Thermo, 78833). Cytoplasmic and nuclear fractions were extracted using cytoplasmic/nuclear extraction reagents (CER I/CER II/NER) at a volume and ratio corresponding to the initial packed cell pellet in µl. Lysates were stored at -20°C or used immediately. Protein concentrations of all samples were determined using the BCA Protein Assay (Pierce™, 23227) and a Mithras Plate Reader (Berthold Technologies).

2.4.3 BCA assay

BCA assay was carried out using the BCA Protein Assay Kit (Pierce™, 23227). Briefly, samples were diluted 1 in 5 in their corresponding diluent and boiled at 90°C for 5 minutes. BCA standards were made up for a working range of 20-2,000 µg/mL. Working reagent (WR) was prepared in a 1:50 ratio (reagent A: reagent B). Samples/BCA standards and WR were mixed 1:8 in a 96-well plate which was incubated for 30 minutes at 37°C. The plate was left to cool to room temperate for subsequent absorbance analysis using a Mithras Plate Reader (Berthold Technologies).

2.4.4 SDS-PAGE/western blotting

Western blots were carried out under denaturing conditions with SDS-PAGE and proteins were wet-transferred to nitrocellulose membranes. Membranes were blocked with either 5% BSA or 5% milk (for phospho-antibodies) for 1 hour at room temperature. Membranes were incubated at 4°C overnight with primary

antibodies against ZIPK at 1:1000 (Bethyl; A304-221A-1), ZIPK-T265-P at 1:500 (Abcam; ab63395 and ThermoFisher; PA5-40234) STAT3 at 1:1000 (Santa Cruz Biotech; C-20: sc-482), STAT3-S727-P at 1:1000 (Abcam; ab30647), STAT3-Y705-P at 1:1000 (CST; #9131) p65 at 1:1000 (Santa Cruz Biotech; C-20: sc-482), H3T6-P at 1:500 (Diagenode; C15410282), H3T11-P at 1:500 (Abcam; ab5168), EGR1 at 1:1000 (CST; #4153), RNA pol II S2-P at 1:1000 (Abcam; ab5095), Vinculin at 1:10,000 (CST; #4650), HDAC2 at 1:5000 (Santa Cruz Biotech; C-19: sc-6296) and B-actin at 1:2000 (ThermoFisher; PA1-183). HRP-conjugated secondary antibodies against rabbit (Jackson-ImmunoResearch; 111-035-003) and mouse (Jackson-ImmunoResearch; 315-035-003) were used at 1:10,000 in 5% milk. Membranes were analysed using ECL (ThermoFisher; Pierce™) and a ChemiDoc system. Bands were quantified with Image LabTM software as indicated.

2.5 Co-immunoprecipitation (Co-IP)

2.5.1 Co-IP lysis

For co-immunoprecipitation (co-IP), cells were lysed with cold immunoprecipitation buffer (IP buffer) (150 mM NaCl, 10 mM Tris-HCl pH 7.4, 1 mM EDTA, 1 mM EGTA, 1% Triton X-100 and 0.5% NP-40) complete with 1x protease inhibitor cocktail (NEB; 5871S) for 30 minutes at 4°C maintaining agitation. Lysates were centrifuged and supernatants stored at - 80°C for co-IP. Protein concentrations of all samples were determined using the BCA Protein Assay (Pierce™) and a Mithras Plate Reader (Berthold Technologies).

2.5.2 Co-IP

Cell lysates were adjusted to 1mg/ml with IP buffer. Lysates were pre-cleared with Protein G Dynabeads™ (Invitrogen, 1004D) for 1 hour or overnight at 4°C while maintaining agitation. Supernatants were incubated with 1-5 µg of anti-ZIPK (Bethyl Laboratories; A304-222A-1), ZIPK-T265-P (ThermoFisher; PA5-40234), STAT3 (Santa Cruz Biotech; C-20: sc-482 and CST; #9139), STAT3-S727-P (CST; #9134), p65 (Santa Cruz Biotech; C-20: sc-372 and CST; #8242), histone H3 (Abcam; ab1791), RNA polymerase II (Abcam; ab817), RNA polymerase II S2-P (Abcam; ab5095) and HRP-conjugated anti-Rat IgG (e-Bioscience/Thermo; 18- 4818-12) for 1 hour at 4°C maintaining agitation. The antibody-lysate immune complexes were captured with 12.5 µl Protein G Dynabeads™ per 100 µg lysate by maintaining agitation for 1 hour at 4°C. Immobilised complexes were washed

up to 5 times with IP buffer and eluted in 4x SDS-PAGE loading buffer (200 mM Tris-HCl pH 6.8, 400 mM DTT, 8% SDS, 0.4% bromophenol blue and 40% glycerol) at 70°C for 5 minutes. Samples were stored at -20°C or electrophoresed on SDS-polyacrylamide gels (PAGE) and detected with primary antibodies by western blot (see methods 2.4.4).

2.6 RNA analysis

2.6.1 Preparation of total RNA

Total RNA was prepared from 10^5-$5x10^6$ cells. Cell pellets were washed with cold PBS and then resuspended in TRIzol® reagent (Invitrogen) at a volume according to the manufacturer's recommendations. RNA was prepared using the Direct-zol™ RNA MiniPrep kit (Zymo Research) including a DNase I treatment. RNA was eluted in DNase/RNase-free water and concentration was determined using the NanoDrop™ spectrophotometer. RNA was subsequently stored at -80°C.

2.6.2 cDNA synthesis

cDNA was synthesised from 1 µg of RNA diluted in nuclease free water with Random Primers (Invitrogen) or Oligo(dT) (Invitrogen). Samples were incubated at 70°C for 5 minutes and then placed on ice for the addition of PCR master-mix: 4 µl 5x FS buffer (Invitrogen), 1µl MLV-reverse transcriptase (Invitrogen), 0.5 µl RNase-Out (Invitrogen) and 0.5 µl dNTPs (Invitrogen) per reaction. The cDNA synthesis was carried out at 37°C for 1 hr, followed by a 5 min denaturation at 95°C. cDNA was subsequently diluted 1:5 in 1x TE and stored at -20°C.

2.6.3 RT-PCR and qPCR

For qPCR, cDNA was diluted 1:10 in nuclease free water. 5 µl reactions were carried out in triplicate in clear 384-well plates. using Luna® Universal qPCR Master Mix (NEB) on a QuantStudio 7 Flex Real-Time PCR System (ThermoFisher) under the following conditions:

Table 3: qPCR conditions

Temperature (ºC)	Time	Cycles
50	2 min	x 1
95	10 min	x 1
95	15 sec	x 40
60	1 min	

Melting curve analysis for each primer set was carried out to ensure the specificity of the amplification. Primers were deemed acceptable when the melting curve had only one peak with high amplitude (for primer sequences see Table 2).

For RT-PCR, cDNA was diluted to a final concentration of 50 ng. The reactions were assembled on ice with 1x standard *taq* reaction buffer (- Mg) (NEB), 1.5 mM $MgCl_2$ (NEB), 200 µM dNTPs (NEB), *taq* DNA polymerase at 1.25 units per 50 µl PCR reaction and 0.2 µM forward and reverse primers, then made up to 25 µl with nuclease-free water. RT-PCR reactions were carried out using a thermal cycler (BioRad) under the following conditions:

Table 4: RT-PCR conditions

Step	Temperature (ºC)	Time	Cycles
Denaturation	95	30 sec	x 1
Cycling	95	20 sec	18-25 depending on linear amplification range
	50-54	30 sec	
	68	2-3 min	
Final extension	68	5 min	x 1
Hold	4	Indefinite	Indefinite

RT-PCR products were run on 1.5% agarose gels for 30-40 minutes at 100 V and visualised with a ChemiDoc system (for primer sequences see Table 2).

2.6.4 qPCR analysis

Relative expression was calculated as a ratio of specific transcript to one/several housekeeping genes using following formula: $2^{-\Delta Ct}$, where ∆Ct equals:

$$\Delta Ct = Ct\ (gene\ of\ interest) - Ct\ (housekeeping\ gene)$$

Equation 2: ∆Ct formula for qPCR quantification.

This equation utilised the following housekeeping genes: TATA-Box Binding Protein (TPB), protein phosphatase 6 catalytic subunit (PPP6C) or glyceraldehyde 3-phosphate dehydrogenase (GAPDH), as indicated.

2.6.5 qPCR analysis – alternative splicing fold change

To assess the impact of ZIPK inhibition on alternative splicing we used calculations described in Harvey and Cheng (2016) [244]. To calculate the fold change in alternative splicing, the quantity of each splice isoform was first determined using the $2^{-\Delta Ct}$ formula, where ∆Ct equals:

$$\Delta Ct = Ct\ (splice\ isoform) - Ct\ (housekeeping\ gene)$$

Equation 3: ∆Ct formula for quantification of splice isoforms.

The relative levels of different splice isoforms of the same gene were expressed as a ratio of one splice isoform to another using the following formula: $2^{-\Delta Ct}$, where ∆Ct equals:

$$\Delta Ct = (Ct\ inclusion\ splice\ isoform\ mRNA - Ct\ exclusion\ splice\ isoform\ mRNA\ in\ the\ same\ sample)$$

Equation 4: formula for quantifying the relative levels of different splice isoforms in relation to one another.

Then, relative comparison of this ratio between different experimental samples was accomplished via the formula:

$$\frac{2^{-\Delta Ct(\text{experiment})}}{2^{-\Delta Ct(\text{control})}}$$

Equation 5: formula for comparing the ratio of splice isoforms between samples and control.

where ∆Ct(experiment) equals:

$$(Ct\ inclusion\ splice\ isoform\ mRNA\ in\ experimental\ sample - Ct\ exclusion\ splice\ isoform\ mRNA\ in\ experimental\ sample)$$

and ∆Ct(control) equals:

$$(Ct\ inclusion\ splice\ isoform\ mRNA\ in\ control\ sample - Ct\ exclusion\ splice\ isoform\ mRNA\ in\ control\ sample)$$

The calculation is identical when assessing exon inclusion versus intron retention alternatively spliced *DUSP2* transcripts by replacing 'Ct exclusion splice isoform' with 'Ct intron retained splice isoform' in all equations. With this methodology, the relative levels of splice isoforms can be expressed as a ratio of one splice isoform to another e.g. an exon inclusion vs. exon exclusion or intron retention ratio. By giving the control sample a baseline value of 1, this ratio can then be compared between different experimental samples.

2.7 Chromatin analysis

2.7.1 Chromatin preparation

ChIP was performed as follows: 10^7 cells were crosslinked with 1.5% formaldehyde for 8 minutes at room temperature. Cells were harvested by centrifugation at 400 x *g* for 4 minutes at 4°C and washed twice with ice cold PBS supplemented with 1x protease inhibitor cocktail (NEB; 5871S). Pellets were resuspended in 10 ml of buffer A (10 mM HEPES (pH 8), 10 mM EDTA (pH 8.0), 0.5 mM EGTA (pH 8.0), and 0.25% Triton X-100) and incubated at 4°C for 10 min with gentle agitation. After centrifugation at 500 x *g* at 4°C for 5 min, cells were resuspended into 40 ml of buffer B (10 mM HEPES (pH 8), 200 mM NaC1, 1 mM EDTA (pH 8.0), 0.5 mM EGTA (pH 8.0), and 0.01% Triton X-100) and incubated

10 min, and centrifuged as before. Nuclei were sonicated in immunoprecipitation buffer (25 mM Tris-HCl (pH 8), 2 mM EDTA, 150 mM NaC1, 1% Triton X-100, 0.1% sodium dodecyl sulphate and 1x protease inhibitor cocktail). Nuclei were sonicated for 15 (RNA polymerase ChIP) or 20 (histone H3 and transcription factor ChIP) cycles (30 seconds on/30 seconds off) using a Bioruptor® Pico sonication device (Diagenode). After centrifugation at 14,000 x *g* for 10 min at 4°C, chromatin preparations were stored at −80°C. 12 µl of chromatin was taken and stored as input for qPCR normalisation.

2.7.2 Chromatin sonication optimisation

The optimal shearing was determined for each cell line individually. 10^7 cells were crosslinked with 1.5% formaldehyde for 8 minutes at room temperature and prepared for sonication as described above. Nuclei were sonicated for 10-25 cycles with 2 cycle gaps (e.g. 16, 18, 20, 22). Sonication products were run on 1.5% agarose gels for 40 minutes at 100 V and visualised with a ChemiDoc system. Optimised sonication was determined as having chromatin fragments in the range of 100 - 600 bp with 1000 bp as the upper limit.

2.7.3 Chromatin immunoprecipitation (ChIP)

Sonicated chromatin from 10^7 cells was used for each immunoprecipitation. The volume was adjusted to give 100 µl per IP with fresh immunoprecipitation buffer. Immunoprecipitation was achieved using Dynabeads™ Protein G (ThermoFisher) with 2.4 µg of anti-histone H3T11-P (Abcam; ab5168), anti-histone H3T6-P (Diagenode; C15410282), anti-STAT3 (Santa Cruz Biotech; C-20: sc-482 and CST; #9139), anti STAT3-S727-P (CST; #9134), anti-p65 (Santa Cruz Biotech; C-20: sc-372 and CST; #8242), anti-ZIPK (Bethyl Laboratories; A304-222A-1), anti-ZIPK-T265-P (ThermoFisher; PA5-40234) anti-RNA polymerase II (Abcam; ab817) or anti-RNA polymerase II S2-P (Abcam; ab5095) per 10 µl of beads. Beads were washed twice with ice cold immunoprecipitation buffer prior to use. Beads and antibodies were incubated for 2 hours at 4°C with gentle agitation. After 2 hours the bead-antibody mixture was pelleted using a magnet and the beads were washed once with ice cold immunoprecipitation buffer. 100 µl of sonicated chromatin was added to achieve a bead to chromatin ratio of 1:10. Chromatin was incubated for 2 hours at 4°C with gentle agitation. After 2 hours, beads were pelleted using a magnet and washed once with washing buffer A (20 mM Tris-HCl (pH 8), 2 mM EDTA, 1% Triton X-100, 0.1% sodium dodecyl sulphate and 150 mM NaCl supplemented with 1x protease

inhibitor cocktail), once with washing buffer B (20 mM Tris-HCl (pH 8), 2 mM EDTA, 1% Triton X-100, 0.1% sodium dodecyl sulphate and 500 mM NaCl supplemented with 1x protease inhibitor cocktail), once with LiCl buffer (0.25 M LiC1, 0.5% NP-40, 0.5% sodium deoxycholate, 1 mM EDTA, and 10 mM Tris-HCl (pH 8) supplemented with 1x protease inhibitor cocktail), and twice with TE buffer (10 mM Tris-HCl (pH 8.0) and 1 mM EDTA). The immune complexes were eluted by adding 50 µl of elution buffer (1% sodium dodecyl sulphate, 100 mM $NaHCO_3$, 200). The cross-link was reversed at 65°C overnight. Inputs were treated with RNAse A for 30 minutes at 36°C and reverse-crosslinked at 65°C overnight with proteinase K.

2.7.4 DNA purification/clean-up for ChIP-qPCR

Reverse cross-linked DNA was purified using AxyPrep™ MAG PCR clean-up kit (Appleton Woods Ltd) according to manufacturer's instructions. qPCR reactions were carried out using Luna® Universal qPCR Master Mix (NEB) on a QuantStudio 7 Flex Real-Time PCR System (ThermoFisher) (for primer sequences see Table 2). For ChIP-qPCR, cDNA was diluted 1:5 in nuclease free water while inputs were diluted 1:50. Standard curves were prepared with input cDNA in a 1:5 dilution series. 5 µl reactions were carried out in duplicate in clear 384-well plates. using Luna® Universal qPCR Master Mix (NEB) on a QuantStudio 7 Flex Real-Time PCR System (ThermoFisher) under the same conditions described in methods 2.6.3.

2.7.5 ChIP-qPCR analysis

ChIP-qPCR data were analysed as follows. First, the average of duplicate Ct values was calculated relative to the intercept and the slope of the standard curve generated for each primer pair representing a genomic region with the following calculation, where *E* is a numeric constant relating to exponential growth and decay:

$$E = \frac{Ct\ target - standard\ curve\ intercept}{standard\ curve\ slope}$$

Next, the values for *E* are compared for each target and control (input):

$$relative\ amount\ of\ DNA = \frac{E_{target}}{E_{control}}$$

Equation 6: formula for quantifying relative amount of ChIP DNA detected by ChIP-qPCR analysis.

Data were then normalised to input and expressed relative to invariant genomic regions CTCF1 and CTCF3 Note: Histone H3T6-P and H3T11-P ChIP was exclusively normalised to histone H3.

Chapter 3 Results 1: ZIPK catalyses histone H3 threonine phosphorylation and regulates lymphoid cell IEG expression

In a previous study, the Lefevre group determined that crosslinking and activation of the BCR induces the expression of IEGs together with phosphorylation of histone H3 at threonine 6 and threonine 11 (see Figure 1.7 – Figure 1.9) (Thomas et al., forthcoming 2020). These IEGs included genes known to promote CLL cell proliferation and survival – making an interesting link between H3T6-P and H3T11-P and IEG expression. Therefore, the group initially sought to identify the kinase mediating this phosphorylation through *in silico* kinase predication software (Figure 1.8). Each candidate kinase provided by the software was tested with a specific kinase inhibitor by looking for changes in IEG expression and a loss of H3T6 and T11 phosphorylation (Thomas et al., forthcoming 2020). ZIPK was the only kinase whose inhibition resulted in both a loss of IEG expression and histone phosphorylation – but it was not clear if this effect was a direct result of the kinase inhibition or an indirect one.

ZIPK is a serine-threonine kinase which mediates a variety of cellular functions. These include both apoptotic and autophagic cell death [225, 229] and the regulation of smooth muscle contraction [222]. Upon its initial discovery ZIPK was reported to interact with chromatin [229]. ZIPK has been observed to phosphorylate H3T11 during mitosis to promote chromosome condensation [230], and PRK1-mediated H3T11-P has been shown to activate AR-dependent gene transcription [220]. However, there is no current literature linking ZIPK and both H3T11 and H3T6 phosphorylation during transcription.

From a therapeutic view, there is an interest to studying ZIPK alongside ibrutinib owing to observed similarities in the reduction of these histone marks in response to ibrutinib treatment (Figure 1.7C-D). As ibrutinib is well known to be a successful CLL therapeutic, we hypothesised that whichever kinase was mediating H3T6 and H3T11 phosphorylation could play a key role in the transcription of genes known to be involved in CLL pathogenesis.

In summary, based on the results from the kinase prediction software and experiments in the Lefevre lab (Figure 1.8A), we initially wanted to question whether ZIPK could directly phosphorylate both H3T11-P and H3T6-P *in vitro.*

Should this be the case and in light of our preliminary observations comparing the ZIPK inhibitor to ibrutinib, we hypothesised that we may see similar ZIPK function in CLL cells, and that further study of ZIPK could be important in the context of CLL therapy.

3.1 ZIPK directly phosphorylates H3T6 and H3T11 in vitro

Preliminary data from the Lefevre group showed that ZIPK inhibition could reduce phosphorylation of histone H3T6 and H3T11. In order to determine whether this was a direct or indirect effect we initially wanted to assess the ability of ZIPK to directly phosphorylate histone H3T6 and H3T11 by *in vitro* kinase assay.

We incubated recombinant histone H3 and ZIPK proteins with ATP and examined the reaction over time (0-60 minutes) by dot blot, probing with antibodies against H3T6-P and H3T11-P (Figure 3.1B-C). ZIPK could phosphorylate both histone marks, showing rapid phosphorylation of H3T6 after just 5 minutes with a gradual increase over time from 5-60 minutes. The catalysis of H3T11 phosphorylation by ZIPK displayed slower kinetics, with minimal H3T11-P detectable by dot blot after 5 minutes. However, by 60 minutes the absolute level of H3T11-P was comparable to H3T6-P.

We also wanted to assess the ability of ZIPK to phosphorylate H3T6 and H3T11 in the presence of the same death associated protein kinase inhibitor (DAPKi) used in the preliminary experiments (Figure 3.1A) – with the expectation that by inhibiting ZIPK kinase activity we could impede its ability to phosphorylate histones. The DAPKi is noted to be an ATP-competitive and highly selective inhibitor of DAPK1 and DAPK3. We added the DAPKi to our kinase assay reactions alongside ibrutinib (Figure 3.1B-C). In this experiment, using recombinant proteins, we expected ibrutinib to have little impact on ZIPK kinase activity. The DAPKi reduces ZIPKs ability to phosphorylate H3T6 and H3T11, with the most significant reduction at 60 minutes in both cases. The effect is most profound with regard to H3T11-P. Ibrutinib has a small but non-significant ($P > 0.05$) effect in all cases apart from H3T11-P at 60 minutes. This may be due to a combination of experimental variability and unexpected impacts arising from the addition of ibrutinib to the reaction e.g. stoichiometric explanations such as ibrutinib physically blocking the protein-protein interactions required for ZIPK-mediated histone phosphorylation.

3.1.1 ZIPK inhibition reduces the levels of active ZIPK T265-P in CLL cells

A series of *in vitro* kinase assays have shown that ZIPK can directly phosphorylate histone H3 at T6 and T11 in a manner preventable by a DAPKi. In order to validate the results observed in Figure 3.1, and future experiments, we

needed to confirm that the ZIPK inhibitor was efficiently repressing ZIPK activity. Further, this is necessary to confirm that the loss of histone threonine phosphorylation observed with DAPKi treatment in Figure 3.1 is due to loss of ZIPK function as opposed to any off-target or alternative effects of the drug.

To assess the efficacy of the inhibitor, CLL cells were treated with increasing doses of DAPKi (0-80 μM) for 60 minutes. The cells were then lysed for western blot analysis with antibodies against total ZIPK and ZIPK T265-P, an autophosphorylation site indicative of active ZIPK [223] (see 1.5.3 on ZIPK function). The protein levels of ZIPK T265-P began to decrease between inhibitor doses of 20 and 40 μM, with very low levels remaining at 80 μM. We recognise the high concentrations of DAPKi required to inhibit ZIPK phosphorylation and activity, especially when compared with the highly potent, small molecule inhibitor, ibrutinib, which has sub-nanomolar activity against BTK (IC50, 0.5 nM) [245]. We partly attribute this to the relatively under-developed nature of the DAPKi which may lack stability (this is discussed further in discussion section 6.2.1). Therefore, off-target effects cannot be completely ruled out at the tested DAPKi concentrations. For the DAPKi, ERK2 has an IC50 > 10 μM, and it may represent the most relevant alternative target [94]. In our preliminary work we have previously assessed the consequences of treating CLL cells with a MEK inhibitor to directly inhibit ERK. In this experiment we observed no effect on *EGR1* and *DUSP2* expression as well as on H3T6 and H3T11 phosphorylation after directly targeting MEK (Figure 1.8), suggesting that ERK might not mediate DAPKi effect. Total ZIPK remains unchanged throughout the experiment, highlighting the specificity of the inhibitor for reducing the levels of active ZIPK and thereby decreasing its kinase activity as seen in Figure 3.1.

A

Table 3. Kinase Selectivity of Compound **6** As Determined in Broad Protein Kinase Panel Screening

no inhibition at 10 μM			
ABL	Erk1	MARK1	PKCζ
AKT1	FLT3	MAPKAPK2	PKD2
AKT2	FYN	MET	PKGα
AMPK	GSK3β	MSK1	PRAK
AurA	HGK	MST2	ROCK2
BTK	IGF1R	p38α	RSK1
CAMK2	INSR	PAK2	SRC
CAMK4	IRAK4	PIM2	SYK
CDK2	LCK	PKA	c-TAK1
CHK1	LYN	PKCβ2	c-Raf
CHK2			
IC_{50} > 10 μM		1 μM < IC_{50} < 10 μM	IC_{50} < 1 μM
CK1δ	FGFR1	p70S6K	DAPK1
DYRK1α	KDR		DAPK3
Erk2	SGK1		

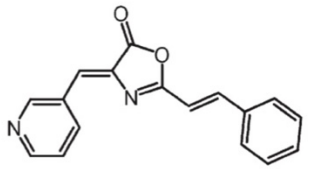

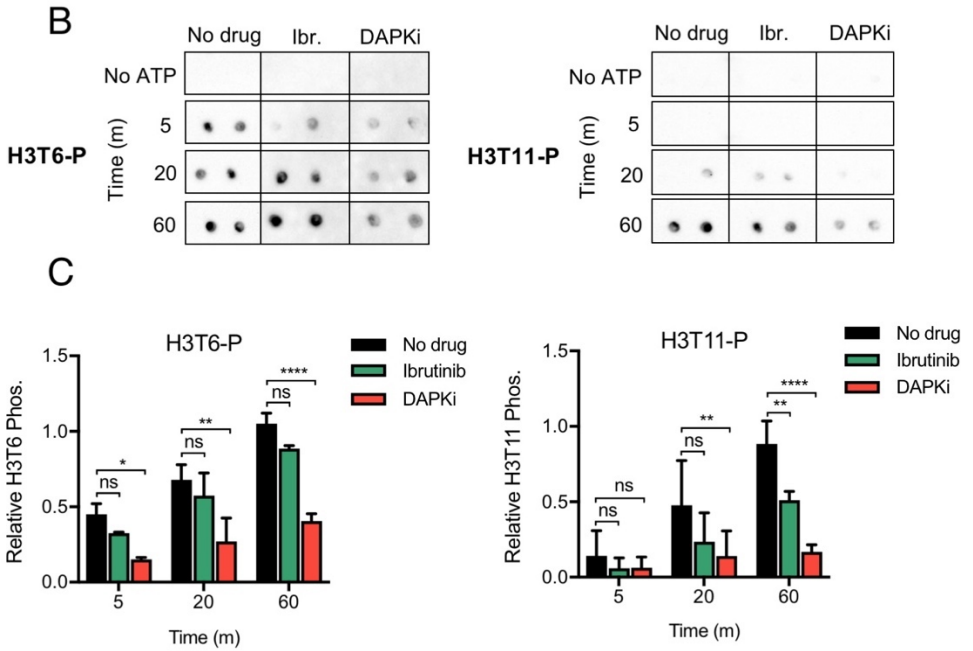

Figure 3.1: ZIPK phosphorylates H3T6 and H3T11 *in vitro*. (A) DAPKi structure and kinase selectivity: (Okamoto et al. 2009 J. Med. Chem.) DAPKi binds to active site of protein. DAPK1 IC50 = 69nM while DAPK3 (ZIPK) IC50 = 225nM indicating moderate specificity. DAPK1 is silenced in CLL. **(B)** Kinase assay quantified by dot-blot with recombinant histone H3 and recombinant ZIPK to measure ZIPK kinase activity over time (5-60 minutes) with or without (negative control) ATP and in the presence of ibrutinib and DAPK inhibitor. **(C)** Kinase assay displaying histone H3 phosphorylation quantified relative to untreated assay with error bars representative of 3 independent experiments. Significant differences calculated using two-way ANOVA followed by Dunnett's multiple comparison test with the untreated sample as control for each time point. H3T6-P P values = 0.3075 & 0.0139 (5 m), 0.4157 & 0.0021 (20 m), 0.1583 & 0.0001 (60 m) for untreated vs. Ibr and DAPKi respectively. H3T11-P P values = 0.6679 & 0.6844 (5 m), 0.0672 & 0.0095 (20 m), 0.0043 0.0001 (60 m) for the same comparisons.

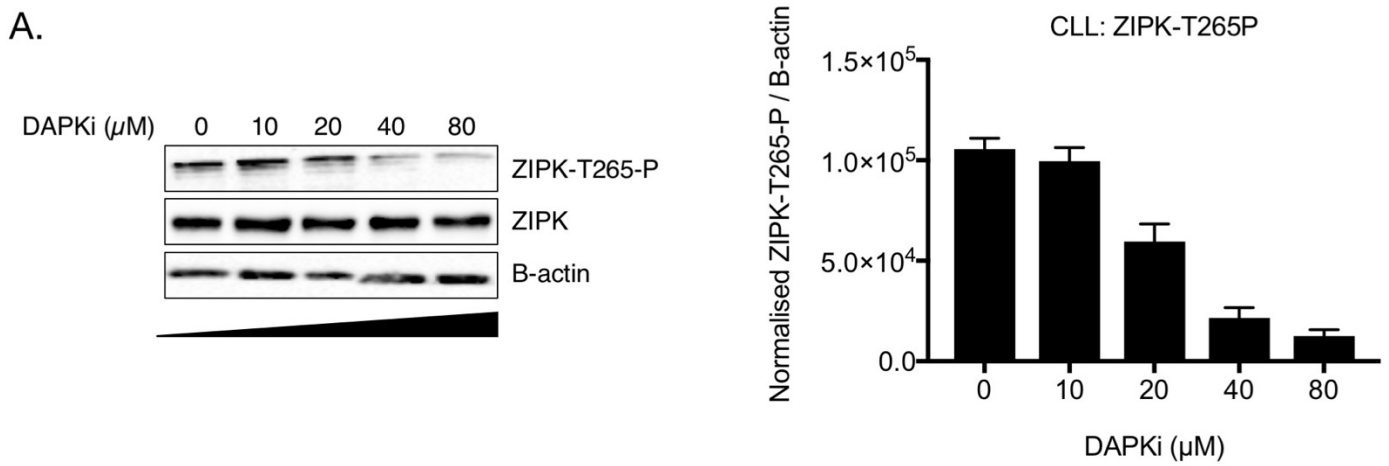

Figure 3.2: DAPKi reduces levels of active ZIPK in CLL cells. (A) western blot displaying levels of phosphorylated/active ZIPK-T265P in untreated CLL cells vs. CLL cells treated with 10-80 μM DAPKi. Cells were pre-treated with DAPKi for 60 mins before anti-IgM stimulation of the BCR for a further 60 mins. Western blot is representative of 2 individual experiments in CLL cells and numerous other experiments in lymphoid cell lines. β-actin was used as a loading control and for normalisation with Image Lab software (right).

3.2 The role of ZIPK in BCR-mediated immediate early gene expression in CLL cells

The importance of cell signalling pathways in cancer cell proliferation and survival is well established and this is no less true in chronic lymphocytic leukaemia (CLL). CLL cells in the microenvironment are influenced by a multitude of signals which work together to activate pro-survival and pro-proliferative gene programmes [93, 94, 96].

The B cell receptor (BCR) pathway is critical for the development of mature, healthy B lymphocytes so it is not surprising that CLL cells may co-opt the pathway for their own malignant development [114]. CLL cells which react to antigen/auto-antigen crosslink the BCR on their cell surface and rapidly upregulate immediate early genes (IEGs). IEGs are genes which are rapidly and transiently upregulated in response to a variety of external stimuli [173]. The proteins for which IEGs code include cytoplasmic enzymes and transcription factors of which many are known to be oncogenic through their regulation of differentiation and proliferation. It is for this reason that understanding IEG expression, function and regulation is of interest in haematological malignancies where they are known to be overexpressed or dysregulated in some way.

Early growth response factor 1 (EGR1) [178, 180], a key regulator of transcription, and dual specificity phosphatase 2 (DUSP2) [187], an important signal transduction enzyme and regulator of the MAPK pathway, are classical IEGs known to be upregulated in CLL and a variety of other haematological malignancies. Previous data from the Lefevre group has implicated ZIPK as a potential regulator of these two genes (Thomas et al., forthcoming 2020 and Figure 1.7 – Figure 1.9). To this end, we first aimed to assess the levels of both *EGR1* and *DUSP2* in a cohort of CLL patients by subjecting primary patient cells to gene expression analysis following activation of the BCR pathway.

3.2.1 Immediate early gene response is dictated by IgHV status in CLL cells

Before we could accurately assess CLL IEG expression in response to BCR signalling, we needed to understand the inherent characteristics of a CLL cell which can play a role in gene expression. One such factor is a CLL cells immunoglobulin heavy chain variable region (IgHV) status. CLL patients are

typically categorised into subtypes depending on the mutational status of the BCR present on the surface of CLL cells, which can either be mutated or unmutated. This refers to the stage in B cell development from which the CLL clone might have originated. In general, U-CLL cells arise from pre-germinal centre B cells and M-CLL cells result from the transformation of mature, antibody producing memory B cells which have undergone a germinal centre reaction (see 1.1.3 on the germinal centre reaction).

To clarify the effect of this trait on gene expression we sought to compare the response of primary, patient U-CLL and M-CLL cells to activation of the BCR pathway. Of our 10 patient cohort, 4 patients were classified as M-CLL (P1, P6, P8 and P9) while the remaining 6 were U-CLL (P2-P5, P7 and P10) and all patients had not previously been treated for their disease. These CLL cells were stimulated with anti-IgM for 30 (6 U-CLL and 4 M-CLL patients) or 60 minutes (4 U-CLL and 3 M-CLL patients) before lysis for RNA extraction. *EGR1* and *DUSP2* gene expression was subsequently analysed by qPCR.

The U-CLL patients showed a varied but pronounced IEG response to anti-IgM stimulation which is highly significant by 60 minutes ($P \leq 0.01$), highlighting the rapid nature in which *EGR1* and *DUSP2* are upregulated in response to external stimuli and BCR pathway activation (Figure 3.3A-B). These data are in line with our preliminary data for *EGR1* and *DUSP2* anti-IgM response kinetics (Figure 1.7). The M-CLL patients presented with two differing phenotypes displaying either (i) very low expression overall (P1 and P8) or (ii) chronic, mid-to-low range expression (P6 and P9) (Figure 3.3C-D). In both cases however, neither responded to anti-IgM stimulation or showed an increase in IEG expression.

In an attempt to elicit a gene expression response in M-CLL cells, we stimulated both U and M-CLL patient cells (for direct comparison) with both anti-IgM and anti-IgD (Figure 3.4A-B). Anti-IgD was chosen as some M-CLL cells may have undergone class switch recombination during the germinal centre reaction and therefore express IgD B cell receptors on their cell surface, potentially explaining their limited response to anti-IgM stimulation. In all cases, we were unable to replicate the robust response seen in U-CLL patient cells stimulated with anti-IgM. However, anti-IgD was able to activate M-CLL cells by a small but significant amount at 30 minutes post stimulation for both *EGR1* and *DUSP2* while anti-IgM stimulation remained non-significant at both time points (Figure 3.4A). In the U-CLL patients we observed the classical anti-IgM response of strong activation at

both time points. Anti-IgD was unable to elicit a significant gene expression response for *DUSP2* in the U-CLL patients and we observed a small but significant impact on *EGR1* expression at 30 minutes which was no longer significant by 60 minutes (Figure 3.4B).

Anti-IgD was generally less effective than anti-IgM for both genes at all timepoints with some exceptions: notably, we observed an increase in *EGR1* and *DUSP2* gene expression in M-CLL at 30 minutes only, suggesting IgD may be able to promote weak but rapid expression in this cell type.

3.2.2 ZIPK inhibition mimics BTK inhibition in preventing CLL immediate early gene expression

We have observed a mixed IEG response to anti-IgM stimulation dependent on the CLL subtype whereby U-CLL cells generally responded well to BCR crosslinking and upregulated *EGR1* and *DUSP2* gene expression (Figure 3.3 & Figure 3.4). We have also observed a loss of ZIPK kinase activity in the presence of the DAPKi (Figure 3.1 & Figure 3.2). With these data in mind, we wanted to address the effect of both ibrutinib and the DAPKi in preventing IEG expression in CLL cells. Firstly, in assessing U-CLL response alone we aimed to achieve a clearer picture of the effect of both inhibitors in the context of cells which can activate BCR signalling. Additionally, by examining the M-CLL response we can compare the effects of the inhibitors in the context of cells which may not strongly activate their BCR, or present with chronic activation.

The small molecule inhibitor, ibrutinib, exploits the dependency of CLL cells on the BCR-signalling pathway by blocking BTK and shutting off the downstream signalling cascade [128]. It was anticipated that ibrutinib would prevent the expression of both *EGR1* and *DUSP2* – as we have concluded both genes are downstream of the BCR. We believe ZIPK is also downstream of the BCR, owing to previously identified similarities observed when treating CLL cells with ibrutinib and the DAPKi, and blocking ZIPK kinase activity should have a similar effect to ibrutinib. We therefore wanted to assess the effects of ibrutinib and the DAPKi in both CLL subtypes.

The patient data is presented at each time point post stimulation with 7 patients, P4-10, with data for both 30 and 60-minute timepoints while 3 patients, P1-3, have data only for 30 minutes. In the U-CLL patients, we observed a significant

increase in *EGR1* and *DUSP2* (Figure 3.5A-B) gene expression at both 30 and 60 minutes, where both genes showed higher expression at 60 minutes – highlighting the rapid nature in which these genes are upregulated in response to stimuli. The significance of the data at 30 minutes was affected by patient 4 (green circle), who displayed slow kinetics in response to anti-IgM stimulation, presenting with an M-CLL like response initially but showed an 8-fold increase in gene expression by 60 minutes for both genes. Where the U-CLL cells had been pre-treated with either ibrutinib or the DAPKi, we observed a significant decrease in the expression of both genes (Figure 3.5A-B). The effect of both drugs was comparable in all cases, with *EGR1* and *DUSP2* gene expression reduced to a level comparable with that observed in the unstimulated control CLL cells, suggesting that ZIPK is either downstream of the BCR, or that both these proteins can indirectly regulate IEG expression.

For the M-CLL patients there were several observations: M-CLL patients presented with either very low baseline IEG expression, or mid-to-low chronic expression – neither of which are altered by stimulation (see Figure 3.3C-D). In these experiments (Figure 3.5C-D), the 2 patients with very low *EGR1* and *DUSP2* gene expression showed no effect when treated with either inhibitor – it is expected that adding inhibitors will have no effect on CLL cells which do not respond to anti-IgM stimulation. More interestingly, of the 2 patients with mid-to-low expression (P6 and P9), one (P6) shows a response to the inhibitors which is similar to the U-CLL patients, while the other patient (P9) is unaffected. Assuming *EGR1 and DUSP2* expression correlates with CLL cell proliferation, these observations broadly fit with the literature suggesting that BTK inhibitors are more effective in treating those patients with U-CLL, while M-CLL patients show a mixed response to treatment [118].

3.2.3 In accordance with gene expression data, ZIPK inhibition reduces IEG protein levels in CLL cells

We have observed a convincing decrease in IEG expression in CLL cells in response to ZIPK inhibition (see Figure 3.5). However, there are circumstances whereby the relative amount of mRNA in a cell as measured by qPCR does not correlate with the protein translated thereafter. Thus, we wanted to assess IEG protein levels to confirm if the complete loss of gene expression observed with ZIPK inhibition led to a corresponding downstream failure to transcribe the protein. U-CLL cells were pre-treated with increasing doses of the DAPKi (0-120

μM) for 60 minutes before stimulation with anti-IgM for 30 minutes. These cells were lysed for western blot and probed with antibody against EGR1.

The western blots correlated with the gene expression data in two ways. We first reinforced that anti-IgM stimulation of the BCR activated IEGs by showing an increase in EGR1 protein after just 60 minutes (Figure 3.6A-B). This increase in protein correlated with *EGR1* mRNA levels post anti-IgM stimulation. Second, at doses > 20 μM we observed a marked loss of EGR1 protein. These doses are relevant, as across all other experiments we employed a dose of 25 μM DAPKi. Between 20-120 μM the loss of EGR1 protein was dose dependent and statistically significant (Figure 3.6B). To further reinforce our observations that the loss of IEG expression is ZIPK-dependent we probed the same western blots with antibody against ZIPK-T265P. As expected, we observed a decrease in active ZIPK protein at doses > 20 μM (Figure 3.6A). We therefore demonstrated that the loss of EGR1 protein not only correlated with *EGR1* mRNA in both a dose and time dependent manner, but that it also is directly related to the levels of active ZIPK in a particular sample.

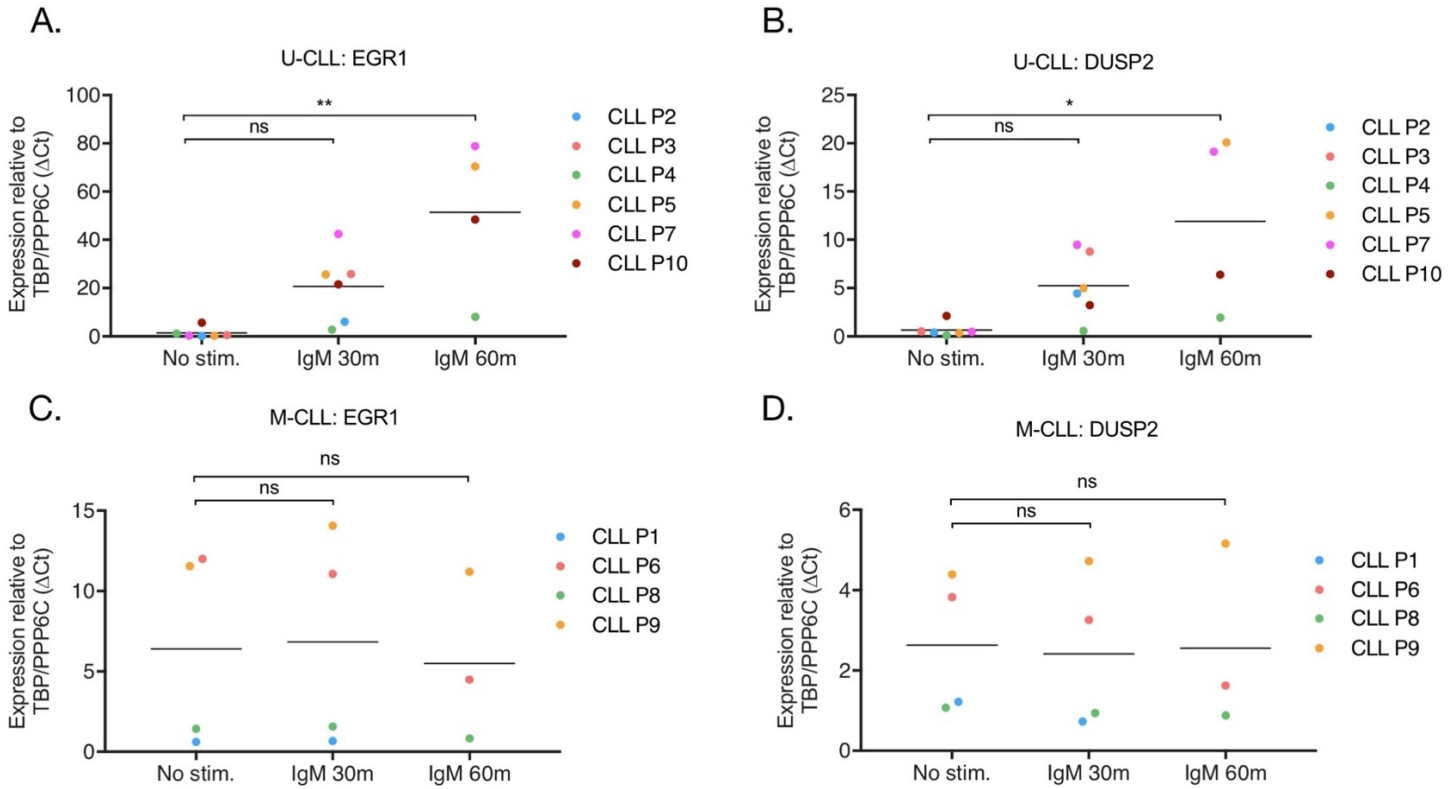

Figure 3.3: CLL IEG response is dictated by IgHV status of the CLL cells. qPCR data analysis of *EGR1* and *DUSP2* gene expression at 30 (n = 6 patients for U-CLL and n = 4 patients for M-CLL) and 60 minutes (n = 4 patients for U-CLL and n = 3 patients for M-CLL) post anti-IgM stimulation in **(A) (B)** U-CLL or **(C) (D)** M-CLL cells. Expression changes were quantified using the ΔCt method with TBP and PPP6C as control genes. Bars represent the grand mean of the samples. Significant differences calculated using two-way ANOVA followed by Dunnett's multiple comparison test with unstimulated as control. U-CLL (*EGR1*) P values = 0.1961 & 0.0095 for no stim vs 30 m and 60 m respectively. U-CLL (*DUSP2*) P values = 0.4818 & 0.0317 for the same comparisons. M-CLL P values not listed for clear insignificance.

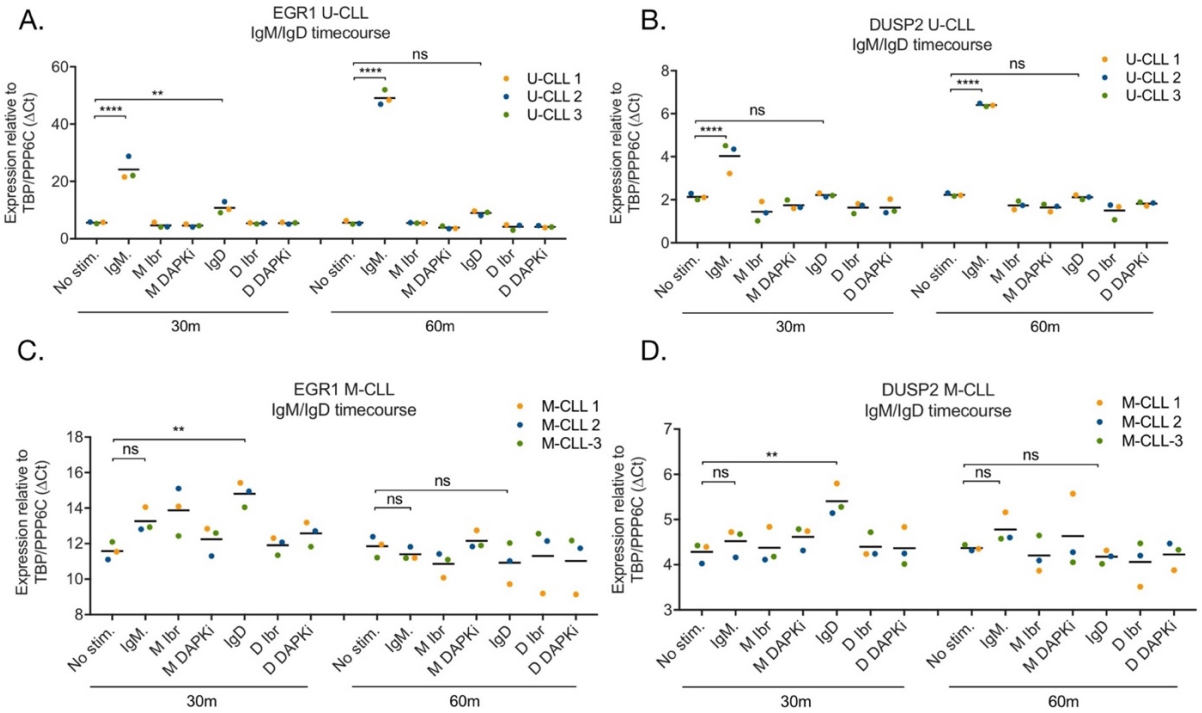

Figure 3.4: CLL IEG response is dictated by IgHV status of the CLL cells. qPCR data analysis of *EGR1* and *DUSP2* gene expression at 30 (n = 3 patients for U-CLL and M-CLL) and 60 minutes (n = 3 patients for U-CLL and M-CLL) post anti-IgM (M) or anti-IgD (D) stimulation in **(A) (B)** U-CLL or **(C) (D)** M-CLL cells. CLL cells were pre-treated with ibrutinib or DAPKi for 1 hour as indicated below the graphs. Expression changes were quantified using the ΔCt method with TBP and PPP6C as control genes. Bars represent the grand mean of the samples. Significant differences calculated using two-way ANOVA followed by Dunnett's multiple comparison test with unstimulated as control. U-CLL (*EGR1*, 30m) P values = 0.0001 & 0.0031 for no stim vs anti-IgM and anti-IgD respectively. U-CLL (*EGR1*, 60m) P values = 0.0001 & 0.0905 for the same comparisons. U-CLL (*DUSP2*, 30m) P values = 0.0001 & 0.9996 for no stim vs anti-IgM and anti-IgD respectively. U-CLL (*DUSP2*, 60m) P values = 0.0001 & 0.9999 for the same comparisons. M-CLL (*EGR1*, 30m) P values = 0.2942 & 0.0046 for no stim vs anti-IgM and anti-IgD respectively. M-CLL (*EGR1*, 60m) not significant. M-CLL (*DUSP2*, 30m) P values = 0.9902 & 0.0099 for no stim vs anti-IgM and anti-IgD respectively. M-CLL (*DUSP2*, 60m) not significant.

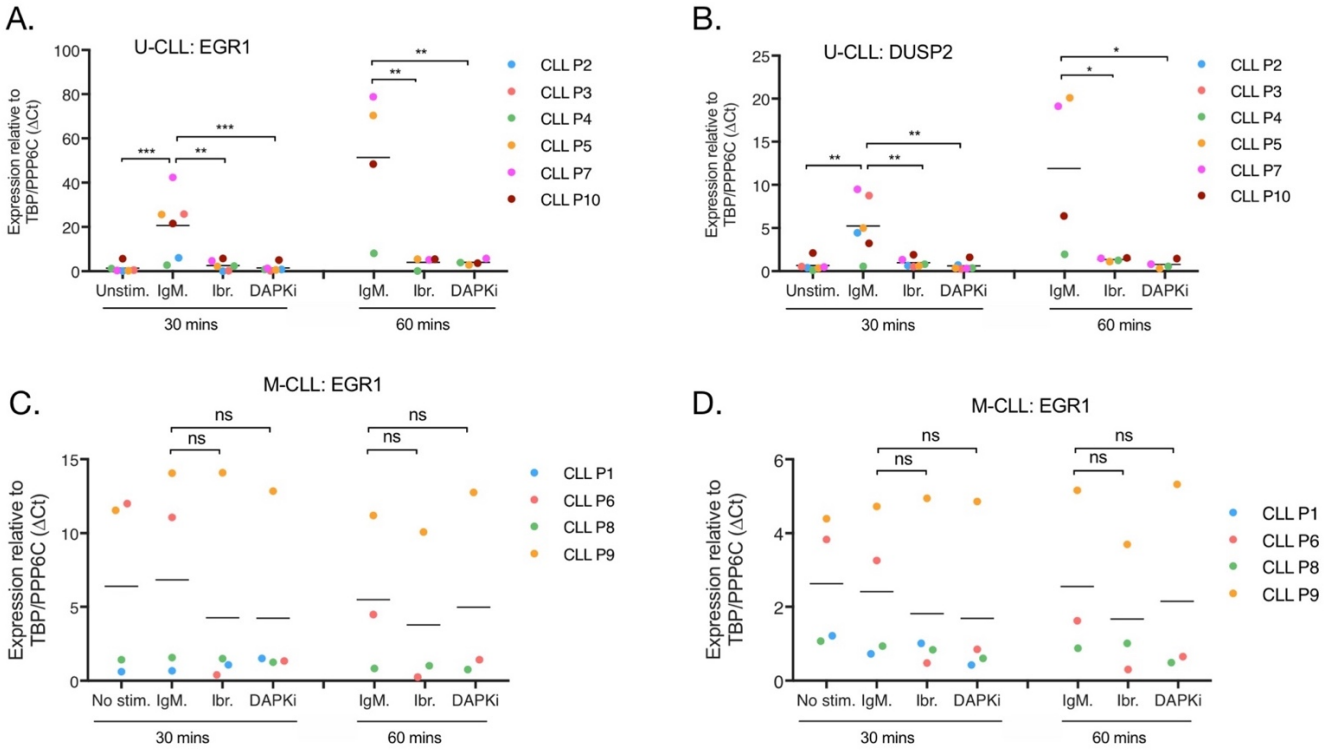

Figure 3.5: ZIPK inhibition mimics ibrutinib in inhibiting CLL IEG expression. qPCR data analysis of *EGR1* and *DUSP2* gene expression at 30 (n = 6 patients for U-CLL and n = 4 patients for M-CLL) and 60 minutes (n = 4 patients for U-CLL and n = 3 patients for M-CLL) post anti-IgM stimulation in **(A) (B)** U-CLL or **(C) (D)** M-CLL cells. CLL cells were pre-treated with ibrutinib or DAPKi for 1 hour as indicated below the graphs. Expression changes were quantified using the ΔCt method with TBP and PPP6C as control genes. Bars represent the grand mean of the samples. Significant differences calculated using two-way ANOVA followed by Dunnett's multiple comparison test with anti-IgM as control. Patient 4 excluded from statistical analysis for M-CLL like anti-IgM response despite U-CLL classification. *EGR1* (30 m) P values = 0.0009, 0.0015 & 0.0009 for anti-IgM vs Unstim, Ibr and DAPKi respectively. *DUSP2* (30 m) P values = 0.0013, 0.0023 & 0.0011 for the same comparisons. *EGR1* (60 m) P values = 0.0039, 0.0052 & 0.0052 for the same comparisons. *DUSP2* (60 m) P values = 0.0204, 0.0269 & 0.0205 for the same comparisons. M-CLL P values not listed for clear insignificance.

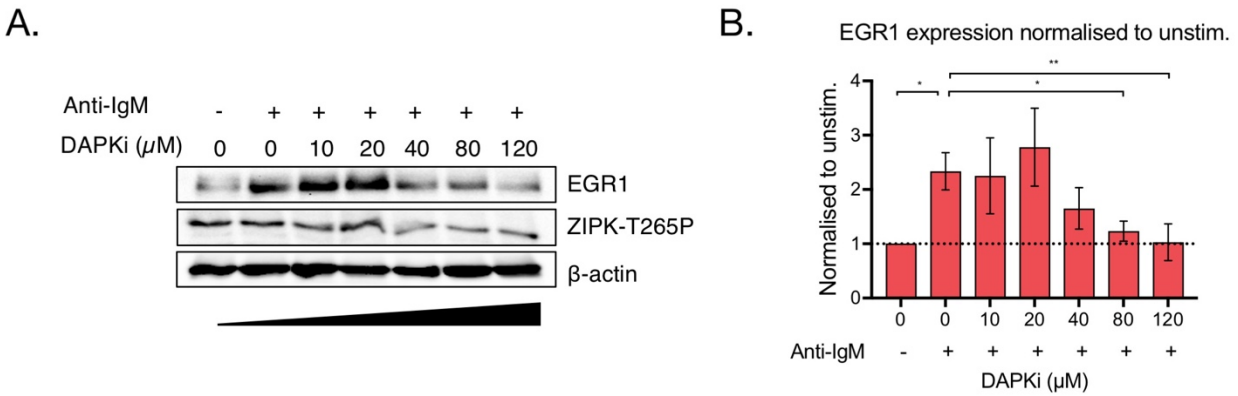

Figure 3.6: ZIPK inhibition reduces the amount of EGR1 protein in CLL cells. (A) (B) Representative western blots displaying levels of EGR1 and ZIPK-T265-P in CLL cells pre-treated with 0-120 μM DAPKi for 60 mins and then stimulated with anti-IgM stimulation for 60 mins. β-actin was used as a loading control. Blots are normalised to unstimulated sample (unstimulated = 1.0) with Image Lab software (below). Error bars are representative of 3 independent experiments. Significant differences calculated using two-way ANOVA followed by Dunnett's multiple comparison test with anti-IgM stimulated 0 μM sample as control. P values = 0.0076, 0.0256 & 0.0087 for unstimulated 0 and 80 and 120 μM samples respectively.

3.3 The effects of BCR pathway activation on immediate early gene expression in lymphoid cell lines

Having characterised the IEG response of CLL cells in the context of BTK and ZIPK inhibition (Figure 3.5), we sought to select a cell line which would show the classical response of rapid but transient expression in order to carry out future experiments in a representative system. The resistance of primary CLL cells to viral transformation by Epstein-Barr virus (EBV) has been cited as a reason for the lack of cell line models which accurately represent the disease [246-248]. MEC1, the most well characterised CLL cell line, has the molecular features of a high risk U-CLL patient, including *TP53* mutation, and lacks many of the other primary characteristics of clinical CLL [249]. Therefore, raji (EBV positive Burkitt's lymphoma), ramos (EBV negative Burkitt's lymphoma) and HBL1 (human diffuse large B cell lymphoma) cell lines were stimulated with anti-IgM $F(ab')_2$ fragment in order to crosslink the BCR and promote IEG expression. *EGR1* and *DUSP2* gene expression was measured over time with real-time/quantitative-PCR (qPCR) (Figure 3.7A-C).

Raji cells displayed a constitutive/underlying baseline expression of both genes in the absence of anti-IgM, which could be increased to higher expression levels with stimulation (Figure 3.7A). Ramos and HBL1 cells showed low/negligible levels of both genes which were dramatically increased with anti-IgM stimulation of the BCR – suggestive of a better model for an inducible system (Figure 3.7B-C). Ramos cells showed upregulation of both *EGR1* and *DUSP2* mRNA just 15 minutes after anti-IgM stimulation. This expression peaked at 30 minutes and decreased between 45-90 minutes and the induction kinetics for both genes were similar. Compared to ramos, HBL1 cells displayed slightly more baseline expression of both genes, similar to raji. However, the subsequent ceiling for mRNA expression post anti-IgM stimulation in HBL1 cells was almost double that observed in raji relative to the expression baseline (102.6% increase in HBL1 0-30 mins compared to 61% in raji at 30 minutes post stimulation). The experiments with HBL1 cells included less timepoints – guided by the observations in raji and ramos cells suggesting the primary expression changes occur between 0-60 minutes. The level of *DUSP2* expression was generally higher in raji cells compared to the other cell lines.

Based on these data we rejected raji cells owing to their high baseline expression and poor inducibility, while both ramos and HBL1 show a more usable IEG

response. In order to further classify which of these cell lines is most CLL-like with regard to IEG expression, we proceeded to assess the effects of treating ramos and HBL1 with ibrutinib and the DAPKi.

3.3.1 The effects of BTK and ZIPK inhibition on BCR-mediated immediate early gene expression in lymphoid cell lines

We have observed an effect of ibrutinib and the DAPKi on the expression of IEGs in CLL cells (Figure 3.5). Therefore, we similarly sought to examine the effects of ibrutinib and the DAPKi on BCR-mediated IEG expression, in order to utilise a cell line with the closest similarities to the primary patient material.

Since ramos and HBL1 cells show the most promising IEG response (see Figure 3.7), we pre-treated both cell lines with either ibrutinib or the DAPKi and assessed the levels of *EGR1* and *DUSP2* gene expression. Initially, we chose to examine the effects of these inhibitors at both 30 and 60 minutes post anti-IgM stimulation in HBL1 cells and at 60 minutes only in ramos cells. These times were selected as they were shown to be timepoints at which high expression of both genes was expected (see Figure 3.7).

For HBL1 cells: the ibrutinib pre-treatment did little to prevent IEG expression, while DAPKi treatment prevented *EGR1* and *DUSP2* gene expression to levels comparable to the reduction observed in CLL cells i.e. unstimulated baseline (Figure 3.8A-B). Ibrutinib had a small but non-significant ($p = 0.9960$ for *EGR1* and $p = 0.0599$ for *DUSP2*) effect on IEG gene expression. In contrast, the DAPKi was consistently able to completely prevent IEG expression in HBL1 cells ($p = 0.0058$ for *EGR1* and $p = 0.0002$ for *DUSP2*). These observations suggest that the regulation of these exemplary IEGs is more dependent on ZIPK than BTK in HBL1 cells. The fact that HBL1 cells are relatively unaffected by ibrutinib treatment may be due to compensation from other transcription factors: while CLL cells rely greatly on BTK-mediated activation of transcription factors, HBL1 cells carry a MYD88-mutation leading to hyperactivation of NF-κB subunits [250].

For ramos cells: neither inhibitor was able to prevent IEG expression following 60 minutes pre-treatment (Figure 3.9B). Following this observation, we decided to pre-treat ramos cells with ibrutinib and the DAPKi for 30 minutes and 120 minutes, to evaluate whether shorter or longer incubation times may affect the

drug's efficacy (Figure 3.9A-C). Additionally, in a further attempt to prevent ramos IEG expression we also treated the cells with cucurbitacin, an inhibitor of STAT3 (STAT3i), a transcription factor and known ZIPK binding partner (Figure 3.9A-C) (see 1.5.6 for the relationship between ZIPK and STAT3).

The response to all three inhibitors (ibrutinib, DAPKi & STAT3i) was mixed across all inhibition time points (30, 60 & 120 minutes). In most cases there was no effect in decreasing IEG expression while in some cases we observed an increase in gene expression, especially in those ramos cells pre-treated with the STAT3i. We believe that the lack of effect seen with ibrutinib and the DAPKi compared to CLL cells or even HBL1 may be due to the multitude of alternative signalling pathways which are active in ramos cells. Further, by inhibiting STAT3, we may have encouraged the cells to upregulate other transcription factors to compensate for its loss.

Based on the results of these experiments, ramos cells provide an ideal model to study anti-IgM mediated activation of the BCR, owing to a rapid but transient IEG response, but are not adequate to assess the effects of BTK or ZIPK inhibition. HBL1 cells are a good anti-IgM responding cell line which is susceptible to ZIPK inhibition, and while slightly less sensitive to ibrutinib, are is the most similar to CLL cells for our criteria.

3.3.1.1 The effects of STAT3 inhibition on IEG expression in CLL cells

When treating ramos cells with a STAT3i (Figure 3.9), we observed that the inhibitor was not particularly effective at preventing IEG expression. Additionally, the STAT3i seemed to have the opposite effect in some cases, resulting in an increase in IEG expression, contrary to our initial hypothesis, that inhibition of STAT3 may be comparable to inhibition with ibrutinib or the ZIPK inhibitor.

In order to understand the puzzling results in ramos cells, we wanted to compare the effect of the STAT3i in patient CLL cells. Primary cells from 4x U-CLL patients (P2-5) were pre-treated with either ibrutinib, the DAPKi or the STAT3i for 60 minutes before stimulation with anti-IgM. *EGR1* and *DUSP2* gene expression was measured by qPCR (Figure 3.10A-B). For both genes, while STAT3i does reduce their expression somewhat, the inhibitor is generally less effective than either ibrutinib or the DAPKi. In one patient (P5, orange circle), we observed an increase in IEG expression as previously seen in ramos cells. For both genes,

this increase is more than double the effect seen from anti-IgM stimulation itself. We conclude that, similar to ramos cells, the inhibition of STAT3 may alter the balance between transcription factors and encourage compensation from others.

3.3.2 Assessing the level of ZIPK protein in lymphoid cell lines

HBL1 and ramos cells responded differently to ZIPK inhibition: while the former showed a convincing loss of IEG expression, ramos cells did not respond well to DAPKi treatment and we did not observe a strong repression of *EGR1* and *DUSP2* expression (see Figure 3.8 & Figure 3.9). In order to understand this response, we sought to quantify the levels of ZIPK protein in each cell line. We took HBL1, ramos, raji and, for comparison, U-CLL and M-CLL cells and lysed them for western blot analysis. Following SDS-PAGE the blot was probed with antibody against ZIPK (Figure 3.11A).

The western blot data showed varying levels of ZIPK expression across the cell lines and the absolute level of ZIPK protein may predict the efficacy of the DAPKi in preventing ZIPK kinase activity. Of note, ramos displayed the highest level of ZIPK – perhaps explaining the ineffectiveness of the DAPKi in preventing IEG expression. M-CLL cells showed the lowest levels of ZIPK but we do not see great differences between the effectiveness of the DAPKi in U-CLL vs M-CLL as it works well in both cases (excluding patient 9). HBL1 and raji cells had similar levels of ZIPK protein and are closest to the CLL cells (U-CLL in particular). This may explain the relative efficacy of the DAPKi in preventing IEG expression in HBL1 cells. We did not test the DAPKi in raji cells owing to their high baseline IEG expression.

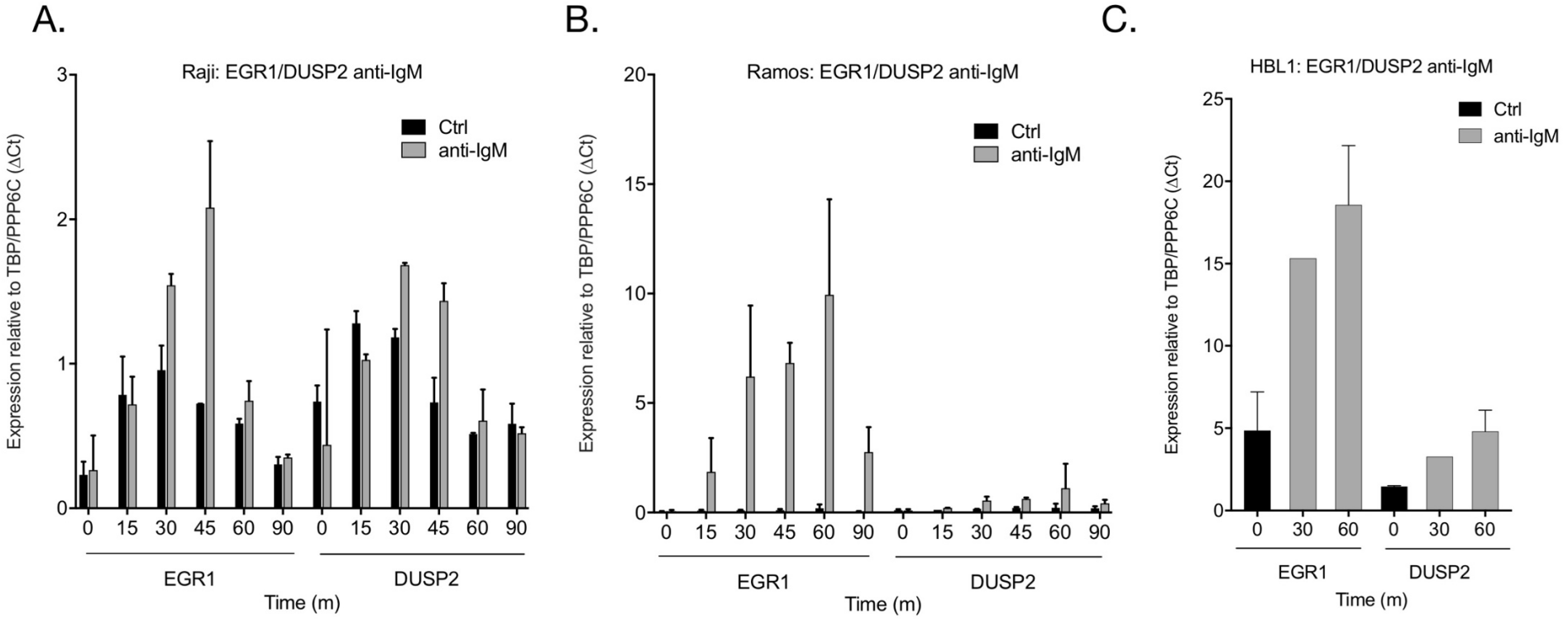

Figure 3.7: IEG expression response in lymphoid cell lines. qPCR data analysis of *EGR1* and *DUSP2* gene expression at 0-90 minutes post anti-IgM stimulation in **(A)** raji, **(B)** ramos and 0-60 minutes in **(C)** HBL1 cells. Cells were taken at indicated time points for RNA extraction and qPCR analysis. Expression changes were quantified using the ΔCt method with TBP and PPP6C as control genes. Error bars are representative of 3 individual stimulations.

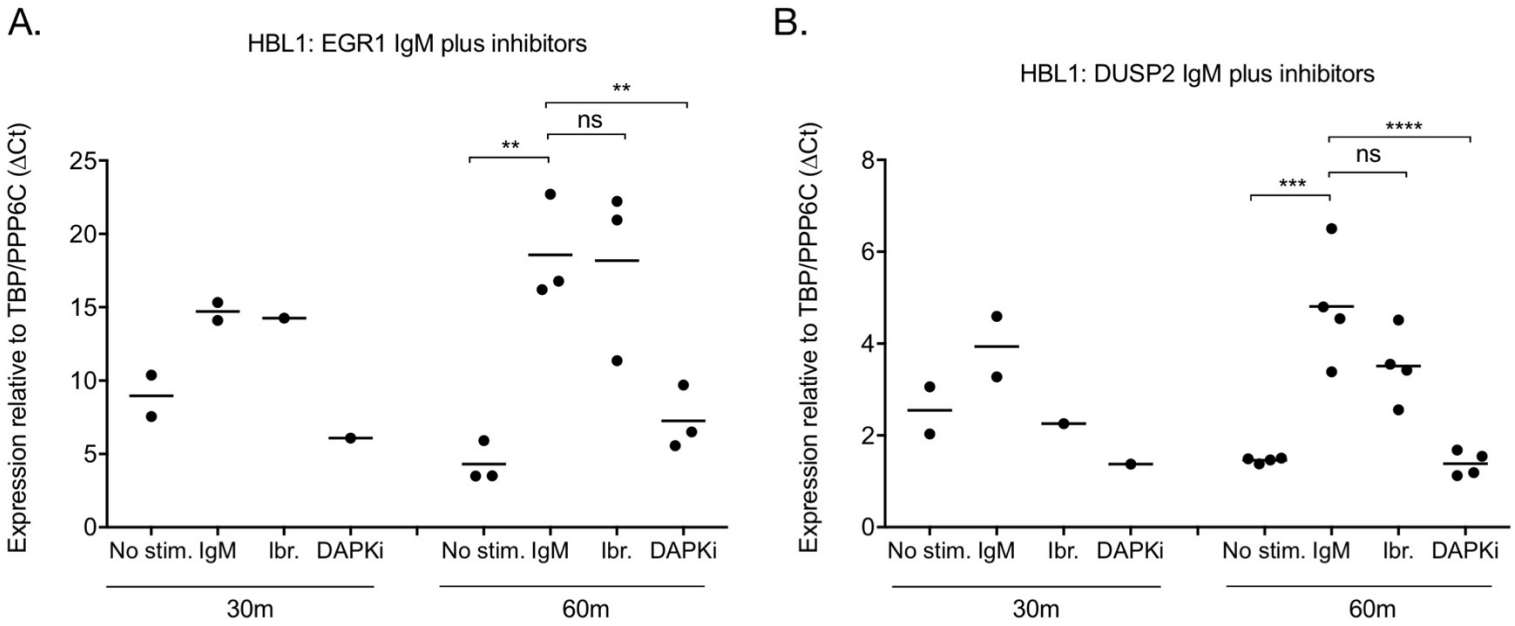

Figure 3.8: IEG response in HBL1 cells. qPCR data analysis of **(A)** *EGR1* (n = 3 independent stimulations at 60 m) and **(B)** *DUSP2* (n = 4 independent stimulations at 60 m) gene expression in HBL1 cells pre-treated with ibrutinib or DAPKi for 60 mins and then stimulated with anti-IgM for 30-60 mins. Expression changes were quantified using the ΔCt method with TBP and PPP6C as control genes. Bars represent the grand mean of the samples. Significant differences calculated using two-way ANOVA followed by Dunnett's multiple comparison test with anti-IgM as control. *EGR1* (60 m) P values = 0.0018, 0.9960 & 0.0058 for anti-IgM vs no stim, Ibr and DAPKi respectively. *DUSP2* (60 m) P values = 0.0002, 0.0599 & 0.0002 for the same comparisons.

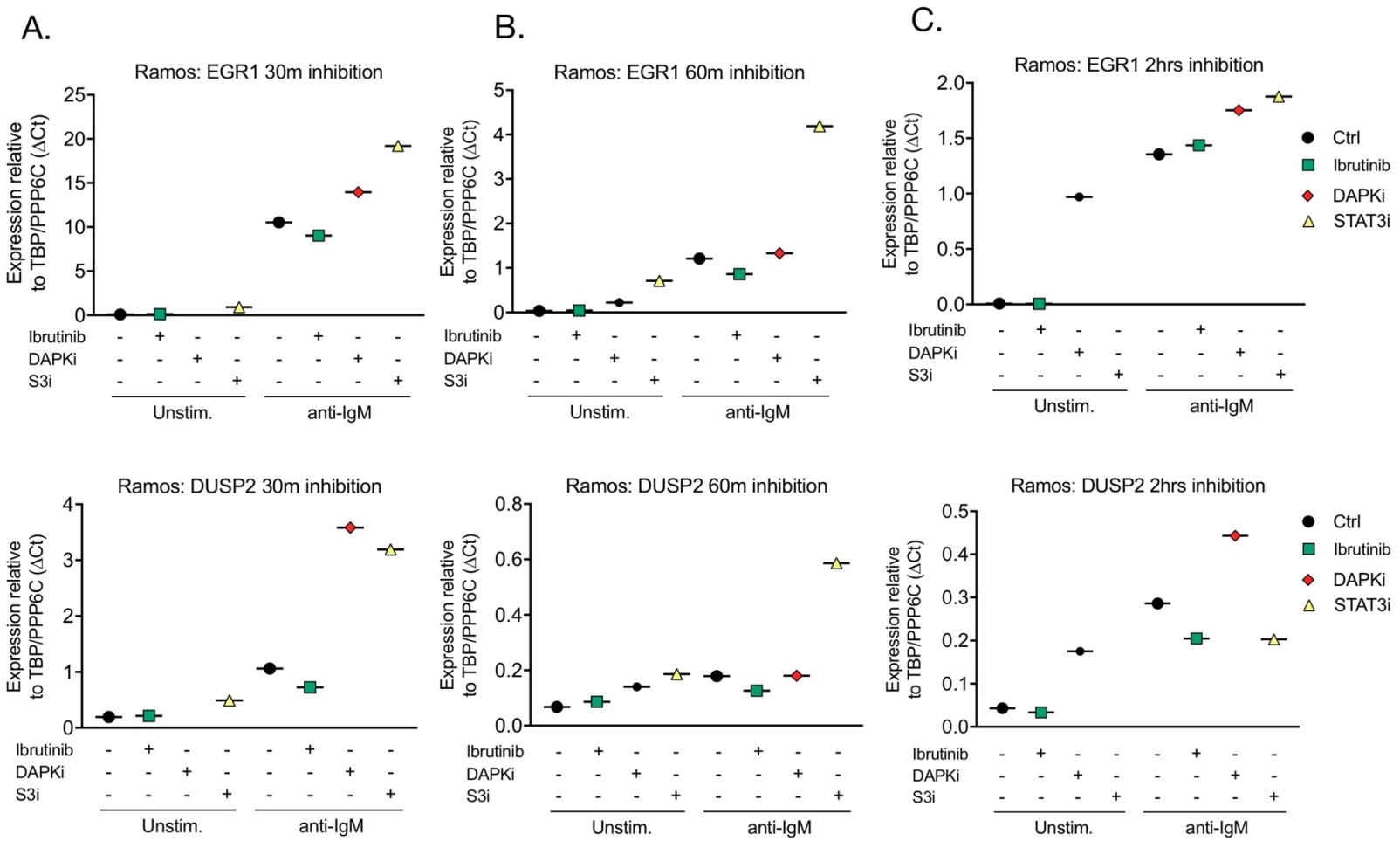

Figure 3.9: IEG response in ramos cells. qPCR data analysis of *EGR1* and *DUSP2* gene expression at 60 minutes post-IgM stimulation in ramos cells. Cells were first (before stimulation) pre-treated with either ibrutinib, the DAPKi or a STAT3i, as indicated, for either **(A)** 30 **(B)** 60 or **(C)** 120 minutes. Expression changes were quantified using the ΔCt method with TBP and PPP6C as control genes.

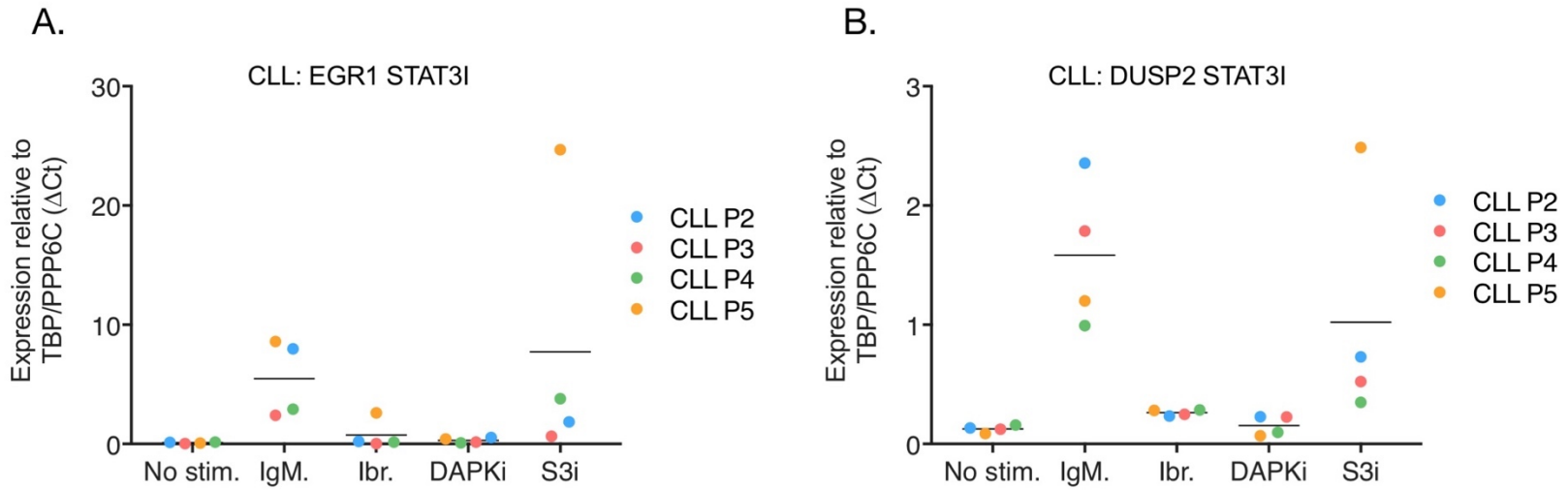

Figure 3.10: ZIPK inhibition mimics ibrutinib in inhibiting CLL IEG expression, while S3i is less effective. qPCR data analysis of **(A)** *EGR1* and **(B)** *DUSP2* gene expression in U-CLL cells (n = 4 U-CLL patients) pre-treated with ibrutinib, STAT3i or DAPKi for 60 mins and then stimulated with anti-IgM for 60 mins. Expression changes were quantified using the ΔCt method with TBP and PPP6C as control genes.

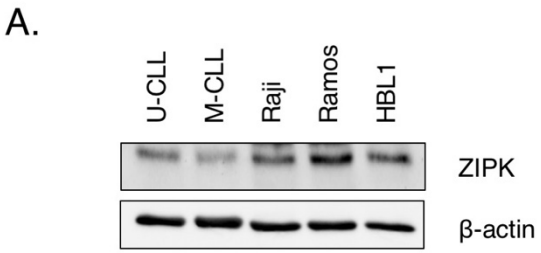

Figure 3.11: ZIPK expression in CLL and lymphoid cell lines. (A) Representative western blot displaying levels of ZIPK in unstimulated U-CLL, M-CLL, raji, ramos and HBL1 cells. CLL cells are representative of an individual patient while the western blot is representative of 2 individual experiments where patients P5 and P10 (U-CLL) and patients P6 and P9 (M-CLL) were assessed. β-actin was used as a loading control.

3.4 The effects of ZIPK knockdown on global histone phosphorylation and immediate early gene expression

We have observed that ZIPK inhibition is as effective as BTK inhibition in preventing IEG expression in CLL cells and HBL1 cells (see Figure 3.5 & Figure 3.8). Ibrutinib, alone or in combination with other inhibitors, is the current gold standard treatment option for patients suffering from CLL. Accordingly, ibrutinib is a highly optimised drug with limited off-target effects and high specificity for BTK, providing a robust loss of enzymatic activity. The DAPKi, while reported to be selective for DAPK1 and DAPK3 over numerous other kinases, has the potential for more off-target effects due to its non-clinical nature. For these reasons, and in order to gain more insight into the cellular consequences of ZIPK loss, we decided to knockdown ZIPK in the HBL1 cell line via small interfering RNA (siRNA) and assess the effect on IEG expression. The HBL1 cell line was chosen for its similarities to CLL cells in the context of IEG expression and inhibition (see 1.1).

HBL1 cells were electroporated with siRNAs directed against ZIPK and a negative control siRNA – an siRNA with a sequence that does not target any gene product to provide a baseline to compare siRNA-treated samples. In order to confirm the effectiveness of the knockdown, cells were taken for analysis at day 3 and day 5. These samples were lysed and ZIPK protein levels were assessed via SDS-PAGE and western blot using antibodies against ZIPK and ZIPK T265-P. By day 5, of the two siRNAs which were tested, both were able to reduce the protein levels of ZIPK and ZIPK T265-P compared to the negative control, with siRNA #2 the more efficient of the pair (Figure 3.12A-B).

Next, we examined the effect of ZIPK knockdown on its downstream histone targets, H3T6-P and H3T11-P (Figure 3.12C). Western blot analysis revealed a loss of both histone marks with either siRNA, giving further evidence to our initial observations that ZIPK is indeed the histone kinase responsible for the phosphorylation of these targets.

In order to assess the functional consequences of knocking down ZIPK with regard to IEG expression, we stimulated siCtrl and siZIPK-transfected HBL1 cells with anti-IgM 5 days post-transfection and assessed the levels of *EGR1* and *DUSP2* gene expression via qPCR (Figure 3.13A-B). For those cells transfected with the siRNA control, anti-IgM stimulation increased IEG expression as

expected. In contrast, cells which carried the ZIPK knockdown failed to induce expression of *EGR1* and *DUSP2* in response to BCR crosslinking via anti-IgM. It is important to note that while the reduction in gene expression was significant it was not as pronounced as the effect we observe when treating CLL or HBL1 cells with a DAPKi. Still, these data reinforced our observations that the DAPKi mimics ibrutinib in its ability to prevent the expression of genes important to CLL progression, and further highlights the role of ZIPK as a transcriptional co-regulator.

3.4.1 The effects of ZIPK inhibition on global histone H3T6 and H3T11 phosphorylation

Having observed that siRNA-mediated knockdown of ZIPK resulted in a loss of global H3T6-P and H3T11-P, we sought to compare this with the effects of the DAPKi. We aimed to further improve our confidence that using the inhibitor to prevent ZIPK activity is comparable to the effects of a loss of ZIPK protein via siRNA. Therefore, we pre-treated HLB1 cells (as it was the cell line used for the siRNA transfection) with increasing concentrations of the DAPKi (10-120 μM) for 60 minutes before stimulation with anti-IgM to activate the BCR. Cells were lysed 60 minutes post stimulation for SDS-PAGE and western blot analysis with antibodies against H3T6-P and H3T11-P (Figure 3.14A-B).

In general, DAPKi treatment did reduce levels of H3T6-P and H3T11-P when compared with non-DAPKi treated samples (0 μM with or without anti-IgM treatment i.e. first two bands). We do not see a noticeable increase in either histone mark with anti-IgM stimulation at the global level. We hypothesise there may be rapid but transient increases in histone phosphorylation specifically in and around the loci of key IEGs which we suggest may be more visible via chromatin immunoprecipitation analysis and is not reflected in a western blot. Finally, the DAPKi-mediated loss of histone phosphorylation was not dose dependent e.g. we see the greatest loss of H3T6-P between 20-40 μM with partial recovery at 80 μM. H3T11-P follows a similar trend with less pronounced differences. This suggests that while the presence of the DAPKi is detrimental to H3T6-P and H3T11-P it is not strictly related to dose and the observed differences may be explained by other cellular factors e.g. cell cycling.

3.5 ZIPK directly interacts with histone H3 to phosphorylate H3T6 and H3T11

Based on our observations that ZIPK's ability to phosphorylate H3T6 and H3T11 is stymied by ZIPK inhibition (3.1) or ZIPK knockdown (3.4.1) we hypothesised that ZIPK that may interact with histone H3 directly to catalyse the reaction. We also considered early literature which suggested ZIPK was a chromatin-associated kinase [229]. Despite this, we did not necessarily expect a positive result as the protein-protein interactions necessary for phosphorylation are often transient owing to the rapid nature of the modification, as seen in signalling cascades. To assess the interaction, HBL1 cells were stimulated with anti-IgM for 60 minutes and then lysed for co-immunoprecipitation (co-IP). The lysates were incubated with protein G magnetic beads and then immunoprecipitated with antibody against histone H3. The interaction was examined by SDS-PAGE and western blot, using antibodies against both ZIPK and ZIPK-T265P (Figure 3.15A).

In assessing the results of the co-IP, we firstly observed an increase in the level of active ZIPK-T265-P in the input (untreated crude cell lysate e.g. a positive control for the presence of ZIPK in the sample). The IgG-immunoprecipitates showed a negative interaction (negative control for non-specific binding). For the co-IP itself, the interaction between total ZIPK and histone H3 was largely negative, or very faint. However, we observed a positive result, suggesting strong interaction, with active/phosphorylated ZIPK and histone H3, regardless of anti-IgM stimulation of the BCR. This suggests that ZIPK specifically interacted with chromatin when it was enzymatically active, or that a closed chromatin configuration makes it difficult to pull down inactive ZIPK.

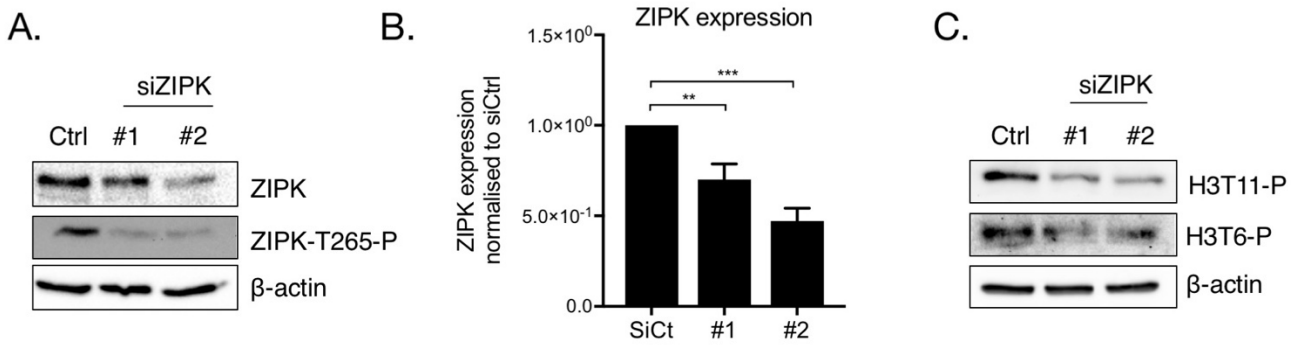

Figure 3.12: ZIPK knockdown reduces level of ZIPK and its histone targets. Western blots of HBL1 cells transfected with siRNAs against ZIPK (#1 and #2) and with a non-specific control siRNA (siCtrl). On day 5 post transfection cells were harvested and lysates probed with antibodies against **(A)** ZIPK, ZIPK-T265-P, **(C)** histone H3T6-P and histone H3T11-P. **(B)** β-actin was used as a loading control and for normalisation to siCtrl using Image Lab software (right). Blots are representative of 3 independent transfections. Significant differences calculated using two-way ANOVA followed by Dunnett's multiple comparison test. P values for ZIPK expression normalised to siCtrl = 0.0036 & 0.0004 for siCtrl vs. siZIPK #1 & siZIPK #2 respectively.

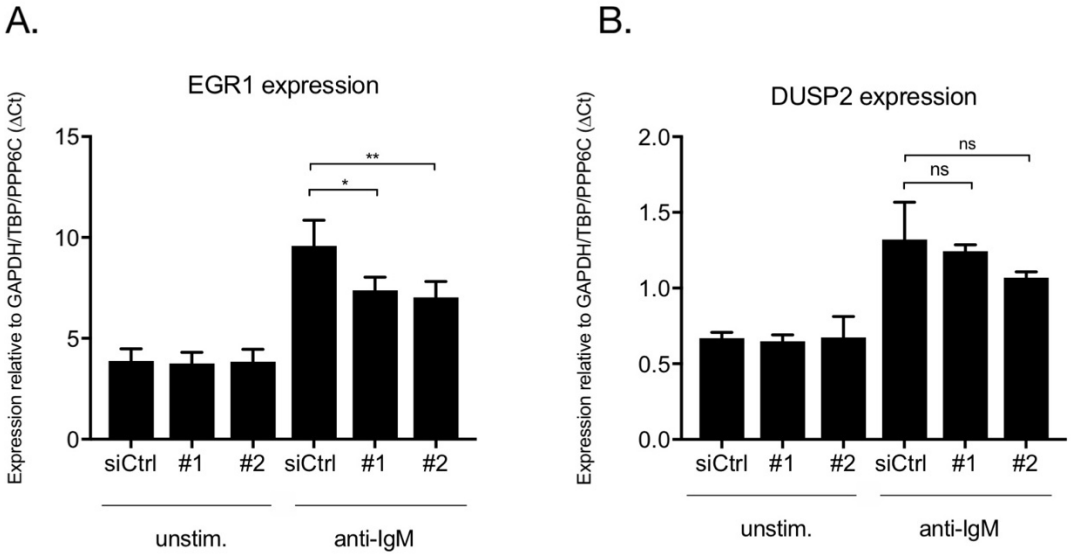

Figure 3.13: ZIPK knockdown mimics DAPKi treatment in preventing IEG expression. qPCR analysis of **(A)** *EGR1* and **(B)** *DUSP2* gene expression in HBL1 cells transfected with siRNAs against ZIPK (#1 and #2) and with a non-specific control siRNA (siCtrl). On day 5 post transfection, HBL1 cells were stimulated with anti-IgM for 1 hour and then harvested for analysis. Expression changes were quantified using the ΔCt method with TBP, GAPDH and PPP6C as control genes. Error bars representative of 3 independent transfections. Significant differences calculated using two-way ANOVA followed by Dunnett's multiple comparison test with anti-IgM stimulated siCtrl as control. P values for *EGR1* = 0.0082 & 0.0009 for siCtrl vs. siZIPK #1 & siZIPK #2 respectively. P values for *DUSP2* = 0.8242 and 0.0995 for the same comparisons.

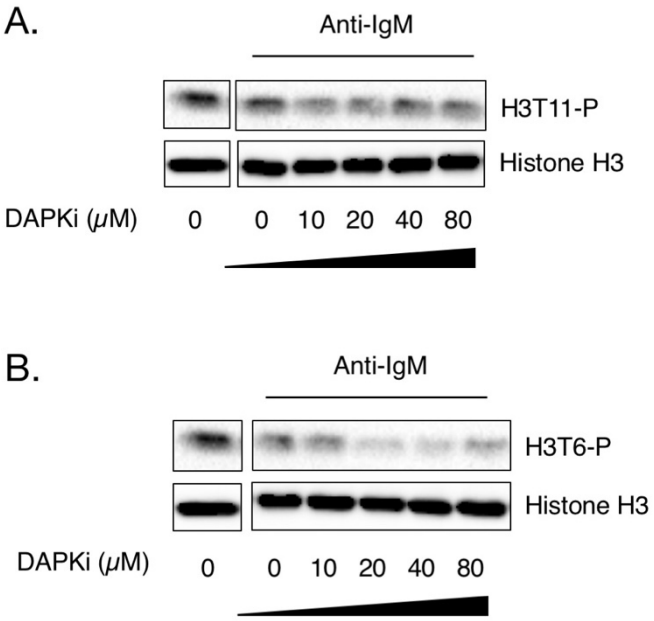

Figure 3.14: ZIPK inhibition reduces levels of H3T6-P and H3T11-P. Western blots displaying levels of **(A)** H3T11-P and **(B)** H3T6-P in untreated CLL cells vs. CLL cells treated with 0-80 μM DAPKi for 60 mins before anti-IgM stimulation of the BCR for a further 60 mins. Western blot is representative of 2 individual experiments in CLL cells. Histone H3 was used as a loading control.

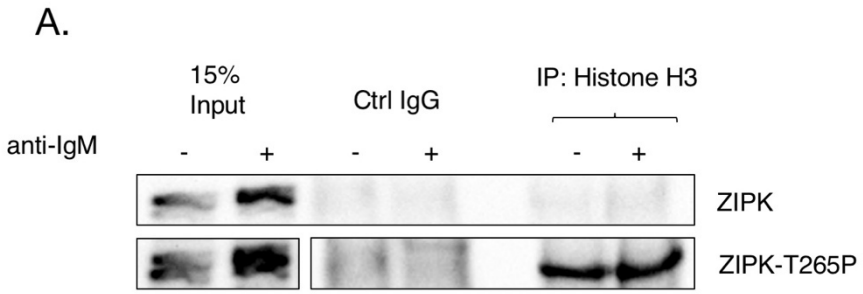

Figure 3.15: ZIPK directly interacts with histone H3 to phosphorylate histones. (A) Co-immunoprecipitation of CLL cells stimulated with anti-IgM for 60 mins as indicated. Immunoprecipitates from histone H3 pulldown were analysed by SDS-PAGE followed by Western blot probing for ZIPK-T265P. Untreated, crude cell lysate was used as positive control (input) and IgG beads were used for negative control (Ctrl IgG). Blot is representative of 3 independent co-IP experiments. Western blot is cropped due to different exposure times for input and co-IP lysates.

Chapter 4 Results 2: ZIPK is required for the effective transcription of critical CLL immediate early genes

Transcriptional regulation is not solely dependent on transcription factor-promoter binding but involves a host of transcriptional co-activators, co-repressors and chromatin remodelling enzymes which mediate the dynamic processes controlling transcription.

4.1 The dynamic interaction between ZIPK and STAT3

Signal transducer and activator of transcription 3 (STAT3) is a well-known member of the STAT3 protein family. These proteins are transcription factors which mediate a variety of critical cellular pathways and mechanisms with functions ranging from growth, proliferation and programmed cell death [238]. STAT3 plays an important role in the development of healthy B cells and it is often seen overexpressed in a variety of cancers [251], including CLL [111, 116, 252, 253]. It has been well demonstrated that STAT3 is activated downstream of the BCR signalling pathway [115] and numerous proteins have been shown to interact with STAT3 to regulate its activity through controlling when and where STAT3 signalling is required. This can include mediating STAT3 crosstalk with other signalling pathways and guiding STAT3 to activate transcription at its target binding sequences [254].

ZIPK has been reported to preferentially (over other STATs) interact with and phosphorylate STAT3 specifically at its serine 727 residue (STAT3 S727-P) [116]. This finding was of particular interest to us as in CLL patients STAT3 is preferentially and constitutively phosphorylated at S727 over its typical phosphorylation sites such as tyrosine 705 (STAT3 Y705-P). These observations led us to consider the ZIPK-STAT3 interaction in CLL. We hypothesised that the loss of IEG expression seen in the context of ZIPK inhibition may be linked to the ZIPK-STAT3 interaction, and that STAT3 may well be a candidate transcription factor responsible for the activation of our IEGs of interest. In summary, while the ZIPK-STAT3 interaction and STAT3 S727-P have been implicated in CLL as separate entities, and both ZIPK and STAT3 have been reported to be upregulated in CLL, at time of writing there is no literature on the interaction between ZIPK and STAT3 in CLL.

4.1.1 STAT3 is activated in response to BCR signalling

In order to begin studying the ZIPK-STAT3 interaction in CLL, we first wanted to understand the kinetics of STAT3 activation after stimulation of the BCR via anti-IgM stimulation. For this, CLL and HBL1 cells (cell line chosen for its similarities to CLL cells – see Chapter 3 Results 1) were stimulated with anti-IgM for 30 minutes before lysis for western blot analysis. Blots were probed with antibodies against total STAT3, STAT3 Y705-P and/or STAT S727-P.

In HBL1 cells, we observed a marked increase in STAT3 S727-P by 30 minutes with even greater levels of phosphorylation by 60 minutes (Figure 4.1A). In contrast, STAT3-Y705-P had slower kinetics showing no increase in phosphorylation until 60 minutes – at which point it was comparable to the levels of STAT3-S727-P (Figure 4.1A). We hypothesise this may suggest a sequential activation of phosphorylation sites on STAT3 in response to BCR activation in HBL1 cells. In CLL cells we saw a moderate increase in the levels of STAT3-S727-P in response to anti-IgM signalling at 30 minutes post-stimulation (Figure 4.1B), this is similar to the response observed in HBL1 cells. These data suggested a rapid activation of STAT3 signalling in response to anti-IgM stimulation of the BCR and confirmed that STAT3 is activated downstream of the BCR in HBL1 and CLL cells.

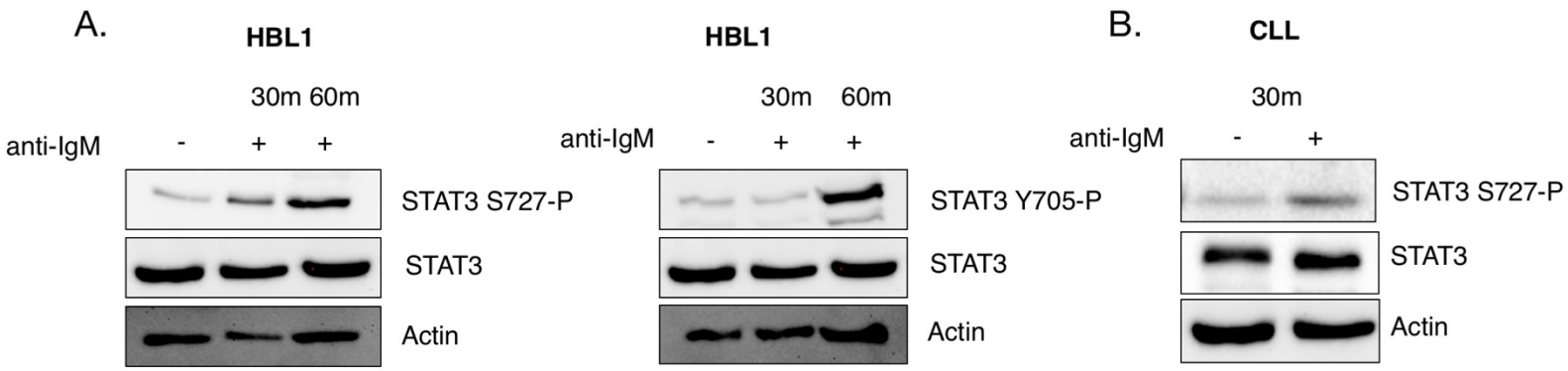

Figure 4.1: STAT3 is activated by BCR signalling in HBL1 and CLL cells. Western blot showing levels of STAT3 phosphorylation at tyrosine 705 and serine 727 in **(A)** HBL1 and **(B)** CLL cells. HBL1 and CLL cells were treated with anti-IgM as indicated and harvested at 30 and/or 60 minutes. β-actin was used as a loading control.

4.1.2 ZIPK interacts directly with STAT3 in CLL cells and lymphoid cell lines

In order to assess the interaction between ZIPK and STAT3 in the context of CLL and BCR signalling, we stimulated CLL cells with anti-IgM for 30 minutes and lysed the cells for reciprocal co-IP. The lysates were incubated with Protein G magnetic beads and then immunoprecipitated with antibodies against ZIPK and STAT3. STAT3 immunoprecipitates were analysed by SDS-PAGE with anti-ZIPK antibody and ZIPK immunoprecipitates with anti-STAT3 antibody. Input samples corresponding to untreated CLL cell lysate (with and without anti-IgM stimulation) were run as a positive control (no inputs were included for the ibrutinib/DAPKi conditions due to 1) limited CLL cell counts and 2) lack of physical space on the gel to run all the samples simultaneously). SDS-PAGE and western blot analysis showed that ZIPK and STAT3 complex together in CLL cells (Figure 4.2A-B). The interaction could be slightly strengthened by anti-IgM stimulation of the BCR, suggesting a functional impact of BCR cross-linking on the ZIPK-STAT3 interaction. In the STAT3 pull-down, we saw the most pronounced anti-IgM dependent increase in the ZIPK-STAT3 interaction (Figure 4.2B upper panel).

We next assessed the interaction between STAT3 and active ZIPK phosphorylated at T265 (Figure 4.2B). When specifically probing for phosphorylated ZIPK the interaction was weaker and could not be as clearly increased by anti-IgM stimulation. We also pulled down with phosphorylated STAT3 (STAT-S727-P) and assessed its interaction with phosphorylated ZIPK (Figure 4.2C). While the proteins still appeared to interact, we did not observe the anti-IgM dependent increase as seen above.

To remain consistent in our assessment of HBL1 cells, we also sought to examine the ZIPK-STAT3 interaction in this cell line. We first assessed the interaction between active ZIPK and both total STAT3 and STAT3-S727-P (Figure 4.2D). In HBL1, we observed ZIPK-STAT3 interaction and although it appeared weaker than in CLL, the interaction remained anti-IgM dependent. We also observed an increase in the interaction when we performed ZIPK-T265-P pull-down and assessed binding of STAT3-S727-P. We have shown that upon anti-IgM stimulation of the BCR, STAT3-S727-P levels are increased in CLL cells (Figure 4.1B). This suggested that not only is more STAT3 phosphorylated as a result of BCR crosslinking, but that more of the active protein then interacted with ZIPK and ZIPK-T265-P. We also sought to examine this interaction reciprocally, pulling

down with STAT3-S727-P antibody and assessing the levels of total ZIPK and ZIPK-T265-P (Figure 4.2E). In these experiments, the interaction remained anti-IgM dependent for the two phosphorylated proteins (Figure 4.2E lower panel), but was clearly weaker between STAT3 S727-P and total ZIPK (Figure 4.2E upper panel).

We also assessed the interaction in ramos cells. When pulling down with total ZIPK and assessing the interaction of STAT3 and STAT3-S727-P we observed a strong anti-IgM dependent increase (Figure 4.2F). We did not observe an anti-IgM dependent increase in the reciprocal experiment when pulling down with STAT3 antibody (Figure 4.2G). The cuts between input/IgG/pull-down in the co-IP western blots shown in Figure 4.2 & Figure 4.3 are due to either having to alter the saturation for faint input samples or were necessary to re-order the bands in order to maintain consistency between sample/condition order across the figures. Full, un-cut co-IP western blots can be found in Appendix 8.2.

4.1.3 ZIPK-STAT3 interactions are inhibited by both BTK and ZIPK inhibition

Having shown that BCR stimulation could promote ZIPK-STAT3 interactions in a seemingly functional, anti-IgM dependent manner, we sought to understand if this interaction was preventable though inhibition of either ZIPK or BTK function. Therefore, we pre-treated CLL cells with either ibrutinib or the DAPKi for 1 hour before anti-IgM stimulation. After 45 minutes the cells were then lysed for co-IP. In our first experiment we sought to assess the interactions reciprocally between total ZIPK and STAT3 (Figure 4.3A-B). First, we confirmed our observations from the previous experiment that anti-IgM stimulation increased the ZIPK-STAT3 interaction. When the CLL cells were pre-treated with ibrutinib the interaction appeared to increase, but only after anti-IgM stimulation. We observed little effect on the interaction for CLL cells pre-treated with the DAPKi. Of note, when we pulled down with ZIPK and assessed the total STAT3 interaction we observed that addition of the DAPKi reduced the interaction to a level comparable with the unstimulated control: but only in the presence anti-IgM stimulation

Our previous experiments have indicated that in examining the interaction between the phosphorylated proteins we observed the largest variation after anti-IgM stimulation (Figure 4.2D lower panel, Figure 4.2E lower panel, Figure 4.2F), suggesting that it may be the active, phosphorylated forms of the proteins which

play the most dynamic roles in the interaction and are the most important functionally. Therefore, we decided to assess the interactions between ZIPK and ZIPK-T265-P and STAT3-S727-P (Figure 4.3C-D). We observed the expected increase in the level of STAT3-S727-P in both inputs following anti-IgM stimulation, indicating the CLL cells have been activated. The co-IP showed the expected increase in ZIPK-STAT3-S727-P interaction following anti-IgM stimulation (Ctrl). The addition of ibrutinib or the DAPKi resulted in a decrease in interaction, with the greatest loss observed after DAPKi treatment. When the CLL cells were not stimulated with anti-IgM both inhibitors showed less of an impact on ZIPK and STAT3-S727-P interaction.

We saw similar results for the ZIPK-T265-P immunoprecipitates (Figure 4.3D). Anti-IgM stimulation increased the interaction between active ZIPK-T265-P and active STAT3-S727-P (Ctrl). The addition of ibrutinib decreased this interaction to a level comparable with unstimulated cells without drug treatment (Ctrl; no stim). Ibrutinib treatment also reduced the interaction in absence of anti-IgM stimulation, in contrast with the results we obtained with total ZIPK where no change in interaction was observed (Figure 4.3A-B).

4.1.4 The effect of ZIPK inhibition on STAT3 phosphorylation in CLL and lymphoid cells

We have demonstrated that STAT3 is activated in response to anti-IgM stimulation, with residues Y705 and S727 showing phosphorylation after 30-60 minutes (Figure 4.3). Further, activation of BCR signalling increased the interaction between STAT3 and ZIPK and this could be inhibited by ibrutinib or DAPKi treatment (Figure 4.2 & Figure 4.3). Consequently, we wanted to assess whether or not inhibition of ZIPK would impact STAT3 phosphorylation directly, perhaps providing an explanation for the loss in interaction. CLL, ramos and HBL1 cells were pre-treated with increasing concentration of the DAPKi (10-120 μM) for 60 minutes before stimulation with anti-IgM. Cells were lysed for western blot analysis, probing with antibody against STAT3 S727-P.

For both CLL and HBL1 cells, we observed only a small decrease in STAT3 phosphorylation in response to ZIPK inhibition, which was most evident only at the highest concentration (120 μM) (Figure 4.4A-B). Overall this decrease was not significant and it appeared that while ZIPK inhibition could impact ZIPK-STAT3 interaction, the level of phosphorylation was not affected. Further, the

anticipated activation of STAT3 S727-P, as seen previously (Figure 4.1), was not observed, with the cells having been stimulated for 30 minutes in both experiments. These data demonstrated the heterogenous response of different CLL patients to anti-IgM stimulation of the BCR – it is possible we may have observed a stronger STAT3 S727-P response after 60 minutes.

Next, we wanted to compare these data with the same experiments performed in ramos cells, which we have already shown to have a very robust anti-IgM response. In ramos, STAT3 S727-P was not inducible and increasing the concentration of DAPKi increased the amount of STAT3 S727-P (Figure 4.4C). This result was unexpected, and to assess this further we examined the same ramos lysates for STAT3 Y705-P. Interestingly, we observed the same trend for this phosphorylation mark, although Y705-P was slightly more inducible by anti-IgM stimulation (Figure 4.4C). Indeed, when quantified, the level of STAT3 Y705-P correlated with the dose of DAPKi. In an effort to understand these data, we also assessed the levels of ZIPK T265-P in response to the inhibitor to confirm its specific function in this cell type (Figure 4.4C). We observed that the anticipated decrease in ZIPK T265-P was marginal in ramos cells, suggesting that this cell line does not respond well to the DAPKi, especially when compared to the data from CLL cells (Chapter 3 Results 1). These data might be explained by the gene expression data from ramos cells (Chapter 3 Results 1), whereby ZIPK inhibition had either no effect on IEG expression or in some cases, increased it. Further, we have shown that of all our tested cell lines and primary cells, ramos displayed the highest levels of ZIPK (Figure 3.11), suggesting that our DAPKi may have been unable to overcome the high protein expression in this cell type.

Based on the data for STAT3 phosphorylation in response to DAPKi from HBL1, ramos and CLL cells we concluded that the total loss of IEG expression observed in response to the drug is not likely linked to a loss of STAT3 phosphorylation; but may still be linked to the reduction in ZIPK-STAT3 interaction observed in our co-IP experiments.

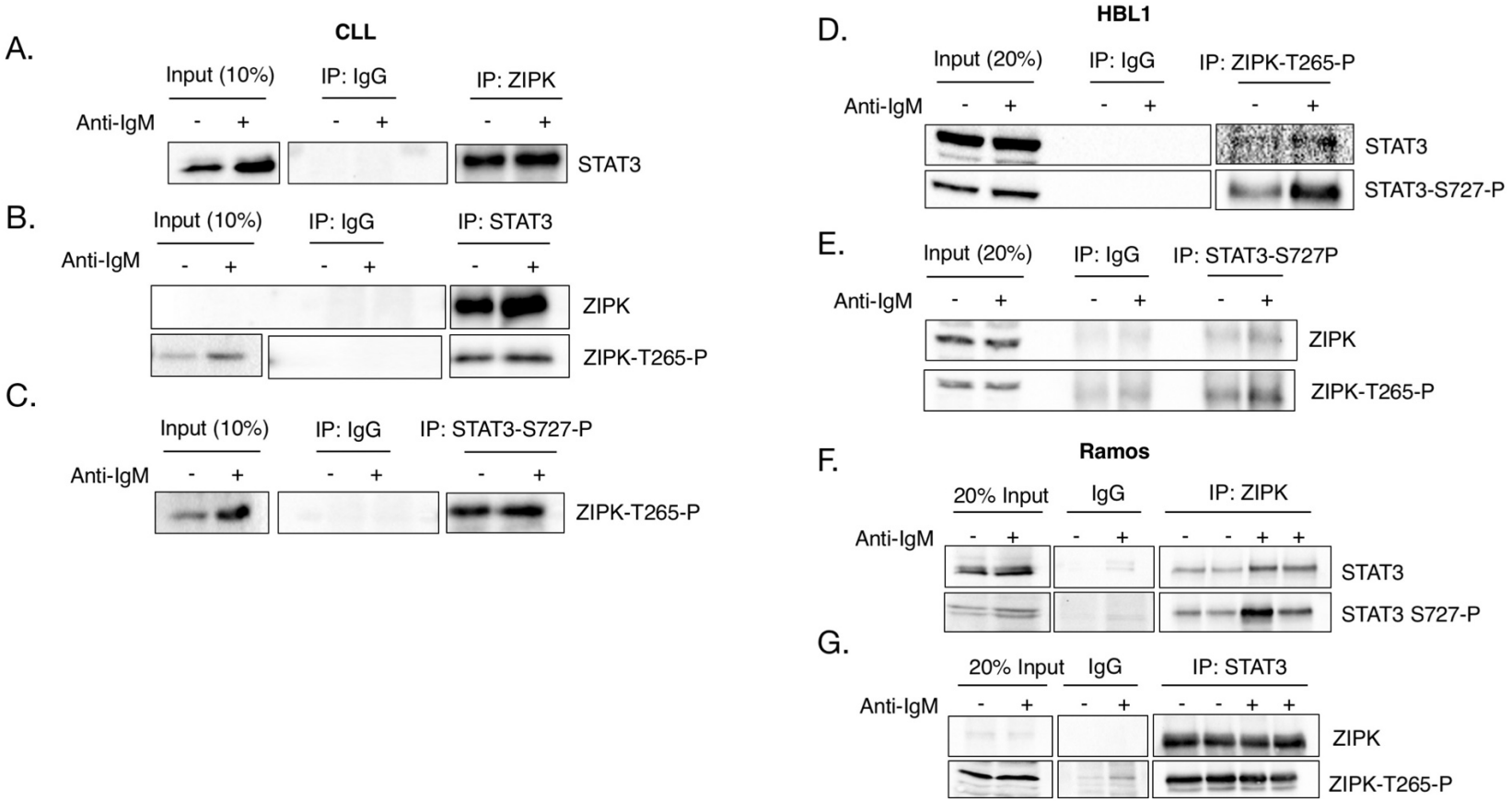

Figure 4.2: ZIPK and STAT3 interact in CLL and lymphoid cell lines. Co-immunoprecipitation of **(A) (B) (C)** CLL, **(D) (E)** HBL1 and **(F) (G)** ramos cells stimulated with anti-IgM for 1 hour as indicated. Immunoprecipitates from ZIPK, STAT3, STAT3 S727-P and ZIPK T265-P pulldown were analysed by SDS-PAGE followed by Western blot probing for ZIPK, ZIPK T265-P, STAT3 and STAT3 S727-P. Untreated, crude cell lysate was used as positive control (input) and IgG beads were used for negative control (Ctrl IgG). Blots are representative of 2-3 independent co-IP experiments. Western blots are cropped due to different exposure times between input and co-IP lysates or due to the order of samples on the original membrane. See full uncropped examples in Appendix 8.2.

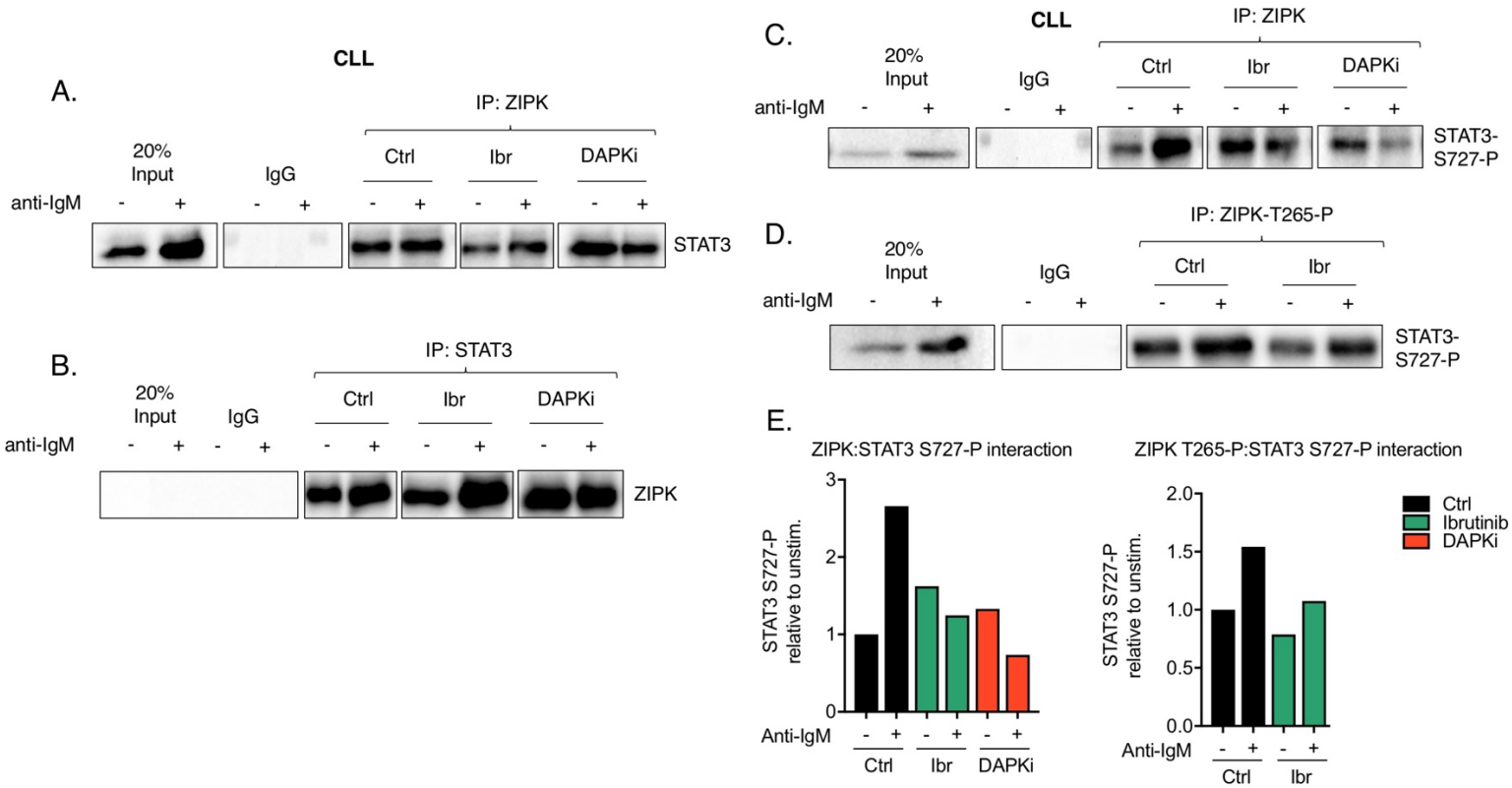

Figure 4.3: ZIPK-STAT3 interaction can be prevented by ZIPK or BTK inhibition. Co-immunoprecipitation of **(A) (B) (C) (D)** CLL cells pre-treated with either ibrutinib or DAPKi for 60 mins and then stimulated with anti-IgM for 60 mins as indicated. Immunoprecipitates from ZIPK, STAT3 and ZIPK T265-P pulldown were analysed by SDS-PAGE followed by western blot probing for ZIPK, STAT3 and STAT3 S727-P. Untreated, crude cell lysate was used as positive control (input) and IgG beads were used for negative control (Ctrl IgG). Blots are representative of 2 independent co-IP experiments. Western blots are cropped due to different exposure times for input and co-IP lysates. **(E)** Interactions were normalised relative to Ctrl (relative value = 1.0) for quantification using Image Lab software. Western blots are cropped due to different exposure times between input and co-IP. Original membranes in panels (A) (B) and (C) were cut between Ctrl, Ibr and DAPKi to reorganise the bands for consistency. See full uncropped examples in Appendix 8.2.

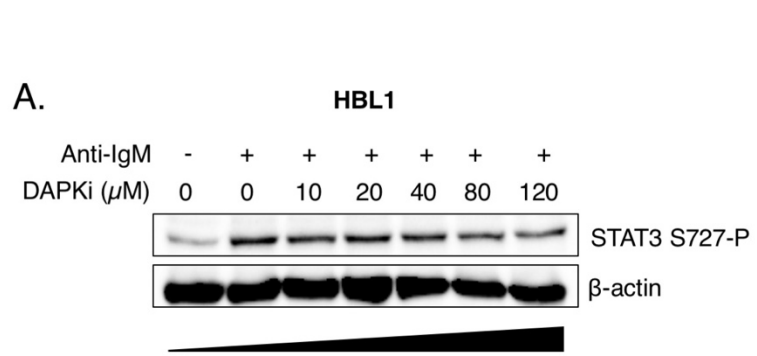
A.
HBL1
Anti-IgM - + + + + + +
DAPKi (μM) 0 0 10 20 40 80 120
STAT3 S727-P
β-actin

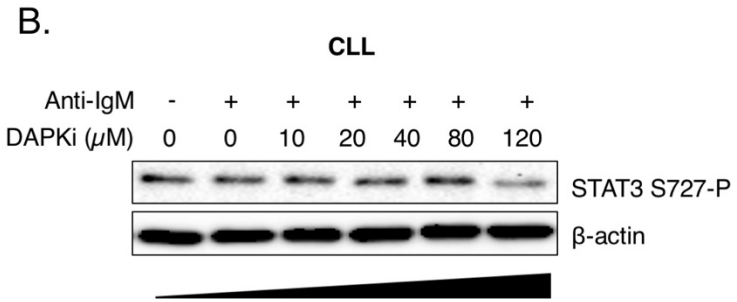
B.
CLL
Anti-IgM - + + + + + +
DAPKi (μM) 0 0 10 20 40 80 120
STAT3 S727-P
β-actin

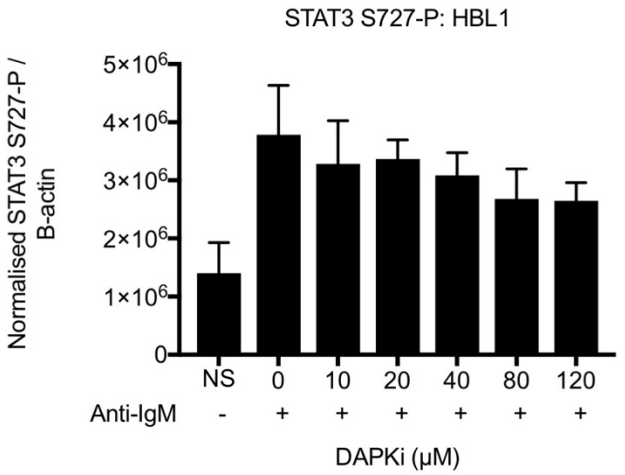
STAT3 S727-P: HBL1
Normalised STAT3 S727-P / B-actin
5×10^6
4×10^6
3×10^6
2×10^6
1×10^6
0
NS 0 10 20 40 80 120
Anti-IgM - + + + + + +
DAPKi (μM)

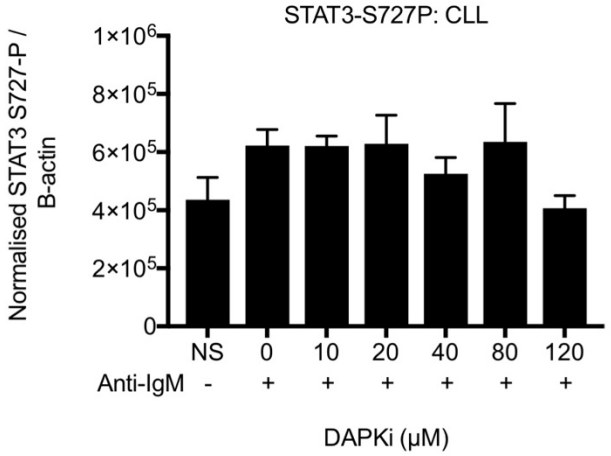
STAT3-S727P: CLL
Normalised STAT3 S727-P / B-actin
1×10^6
8×10^5
6×10^5
4×10^5
2×10^5
0
NS 0 10 20 40 80 120
Anti-IgM - + + + + + +
DAPKi (μM)

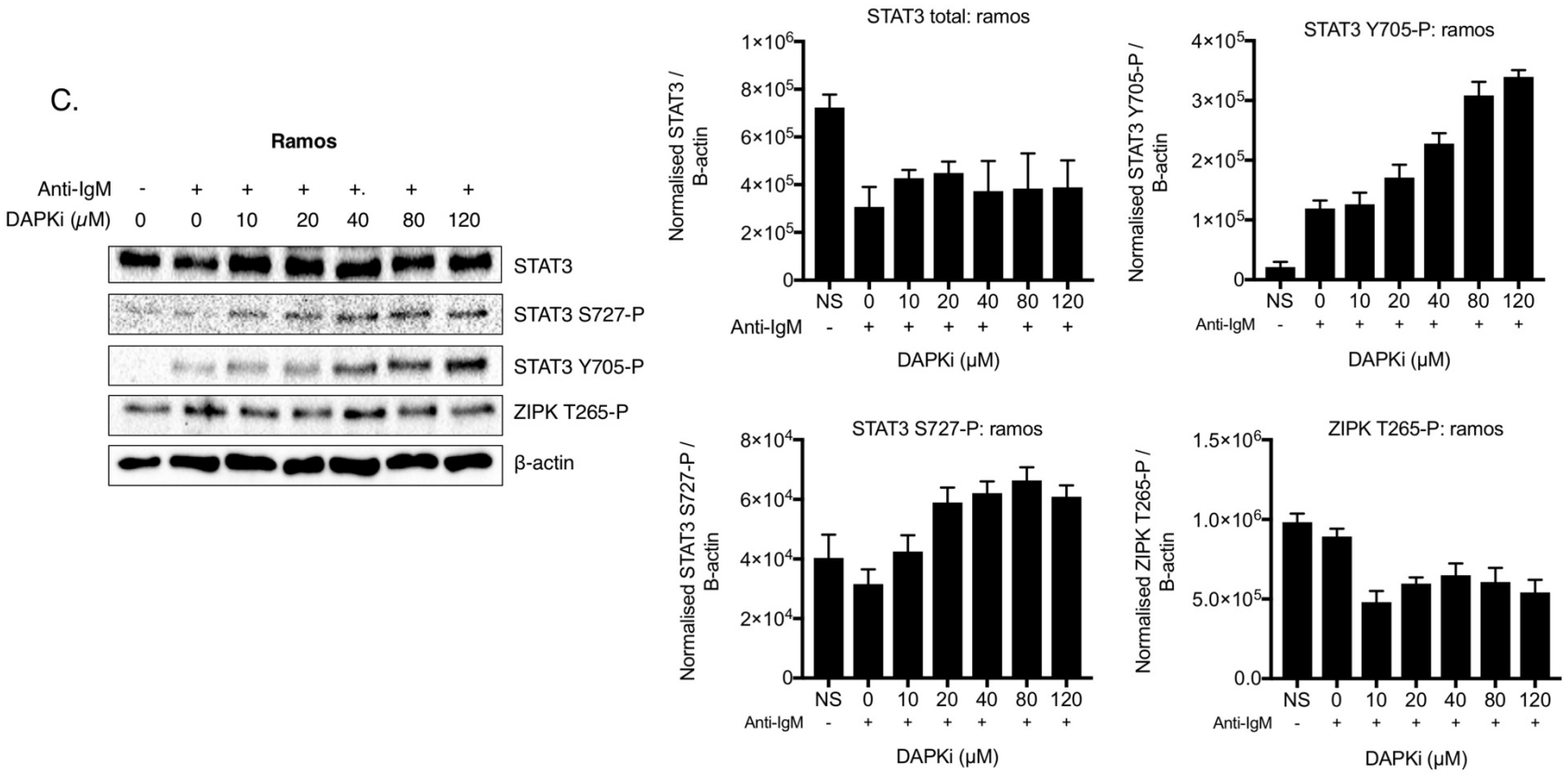

Figure 4.4: The effects of ZIPK inhibition on STAT3 phosphorylation. (A) western blot displaying levels of STAT3-S727P in HBL1 cells pre-treated with 0-120 μM DAPKi for 60 mins and then stimulated with anti-IgM for 30 mins, as indicated. β-actin was used as a loading control and for normalisation with Image Lab software (right). **(B)** western blot displaying levels of STAT3-S727P in CLL cells pre-treated with 0-120μM DAPKi for 60 mins and then stimulated with anti-IgM for 30 mins, as indicated. NS, no stimulation. β-actin was used as a loading control and for normalisation with Image Lab software (right). **(C)** western blots displaying levels of STAT3, STAT3-Y705-P, STAT3-S727-P and ZIPK-T265-P in ramos cells pre-treated with 0-120 μM DAPKi for 60 mins and then stimulated with anti-IgM for 30 mins, as indicated. NS, no stimulation. β-actin was used as a loading control and for normalisation with Image Lab software (below).

4.2 STAT3 binds IEG promoters in response to BCR activation

We have determined that ZIPK and STAT3 interact after BCR cross-linking in CLL cells – an interaction which could be reduced by ibrutinib or DAPKi treatment (Figure 4.2 & Figure 4.3). We have shown that ZIPK inhibition could completely prevent IEG expression in CLL despite little to no impact on STAT3 phosphorylation (Chapter 3 Results 1 & Figure 4.4). In order to increase our understand of how STAT3 may play a role in the mechanism of IEG-repression mediated by DAPKi, we wanted to assess the role of STAT3 in the transcriptional regulation of the two IEGs studied.

To understand how a loss of ZIPK function might impact the gene expression of our model genes, *EGR1* and *DUSP2*, we assessed STAT3-DNA binding through a series of ChIP experiments. STAT3 is a known regulator or *EGR1*, but not *DUSP2*, which is considered to be regulated by NF-κB family members. Therefore, most of the experiments were performed looking at the *EGR1* locus. We designed a series of primers to cover regions around the loci of both genes using publicly available data [255] and ChIP-seq databases [256] as a guide to probe for regions where STAT3 was predicted to bind.

Cells from a U-CLL patient (CLL P3) were stimulated with anti-IgM for 60 minutes before formaldehyde-induced cross-linking and ChIP analysis using antibodies against STAT3 and STAT3-S727-P to pull-down protein-associated DNA of interest. The ChIP-qPCR analysis revealed that STAT3 predominantly binds in response to BCR crosslinking at a region 1.0 kb upstream (3') of the *EGR1* transcription start site (TSS) (Figure 4.5A). This region is one of several predicted STAT3-binding promoters. There was further STAT3 binding at a predicted enhancer region (-6.1 kb) and in the gene body itself (+2.2 kb); yet in both cases the enrichment is approximately half of what we observed at -1.0 kb. STAT3-S727-P had a similar but mirrored profile with strong binding at -6.1 kb and less at -1.0 kb, with a comparable amount in the gene body (+2.2 kb) in response to anti-IgM stimulation (Figure 4.5A). The fact that the active, phosphorylated form of STAT3 preferentially binds the enhancer could have functional consequences but this conclusion would require further investigation.

Total STAT3 displayed relatively poor binding at the *DUSP2* locus with a two-fold increase seen at +4.2 kb from the TSS in absence of stimulation (Figure 4.5B). STAT3-S727-P displays moderate binding just downstream of the *DUSP2*

transcription end site (TES; +2.4 kb) (Figure 4.5B). We hypothesised that the transcription factor binding observed in the gene bodies of both genes could be attributed to the presence of an intronic enhancer [257] or chromatin looping and other higher order architectural changes to the epigenetic landscape which may bring the promoter region in close contact with the gene body.

4.2.1 The effects of ibrutinib and DAPKi on STAT3 IEG binding

Having begun to assess STAT3 binding in CLL cells, we moved to examine the effect of both the DAPKi and ibrutinib on STAT3-DNA binding at IEG loci. We took U-CLL patient cells (CLL P5) and pre-treated them with either ibrutinib or the DAPKi for 60 minutes. The cells were then stimulated for a further 60 minutes with anti-IgM to activate STAT3. The cells were then crosslinked and lysed for ChIP following our standard protocol.

The ChIP-qPCR data for CLL P5 showed some similarities to the data for CLL P3: notably that the region -1.0 kb from the *EGR1* TSS seemed to be the area of most STAT3 enrichment (Figure 4.6A). However, there were also inconsistencies when comparing the ChIP data between individual patients, for example: we did not observe a BCR-dependent increase in binding for STAT3 or STAT3-S727-P and instead observed the presence of STAT3 at the *EGR1* locus in absence of BCR stimulation. The inhibitors (ibrutinib and the DAPKi) did appear to reduce the level of STAT3 binding for STAT3-S727-P but had less effect for total STAT3. In this experiment, we also observed a stronger enrichment for STAT3 at the *DUSP2* locus – with recruitment to the predicted promoter region -0.6 kb upstream of the *DUSP2* TSS (Figure 4.6B). This recruitment was inhibited by both ibrutinib and the DAPKi. However, no binding was observed for phosphorylated STAT3 at the *DUSP2* locus.

We similarly carried out ChIP-qPCR analysis using HBL1 cells to assess STAT3-binding. In this experiment, we treated some of the cells with a DAPKi to understand whether or not a loss of ZIPK function could impact STAT3 binding. While the data were predominantly negative, we observed enrichment of STAT3 upstream of the *EGR1* TSS at -1.3 kb in HBL1 cells (Figure 4.6C). This region is 300 base pairs upstream of the promoter-associated binding region we observed in CLL cells. The purported enhancer was negative for STAT3 binding in HBL1 cells (data not shown), suggesting this enhancer may be CLL-specific. The

DAPKi had a small effect in reducing STAT3 binding, which was slightly reduced at the -1.3 kb region upstream of the *EGR1* TSS after treatment with DAPKi.

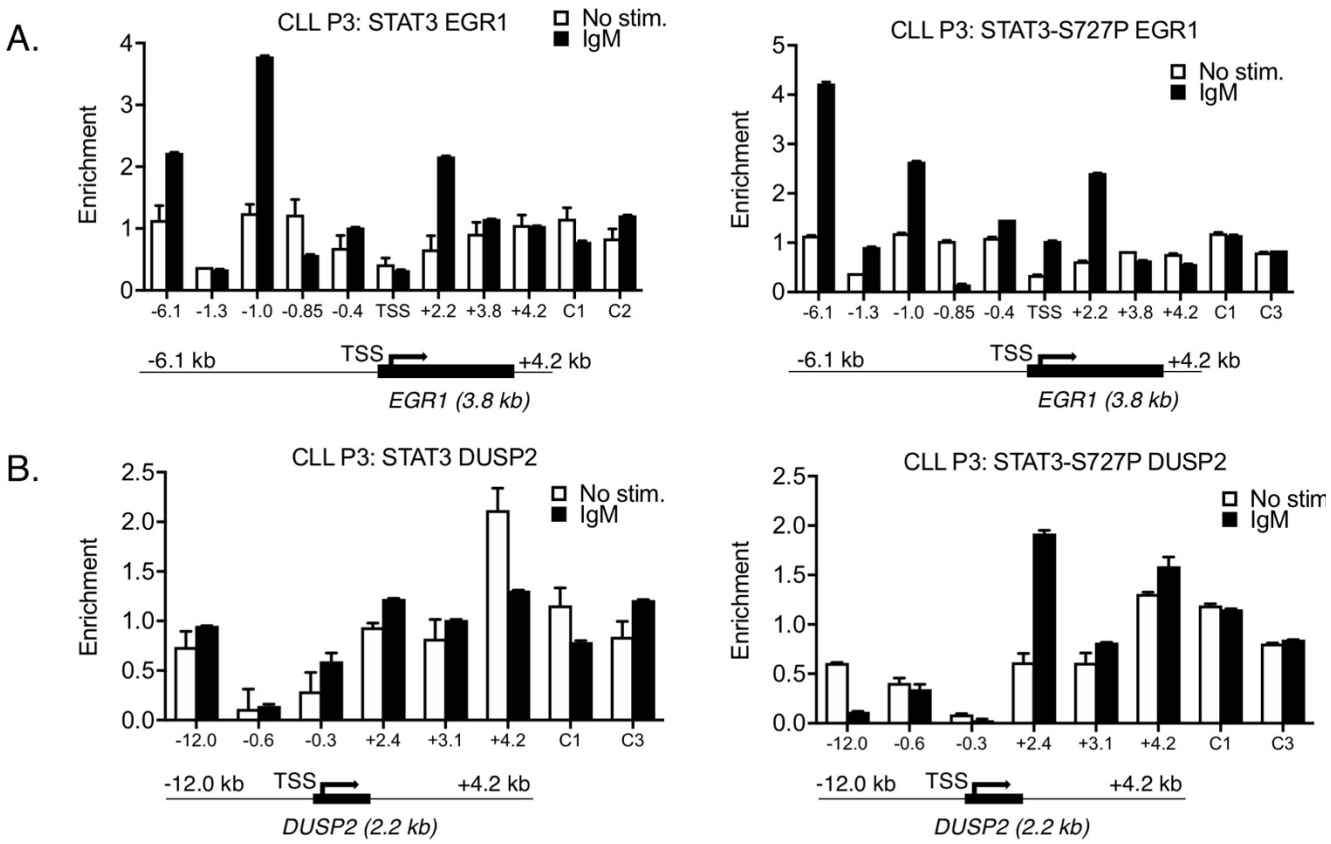

Figure 4.5: STAT3 binds IEG promoters in CLL cells. ChIP-qPCR data assessing levels of STAT3 and STAT3 S727-P at the **(A)** *EGR1* and **(B)** *DUSP2* gene loci at 30 minutes post stimulation with anti-IgM. The values on the x axis refer to specific gene regions relative to the transcription start site (TSS) in kilobases (kb) as indicated on the gene schematics below (not to scale). CTCF1/3 (C1/C3) were used as negative control regions which are not indicated on the gene schematics. Error bars correspond to variations in the ChIP-qPCR repeats.

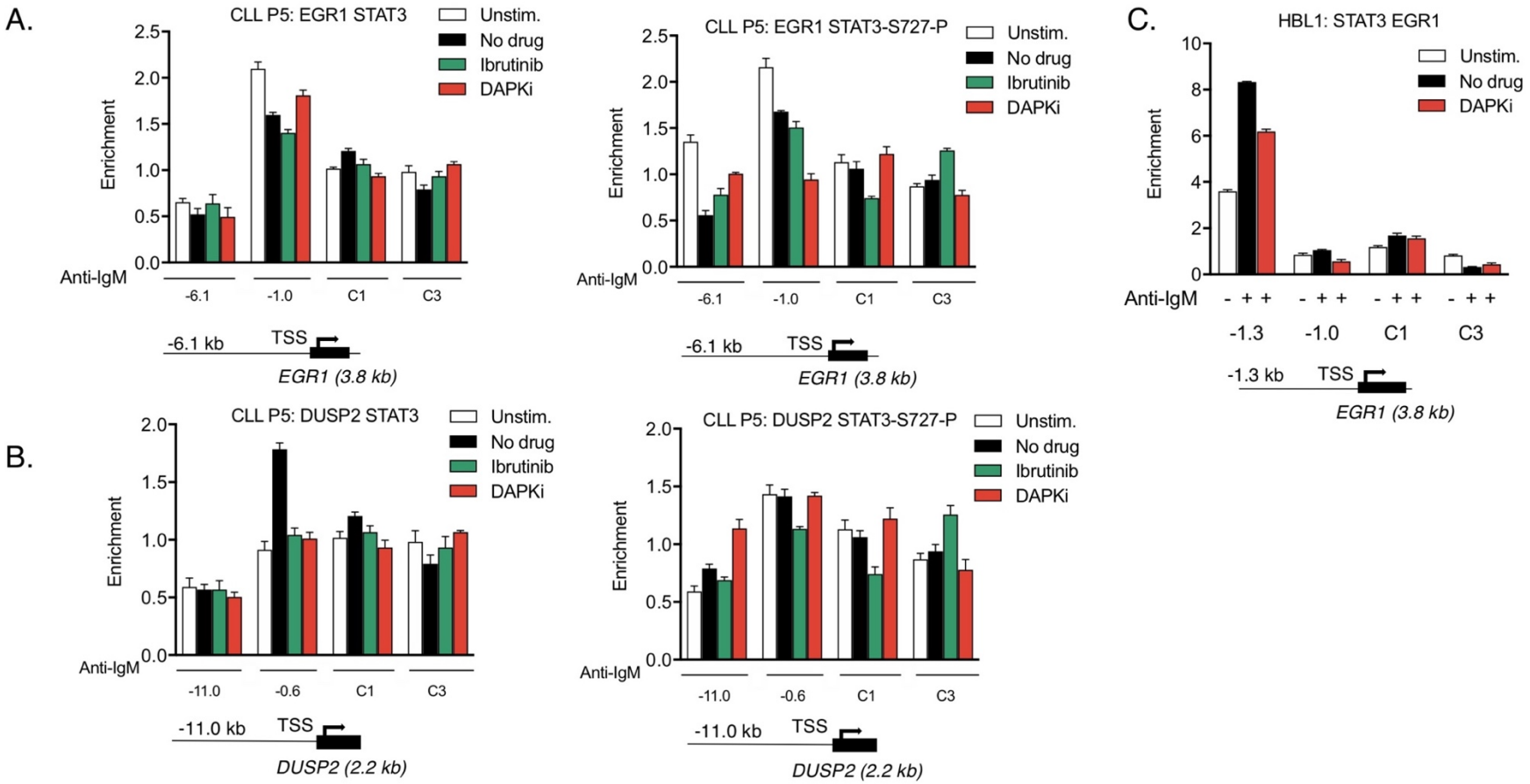

Figure 4.6: STAT3 binds IEG promoters in CLL cells. ChIP-qPCR data assessing levels of STAT3 and STAT3 S727-P at the **(A)** *EGR1* and **(B)** *DUSP2* gene loci in CLL or **(C)** HBL1 cells. Cells were pre-treated with either 1 μM ibrutinib (green) or 25 μM DAPKi (red) for 60 mins as indicated and then stimulated with anti-IgM for 30 mins. The values on the x axis refer to specific gene regions relative to the transcription start site (TSS) in kilobases (kb) as indicated on the gene schematics below (not to scale). CTCF1/3 (C1/C3) were used as negative control regions which are not indicated on the gene schematics. Error bars correspond to variations in the ChIP-qPCR repeats.

4.3 Combined anti-IgM/CD40L stimulation increases IEG expression in an additive and/or synergistic fashion in CLL cells and lymphoid cell lines

Our combined co-IP, western blot and ChIP data for STAT3 suggested it may well function as one of the transcription factors responsible for the activation of IEGs known to promote CLL cell proliferation. However, it is not STAT3 but NF-κB subunits which are thought to be the predominant transcription factor acting on *DUSP2* transcription. Current literature suggests that STAT3-NF-κB crosstalk can synergistically promote gene expression in CLL [111, 112, 258] and we therefore wanted to probe the effects of activating the NF-κB pathway alongside the BCR pathway in our system.

We began by assessing *EGR1* and *DUSP2* gene expression after addition of both CD40L and anti-IgM with the aim of activating both NF-κB subunits and STAT3, in the chosen lymphoid cell lines. We have previously assessed that ramos cells were the strongest anti-IgM responders (Chapter 3 Results 1) and would provide a clear baseline to examine the CD40L effect in IEG expression. Therefore, ramos cells were stimulated with anti-IgM, CD40L or both for 0-90 minutes with samples taken every 15 minutes for gene expression analysis. Samples were lysed for RNA extraction followed by cDNA synthesis and qPCR analysis (Figure 4.7A). The data in ramos cells showed the classical anti-IgM activation of *EGR1* and *DUSP2*, which peaked at 30 minutes and gradually decreased over the 90 minute time-course. CD40L stimulation alone elicited a similar peak expression response to anti-IgM with slightly slower kinetics which peaked at 45 minutes for both genes. Of note, *DUSP2* gene expression showed more than a two-fold increase in the context of CD40L stimulation versus anti-IgM stimulation – lending credence to our hypotheses that *DUSP2* is an NF-κB target gene. When combining anti-IgM and CD40L, we observed an additive (30 mins) and eventually synergistic (45 mins) expression response for both genes which peaked at 45 minutes. Dual stimulation (DS) strongly promoted expression of both genes, in comparison to CD40L alone which had a strong effect on DUSP2 expression only.

Next, we assessed the IEG expression response to CD40L in HBL1 cells (Figure 4.8A-B). In replicate experiments stimulating HBL1 for 60 mins, we observed the same additive effect of CD40L when combined with anti-IgM. As in ramos, *DUSP2* gene expression displayed the greatest synergistical activation from

combining the two stimulants. *EGR1* is less CD40L dependent in HBL1 cells than in ramos cells, whereby dual-stimulation only marginally increased overall *EGR1* gene expression.

Subsequently, we wanted to assess the CD40L effect in CLL cells (Figure 4.9A-D). We took the cells from 3 U-CLL (CLL P4, 5 and 7) and 2 M-CLL patients (CLL P6 and 8) and stimulated them as described above, taking RNA samples at 30 and 60 minutes. In the U-CLL cells, the results were similar to HBL1. The qPCR data for *EGR1* after dual stimulation showed a small additive effect on gene expression at 30 minutes which was lost by 60 minutes. *DUSP2* however, as in HBL1 and ramos cells, showed a strong additive response at 30 and 60 minutes with the addition of CD40L with anti-IgM, and a stronger overall response to CD40L alone (Figure 4.9A). The M-CLL cells showed a typical non-response to anti-IgM but were stimulated by CD40L to levels of gene expression that exceeded the small increase seen by the addition of IgD (Chapter 3 Results 1). After dual-stimulation, marginally lower gene expression was observed in these M-CLL cells (Figure 4.9B). Overall, for both CLL subtypes, *DUSP2* gene expression benefited primarily from the addition of CD40L while *EGR1* remained predominantly anti-IgM dependent (Figure 4.9C-D).

4.3.1 ZIPK inhibition can overcome dual anti-IgM/CD40L stimulation to reduce IEG expression

Having determined that dual anti-IgM/CD40L stimulation could boost IEG expression in CLL and lymphoid cell lines, we wanted to assess if expression could be impacted through pre-treatment with either ibrutinib or the DAPKi. These experiments are particularly important in the context of mechanisms of acquired resistance to ibrutinib such as activating mutations in signalling pathways parallel to the BCR pathway such as the CD40 pathway [143, 146, 147].

We took the cells from 3 U-CLL (CLL P4, 5 and 7) and 2 M-CLL patients (CLL P6 and 8) and pre-treated them with ibrutinib or the DAPKi for 60 minutes. The cells were then stimulated with both anti-IgM and CD40L with samples taken at 30 and 60 minutes for gene expression analysis. The qPCR data reveals that ZIPK inhibition blocked both *EGR1* and *DUSP2* gene expression (Figure 4.10A-B). Both U- and M-CLL cells were affected similarly with all 5 patients showing a complete and significant loss of IEG expression. For the cells pre-treated with ibrutinib, we observed only a partial reduction of IEG expression (Figure 4.10A-

B). In conclusion, while these inhibitors had a completely comparable effect when used on cells which had undergone anti-IgM stimulation alone (Chapter 3 Results 1), ibrutinib could not block dual activation in contrast to DAPKi, which appeared to have a broader repressive potential.

Finally, we took HBL1 cells and pre-treated them with either ibrutinib or the DAPKi. Following this, the cells were stimulated with anti-IgM, CD40L or both and samples were taken at 60 minutes post-stimulation for RNA analysis. For both *EGR1* and *DUSP2*, we observed that the DAPKi could overcome dual anti-IgM/CD40L stimulation while ibrutinib could not, as observed for CLL cells (Figure 4.10C-D). As seen in Chapter 3 Results 1 when comparing CLL to HBL1 cells, ibrutinib was not as effective at preventing IEG expression. CD40L stimulation alone primarily promoted *DUSP2* gene expression, and both inhibitors could moderately reduce this expression – while the DAPKi remains the more effective of the pair.

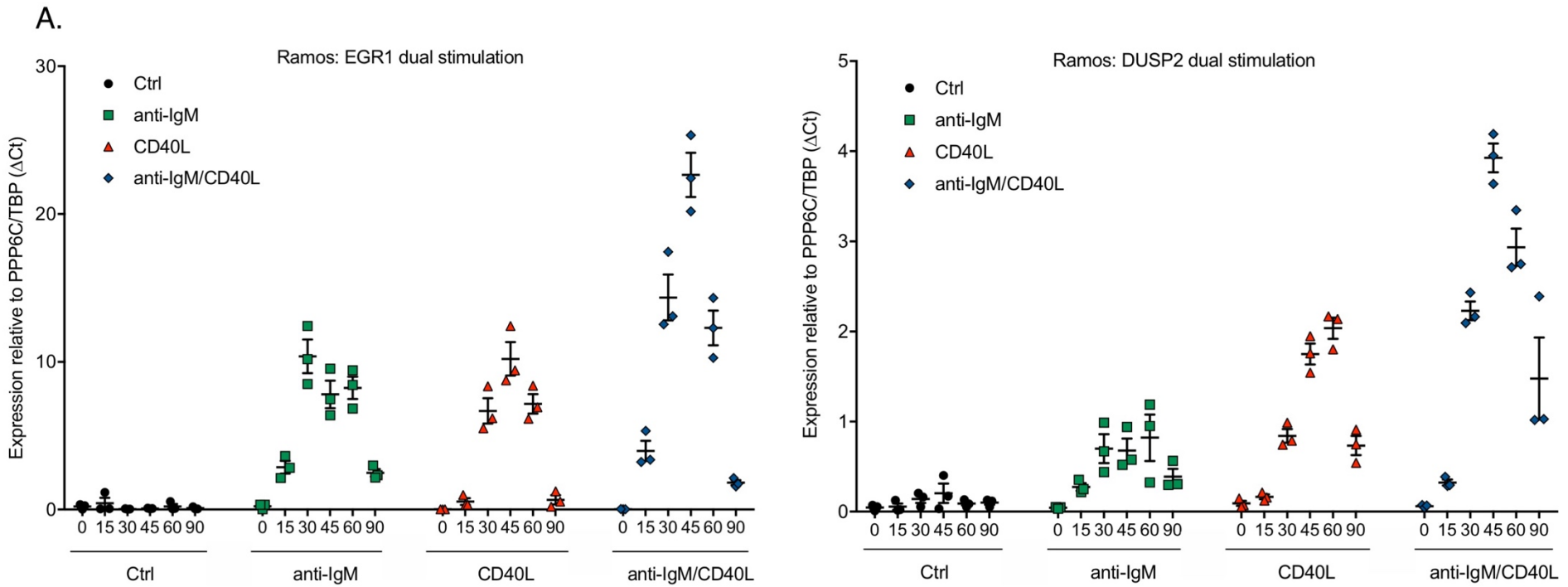

Figure 4.7: Combined anti-IgM/CD40L stimulation increases IEG expression in an additive and/or synergistic fashion in ramos cells. (A) qPCR data analysis for *EGR1* and *DUSP2* gene expression over time (0-90 minutes) in ramos cells stimulated with either anti-IgM, CD40L or both, as indicated. Error bars representative of 3 independent experiments. Expression changes were quantified using the ΔCt method with TBP and PPP6C as control genes.

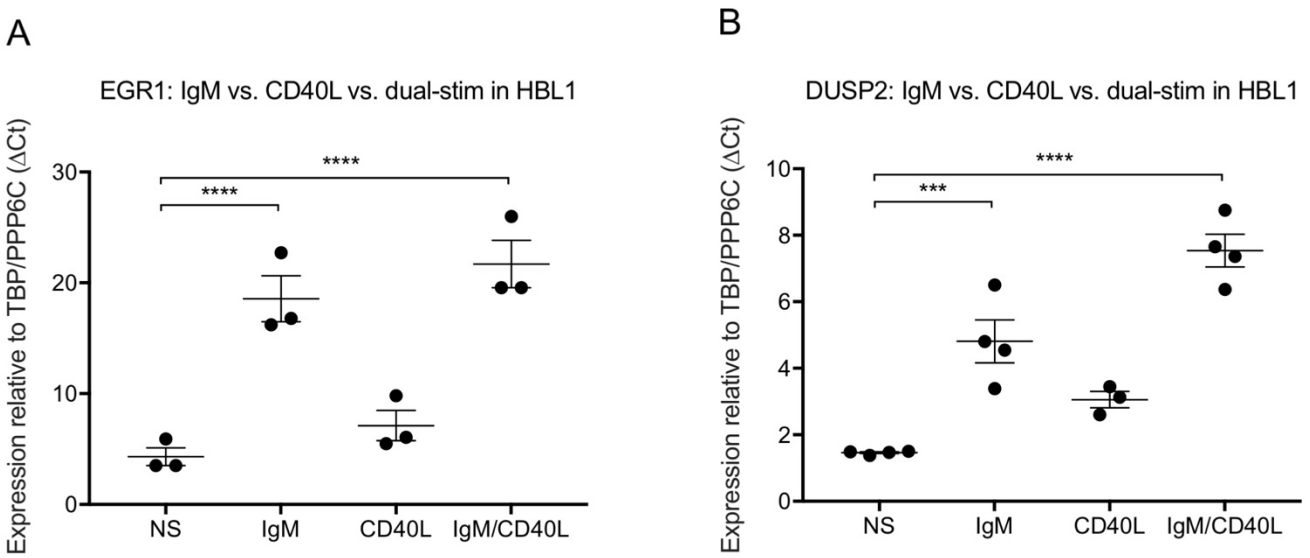

Figure 4.8: Combined IgM/CD40L stimulation increases IEG expression in HBL1 cells. qPCR data analysis for **(A)** *EGR1* and **(B)** *DUSP2* gene expression in HBL1 cells stimulated with either anti-IgM, CD40L or both, as indicated, for 60 minutes. Error bars representative of 3 independent experiments. Expression changes were quantified using the ΔCt method with TBP and PPP6C as control genes. Significant differences calculated using two-way ANOVA followed by Dunnett's multiple comparison test with unstimulated as control. *EGR1* P values = 0.0018 & 0.0000 for no stim vs anti-IgM and anti-IgM/CD40L respectively. *DUSP2* P values = 0.0002 & 0.0002 for the same comparisons.

A

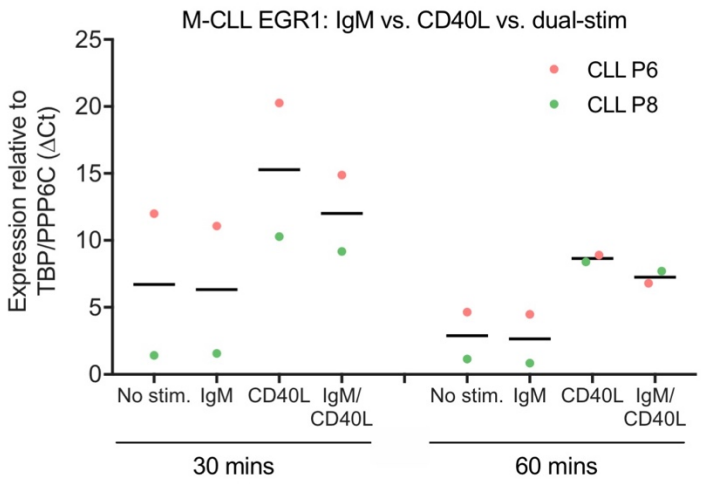
M-CLL EGR1: IgM vs. CD40L vs. dual-stim
Expression relative to TBP/PPP6C (ΔCt)
25
20
15
10
5
0
CLL P6
CLL P8
No stim.
IgM
CD40L
IgM/ CD40L
30 mins
60 mins

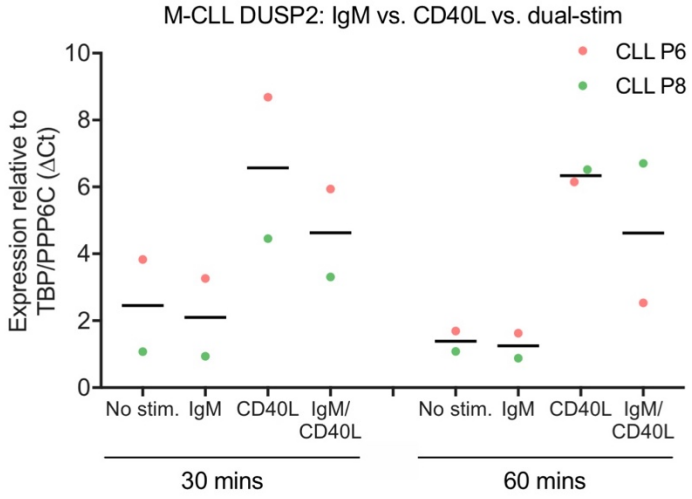
M-CLL DUSP2: IgM vs. CD40L vs. dual-stim
Expression relative to TBP/PPP6C (ΔCt)
10
8
6
4
2
0
CLL P6
CLL P8
No stim.
IgM
CD40L
IgM/ CD40L
30 mins
60 mins

B

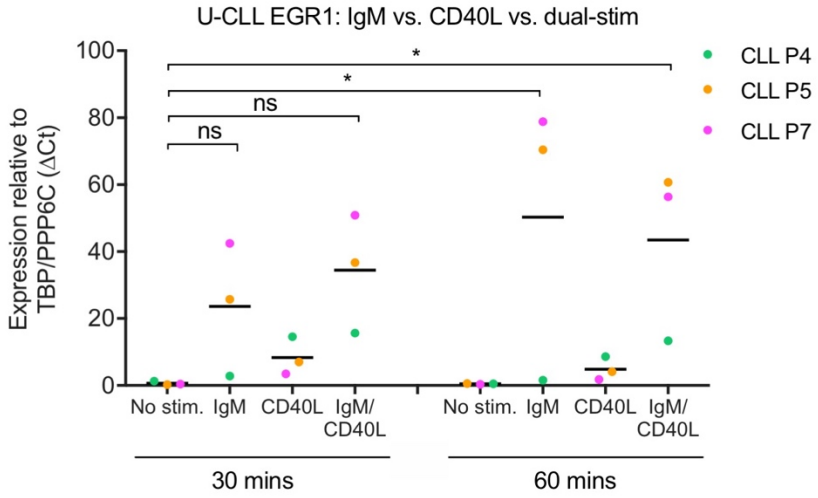
U-CLL EGR1: IgM vs. CD40L vs. dual-stim
Expression relative to TBP/PPP6C (ΔCt)
100
80
60
40
20
0
*
*
ns
ns
CLL P4
CLL P5
CLL P7
No stim.
IgM
CD40L
IgM/ CD40L
30 mins
60 mins

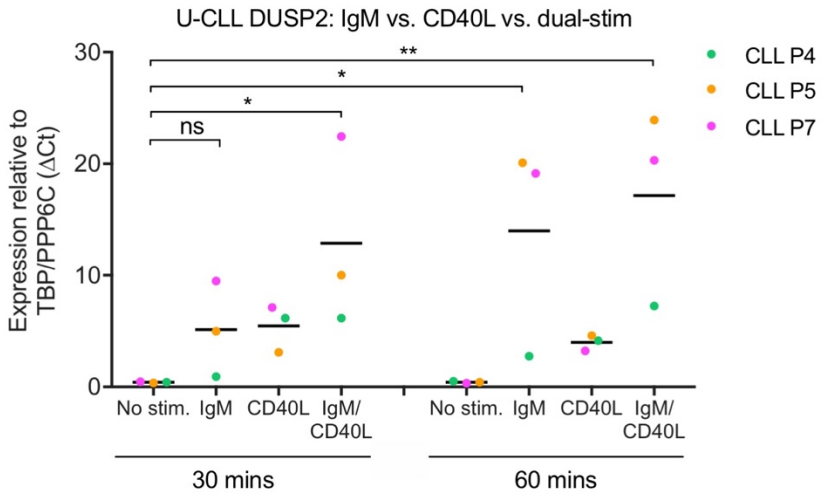
U-CLL DUSP2: IgM vs. CD40L vs. dual-stim
Expression relative to TBP/PPP6C (ΔCt)
30
20
10
0
**
*
*
ns
CLL P4
CLL P5
CLL P7
No stim.
IgM
CD40L
IgM/ CD40L
30 mins
60 mins

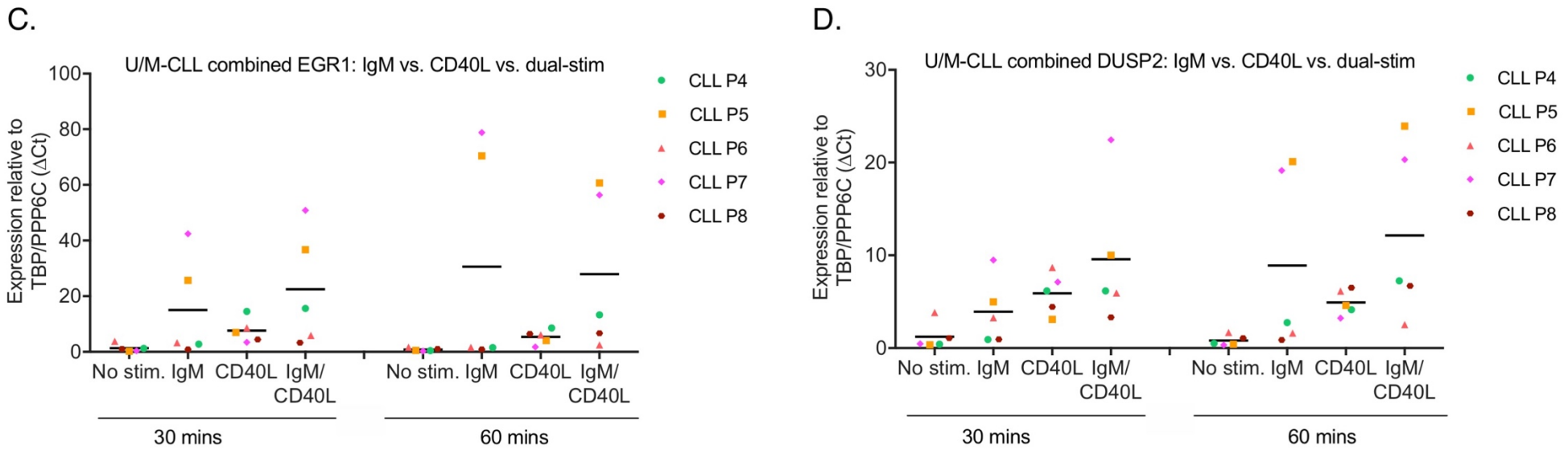

Figure 4.9: Combined IgM/CD40L stimulation increases IEG expression in CLL cells. qPCR data analysis for *EGR1* and *DUSP2* gene expression in **(A)** U-CLL and **(B)** M-CLL cells stimulated with either anti-IgM, CD40L or both, as indicated, for 30-60 minutes. Bars representative of the grand mean. Expression changes were quantified using the ΔCt method with TBP and PPP6C as control genes. Significant differences calculated using two-way ANOVA followed by Dunnett's multiple comparison test with unstimulated as control. *EGR1* P values = 0.4606, 0.1451, 0.0189 & 0.0466 for no stim vs anti-IgM/CD40L (30m), anti-IgM (60m) and anti-IgM/CD40L (60m) respectively. *DUSP2* P values = 0.7479, 0.0398, 0.0236 & 0.0053 for the same comparisons. qPCR data analysis for **(C)** *EGR1* and **(D)** *DUSP2* gene expression in U-CLL/M-CLL cells stimulated with either anti-IgM, CD40L or both, as indicated, for 30-60 minutes. Bars representative of the grand mean. Expression changes were quantified using the ΔCt method with TBP and PPP6C as control genes.

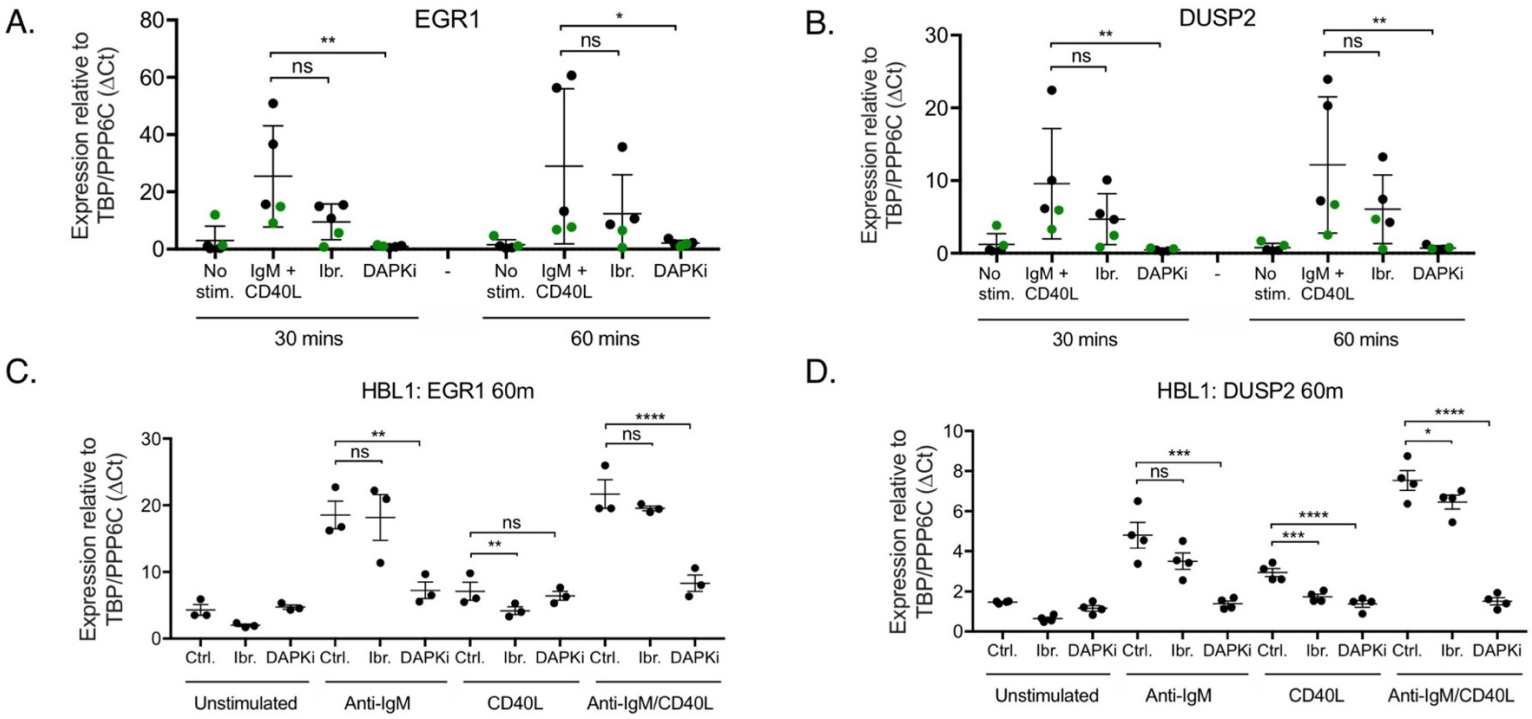

Figure 4.10: ZIPK inhibition can overcome dual anti-IgM/CD40L stimulation, while ibrutinib cannot. qPCR data analysis for *EGR1* and *DUSP2* gene expression in **(A) (B)** U/M-CLL (black circles for U-CLL and green circles for M-CLL) and **(C) (D)** HBL1 cells. Both CLL and HBL1 cells were pre-treated with ibrutinib or DAPKi for 60 mins. CLL cells were then stimulated with anti-IgM/CD40L for 30-60 mins. HBL1 cells stimulated with either anti-IgM, CD40L or both for 60 mins. Bars representative of the grand mean. Expression changes were quantified using the ΔCt method with TBP and PPP6C as control genes. Significant differences calculated using two-way ANOVA followed by Dunnett's multiple comparison test with anti-IgM/CD40L as control. CLL cell statistics: *EGR1* P values = 0.0626, 0.0054, 0.1893 & 0.0245 for anti-IgM/CD40L vs ibrutinib and DAPKi at 30 and 60 minutes, respectively. *DUSP2* P values = 0.1713, 0.0086, 0.1507 & 0.0064 for the same comparisons. HBL1 cell statistics: *EGR1* P values = 0.9960, 0.0058, 0.0069, 0.5620, 0.2339 & 0.0001 for ctrl vs ibrutinib and DAPKi with anti-IgM, CD40L and anti-IgM/CD40L stimulation, respectively. *DUSP2* P values = 0.0599, 0.0002, 0.0004, 0.0001, 0.0383 & 0.0001 for the same comparisons.

4.4 The cellular consequences of dual anti-IgM/CD40L stimulation

We have shown that targeting ZIPK kinase activity prevented the anti-IgM/CD40L-mediated activation of IEGs known to promote CLL cell proliferation, whereas ibrutinib does not.

It has been shown that cooperative/dual stimulation can allow one transcription factor to assist the loading of another onto the chromatin at promoters and/or enhancers to promote synergistic gene expression [259]. In particular, there are genes whose expression has been shown to be enhanced by the cooperative effects of STAT3 and NF-κB subunit p65 (RelA) [259]. As p65 is known to be activated downstream of CD40, we naturally sought to assess whether p65 was playing a role in enhancing the gene expression of our model IEGs in cooperation with STAT3. We initially chose to carry out these experiments in both CLL and ramos cells, selecting ramos as they showed more pronounced IEG activation in response to dual stimulation compared to HBL1. Further, the data from Figure 4.4 showed an increase in phosphorylated STAT3 in response to the DAPKi in ramos cells. In light of this experiment, we wanted to understand if ZIPK inhibition could impact p65-induced transcription in ramos cells; as increased STAT3 phosphorylation was anti-correlated with IEG expression.

4.4.1 Combined anti-IgM/CD40L stimulation increases p65 nuclear localisation

First, we wanted to assess whether p65 was activated in response to anti-IgM, CD40L or, specifically, after dual anti-IgM/CD40L stimulation. P65 migration from the cytoplasm to the nucleus is a hallmark of NF-κB activation as it indicates degradation of the IκB proteins responsible for the cytoplasmic sequestration of p65 [105].

We stimulated ramos cells with either anti-IgM, CD40L or both for 45 minutes (time at which dual stimulation-induced gene expression peaked) and then lysed the cells for nuclear-cytoplasmic separation and western blot. While the levels of cytoplasmic p65 protein remain stable throughout all stimulation conditions, we observed a marked increase in levels of nuclear p65 in response to CD40L stimulation (Figure 4.11A-B). Anti-IgM stimulation alone does very little to increase p65 nuclear localisation, but when combined with CD40L we observed

an additive increase in p65 translocating to the nucleus. These data showed that dual anti-IgM/CD40L stimulation could promote an increase in p65 nuclear localisation.

4.5 The effects of combined anti-IgM/CD40L stimulation on transcription factor binding

We have observed an anti-IgM/CD40L-mediated increase in p65 nuclear localisation (Figure 4.11). In order to determine if this correlated with an increase in p65 recruitment to the *EGR1* and *DUSP2* loci we performed a series of ChIP experiments. Moreover, we wanted to assess whether or not STAT3-DNA binding could be impacted by the addition of CD40L. Our previous STAT3 ChIP data provided a basis for our understanding of how STAT3 could regulate *EGR1*, but were not fully conclusive.

Increasing our understanding of how these transcription factors promote IEG expression in response to anti-IgM and/or CD40L stimulation will help to unravel how repression of ZIPK enzymatic activity in CLL cells can prevent the transcription of these genes. Therefore, the next sections present ChIP-qPCR data for (i) p65 and (ii) STAT3 at the *DUSP2* and *EGR1* loci in turn in both (i) ramos and (ii) CLL cells.

4.5.1 The effects of combined anti-IgM/CD40L stimulation on p65-DNA binding at the DUSP2 locus

First, we wanted to continue our assessment of p65 in response to dual stimulation. We took ramos cells and stimulated them with either anti-IgM, CD40L or both for 45 minutes, taking samples for ChIP analysis at 30 and 45 minutes. We used antibody against p65 to assess binding across both the *EGR1* and *DUSP2* loci.

The ChIP-qPCR data showed a strong p65 binding at the region -0.6 kb upstream from the *DUSP2* TSS when the cells are treated with CD40L or the anti-IgM/CD40L combination (Figure 4.12A-B). The p65 binding increased over time from 30-45 minutes for both CD40L alone and after dual stimulation (3 fold and 2 fold respectively). It is interesting to note the correlation between this data and the p65 nuclear localisation, specifically: anti-IgM stimulation alone had no effect

on p65-DNA binding at the *DUSP2* promoter, but when used in conjunction with CD40L we saw a strong synergistic effect – also as reflected in the gene expression. Notably, this binding enrichment (almost 40 fold over the CTCF controls) was far stronger than any of our previous anti-IgM induced STAT3 binding and highlights the NF-κB-driven nature of *DUSP2*. We concluded that increased nuclear localisation correlated with increased p65-DNA binding and upregulation of *EGR1* and *DUSP2* gene expression.

Having determined the effects of dual anti-IgM/CD40L stimulation on ramos cells we moved to assess the effect of the same activation in U-CLL cells. U-CLL cells (patient P7) were either pre-treated with ibrutinib, the DAPKi or neither and then stimulated with anti-IgM/CD40L for 45 minutes. The ChIP-qPCR data showed similar binding of p65 to the region -0.6 kb from the *DUSP2* TSS (Figure 4.12C). We first observed that, in CLL, p65 was bound prior to anti-IgM/CD40L stimulation. Further, p65 binding after dual stimulation was considerably weaker than that observed in ramos cells. This suggested that the activation of the NF-κB pathway may be less robust in CLL cells after dual stimulation compared to the ramos cell line, or that the kinetics of p65-binding are considerably slower. The ChIP-qPCR data also showed that while the DAPKi had little effect on p65 binding at the *DUSP2* promoter, we observed a pronounced increase in response to ibrutinib treatment. While it is difficult to conclude with certainty the reason behind this increase, we hypothesised that ibrutinib-mediated prevention of STAT3-binding could shift the transcription factor balance, promoting an alternative p65-mediated increase in *DUSP2* gene expression.

However, we must take into account the potential technical limitations of performing ChIP experiments in primary CLL cells compared to cell lines. Such limitations included the limited number of primary CLL cells which were available for these analyses, promoting a lack of reproducibility for these data (a point which is relevant to all the CLL ChIP data in this chapter). Further, when working with a primary cell line which is adverse to cell culture, there is an inherent likelihood that the cells which are harvested for ChIP experiments will not be as healthy as those from a traditional, immortalised cell line. Indeed, without the ability to reproduce these data in other patients, we cannot say with certainty why ibrutinib promotes p65 binding or why there is a discord between the data from ramos cells above (Figure 4.12A-B). There is particularly interest in repeating this experiment with the cells from those patients who are resistant to ibrutinib to assess whether or not long-term shutdown of the BCR pathway can promote the activation of alternative transcription factors such as p65.

4.5.2 The effects of combined anti-IgM/CD40L stimulation on p65-DNA binding at the *EGR1* locus

In addition to examining the dynamics of p65-DNA binding at the *DUSP2* locus, we also used a series of primers in and around the *EGR1* locus to assess p65 binding at this IEG.

Ramos cells were treated with either anti-IgM and/or CD40L for 60 minutes and prepared for ChIP analysis with antibodies against p65. In replicate experiments we saw some variation in p65 binding at the *EGR1* promoter. Firstly, the majority of p65 binding at the *EGR1* locus was around the -1.0 and 1.3 kb regions upstream of the TSS (Figure 4.13A-C) – the same regions where we saw STAT3 binding under anti-IgM stimulation. This correlation suggests these regions may contain some cis-regulatory elements which are important to *EGR1* expression. In the first experiment, we saw comparable levels of p65 enrichment at the regions -1.3 and -1.0 kb from the TSS for all conditions, including without stimulation, and a CD40L-dependent enrichment at the region -0.4 kb from the TSS (Figure 4.13A). Our second experiment compared unstimulated cells with dual anti-IgM/CD40L stimulated cells (Figure 4.13B). In this experiment, for similarities, we saw a 3-fold increased stimulation-dependent response in p65-DNA binding at the -1.0 kb region and further, weaker, binding at the +3.8 kb region or at the 3' end of the gene. However we no longer observed the CD40L-dependent enrichment at the -0.4 kb region.

Finally, we took the CLL cells from a U-CLL patient (CLL P7) and prepared them for ChIP analysis. The cells were either pre-treated with ibrutinib, the DAPKi or neither and then stimulated with anti-IgM/CD40L for 45 minutes (Figure 4.13C). The ChIP-qPCR data for CLL P7 was consistent with our *DUSP2* CLL ChIP data (Figure 4.13A) in that we observed p65 bound at the -1.3 kb region independently of anti-IgM/CD40L stimulation. Ibrutinib was able to prevent this binding while the DAPKi did not – suggesting the DAPKi mechanism of action in preventing p65-mediated IEG expression was not outright linked to preventing p65 binding.

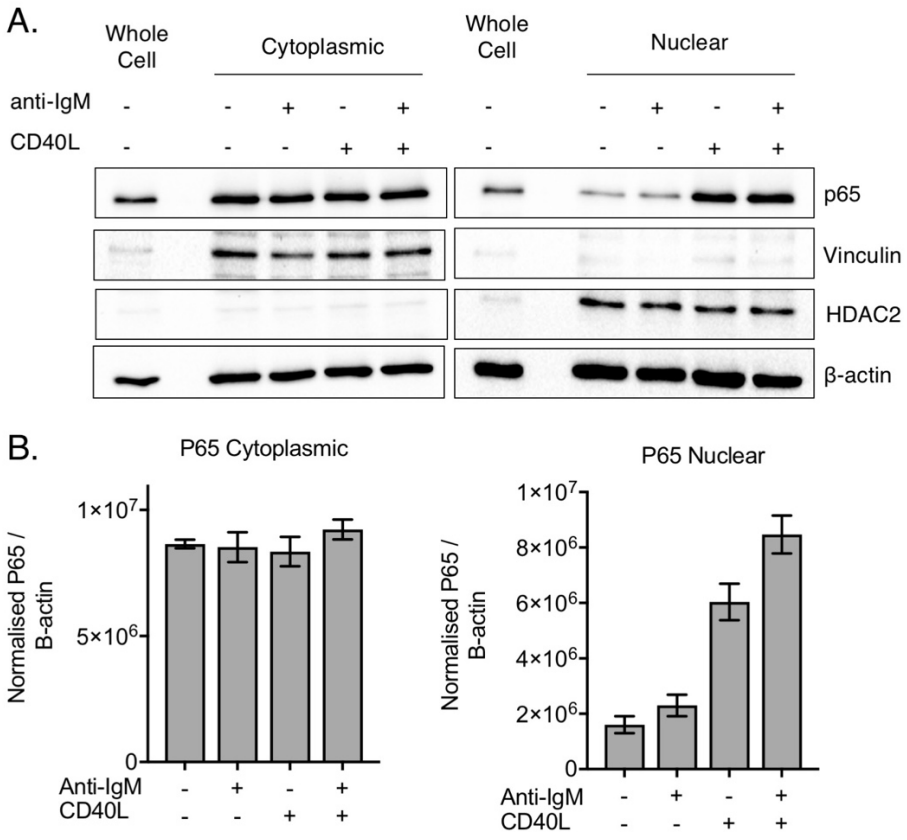

Figure 4.11: Combined anti-IgM/CD40L stimulation increases p65 nuclear localisation. (A) cytoplasmic and nuclear extracts from ramos cells were subjected to SDS-PAGE for western blot analysis. Cells were stimulated for 1 hour with either anti-IgM, CD40L or both as indicated. **(B)** HDAC2 and vinculin were used as loading controls for cytoplasmic and nuclear extracts respectively and for normalisation with Image Lab software (below). Error bars from 2 representative experiments.

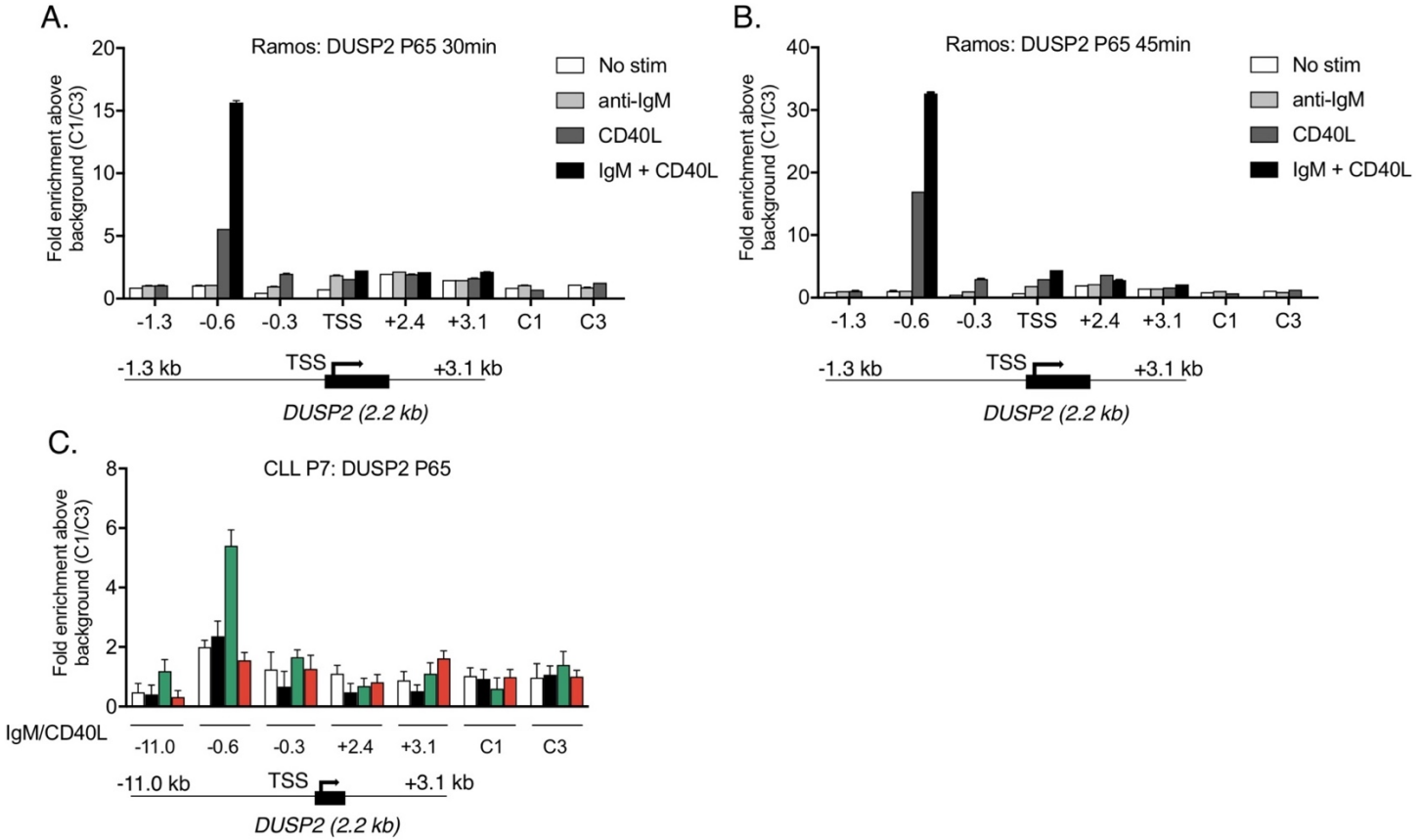

Figure 4.12: The effects of combined IgM/CD40L stimulation on p65 *DUSP2* DNA binding. ChIP-qPCR data assessing levels of p65-binding across the *DUSP2* locus. Ramos cells were stimulated with anti-IgM, CD40L or both and samples were taken for ChIP analysis at **(A)** 30 and **(B)** 45 minutes. **(C)** CLL cells were pre-treated with either 1 μM ibrutinib (green) or 25 μM DAPKi (red) for 60 mins as indicated and then stimulated with combined anti-IgM/CD40L for 45 minutes. The values on the x axis refer to specific gene regions relative to the transcription start site (TSS) in kilobases (kb) as indicated on the gene schematics below (not to scale). CTCF1/3 (C1/C3) were used as negative control regions which are not indicated on the gene schematics. Error bars correspond to variations in the ChIP-qPCR repeats.

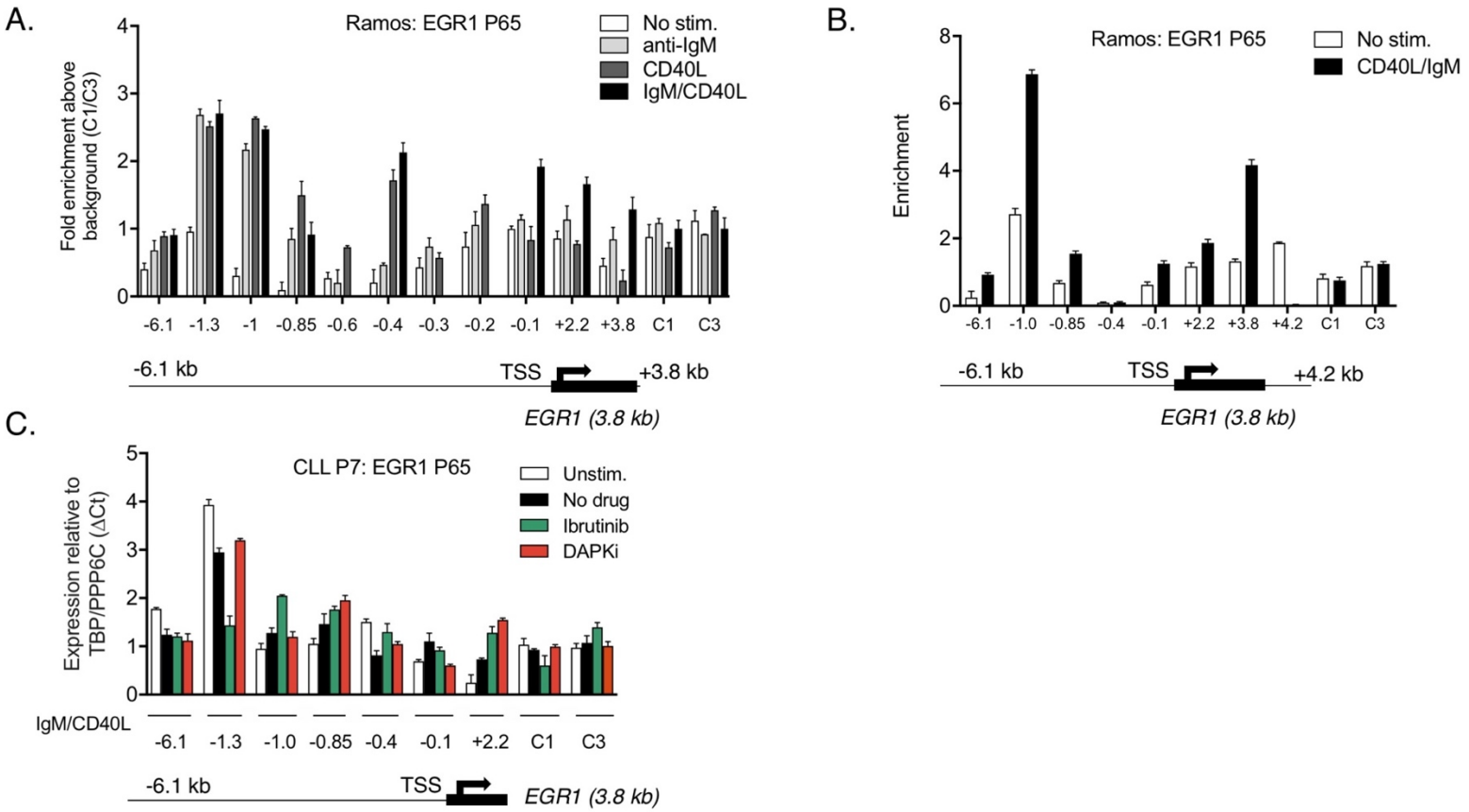

Figure 4.13: The effects of combined IgM/CD40L stimulation on p65 *EGR1* DNA binding. ChIP-qPCR data assessing levels of p65-binding across the *EGR1* locus. **(A) (B)** Ramos and **(C)** CLL cells were stimulated with anti-IgM, CD40L or both for 45 minutes. CLL cells were pre-treated with either 1 μM ibrutinib (green) or 25 μM DAPKi (red) for 1 hour as indicated before anti-IgM/CD40L stimulation. The values on the x axis refer to specific gene regions relative to the transcription start site (TSS) in kilobases (kb) as indicated on the gene schematics below (not to scale). CTCF1/3 (C1/C3) were used as negative control regions which are not indicated on the gene schematics. Error bars correspond to variations in the ChIP-qPCR repeats.

4.5.3 The effects of combined anti-IgM/CD40L stimulation on STAT3-DNA binding at the *EGR1* locus

To assess the effect of combined anti-IgM/CD40L stimulation on STAT3-DNA binding we took a similar approach as to that described above for p65. We initially took ramos cells and stimulated them with either anti-IgM, CD40L or both for 45 minutes taking samples for ChIP analysis at 30 and 45 minutes. We used antibodies against STAT3, STAT3-Y705-P and STAT3-S727-P to assess binding across the *EGR1* locus. We chose to include both phosphorylation sites as while S727-P is known to activate transcription in CLL, Y705-P is more often phosphorylated in correlation with STAT3 activity in other diseases/tissues.

The ChIP-qPCR data showed that at 30 minutes post-stimulation STAT3 and STAT3-Y705-P were bound -1.0 kb from the *EGR1* TSS independent of anti-IgM and CD40L stimulation while STAT-S727-P was inducible at this region (-1.0 kb) and at the regions -0.4 and -0.2 kb from the TSS (Figure 4.14A-C).

Next, we again took the cells from U-CLL patient 7 and prepared them for ChIP analysis. The cells were either pre-treated with ibrutinib, the DAPKi or neither and then stimulated with anti-IgM and CD40L for 45 minutes (Figure 4.15A-B). As seen in the ramos cells, STAT3 appeared to be present at the region -1.3 kb from the TSS prior to stimulation and was not inducible while STAT3-S727-P recruitment increased after dual anti-IgM/CD40L stimulation. Both ibrutinib and DAPKi treatment inhibited the recruitment of STAT3-S727-P (Figure 4.15B). These data suggested that STAT3-S727 phosphorylation played an important role in CLL cell transcriptional activation and that its targeting at IEG promoters could be prevented by ibrutinib and the DAPKi. However, these data must be considered with our observations for p65 binding at the *DUSP2* promoter (Figure 4.12C). Here, we observed a strong increase in p65 recruitment to the region -0.6 kb upstream from the *DUSP2* TSS in the presence of ibrutinib suggesting the loss of BTK-mediated STAT3 activation could shift the balance of key transcription factors in CLL and promoted compensation from other transcriptional activators such as p65.

4.5.4 The effects of combined anti-IgM/CD40L stimulation on STAT3-DNA binding at the *DUSP2* locus

While we have shown that combined anti-IgM/CD40L stimulation predominantly induces p65 DNA-binding to the *DUSP2* promoter, we sought to also assess STAT3-binding for comparison. We previously analysed STAT3 binding to the *DUSP2* locus in CLL cells (P3 and P5) in the context of anti-IgM stimulation alone (see Figure 4.5 & Figure 4.6) and the data were not particularly clear. We stimulated ramos cells with both anti-IgM and CD40L and prepared them for ChIP analysis using antibodies against STAT3 and STAT3-S727-P (Figure 4.16A-B). The ChIP-qPCR revealed that in the ramos cells the majority of STAT3 and phosphorylated STAT3 was present independently of stimulation all across the gene body (regions +2.4 and +3.1 kb downstream of the TSS). However, at the promoter region -0.6 kb upstream of the TSS, dual anti-IgM/CD40L stimulation increased the level of phosphorylated STAT3-S727. Noting the data from Figure 4.12 in which dual anti-IgM/CD40L stimulation induced a large increase in p65 binding at the -0.6 kb region, the presence of STAT3 in this region both with and without stimulation suggested evidence for the notion of one transcription factor assisting the loading of another [259].

Next, and in order to directly compare the data for STAT3-binding in CLL cells at the *DUSP2* locus under anti-IgM stimulation alone, we took cells from a U-CLL patient (CLL P7) and prepared them for ChIP analysis (Figure 4.17A-B). The ChIP-qPCR data in CLL provided some differences and some similarities to that observed in ramos. Of the similarities, we observed the same lack of total STAT3 before stimulation at the -0.6 kb promoter region and demonstrated similarly inducible STAT3-S727-P. Here, addition of both stimulating agents caused an increase in the DNA binding of the phosphorylated form of the protein. The main difference between ramos and CLL in this experiment, is that we did not observe STAT3 or STAT3-S727-P bound in the absence of stimulation. We also observed an increase in STAT3-S727-P binding within the gene body and 5' regions after dual stimulation. The observed STAT3-S727-P binding after stimulation could be prevented by either inhibitor (Figure 4.17B). This is similar to the observations at the *EGR1* promoter, whereby both inhibitors could efficiently prevent STAT3-S727-P binding at the 1.3 kb region upstream of the *EGR1* TSS (Figure 4.15B).

4.6 The effects of combined anti-IgM/CD40L stimulation on H3T6-P and H3T11-P deposition at IEG loci

We have assessed the effect of combining anti-IgM and CD40L stimulation on expression of IEGs as well as the DNA-binding of the proteins responsible for their transcription. ZIPK inhibition could reliably prevent expression of *EGR1* and *DUSP2* in CLL cells after BCR cross-linking and/or CD40 activation (Figure 4.10). In some cases, ZIPK inhibition could also reduce transcription factor binding i.e. p65 at the DUSP promoter (Figure 4.12C) and STAT3-S727-P at the *EGR1* (Figure 4.15B) and *DUSP2* promoters (Figure 4.16D). We next wanted to determine whether or not these effects were linked to ZIPKs function as a histone kinase by assessing the levels of H3T6-P and H3T11-P in the context of dual anti-IgM and CD40L stimulation.

Ramos cells were stimulated with anti-IgM and/or CD40L for 45 minutes and prepared for ChIP analysis using antibodies against both histone marks (Figure 4.18A-B). The ChIP-qPCR data showed mixed synergy between the two stimulants. For H3T6-P, the regions +3.8 kb from the *EGR1* TSS and -0.6/+2.4/+3.1 kb from the *DUSP2* TSS showed increased histone phosphorylation in the context of dual anti-IgM/CD40L stimulation. However the H3T6-P data for *DUSP2* were difficult to interpret due to the low levels of enrichment. For H3T11-P, we observed histone phosphorylation in the gene body after anti-IgM stimulation alone (region +2.2 kb) and accumulation in the 3' end of the gene (region +3.8 kb) after CD40L addition. For *DUSP2*, H3T11-P placement across the entire locus consistently required the addition of CD40L.

Finally, HBL1 cells were prepared for ChIP after pre-treatment with ibrutinib, the DAPKi or neither for 60 minutes and then stimulated with both anti-IgM and CD40L for 45 minutes (Figure 4.19A-B). The ChIP-qPCR data showed that under dual stimulation conditions the DAPKi is generally more effective at preventing H3T6-P and H3T11-P deposition, especially at the regions where the histone phosphorylation is strongest e.g. *EGR1* +3.8 kb and *DUSP2* -0.6/-0.3 kb.

It is interesting to note the effect of ibrutinib at the *DUSP2* promoter region (-0.6 kb), where we observed that the drug promoted phosphorylation of both histone marks (Figure 4.19B). The appearance of activatory histone phosphorylation after drug treatment could potentially be linked with the effect ibrutinib had on p65-

binding at this region in CLL whereby the inhibitor appeared to activate alternate transcription factors as a result of shutting off those mediated by BTK.

Taken together, we showed that while ibrutinib is effective at preventing STAT3 DNA binding and histone modifications at the *EGR1* locus, it may have a tendency to shift the transcriptional balance. This is particularly true for the NF-κB mediated *DUSP2*, where treatment with the drug increased histone deposition and p65 binding at the *DUSP2* promoter. These data could help us to understand why ibrutinib was ineffective against anti-IgM/CD40L-mediated IEG expression while the DAPKi appears repress both signalling pathways.

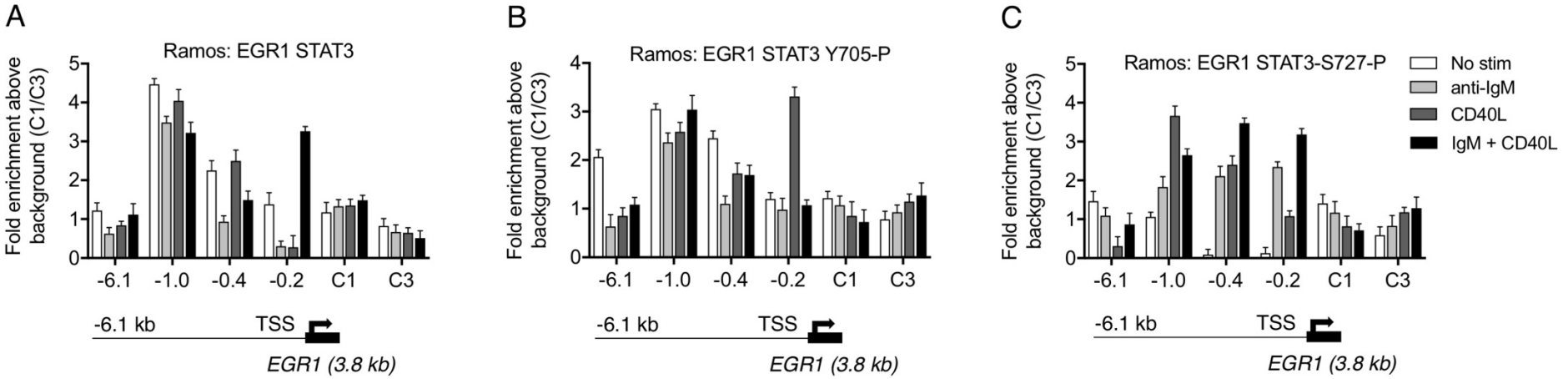

Figure 4.14: The effects of combined IgM/CD40L stimulation on STAT3 *EGR1* DNA binding. ChIP-qPCR data assessing levels of **(A)** STAT3, **(B)** STAT3 Y705-P and **(C)** STAT3 S727-P in ramos cells at the *EGR1* gene locus at 30 minutes post stimulation with either anti-IgM, sCD40L or both, as indicated. The values on the x axis refer to specific gene regions relative to the transcription start site (TSS) in kilobases (kb) as indicated on the gene schematics below (not to scale). CTCF1/3 (C1/C3) were used as negative control regions which are not indicated on the gene schematics. Error bars correspond to variations in the ChIP-qPCR repeats.

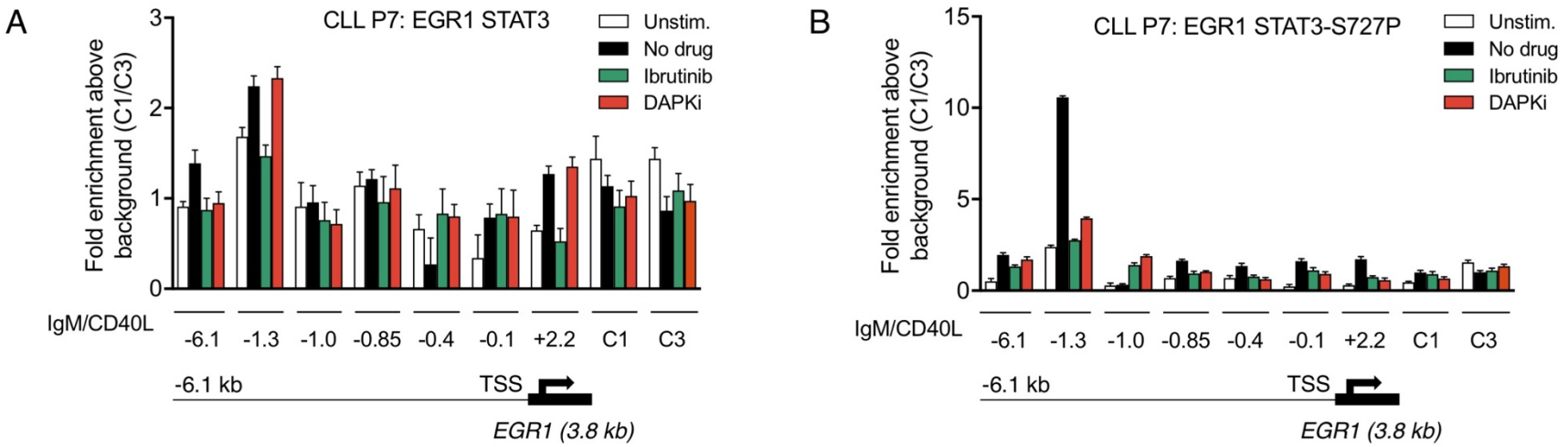

Figure 4.15: The effects of combined IgM/CD40L stimulation on STAT3 *EGR1* DNA binding. ChIP-qPCR data assessing levels of **(A)** STAT3 and **(B)** STAT3 S727-P binding across the *EGR1* locus. CLL cells were pre-treated with either 1 μM ibrutinib (green) or 25 μM DAPKi (red) for 60 mins as indicated before stimulation with both anti-IgM/CD40L for 45 mins. The values on the x axis refer to specific gene regions relative to the transcription start site (TSS) in kilobases (kb) as indicated on the gene schematics below (not to scale). CTCF1/3 (C1/C3) were used as negative control regions which are not indicated on the gene schematics. Error bars correspond to variations in the ChIP-qPCR repeats.

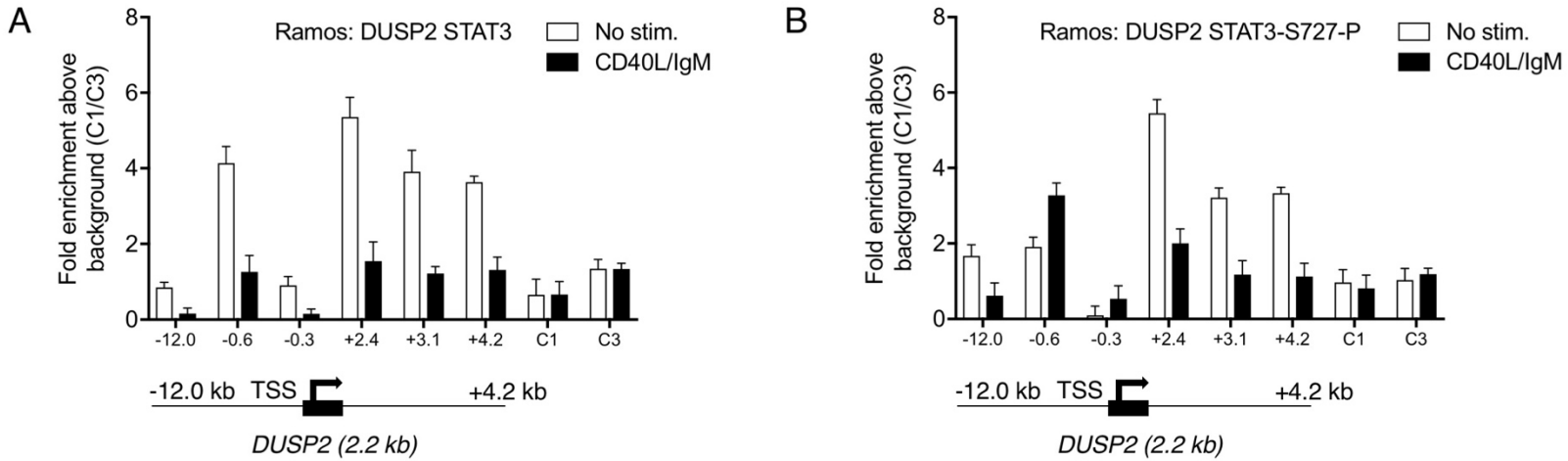

Figure 4.16: The effects of combined IgM/CD40L stimulation on STAT3 *DUSP2* DNA binding. ChIP-qPCR data assessing levels of **(A)** STAT3 and **(B)** STAT3 S727-P binding across the *DUSP2* locus. Ramos cells were stimulated with both anti-IgM/CD40L for 45 mins. The values on the x axis refer to specific gene regions relative to the transcription start site (TSS) in kilobases (kb) as indicated on the gene schematics below (not to scale). CTCF1/3 (C1/C3) were used as negative control regions which are not indicated on the gene schematics. Error bars correspond to variations in the ChIP-qPCR repeats.

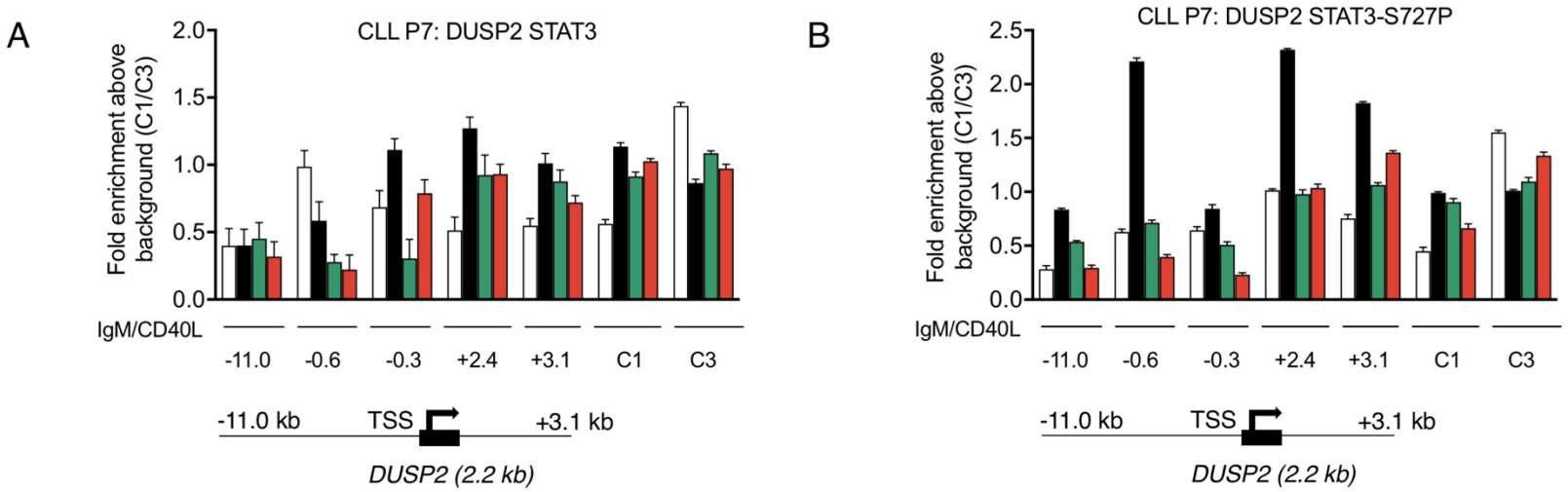

Figure 4.17: The effects of combined IgM/CD40L stimulation on STAT3 *DUSP2* DNA binding. ChIP-qPCR data assessing levels of **(A)** STAT3 and **(B)** STAT3 S727-P binding across the *DUSP2* locus. CLL cells were pre-treated with either 1 μM ibrutinib (green) or 25 μM DAPKi (red) for 1 hour as indicated and then stimulated with both anti-IgM/CD40L for 45 mins. The values on the x axis refer to specific gene regions relative to the transcription start site (TSS) in kilobases (kb) as indicated on the gene schematics below (not to scale). CTCF1/3 (C1/C3) were used as negative control regions which are not indicated on the gene schematics. Error bars correspond to variations in the ChIP-qPCR repeats.

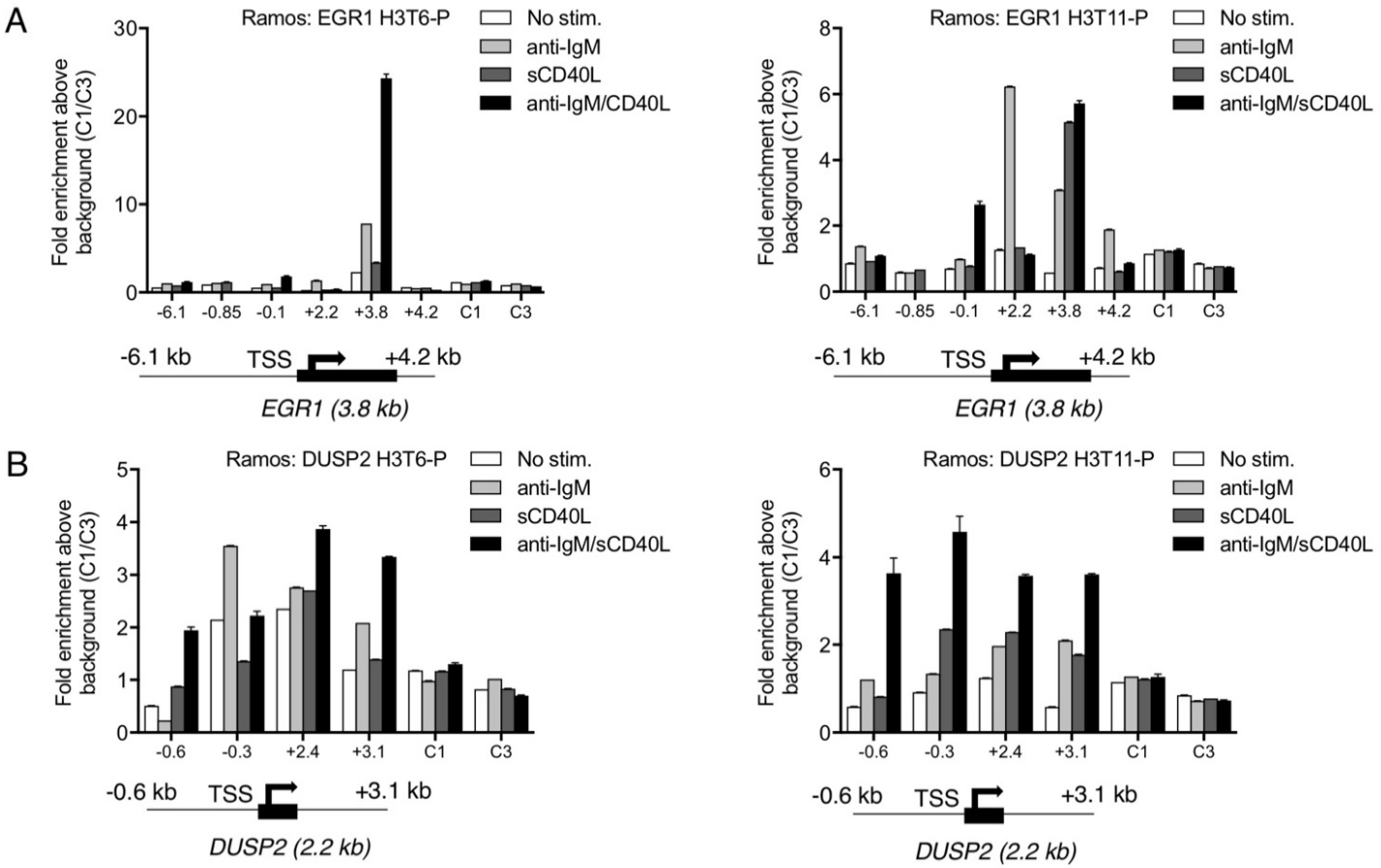

Figure 4.18: Comparing anti-IgM and sCD40L stimulation on the deposition of H3T6-P and H3T11-P at IEG loci in ramos cells. ChIP-qPCR data assessing levels of H3T6-P and H3T11-P at the **(A)** *EGR1* and **(B)** *DUSP2* gene loci. Ramos cells were treated with either anti-IgM, CD40L or both as indicated for 45 mins. The values on the x axis refer to specific gene regions relative to the transcription start site (TSS) in kilobases (kb) as indicated on the gene schematics below (not to scale). CTCF1/3 (C1/C3) were used as negative control regions which are not indicated on the gene schematics. Error bars correspond to variations in the ChIP-qPCR repeats.

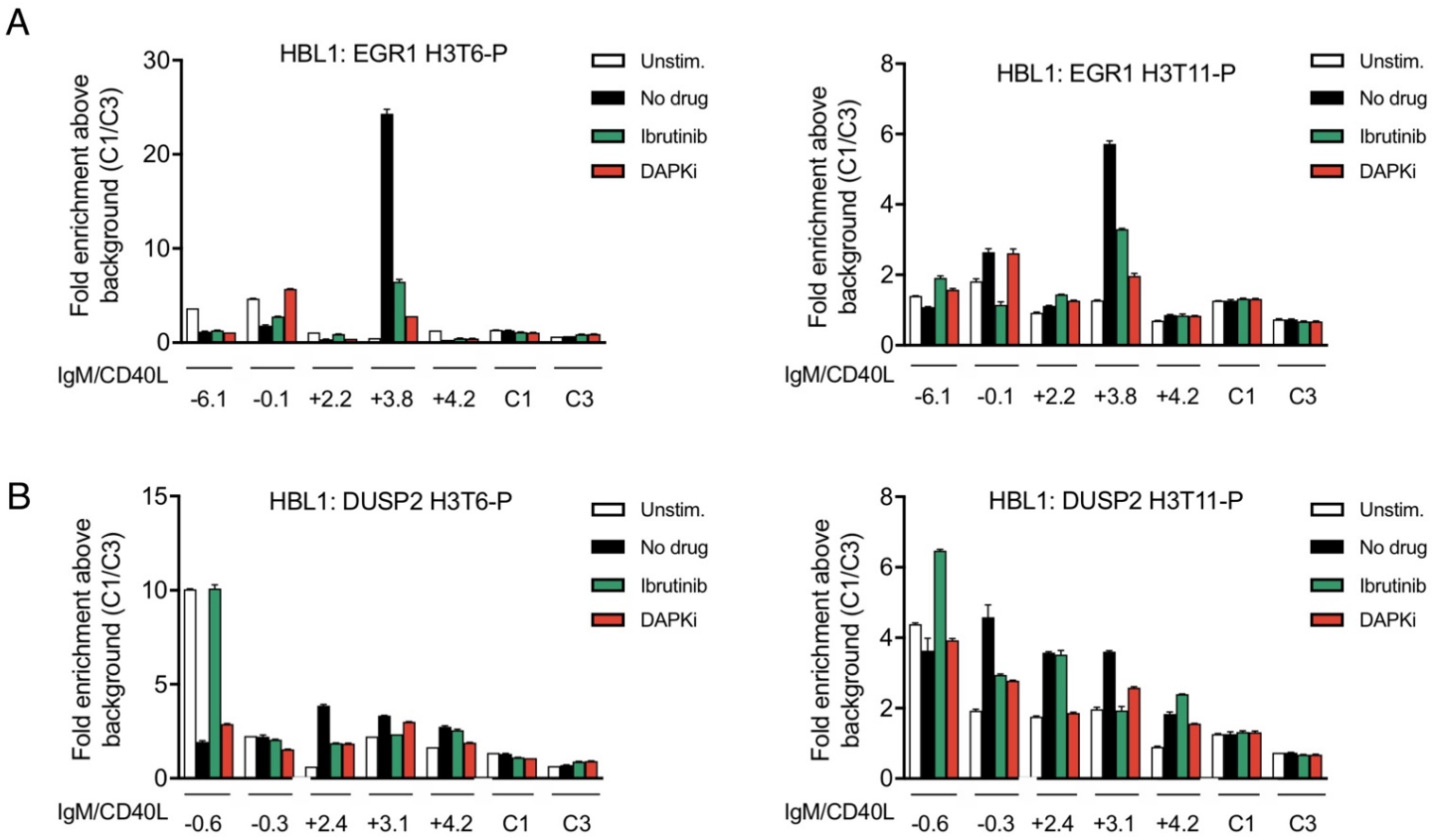

Figure 4.19: The effects of dual anti-IgM/CD40L stimulation on H3T6-P and H3T11-P histone modifications in HBL1 cells. ChIP-qPCR data assessing levels of H3T6-P and H3T11-P at the **(A)** *EGR1* and **(B)** *DUSP2* gene loci. HBL1 cells were pre-treated with either 1 μM ibrutinib (green) or 25 μM DAPKi (red) for 1 hour as indicated before stimulation with combined anti-IgM/CD40L for 45 minutes. The values on the x axis refer to specific gene regions relative to the transcription start site (TSS) in kilobases (kb) as indicated on the gene schematics below (not to scale). CTCF1/3 (C1/C3) were used as negative control regions which are not indicated on the gene schematics. Error bars correspond to variations in the ChIP-qPCR repeats.

Chapter 5 Results 3: The role of ZIPK in RNA polymerase II recruitment and pre-mRNA processing

In chapter 2, we examined the effects and implications of ZIPK and its inhibition on gene expression via the analysis of transcription factor binding to cis-regulatory elements in response to BCR cross-linking and CD40 activation, specifically within the loci of our studied IEGs. While transcription is not necessarily correlated with transcription factor recruitment, its examination can help us to understand this key aspect of the cascade of events necessary for controlling gene expression. Additionally, transcription factor binding to cis-regulatory elements is usually associated with the recruitment of RNA polymerase II (RNA pol II), one of the three eukaryotic RNA polymerases responsible for the transcription of messenger RNAs [260]. RNA pol II recognises the promoter region upstream of the transcription start site of a gene, unwinds the DNA duplex and initiates transcription of RNA. Subsequently, the elongation complex proceeds through the gene before dissociating via a termination signal, releasing the transcribed RNA for pre-mRNA processing [260].

The stages of RNA pol II-mediated transcription are marked by phosphorylation changes to the carboxyl-terminal domain (CTD) of RNA pol II. RNA pol II CTD is observed to be phosphorylated at serine 5 (RNA pol II S5-P) at the 5' end of genes and is associated with transcription initiation [190, 261]. Serine 5 phosphorylation is gradually lost as RNA pol II elongates through the gene, replaced with CTD phosphorylation at serine 2 (RNA pol II S2-P). RNA pol II S2-P is indicative of active transcription as the polymerase elongates through the gene body [190, 261].

Having examined the transcription factors involved in *EGR1* and *DUSP2* transcription we wanted to move further down the transcription cascade in order to more clearly understand the activation of our model IEGs. Therefore, we decided to assess the recruitment of RNA pol II and RNA pol II S2-P to the locus of each gene and examine and compare the effects of ibrutinib and DAPKi treatment on such recruitment. These question are particularly interesting in the context of immediate early gene expression: IEGs show rapid pre-mRNA induction and RNA pol II recruitment compared to secondary/delayed response genes [193]. In fact, it has been suggested that RNA pol II may be poised at the promoter regions of some IEGs before cellular stimulation and transcription factor

activation in order to provide a 'ready-to-go' RNA pol II [191-193]. Further, IEGs have a distinct genomic architecture and chromatin structure to facilitate their rapid transcription characterised by bivalent promoters poised for rapid activation [191].

5.1 RNA polymerase II recruitment to IEG loci

We have now investigated the recruitment of transcription factors to the promoter regions of *EGR1* and *DUSP2* in response to BCR activation and observed mixed response to the addition of ibrutinib or DAPKi treatment (see Chapter 4 Results 2). In order to fully understand the transcription and activation of our model IEGs, we sought to profile RNA pol II and RNA pol II S2-P recruitment in CLL cells following anti-IgM crosslinking of the BCR.

The cells from a U-CLL patient (P3) were stimulated with anti-IgM for 30 minutes to activate transcription. These cells were then lysed and prepared for ChIP analysis with antibodies against RNA pol II (total RNA pol II – will recognise all forms of the enzyme) and RNA pol II S2-P. Broadly, we expected to observe total RNA pol II localised around the gene promoters/upstream of the TSS and RNA pol II S2-P in the gene bodies as an indication of active transcriptional elongation.

The ChIP-qPCR data for RNA pol II at the *EGR1* locus post anti-IgM stimulation showed recruitment of the polymerase to the regions -6.1, -1.0 and -0.85 kb upstream of the TSS as well as +2.2 kb downstream of the TSS (Figure 5.1A). All of the regions downstream of the TSS where we observed recruitment of the polymerase were regions which we have previously identified and associated with transcription factor binding (particularly STAT3 – see Figure 4.5). The ChIP-qPCR data for the elongating polymerase (S2-P) showed recruitment primarily in the gene body (+2.2 and +3.8 kb) and 3' of the TES (+4.2 kb) with additional recruitment upstream of the TSS, closer to the promoter region (-1.0 kb) (Figure 5.1A). The data for *DUSP2* were similar (Figure 5.1B): total RNA pol II was recruited primarily upstream of the TSS (-0.3 kb) and receded along the gene body, whilst elongating RNA pol II S2-P was bound all across the gene body (+2.4 kb) and 3' of the TES (+3.1 and 4.2 kb). Enrichment of RNA pol II downstream of the TES could be attributed to a variety of technical or biological factors. In analysing RNA pol II recruitment by ChIP the chromatin sample could contain large pieces of DNA meaning there is potential for detecting RNA pol II transcribing nearby genes. Additionally, termination of elongating RNA pol II can

occur hundreds of bases downstream of the 3' end site [262]. Taken together these data exemplified classical transcription of our model IEGs.

5.1.1 The effects of combined dual anti-IgM/CD40L stimulation on RNA polymerase II recruitment to IEG loci

Having determined that anti-IgM stimulation of the BCR promotes a classical RNA pol II response at the *EGR1* and *DUSP2* loci, we sought to assess the effects of combining dual anti-IgM/CD40L stimulation on the transcriptional activation of both genes.

The cells from a U-CLL patient (P3) were stimulated with anti-IgM and CD40L for 30 minutes to activate transcription. These cells were then lysed and prepared for ChIP analysis with antibodies against RNA pol II and RNA pol II S2-P. The ChIP-qPCR data showed a strong recruitment of RNA pol II to the *EGR1* and *DUSP2* promoter regions (see *EGR1* -1.3, -1.0, -0.85, -0.4 kb and *DUSP2* -0.6, -0.3, -0.1 kb) and RNA pol II S2-P elongating in the gene bodies (see *EGR1* +2.2, +3.8, +4.2 kb and *DUSP2* +3.1, +4.2 kb) after stimulation (Figure 5.2A-B). These data showed accumulating RNA pol II S2-P at, and beyond, the 3' end of both genes. Further, it is worth noting the enrichment values in this experiment were significantly higher when compared to anti-IgM stimulation alone for the same sample (see Figure 5.1). While this could be attributed to variable experimental response to stimuli, it suggested a synergistic impact of combining dual anti-IgM/CD40L on transcriptional activation of *EGR1* and *DUSP2*.

These data suggested that a poised RNA pol II was present at IEG promoters prior to stimulation and demonstrated textbook recruitment of the polymerase to gene promoter regions followed by RNA pol II S2-P elongating through the gene body and 3' end of the gene.

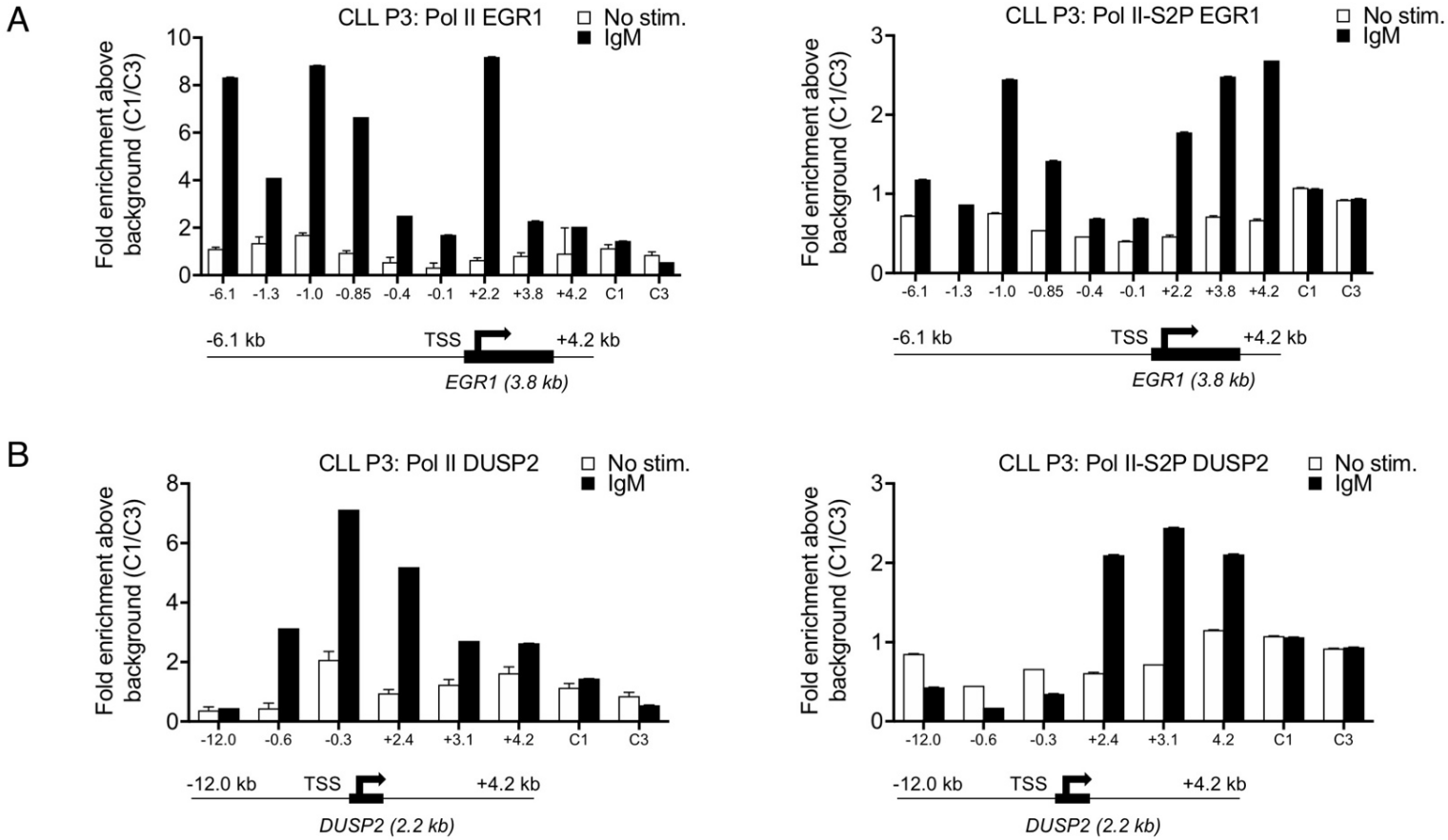

Figure 5.1: RNA pol II recruitment to IEG loci. ChIP-qPCR data assessing RNA pol II and RNA pol II-S2P binding across the **(A)** *EGR1* and **(B)** *DUSP2* locus in CLL cells. CLL cells were stimulated with anti-IgM for 45 mins. The values on the x axis refer to specific gene regions relative to the transcription start site (TSS) in kilobases (kb) as indicated on the gene schematics below (not to scale). CTCF1/3 (C1/C3) were used as negative control regions which are not indicated on the gene schematics. Error bars correspond to variations in the ChIP-qPCR repeats.

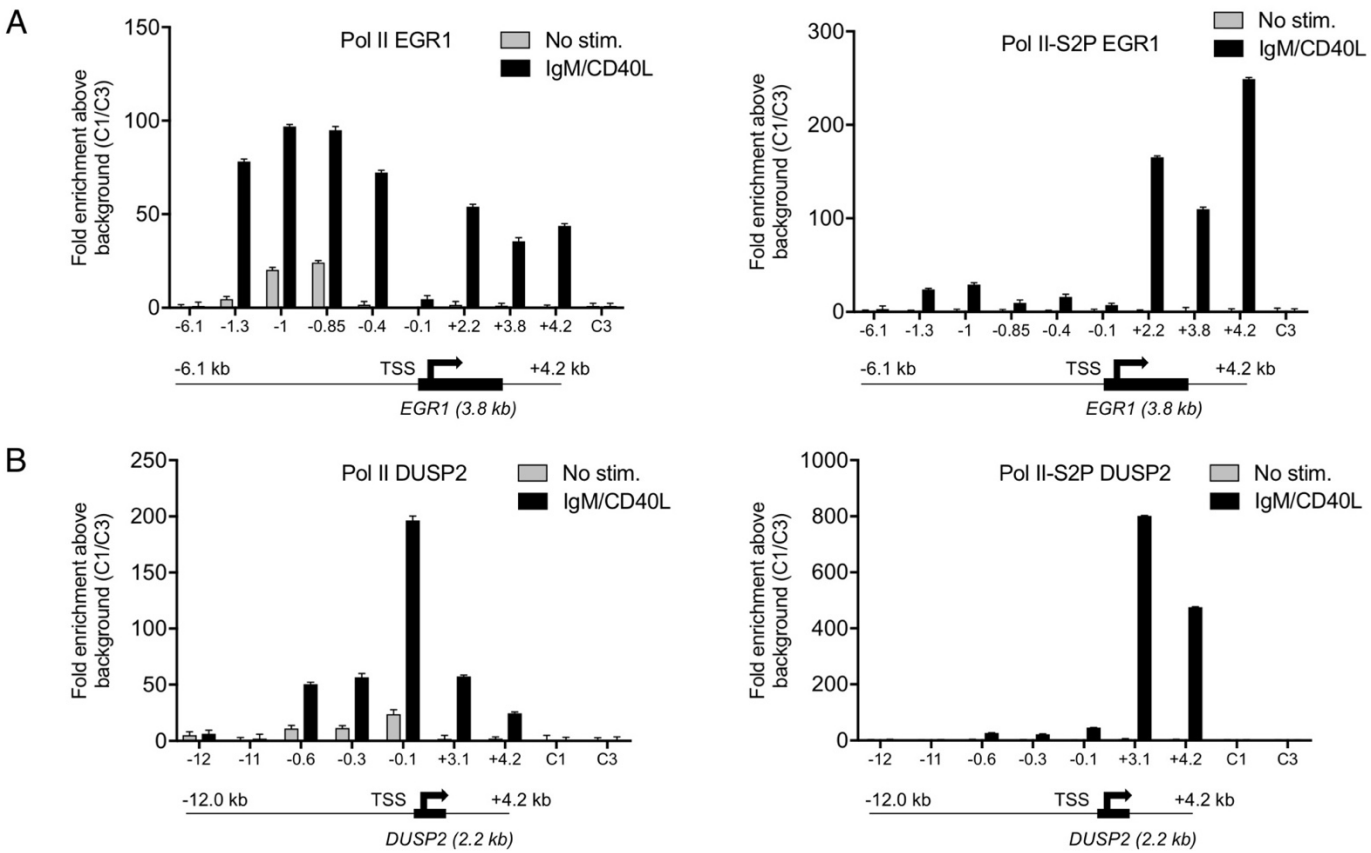

Figure 5.2: RNA pol II recruitment to IEG loci in the context of combined anti-IgM/CD40L stimulation. ChIP-qPCR data assessing RNA pol II and RNA pol II-S2P binding across the **(A)** *EGR1* and **(B)** *DUSP2* locus in CLL cells. CLL cells were stimulated with combined anti-IgM/CD40L for 45 mins. The values on the x axis refer to specific gene regions relative to the transcription start site (TSS) in kilobases (kb) as indicated on the gene schematics below (not to scale). CTCF1/3 (C1/C3) were used as negative control regions which are not indicated on the gene schematics. Error bars correspond to variations in the ChIP-qPCR repeats.

5.2 BTK and ZIPK inhibition differentially effect RNA polymerase II recruitment to IEG loci

We have demonstrated that RNA polymerase II recruitment to the *EGR1* and *DUSP2* loci occurred rapidly after anti-IgM and/or CD40L stimulation. In order to further understand how ZIPK affects the transcriptional activation of our model IEGs we aimed to compare the effects of ibrutinib and DAPKi on RNA pol II recruitment.

We took the cells from a U-CLL patient (P5) and pre-treated them with either ibrutinib or DAPKi before stimulation with anti-IgM for 30 minutes. The cells were then prepared for ChIP analysis with antibodies against RNA pol II and RNA pol II S2-P. The ChIP-qPCR data showed clear recruitment of RNA pol II to *EGR1* and *DUSP2* promoters (see enrichment at *EGR1* -1.0, -0.85 kb and *DUSP2* -0.6, -0.3 kb) and RNA pol II S2-P elongating through the gene bodies (see enrichment at *EGR1* +2.2, +3.8, +4.2 kb and *DUSP2* +2.4, +3.1, +4.2 kb) (Figure 5.3A-B). Ibrutinib could prevent this recruitment throughout both genes, in correlation with our previous data that showed ibrutinib was effective at overcoming anti-IgM-mediated stimulation of IEG transcription in CLL cells (see Chapter 3 Results 1). DAPKi treatment however did not affect RNA pol II (S2-P) recruitment – with only a slight decrease observed at the *DUSP2* locus (Figure 5.3B). These data suggested that a loss of ZIPK function prevented IEG expression through post-transcriptional mechanisms, in a way that leaves RNA pol II recruitment mostly unaffected. Alternatively, we could not rule out that DAPKi may have trapped the elongated polymerase within gene bodies, with this block in transcriptional elongation being undetectable by ChIP.

5.2.1 Comparing the effects of BTK and ZIPK inhibition on RNA polymerase II recruitment to IEG loci in the context of combined anti-IgM/CD40L stimulation

Having demonstrated that Ibrutinib can prevent RNA polymerase II recruitment to IEG loci while DAPKi does not (see Figure 5.3), we wanted to assess if these inhibitors would have a similar effect after stimulation with combined anti-IgM/CD40.

We took the cells from a U-CLL patient (P7) and pre-treated them with either ibrutinib or DAPKi before stimulation with dual anti-IgM/CD40L for 30 minutes. The cells were then prepared for ChIP analysis with antibodies against RNA pol II and RNA pol II S2-P. Without the inhibitors we observed a classical RNA polymerase recruitment with elongating S2-P localised in the gene bodies and 3' of the TES (see enrichment at *EGR1* +2.2, +3.8, +4.2 kb and *DUSP2* +2.4, +3.1, +4.2 kb). After combined anti-IgM/CD40L stimulation ibrutinib was less effective at preventing the recruitment of RNA pol II and RNA pol II S2-P to both the *EGR1* and *DUSP2* loci. In particular, we observed no effect of ibrutinib on RNA pol II recruitment 5' of the *EGR1* TSS (regions -1.0 and -0.85 kb) or at any regions across the *DUSP2* locus (Figure 5.4A-B). Similarly, RNA pol II S2-P recruitment was mostly unaffected across the *DUSP2* locus with partial loss observed at the region 3.1 kb downstream of the TSS (Figure 5.4A-B). In contrast, RNA pol II S2-P recruitment was fully prevented across the *EGR1* locus, as observed for anti-IgM stimulation alone (see Figure 5.3).

At the *EGR1* locus, DAPKi treatment either had no effect (regions +2.2 and +4.2 kb) or induced an accumulation of RNA pol II/RNA pol II S2-P compared to no drug (regions -1.0, -0.85 and +3.8 kb) (Figure 5.4A). For *DUSP2*, we observed similar results with the DAPKi – either no effect (regions +2.4 and +3.1 kb) or increased RNA pol II recruitment compared to no drug (regions -0.6 and -0.3 kb). RNA pol II S2-P recruitment was the most variable, with a combination of regions unaffected (region -0.6 kb), increased (regions -0.3 kb) or decreased (regions +2.4, +3,1 and +4.2 kb) in response to DAPKi treatment (Figure 5.4B). These variations may represent experimental variability and from these data we can only conclude that DAPKi treatment does not fully repress RNA pol II S2-P recruitment.

The reason why Ibrutinib was able to prevent RNA pol II S2-P across the *EGR1* locus while having little effect on *EGR1* gene expression (see Chapter 4 Results 2) was unclear. Clearly, Ibrutinib was least effective at preventing RNA pol II recruitment to *DUSP2* under dual anti-IgM/CD40L stimulation. We hypothesised these differences may arise from contrasting RNA pol II recruitment dynamics which could be dependent on the signalling pathway and downstream TFs (e.g. CD40L/NF-kB versus BCR/STAT3) at the *DUSP2* and *EGR1* loci.

5.2.2 Examining RNA polymerase II recruitment to IEG loci in HBL1 cells

Having assessed RNA polymerase II recruitment to IEG loci in CLL cells, we wanted to continue our assessment of the HBL1 cell line by carrying out further ChIP experiments. HBL1 cells were pre-treated with either ibrutinib or DAPKi before stimulation with dual anti-IgM/CD40L for 30 minutes. The cells were then prepared for ChIP analysis with antibodies against RNA pol II and RNA pol II S2-P.

As expected, the ChIP-qPCR data showed RNA pol II and RNA pol II S2-P binding at IEG promoters in gene bodies (Figure 5.5A-B). Ibrutinib was able to prevent RNA pol II (S2-P) recruitment to some 5' and gene body regions (see *EGR1* -1.0, +2.2 and *DUSP2* -0.6, +2.4 kb) and also caused an accumulation of RNA pol II in the 3' end of the gene (see regions *EGR1* +3.8 and *DUSP2* +3.1 kb). DAPKi treatment had either no effect or caused a locus-wide accumulation of RNA polymerase. These data suggested that the effect of the DAPKi was similar between HBL1 and primary CLL cells and that ZIPK was functioning in a similar manner in both cell types. Again, it was unclear how Ibrutinib was able to prevent RNA pol II recruitment to IEG loci, while it simultaneously was not able to prevent transcription of *EGR1* and *DUSP2* in the context of dual anti-IgM/CD40L stimulation in HBL1 cells.

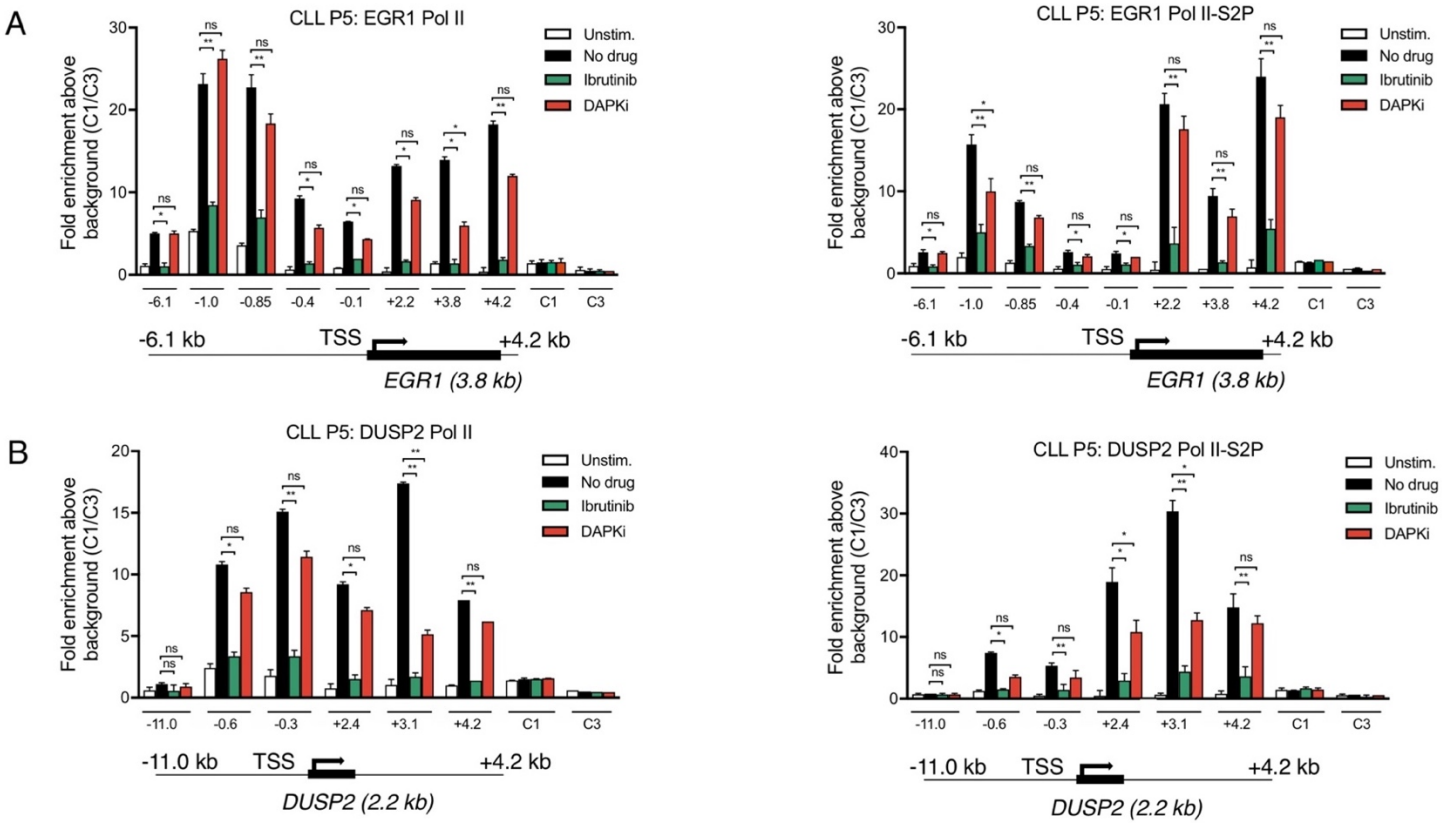

Figure 5.3: Differential effects of ibrutinib and DAPKi treatment on RNA polymerase II recruitment in CLL cells. ChIP-qPCR data assessing RNA pol II and RNA pol II S2-P binding across the **(A)** *EGR1* and **(B)** *DUSP2* locus in CLL cells. Cells were pre-treated with either 1 μM ibrutinib (green) or 25 μM DAPKi (red) for 1 hour as indicated and then stimulated with anti-IgM for 45 minutes. The values on the x axis refer to specific gene regions relative to the transcription start site (TSS) in kilobases (kb) as indicated on the gene schematics below (not to scale). CTCF1/3 (C1/C3) were used as negative control regions which are not indicated on the gene schematics. Significant differences were calculated using two-way ANOVA followed by Dunnett's multiple comparison test for n = 2 independent experiments where 1 representative example is shown in the figure with error bars corresponding to variations in the ChIP-qPCR repeats.

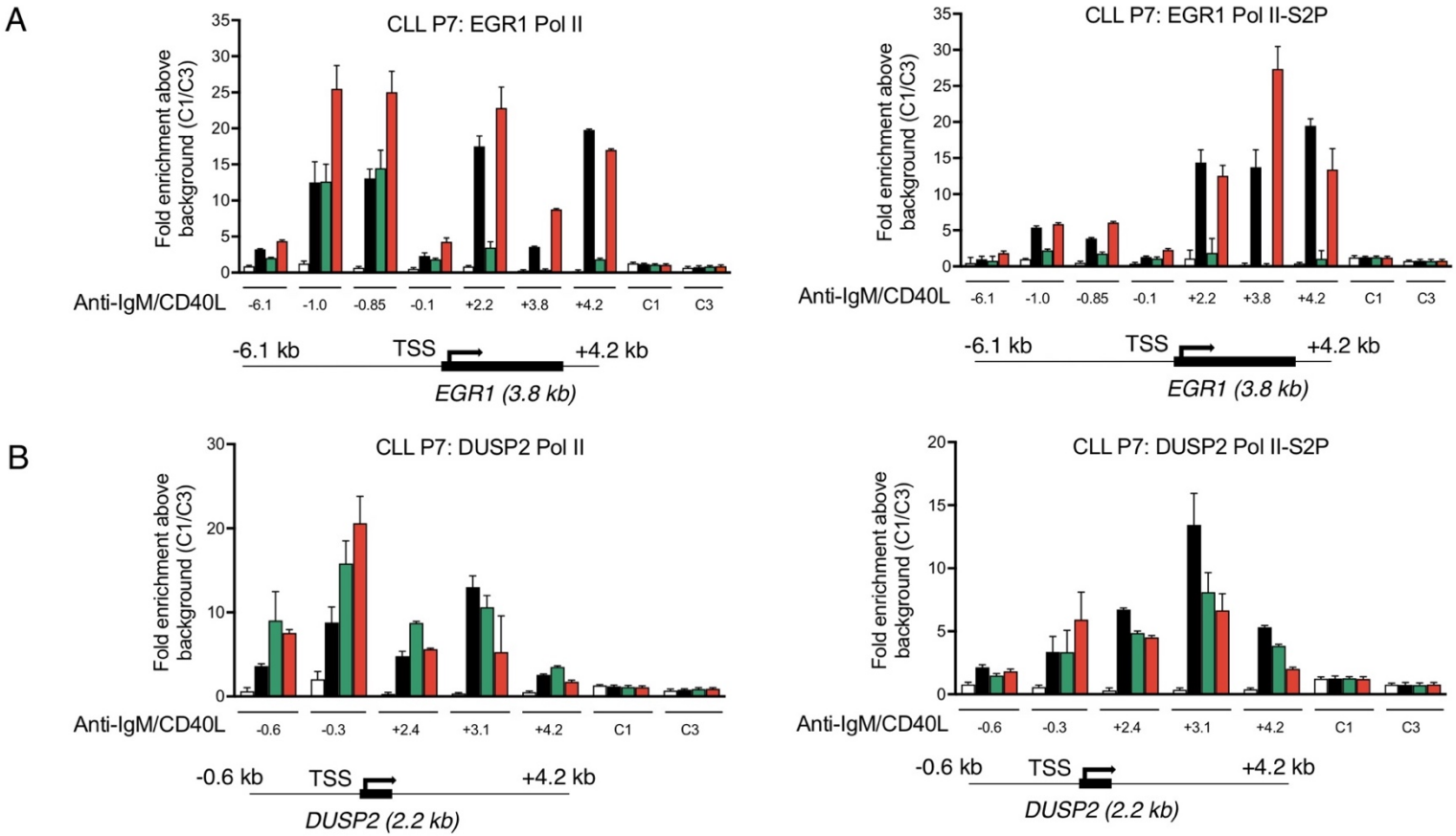

Figure 5.4: Differential effects of ibrutinib and DAPKi treatment on RNA polymerase II recruitment in CLL cells. ChIP-qPCR data assessing RNA pol II and RNA pol II S2-P binding across the **(A)** *EGR1* and **(B)** *DUSP2* locus in CLL cells. Cells were pre-treated with either 1 μM ibrutinib (green) or 25 μM DAPKi (red) for 1 hour as indicated and then stimulated with anti-IgM/CD40L for 45 minutes. The values on the x axis refer to specific gene regions relative to the transcription start site (TSS) in kilobases (kb) as indicated on the gene schematics below (not to scale). CTCF1/3 (C1/C3) were used as negative control regions which are not indicated on the gene schematics. Error bars correspond to variations in the ChIP-qPCR repeats for n = 1 experiment.

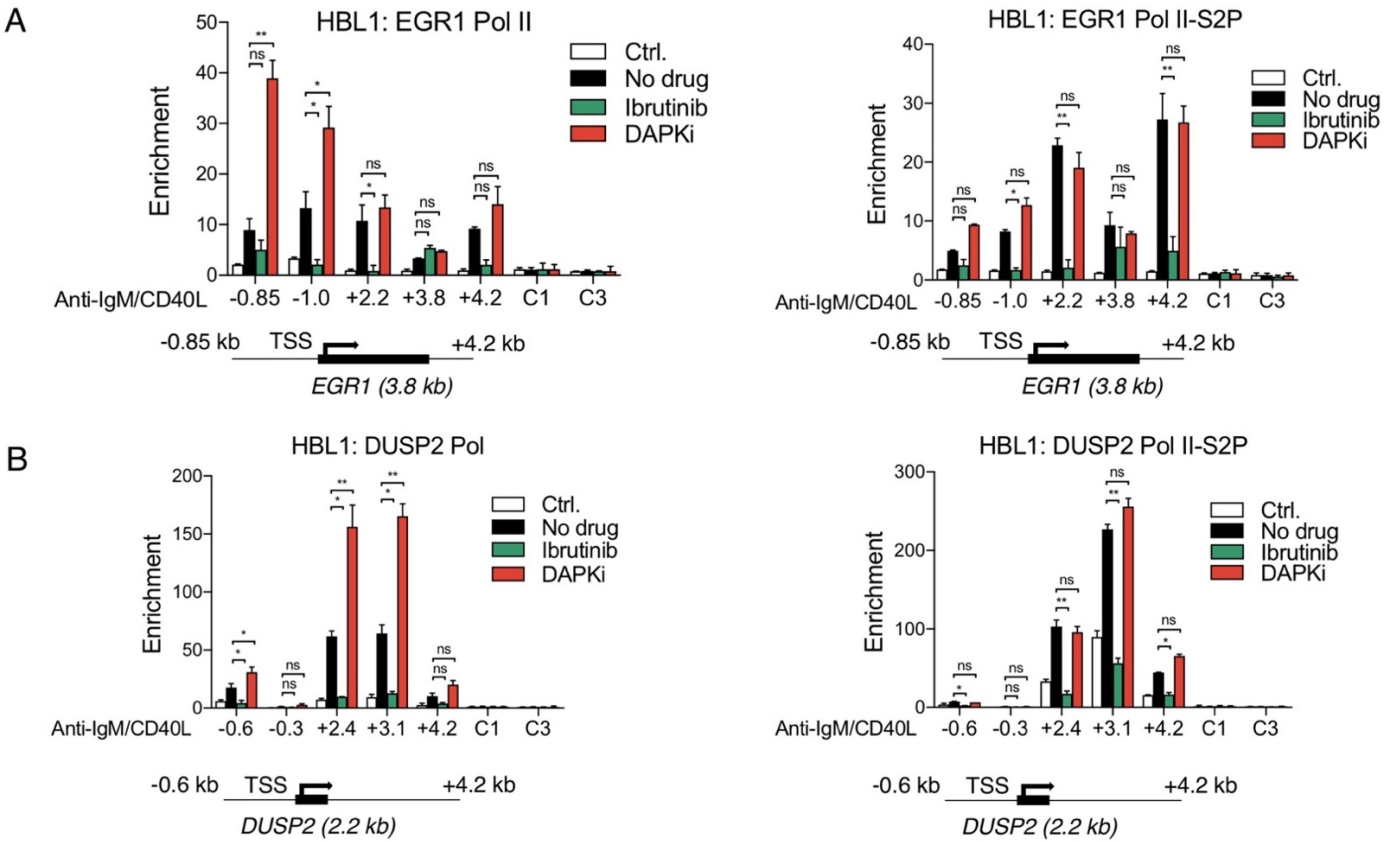

Figure 5.5: Differential effects of ibrutinib and DAPKi treatment on RNA polymerase II recruitment in HBL1 cells. ChIP-qPCR data assessing RNA pol II and RNA pol II S2-P binding across the **(A)** *EGR1* and **(B)** *DUSP2* locus in HBL1 cells. Cells were pre-treated with either 1 μM ibrutinib (green) or 25 μM DAPKi (red) for 1 hour as indicated and then stimulated with anti-IgM/CD40L for 45 minutes. The values on the x axis refer to specific gene regions relative to the transcription start site (TSS) in kilobases (kb) as indicated on the gene schematics below (not to scale). CTCF1/3 (C1/C3) were used as negative control regions which are not indicated on the gene schematics. Significant differences were calculated using two-way ANOVA followed by Dunnett's multiple comparison test for n = 3 independent experiments where 1 representative example is shown in the figure with error bars corresponding to variations in the ChIP-qPCR repeats.

5.3 The effects of ZIPK inhibition on the processing of primary mRNA transcripts

Since treatment of CLL cells with DAPKi prevents IEG expression (see Figure 3.5) but did not seem to impact on RNA pol II elongation (see Figure 5.4), we sought to assess the effect of ZIPK inhibition on steps post-elongation: specifically focussing on the processing of primary mRNA transcripts. The processing or maturation of primary mRNA precursors often will occur simultaneously with their transcription by RNA polymerase II [200, 263]. The co-transcriptional nature of pre-mRNA processing requires alterations to the chromatin structure by histone-modifying enzymes for the recruitment and action of both the RNA polymerase II itself and a raft of RNA processing factors for splicing, intron removal, 3' end processing and 5' capping [203].

We therefore sought to examine any effect of ZIPK inhibition on the processing of pre-mRNA for these reasons:

I. ZIPK inhibition does not prevent RNA pol II S2-P in the gene bodies of IEGs suggesting that its mechanism of action may occur post elongation.
II. ZIPK is a chromatin modifying enzyme and accurate changes to the chromatin structure play a role in the processing of primary mRNA transcripts.

5.3.1 RT-PCR highlights RNA processing defect caused by a loss in ZIPK function

In order to examine the effect of ZIPK inhibition on mRNA processing, we used conventional RT-PCR to compare the effect of DAPKi on mature mRNA and primary mRNA transcripts. CLL cells (P7) were pre-treated with either ibrutinib or DAPKi for 1 hour, stimulated with dual anti-IgM/CD40L for 1 hour before lysis for RNA extraction. cDNA synthesis was carried out with either an oligo-dT (O-dT) or random primers. The random primers would amplify both processed mRNA and unprocessed pre-mRNA, while the O-dT would only amplify polyadenylated transcripts. This would allow us to determine whether or not an mRNA processing defect occurring as a result of ZIPK loss takes place pre- or post-polyadenylation. Samples were analysed with RT-PCR using primers designed for full length, processed mRNA and several primers designed to span intron/exon boundaries or fully intronic regions in order to analyse the level of primary transcripts (Figure 5.6A).

We observed an increase in *EGR1* and *DUSP2* gene transcription following dual anti-IgM/CD40L stimulation (Figure 5.6B top left panel). Ibrutinib had a limited effect on IEG expression under these stimuli, as observed earlier via qPCR (see Figure 3.8), while DAPKi treatment reduced the level of processed, mature mRNA, as expected. DAPKi treatment only impacted the level of primary transcripts when the reverse transcription was carried out with an oligo-dT, when we used random primers there was no effect of DAPKi treatment with a slight increase/accumulation of primary transcript for primers *EGR1* +1.0 and *DUSP2* +0.5 (Figure 5.6B bottom left panel, bottom right panel). There was an effect of the DAPKi on the intro/exon boundary primer *DUSP2* +1.1 (Figure 5.6B top right panel), but the primary transcript was not reduced to a level comparable with processed *DUSP2* mRNA.

These data suggested an effect of ZIPK inhibition on mRNA processing of primary transcripts which impacted on the processing steps pre-polyadenylation, such as 5' capping or splicing, although it should be noted that these steps often occur concurrently.

5.3.2 qPCR demonstrates that DAPKi treatment does not prevent primary mRNA transcript formation, but leads to their accumulation

Having used RT-PCR to determine that DAPKi treatment impacted on mRNA processing we wanted to confirm these observations with qPCR. First, we took the cells from a CLL patient (P7) and pre-treated them with either ibrutinib or DAPKi for 1 hour before stimulation with anti-IgM for 30 minutes. The cells were then lysed for RNA extraction and qPCR analysis. The qPCR data showed an increase in both processed mRNA and unprocessed pre-mRNA upon anti-IgM stimulation for both *EGR1* and *DUSP2* (Figure 5.7A). Ibrutinib and DAPKi pre-treatment reduced the levels of both processed mRNA and unprocessed pre-mRNA, but we observed that the DAPKi was less effective at inhibiting primary transcript. This was particularly true for *DUSP2* where after DAPKi treatment there was a considerable increase/accumulation of primary transcript compared with mature mRNA (Figure 5.7A). To more clearly understand the difference between ibrutinib and DAPKi treatment on primary transcript we can compare the relative change between the anti-IgM stimulated sample without drug vs. the anti-IgM stimulated sample pre-treated with either ibrutinib or the DAPKi (where

relative change was defined as ΔCt drug treated sample / ΔCt un-drugged sample) (Figure 5.7B). By viewing the qPCR data in this way, we observed that ibrutinib affected the processed mRNA and unprocessed pre-mRNA to a similar extent. However, the DAPKi-dependent reduction in RNA production was at least 2-fold less effective for primary transcripts compared to processed mRNA, for all primers tested.

We have shown that the DAPKi had the same effect on recruitment of RNA pol II (S2-P) in both CLL and HBL1 cells (see Figure 5.3-Figure 5.5). Having determined that ZIPK inhibition impacted on pre-mRNA processing post elongation in CLL cells we wanted to assess if the same was true in HBL1. Therefore, HBL1 cells were pre-treated with either ibrutinib or DAPKi for 1 hour before stimulation with dual anti-IgM/CD40L for 30 minutes. The cells were then lysed for RNA extraction and qPCR analysis. The qPCR data showed that DAPKi can prevent transcription of processed mRNA while ibrutinib cannot (Figure 5.7C), as expected from previous experiments with combined anti-IgM/CD40L stimulation (see Figure 4.10). By taking the data in Figure 5.7C and giving the unstimulated control a value of 1.0, we compared the effects of the two inhibitors more clearly. In this way, we observed that DAPKi treatment resulted in an accumulation of *EGR1* primary transcript, even in unstimulated conditions (Figure 5.7D). The effect was less strong for *DUSP2*, but we still observed that the DAPKi had less impact on primary transcripts compared to mature mRNA (Figure 5.7D). The impact of DAPKi on primary transcripts was observed more strongly in HBL1 compared to CLL cells – here we showed that loss of ZIPK function either had little impact on unprocessed mRNA or caused a slight increase/accumulation of the primary transcript, as observed by RT-PCR (see Figure 5.6B). These data confirmed our observations in CLL cells by RT-PCR and qPCR that ZIPK inhibition blocked processing of the pre-mRNA primary transcripts.

5.3.3 The effects of ZIPK knockdown on the processing of IEG primary transcripts

We have shown that loss of ZIPK function prevented the normal processing of both *EGR1* and *DUSP2* primary mRNAs in CLL and HBL1 cells, demonstrating that DAPKi treatment can cause an accumulation of the unprocessed version of these transcripts (see Figure 5.6 & Figure 5.7). We have previously shown that siRNA-mediated knockdown of ZIPK mimics the effects of DAPKi treatment in HBL1 cells with regard to IEG transcription and histone phosphorylation (see Figure 3.12 & Figure 3.13). We now sought to assess whether the effect of ZIPK

knockdown would be comparable to DAPKi with regard to abnormal mRNA processing to determine if it was a direct effect of this inhibitor on ZIPK function.

HBL1 cells were electroporated with siRNAs directed against ZIPK and a negative control siRNA – an siRNA with a sequence that does not target any gene product to provide a baseline to compare siRNA-treated samples. Day 5 post transfection, the cells were stimulated with anti-IgM for 60 minutes and then lysed for RNA extraction and qPCR analysis. As shown by qPCR previously, we observed that ZIPK knockdown mimicked DAPKi in preventing IEG transcription i.e. there was a decrease in processed mRNA in the cells transfected with siRNAs directed against ZIPK (Figure 5.8A-B). For *EGR1*, we observed an accumulation of primary transcript (Figure 5.8A) as observed in the HBL1 qPCR experiment (see Figure 5.7C). The data for *DUSP2* were less convincing in these series of knockdown experiments due to large variation between duplicate transfections, shown with the error bars for both primary transcripts (Figure 5.8B). The data for the intronic primer (*DUSP2* +0.8 kb) when compared with the processed mRNA showed, more convincingly, how a loss of ZIPK function led to impaired pre-mRNA processing. To summarise, ZIPK knockdown had similarities to DAPKi treatment with regard to ZIPKs impact on pre-mRNA processing, particularly for *EGR1*.

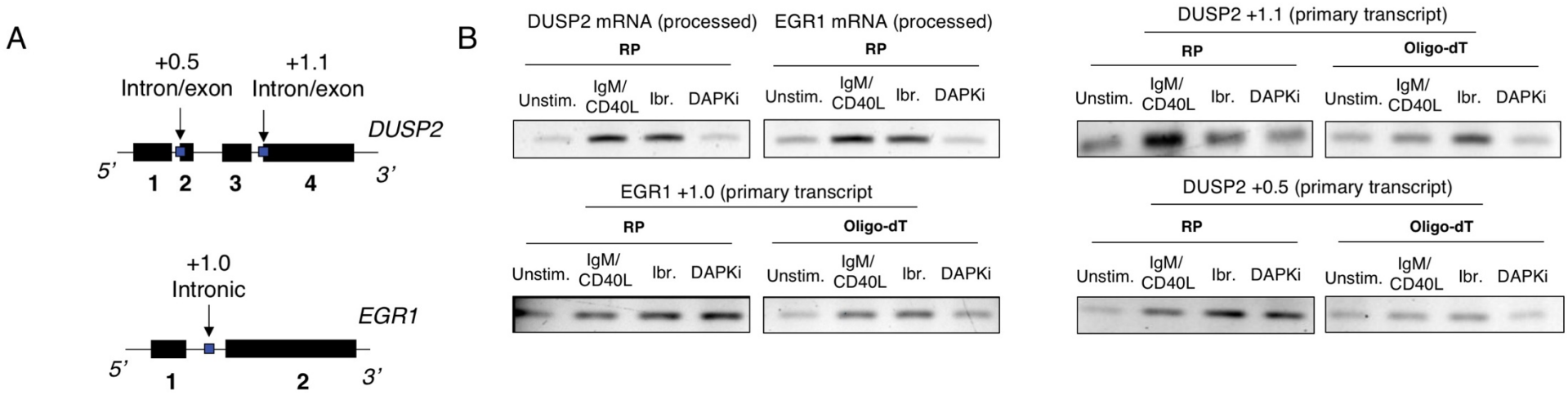

= primer location, as also indicated by the arrows. Text above the arrows refers to the location upstream of the TSS (in kb) and indicates further whether the primer spans an intron/exon junction or is fully intronic. All three primers provide a readout of unprocessed mRNA.

DUSP2 +0.5 kb product 115 bp
DUSP2 +1.1 kb product 102 bp
EGR1 +1.0 kb product 110 bp

Figure 5.6: RT-PCR highlights RNA processing defect caused by a loss in ZIPK kinase activity. (A) *EGR1*/*DUSP2* gene schematics showing introns and exons. Primer locations for qPCR and RT-PCR indicated by vertical arrows and blue boxes. Numbers after gene names correspond to the position of the primers in and around the gene relative to the transcription start site (TSS), where + denotes 3' of the TSS and – denotes 5' of the TSS. **(B)** Reverse-transcription PCR (RT-PCR) analysis comparing levels of processed *EGR1*/*DUSP2* mRNA (top left) with *EGR1*/*DUSP2* primary transcript levels (bottom left, top right, bottom right). CLL cells were pre-treated with either ibrutinib or the DAPKi for 60 mins as indicated and then stimulated with anti-IgM and sCD40L for 60 mins to activate IEG expression. Extracted RNA was reverse transcribed with either random primer (RP) or oligo-dT, subjected to RT-PCR and analysed by agarose gel electrophoresis.

A

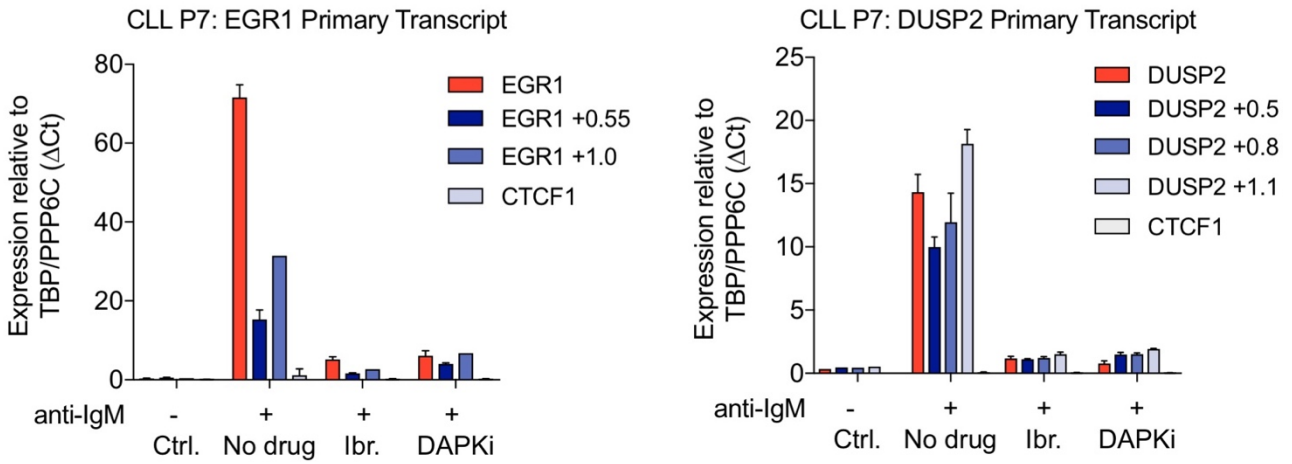
CLL P7: EGR1 Primary Transcript
Expression relative to TBP/PPP6C (ΔCt)
80
60
40
20
0
EGR1
EGR1 +0.55
EGR1 +1.0
CTCF1
anti-IgM - + + +
Ctrl. No drug Ibr. DAPKi
CLL P7: DUSP2 Primary Transcript
Expression relative to TBP/PPP6C (ΔCt)
25
20
15
10
5
0
DUSP2
DUSP2 +0.5
DUSP2 +0.8
DUSP2 +1.1
CTCF1
anti-IgM - + + +
Ctrl. No drug Ibr. DAPKi

B

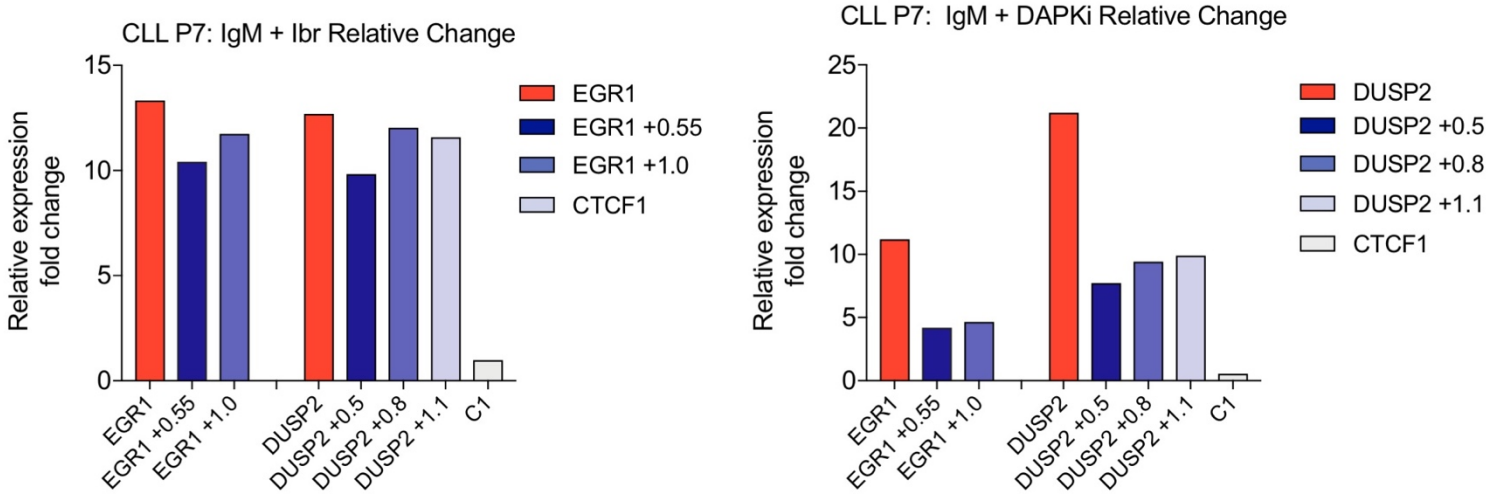
CLL P7: IgM + Ibr Relative Change
Relative expression fold change
15
10
5
0
EGR1
EGR1 +0.55
EGR1 +1.0
CTCF1
EGR1
EGR1 +0.55
EGR1 +1.0
DUSP2
DUSP2 +0.5
DUSP2 +0.8
DUSP2 +1.1
C1
CLL P7: IgM + DAPKi Relative Change
Relative expression fold change
25
20
15
10
5
0
DUSP2
DUSP2 +0.5
DUSP2 +0.8
DUSP2 +1.1
CTCF1
EGR1
EGR1 +0.55
EGR1 +1.0
DUSP2
DUSP2 +0.5
DUSP2 +0.8
DUSP2 +1.1
C1

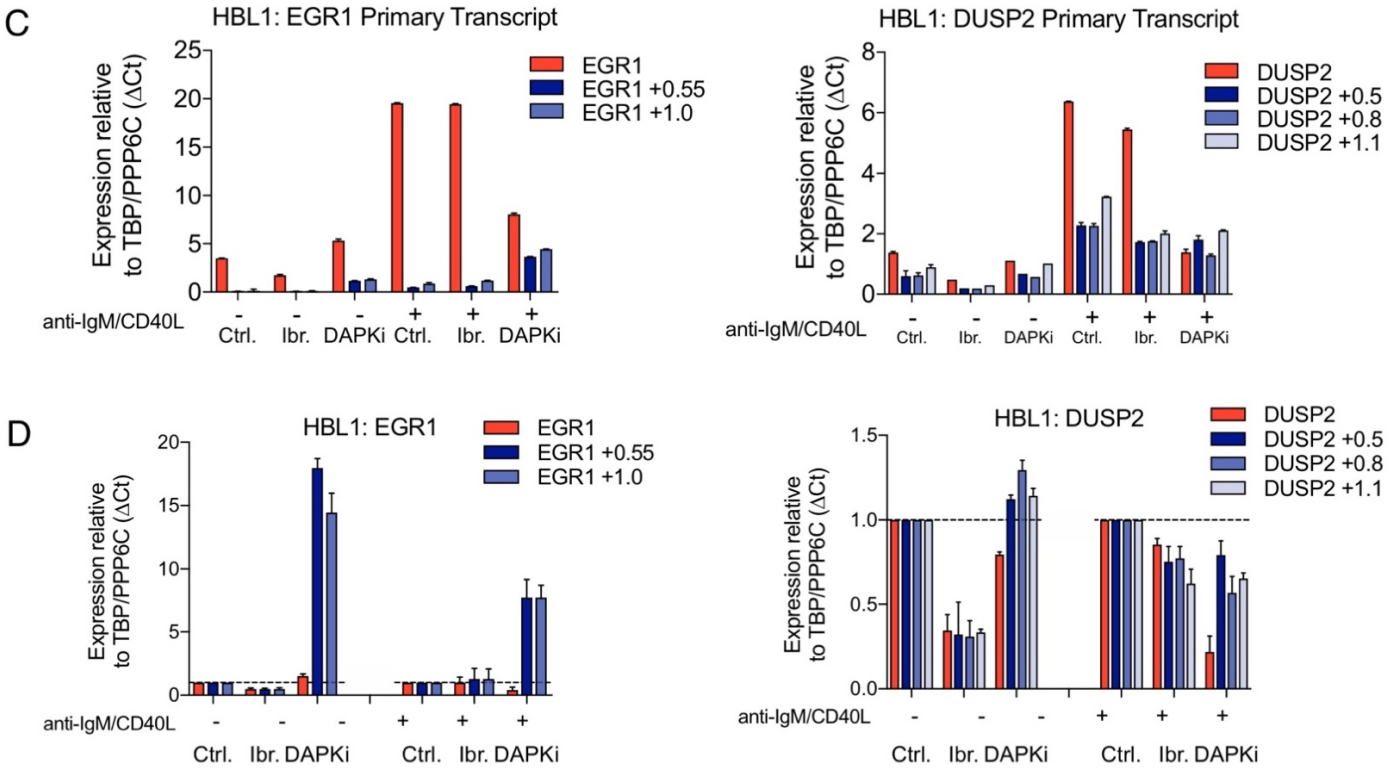

Figure 5.7: DAPKi is less effective at inhibiting IEG primary transcript than mature mRNA in CLL cells while Ibrutinib effects mature mRNA & primary transcripts similarly. (A) qPCR analysis of *EGR1*/*DUSP2* primary transcript (shades of blue) vs processed mRNA (red) from CLL cells pre-treated with either 1 μM ibrutinib or 25 μM DAPKi for 60 mins and then stimulated with or without anti-IgM for 60 mins as indicated. Error bars representative of n = 3 independent experiments. **(B)** Relative change between anti-IgM stimulated and anti-IgM stimulated pre-treated with either Ibrutinib/DAPKi samples (relative change = ΔCt drug treated sample/ΔCt un-drugged sample). C1 and C3 (CTCF1/3) are controls for genomic DNA contamination. **(C)** qPCR analysis of *EGR1*/*DUSP2* primary transcript (shades of blue) vs processed mRNA (red) from HBL1 cells pre-treated with either 1 μM ibrutinib or 25 μM DAPKi for 60 mins and then stimulated with or without anti-IgM/CD40L for 60 mins as indicated. **(D)** The data from (C) presented as fold change relative to control/unstimulated sample (= 1.0).

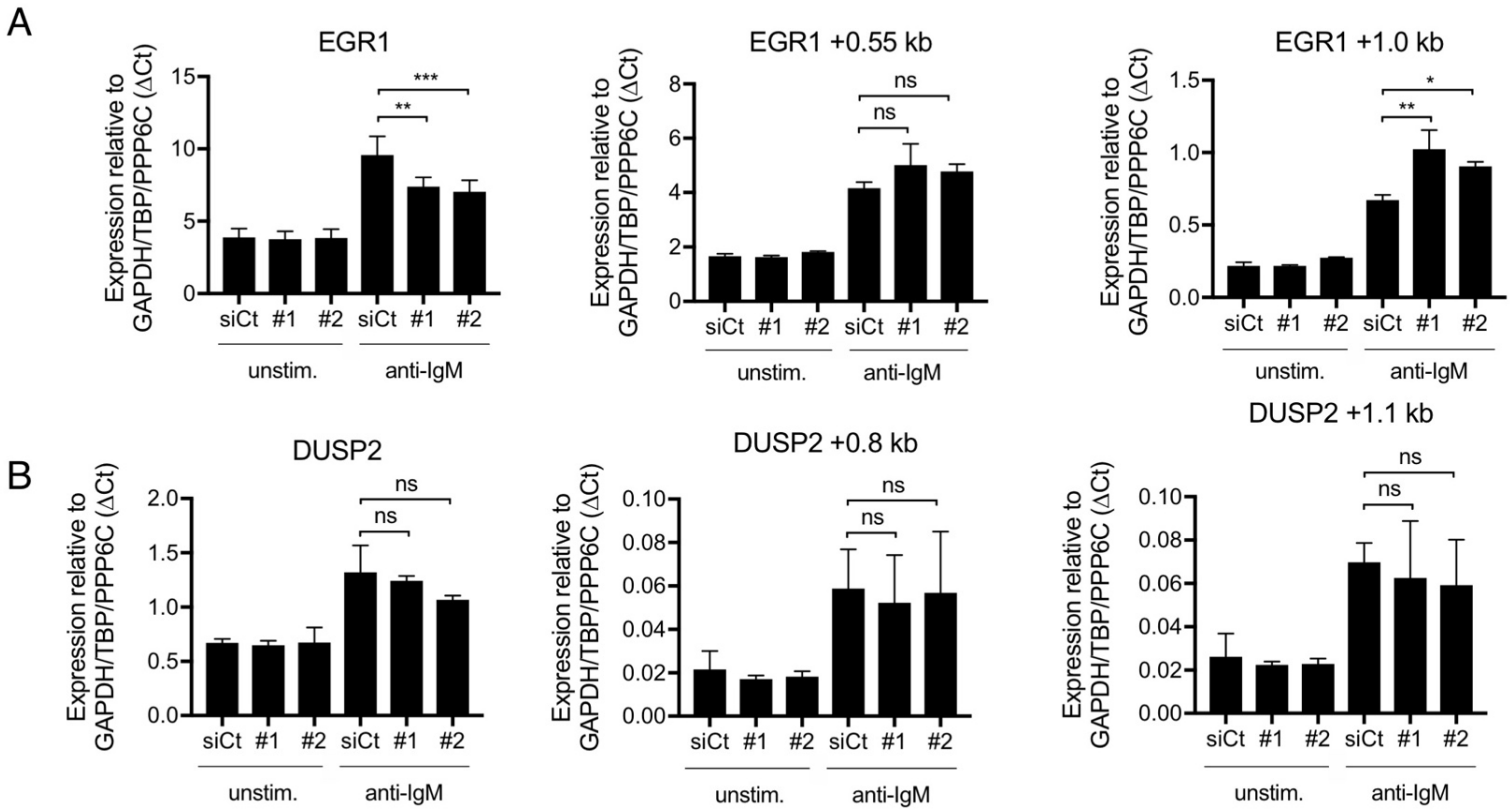

Figure 5.8: ZIPK knockdown mimics DAPKi treatment in preventing IEG expression via impacting pre-mRNA processing. qPCR analysis of **(A)** *EGR1* and **(B)** *DUSP2* mRNA/pre-mRNA from HBL1 cells transfected with siRNAs against ZIPK. 3 days after transfection, the cells were stimulated with or without anti-IgM for 60m. Numbers after gene names correspond to the position of the primers in and around the gene relative to the transcription start site (TSS), where + denotes 3' of the TSS and – denotes 5' of the TSS. Error bars are representative of 3 (*EGR1*) and 2 (*DUSP2*) individual transfections.

5.4 The effects of ZIPK inhibition on alternative splicing

Having determined that ZIPK inhibition or loss of function prevented pre-mRNA processing of IEG nascent transcripts, we wanted to further understand which aspect of processing may be primarily affected by loss of ZIPK kinase activity. The three main events needed to faithfully process a primary mRNA transcript into mature mRNA are 5' capping, 3' processing (cleavage/polyadenylation) and splicing [263]. All three events have been shown to be interpedently stimulated by different regions of the CTD domain of RNA polymerase II [261, 264].

We sought to determine whether ZIPK inhibition could impact splicing. As IEGs, both *DUSP2* and *EGR1* are short genes with only a few exons to ensure the rapid transcription necessary for their immediate function [177]. *EGR1* is a simple gene with only 2 exons and has no functional alternate spice isoforms. *DUSP2* however, has variable exons (exons 2 and 3) which can give rise to a shorter transcript upon their exclusion (data accessible at NCBI AceView [255]). Further, *DUSP2* intron retention (intron 3) has also been shown to give rise to a functional protein [265]. We designed primers to detect both the exon exclusion and intron retention transcripts to examine alternative splicing of *DUSP2* in the context of ZIPK inhibition (Figure 5.9A for primer design).

First, to understand the relative levels of the spliced/unspliced/alternatively spliced *DUSP2* isoforms, HBL1 cells were stimulated with either anti-IgM alone, combined anti-IgM/CD40L, or neither for 1 hour before lysis for RNA extraction and qPCR analysis. The qPCR data detected a small amount of transcripts containing the retained intron with a more significant number of transcripts which were alternatively spliced with exon exclusion/skipping. Under all conditions there was a higher level of spliced *DUSP2* mRNA compared to the alternatively spliced or unspliced transcript (Figure 5.9B).

To understand the effect of ZIPK inhibition on alternative splicing we repeated the experiment pre-treating HBL1 cells with either ibrutinib or DAPKi for 1 hour before stimulation. In order to assess the impact of ZIPK inhibition on splicing, we examined the change in the ratio of splice isoforms between the control (stimulated, un-drugged) and ibrutinib/DAPKi-treated samples. In short, the relative levels of splice isoforms can be expressed as a ratio of one splice isoform to another e.g. an exon inclusion (spliced) vs. exon exclusion or intron retention ratio (unspliced/alternatively spliced). By giving the control sample a baseline

value of 1, this ratio can then be compared between different experimental samples e.g. ibrutinib vs. DAPKi-treated (see Methods 2.6.5 for detailed calculations).

The qPCR data expressed in this way showed that the ratio of exon inclusion transcripts (spliced transcripts) to alternatively spliced transcripts is increased in DAPKi treated samples when compared with control or ibrutinib treated samples (Figure 5.10A). We observed that the value for ibrutinib treated cells was close to the baseline value of 1, suggesting that BTK inhibition affected both isoforms to the same degree and that the ratio between isoforms remains similar as transcription was decreased (Figure 5.10A). This is in agreement with ibrutinib's mechanism of action in preventing transcription via inhibition of the upstream BCR signalling pathway. Conversely, while DAPKi treatment inhibited transcription of the full-length *DUSP2* isoform it even more strongly inhibited alternative splicing of the exon excluded isoform. In the DAPKi treated cells the ratio was increased and strongly skewed away from the alternatively spliced isoform (Figure 5.10A). The same trend holds true when comparing exon included transcripts (spliced transcript) with intron retained transcripts (Figure 5.10B).

These data continue to lend evidence to the fact that ZIPK inhibition negatively impacted on pre-mRNA processing. While it remained unclear exactly how loss of ZIPK prevents faithful pre-mRNA processing, we have now observed an impact on both alternative splicing and an accumulation of both *EGR1* and *DUSP2* primary transcript in the context of ZIPK inhibition (Figure 5.7).

5.5 ZIPK regulates RNA processing through a direct interaction with RNA polymerase II

We have shown links between ZIPK function and pre-mRNA processing (Figure 5.6-Figure 5.10) and discussed how the processing of nascent transcripts was often coupled to and happened simultaneously with RNA pol II-mediated transcription. Further, many proteins responsible for pre-mRNA processing interact directly with the CTD domain of RNA pol II. In order to further understand the role of ZIPK in the transcription of our IEGs we prepared HBL1 cells for co-IP to assess a potential interaction between ZIPK and RNA pol II. The cells were pre-treated with or without DAPKi for 1 hour and then stimulated with anti-IgM for

30 minutes before co-IP lysis and immunoprecipitation with antibodies against both total RNA pol II and elongating RNA pol II S2-P.

The co-IP data showed that ZIPK interacted directly with both RNA pol II and RNA pol II-S2P in an anti-IgM dependent manner whereby stimulation increased the interaction, particularly for RNA pol II S2-P (Figure 5.11A-B). Further, the interaction with RNA pol II S2-P can be marginally decreased by ZIPK inhibition (Figure 5.11B). The signal in the IgG control suggests some non-specific pull-down in this experiment, but the smudged band shaping is not indicative of a false positive result, especially when compared with the pronounced bands in the co-IP.

These data suggested that the impact on pre-mRNA processing resulting from a loss of ZIPK function may be linked to its inability to interact with the elongating polymerase. We also cannot rule out that ZIPK may interact with elements of the processing machinery; the raft of proteins known to bind the RNA pol II CTD, but this requires further investigation.

5.5.1 ZIPK inhibition leads to an accumulation of elongating RNA pol II S2-P

We have shown that:

I. ZIPK can interact directly with RNA pol II (S2-P) in an anti-IgM dependent manner and that this interaction can be prevented by DAPKi treatment (see Figure 5.11).
II. ZIPK inhibition will either have no effect on or lead to an accumulation of RNA pol II (S2-P) at IEG loci (see Figure 5.3-Figure 5.5).

To further understand the impact of ZIPK inhibition on RNA pol II recruitment to IEG loci we sought to assess the level of RNA pol II S2-P after DAPKi treatment by western blot. We pre-treated HBL1 cells with increasing concentrations of DAPKi (0-120 μM) for 1 hour before stimulation with anti-IgM for 30 minutes and subsequent lysis for western blot analysis with antibody against RNA pol II S2-P. At concentrations of DAPKi greater than 20 μM we observed a small increase in the levels of RNA pol II S2-P which may represent an accumulation of the polymerase in the context of ZIPK loss of function (Figure 5.12A-B). These data reinforced the link between ZIPK activity and the functionality of RNA pol II which

we have demonstrated through both accumulation of the polymerase itself and via interference in transcription coupled pre-mRNA processing.

In this chapter we have shown that ZIPK appeared to directly interact with RNA pol II and its inhibition had an impact on pre-mRNA processing steps post-RNA pol II S2-P elongation.

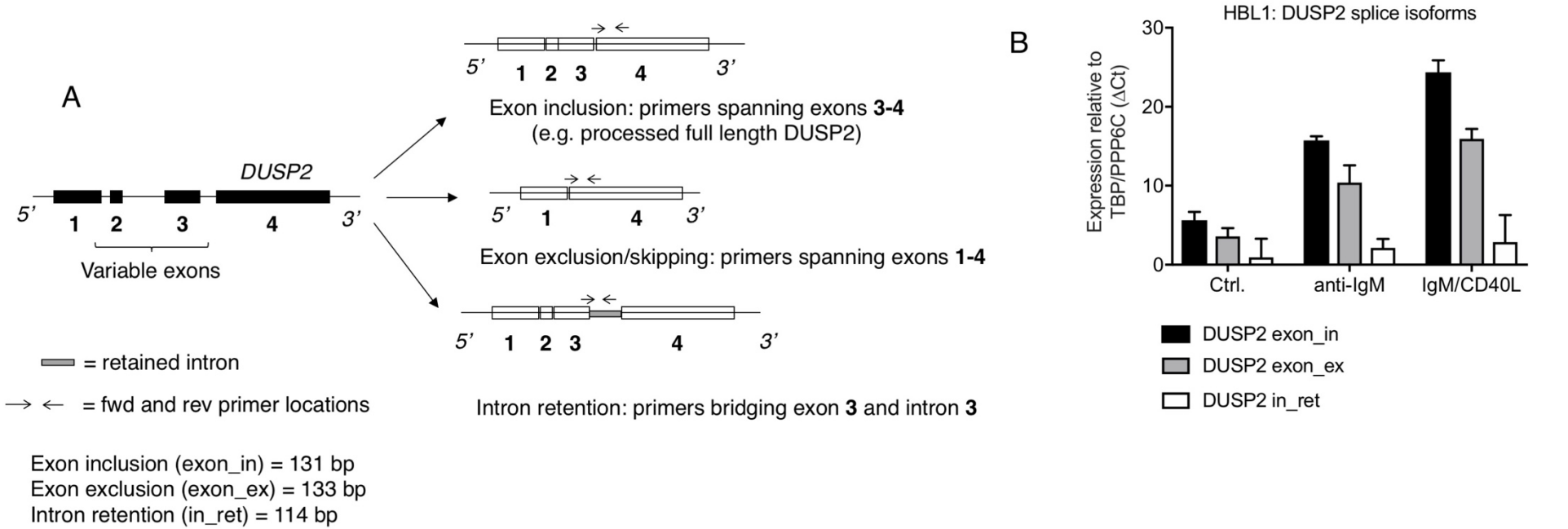

Figure 5.9: Primer design for DUSP2 alternative splicing. (A) *DUSP2* gene schematic showing introns and exons (indicated by numbers in bold), variable exons (exons 2-3) and 3 sets of primers. Primers for mRNA were designed as follows: primers spanning exons 3-4 to detect transcripts which have included the variable exons (top), primers spanning exons 1-4 to detect transcripts which have excluded or skipped the variable exons (middle) and primers bridging the junction between exon 3 and intron 3 to detect the alternatively spliced intron retained *DUSP2* transcript (bottom). **(B)** qPCR data showing the level of constitutively (exon inclusion; exon_in) and alternatively spliced (exon exclusion; exon_ex or intron retention; in_ret) mRNA in HBL1 cells stimulated with anti-IgM or anti-IgM/CD40L for 30 mins.

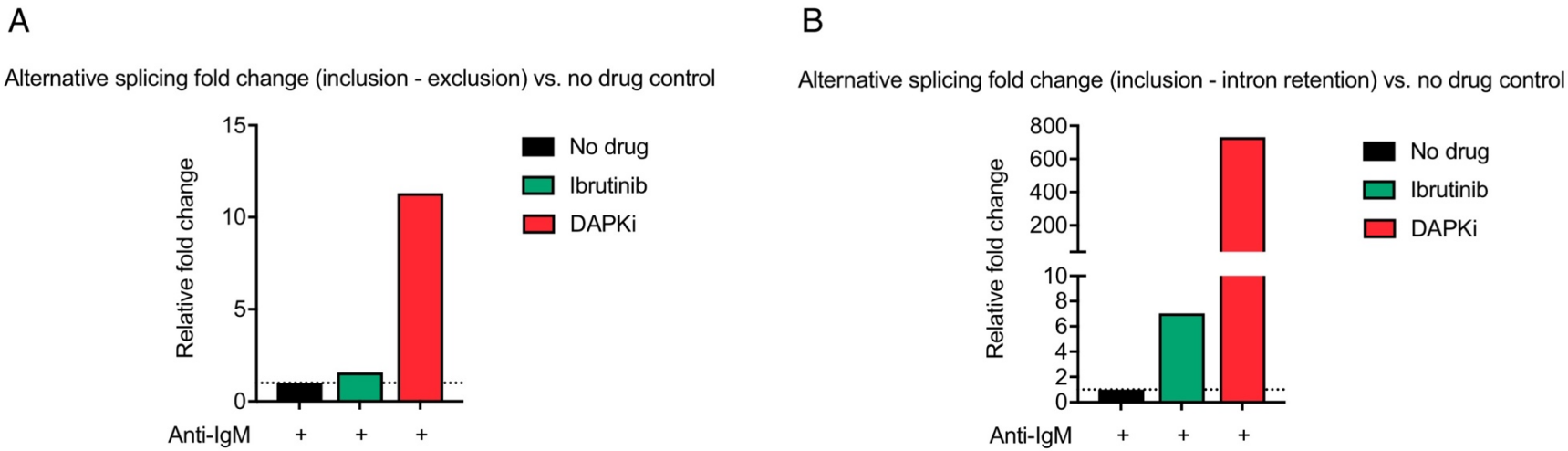

Figure 5.10: ZIPK inhibition reduces levels of alternative splicing. (A) (B) qPCR analysis comparing levels of full length *DUSP2* mRNA with alternatively spliced *DUSP2* mRNA. HBL1 cells were treated with either ibrutinib (green) or DAPKi (red) and stimulated with anti-IgM (black). To calculate the fold change in splicing, first, the ratio of splice isoforms is compared through the equation $2^{-\Delta Ct}$, where ΔCt = (Ct exon inclusion mRNA − Ct exon exclusion/retention mRNA). This ratio is then compared to the value obtained for the same calculation for the control sample through the following equation: $2^{-\Delta Ct(experiment)}/2^{-\Delta Ct(control)}$, where ΔCt(experiment) = (Ct inclusion splice isoform mRNA in experimental sample − Ct exclusion/retention splice isoform mRNA in experimental sample) and ΔCt(control) = (Ct inclusion splice isoform mRNA in control sample − Ct exclusion/retention splice isoform mRNA in control sample) (see methods for more details on the calculations). In this way we can calculate the fold change in full length/intron retention ratio compared to the control sample. In giving the control sample ratio a value of 1, we observe that the value for ibrutinib remains close to this number, suggesting BTK inhibition effects both transcripts equally. DAPKi treatment however dramatically increases the ratio between alternatively and normally transcript transcripts, suggesting an impact on pre-mRNA processing/alternative splicing.

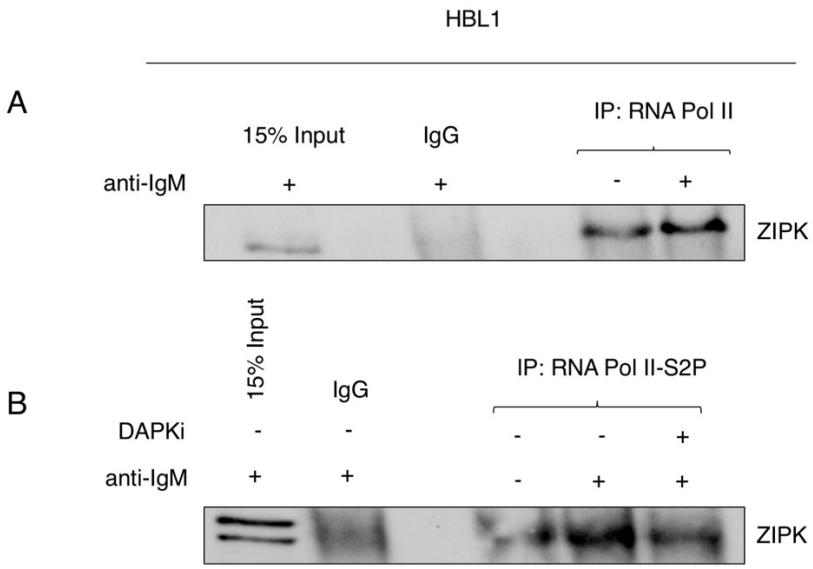

Figure 5.11: ZIPK interacts directly with RNA pol II (S2-P) in HBL1 cells. Co-immunoprecipitation of HBL1 cells stimulated with anti-IgM for 1 hour as indicated. HBL1 cells were pre-treated with DAPKi for 1 hour where indicated. Immunoprecipitates from **(A)** RNA polymerase II and **(B)** RNA polymerase II S2-P pulldown were analysed by SDS-PAGE followed by Western blot probing for ZIPK. Untreated, crude cell lysate was used as positive control (input) and IgG beads were used for negative control (Ctrl IgG). Blots are representative of 3 independent co-IP experiments.

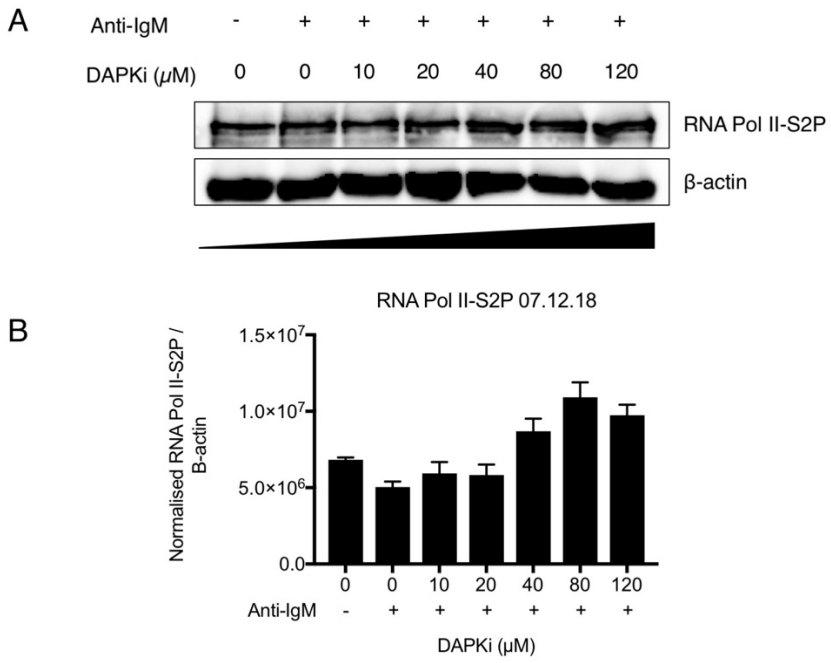

Figure 5.12: RNA polymerase II-S2P is observed to accumulate in the context of ZIPK inhibition. (A) (B) Western blot in HBL1 cells showing the effect of ZIPK inhibition on protein level of RNA Pol II-S2P with 1 hour anti-IgM stimulation of the BCR as indicated. β-actin was used as a loading control and for normalisation with Image Lab software (right).

Chapter 6 Discussion

6.1 Summary of principle findings

Zipper-Interacting Protein Kinase (ZIPK)/Death-Associated Protein Kinase 3 (DAPK3) is a serine-threonine kinase known for its roles in apoptosis, but initially identified as a chromatin-associated enzyme with chromatin modifying potential [229]. Here, we show that ZIPK is recruited to the transcriptional machinery in response to BCR cross-linking where it targets histone H3 at threonine 6 and 11 within the body of immediate early genes (IEGs) involved in CLL pathogenesis. These histone post translational modifications (PTMs) are correlated with IEG transcription and DAPK inhibition prevents their expression.

We confirmed that ZIPK interacted with the non-histone substrates, RNA polymerase II and STAT3 and we demonstrated that the latter is also recruited to IEGs downstream of the BCR. Further, we showed that dual anti-IgM/CD40L stimulation increased IEG expression in CLL in an additive fashion through the activation of transcription factors such as the NF-κB subunit P65. In this context, and unlike ibrutinib, the ZIPK inhibitor was capable of overcoming combined anti-IgM/CD40L-mediated IEG expression. Despite a complete loss of IEG transcription, RNA polymerase II recruitment and elongation were unperturbed by ZIPK inhibition. However, the loss of functional ZIPK impacted co-transcriptional processing of nascent RNA, resulting in a loss of IEG pre-mRNA processing.

From a clinical standpoint, we have determined that DAPK inhibition has similar outcomes to ibrutinib with regard to CLL cell proliferation *in vitro* and repression of IEGs transcribed in response to activation of the BCR pathway. Further, we have shown that DAPK inhibition appeared to have a broader effect in repressing pathways involved in cancer proliferation than ibrutinib – specifically CD40-mediated NF-κB pathway activation

Our principle findings are summarised in Figure 6.1.

6.2 Discussion

6.2.1 DAPK inhibition as an alternative to ibrutinib in CLL?

ZIPK has previously been implicated as having both oncogenic and tumour suppressing functions. For example, a loss of ZIPK function has been associated with reduced apoptosis in squamous cell carcinoma [231], increased tumour invasion in gastric cancer [232] and increased levels of cell survival, proliferation and resistance to chemotherapy in colon, lung and ovarian cancers [233]. Conversely, expression of ZIPK has been linked to metastasis via activation of AKT and NF-κB signalling in gastric cancer [234] and with an ability to provide a growth advantage to prostate cancer cells through androgen receptor gene regulation [220].

In our work in CLL, we have implicated ZIPK function as pro-proliferative, whereby DAPK inhibition reduces CLL cell proliferation with an apparent increase in apoptosis (Thomas et al., forthcoming 2020) and a reduction in IEG expression/histone PTM deposition (Results Figure 3.5 & Figure 3.14). Additionally, we observed a potentially synergistic effect on CLL cell proliferation and apoptosis when combining DAPKi with the CLL therapeutic, ibrutinib. Ibrutinib treatment generally had a similar outcome to DAPK inhibition while their mechanism of action differs and DAPKi had a broader repressive ability and could prevent both BCR- and CD40-mediated IEG expression.

When discussing the impact of DAPK inhibition on CLL and HBL1 cell proliferation, apoptosis and IEG expression we must also address the doses of DAPKi necessary to achieve comparable or superior results to ibrutinib. Our working dose for DAPKi treatment was 20 μM, significantly higher than the 1 μM ibrutinib which was used throughout the project. Firstly, our initial kinase assay (Results Figure 3.1) demonstrated that the commercial DAPKi is not the most refined or potent inhibitor and may lack stability, as H3T6-P was only partially repressed in this experiment when compared to H3T11-P. Although, we observed a similar relative impact of siZIPK on H3T6-P by western blot (Results Figure 3.12) suggesting this histone PTM may be harder to prevent by ZIPK inhibition or may be compensated for by another kinase. Our commercially available DAPKi is being compared to ibrutinib, the gold standard CLL therapeutic used in the clinic for thousands of patients worldwide which has been rigorously refined through numerous clinical trials. While ibrutinib off-target effects are being addressed through the development of highly-specific second generation BTKi

such as acalabrutinib and zanubrutinib, such considerations have not been made for the DAPKi.

Of potential DAPKi off-target effects [266], ERK may be the most relevant to our work considering ERK has been shown to be phosphorylated and activated by anti-IgM stimulation of the BCR in CLL [267]. In the same study, ERK phosphorylation was shown to be also be attenuated by ibrutinib treatment. However, the authors used a co-culture NLC model system to model the lymph node microenvironmental niche. They observed that ERK phosphorylation was markedly decreased in the absence of NLC co-stimulation, suggesting that in an *in vitro* system like ours without co-culture, ERK phosphorylation may play a less significant role. Another study demonstrated that while a proportion (~50%) of their CLL patients presented with constitutive ERK phosphorylation, these patients where characterised by an unresponsiveness to BCR triggering by anti-IgM *in vitro* [268]. Typically, our U-CLL patients responded well to anti-IgM signalling (CLL P4 as the exception), perhaps suggesting a lack of phospho-ERK. Nevertheless, future work with DAPKi would require screening for off target effects on ERK and others proteins.

As discussed, BTK is an important signalling molecule towards the top of the BCR pathway and is implicated in the pathogenesis of several B-cell malignancies. Targeting BTK with ibrutinib provided a breakthrough in the treatment CLL, but cases of resistance associated with mutations in *BTK* and the downstream signalling molecule *PLCγ2*, are now emerging [138]. Further, there are reports of resistance which cannot be explained by genetic alterations [139-141]. In fact, recent studies indicate that alternative, pro-proliferative signalling pathways, primarily NF-κB, could compensate for the inactivation of BCR signalling [142, 143]. Our own data demonstrated strong binding of the NF-κB subunit p65 at the *DUSP2* promoter, replacing STAT3, in the presence of ibrutinib. This could suggest that the loss of BTK-mediated STAT3 activation promoted compensation from other transcription factors such as p65 (Results Figure 4.12).

For additional examples, it has been reported that toll-like receptor (TLR) signalling, which can activate NF-κB in the lymph node, is only partially repressed by ibrutinib [142]. Similarly, ibrutinib does not prevent transcription in response to CD40 activation and this has been described by others [138] and demonstrated by us. CD40 is a key regulator of B cell proliferation and known to activate NF-κB [269]. ZIPK is activated downstream of BTK and PLCγ2, and was effective at

inhibiting both BCR and CD40-mediated IEG expression, suggesting that it could be an attractive alternative to ibrutinib, particularly in CLL cells for which relapse is correlated with mutations of both upstream proteins.

ZIPK mediating the pre-mRNA processing of NF-κB target genes downstream of CD40 activation suggested it might also regulate NF-κB genes activated by other stimuli. In our work we examined IEG expression in response to anti-IgM, anti-IgD and CD40L, but the canonical and non-canonical NF-κB pathways can additionally be activated by tumour necrosis factor (TNF), interleukin 1 (IL-1), lipopolysaccharide (LPS) and via micro-environmental agonists such as CpG-oligodeoxynucleotides. It has been shown that ZIPK also regulates pro-inflammatory genes in response to TNF-dependent activation [270] as well as in response to interferon-gamma (IFNγ) [271]. This suggests that ZIPK may be effective in preventing the pre-mRNA processing of many NF-κB target genes, regardless of the upstream activation pathway. From a clinical standpoint, NF-κB hyper-activation is common in many cancers and ZIPKs efficacy in preventing expression of NF-κB target genes presents an interesting and novel therapeutic option. Such pan-NF-κB deactivation could be considered dangerous to 'normal' cells which rely on NF-κB for various physiological processes. However, we suggest DAPK inhibition may be uniquely effective in cells with DAPK1 silencing (discussed in 6.2.2), and appears to be able to block transcription with a wider effect than ibrutinib, and this may provide a therapeutic window for ZIPK inhibitors.

6.2.2 DAPK inhibition as a therapeutic option for DAPK1-silenced cancers

DAPK1, the first member of the death-associated protein kinase family, can induce apoptosis in response to the IFNγ [272], TNF and FAS pathways [273]. Studies suggest that the DAPK family members form a unique hierarchy to regulate apoptosis and their activation is mediated not only by upstream signals but also through interactions with other DAPK proteins. DAPK1 and ZIPK directly interact to regulate their activity whereby they form a death-associated multi-protein complex to regulate apoptosis [274]. DAPK1 can phosphorylate and regulate ZIPKs cellular localisation and it has been suggested that the cytoplasmic localisation of ZIPK may be imperative for its pro-apoptotic activity [218]. Silencing of DAPK1 via hypermethylation of its promoter has been observed in cancers such as CLL [91] and DLBCL [92] and is suggested to

influence tumour progression, aggressive disease, metastasis and is generally a marker of poor survival [275]. The profound effect of DAPK1 hypermethylation in virtually all cases of sporadic CLL [91, 276] was exemplified by work showing that reconstitution of DAPK1 activity in CLL cells could selectively promote leukaemia cell killing [277]. It was demonstrated that reactivated DAPK1 was able to promote both conventional, caspase dependent apoptosis and autophagy of CLL cells even with the most adverse cytogenetic prognostic features.

ZIPK and DAPK1 share a cooperative relationship in normal tissue whereby both proteins synergise to induce cell death [218]. Work has shown that the presence of both proteins is required for effective apoptosis and that DAPK1 and ZIPK physically interact via their kinase domains [218]. This physical interaction allows DAPK1 to phosphorylate ZIPK at threonine 299 (ZIPK T299-P) in its catalytic domain. Phosphorylation of the T299 residue has been shown to promote cytoplasmic localisation of ZIPK [278]. The T299 residue has been shown to be adjacent to ZIPKs nuclear localisation sequence (NLS) and the authors hypothesised that when phosphorylated it may mask the NLS-function. Indeed, additional mutational analysis studies showed that loss of ZIPK T299-P induced a redistribution of ZIPK to the nucleus [222]. Logically, with DAPK1 silenced in diseases like CLL, ZIPK will lack substantial T299-P and the associated cytoplasmic localisation and cell death functions associated with DAPK1-ZIPK synergy.

In addition to transphosphorylation by DAPK1, ZIPK possesses an autophosphorylation site in its kinase domain at threonine 265 (ZIPK T265-P), which has been shown to be critical for ZIPK kinase activity [223]. Further mutational analyses showed that ZIPK lacking T265-P was unable to effectively promote cell death and ZIPK-mediated STAT3 activation was impaired in the absence of T265 phosphorylation [223]. The same group also showed that leukaemia inhibitory factor (LIF) and interleukin-6 (IL-6) were able to activate and promote phosphorylation of ZIPK at T265, demonstrating the ability for ZIPK to be activated in response to stimuli, as we have also shown using anti-IgM (ZIPK in signalling is expanded on in discussion 6.2.3). It is worth noting that it has been shown that both DAPK1 and ZIPK are unable to phosphorylate any other members of the DAPK protein family, highlighting the specificity of this functional interaction.

In summary, based on the existing evidence regarding the ZIPK-DAPK1 relationship, we suggest that depending on the state of DAPK1 silencing, ZIPK could function to either induce cell death (with DAPK1 expression) or promote proliferation and survival (with DAPK1 silencing). Without DAPK1-mediated ZIPK T299-P, ZIPK appears to be no longer regulated in a pro-apoptotic manner in the cytoplasm and may be equally present in the nucleus. Nuclear localisation could encourage alternative ZIPK functions including the phosphorylation of histones and ZIPK-STAT3 dependent gene expression, culminating in a pro-proliferative phenotype. This is evidenced by DAPKi treatment of CLL cells preventing the activation of pro-proliferative IEGs (Results Figure 3.5), preventing CLL and HBL1 cell proliferation and promoting CLL cell apoptosis (Thomas et al., forthcoming 2020). Due to the resounding evidence in the literature, we did not check our CLL samples for DAPK1 expression. However, if this gene was expressed in some CLL cells, and considering its function as described above, it would be very unlikely that targeting it with our DAPK inhibitor would produce the anti-proliferative and pro-apoptotic effects which we have observed and attributed to a loss of ZIPK function.

Therapeutically, this suggests the possibility of testing ZIPK inhibitors in other malignancies characterised by DAPK1 silencing. For example, outside of CLL, DAPK1 promoter methylation is associated with the severity of the malignancy in various cancers including DLBCL [92], gastrointestinal [275], lung [279], urinary tract carcinomas [280], oesophageal and squamous cell carcinomas [281], head and neck [282], thyroid [283] and even in the brain metastases of solid tumours [284]. In the majority of these cancers DAPK1 is thought to function as a tumour suppressor which can suppress metastasis and tumour proliferation, together with ZIPK, via its apoptosis-inducing abilities. It is interesting to consider that ZIPK inhibitors may have a repressive function that is restricted to DAPK1-silenced cells, where ZIPK may potentially be functioning in a pro-proliferative fashion. We would recommend screening ZIPK inhibitors for anti-proliferative effects in models of those diseases listed above.

Mechanistically, we can consider the signalling pathways which may be inhibited by ZIPK inhibition. As previously stated, constitutive BCR or NF-κB pathway activation is known to be pro-proliferative in many cancers, including CLL, and we have shown that ZIPK inhibition can prevent both anti-IgM and CD40L-mediated IEG expression. However, targeting NF-κB in particular is difficult to its important roles in many normal physiological processes, particularly in preventing

inflammation [285]. Similarly, the BCR pathway is vital for the maturation and development of healthy B cells. Our data suggests that ZIPK inhibition may repress these pathways only in cells with aberrant epigenetic silencing of DAPK1 while sparing cells in which DAPK1 is normally expressed. In summary, we have shown that ZIPK is a potential target in CLL and more generally in cancers characterised by DAPK1-silencing, which is often a marker of poor prognosis.

6.2.3 ZIPK is a signalling-histone kinase

ZIPK has previously been classified as a pro-apoptotic kinase involved in both caspase-dependent and independent pathways [224] as well as an alternative mechanism through autophagic cell death [286]. However, this enzyme was initially identified as a chromatin-associated enzyme phosphorylating the core histones H2A, H3 and H4 [229]. More specifically, ZIPK has been shown to phosphorylate histone H3 at T11 in a mitotic context where it modifies histones at specific regions of centromeric chromatin [230]. ZIPK has not previously been shown to phosphorylate histone H3 at threonine 6 and this is a novel finding. The H3T6-P modification has, however, been previously implicated in mediating gene activation through its phosphorylation by protein kinase C beta I (PKCß-I) [213]. In this example, transcription is promoted via H3T6-P directly preventing LSD1 from demethylating H3K4 during androgen receptor gene activation. This mechanism for H3T6-P-mediated gene activation differs to that which we have described via pre-mRNA processing, but it does implicate this histone mark as activatory.

It is worth noting that in our preliminary work we did consider whether or not PKC or other kinases, which were predicted to/and have previously been show to, phosphorylate H3T6 and H3T11 were functioning in our system. Among these kinases are MEK2, RSK1/2 and various PKCs, all of which are known to function downstream of the BCR signalling pathway. In order to confirm that ZIPK was uniquely responsible for targeting IEGs downstream of the BCR for histone PTMs, inhibitors targeting other kinases were tested for their ability to inhibit expression of *EGR1* and *DUSP2* and phosphorylation of H3T6 and H3T11 along these genes. We tested Gö6983, a pan-PKC inhibitor, RSK inhibitor II, a pan-RSK inhibitor, and U0126, a MEK1/2 inhibitor. None of these inhibitors significantly inhibited the expression of *EGR1* and *DUSP2* or prevented histone H3 phosphorylation after anti-IgM stimulation (Thomas et al., forthcoming 2020). These data confirmed to us that downstream of the BCR in CLL, ZIPK is solely implicated in mediating IEG expression via H3T6 and H3T11 phosphorylation.

We have shown for the first time that ZIPK is activated in response to BCR cross-linking and recruited to the transcriptional machinery where it interacts with RNA pol II in an anti-IgM dependent manner. Such BCR-dependent ZIPK:RNA pol II interaction correlated with IEG mRNA induction kinetics, providing further evidence that ZIPK is activated downstream of the BCR to mediate transcription. Previously, ZIPK had been identified as activated downstream of both TNF-α and IFN-γ. In the context of TNF, ZIPK was shown to mediate the phosphorylation of p38 and Akt as well as reactive oxygen species (ROS) production induced by TNF-α. This study showed for the first time how ZIPK could regulate TNF-α inflammatory responses via ROS-mediated mechanisms. Conversely, IFN-γ activates a kinase cascade which sees DAPK1 activate ZIPK and in turn phosphorylate the ribosomal protein L13a, whose phosphorylation is essential for the translational repression of inflammatory genes by the interferon gamma activated inhibitor of translation (GAIT) complex. Interestingly, in this example, GAIT-dependent inactivation of ZIPK can then reactive gene expression as required by the cell, demonstrating a unique regulatory axis that first represses, then re-permits inflammatory gene expression. While these mechanisms are diverse and differ from our proposed model suggesting ZIPK mediates pre-mRNA processing to regulate gene expression, they highlight the dynamism of ZIPK function and how its role can differ based on DAPK1 expression, subcellular localisation and stimulation source.

STAT3 is well-reported to be activated in response to BCR signalling, as shown by us (Results Figure 4.1) and others [111, 115]. Further, ZIPK has previously been reported to interact with STAT3 and catalyse the phosphorylation of serine 727 [228]. In addition, STAT3 has been shown to be uniquely phosphorylated at S727 in CLL and it has been specifically implicated in binding DNA and activating pro-proliferative gene programmes in the disease [116]. We combined this available data and assessed ZIPK-STAT3 interaction in CLL cells, which has not previously been reported.

We confirmed the interaction in primary cells and demonstrated a BCR-inducible interaction between ZIPK and the CLL-specific phosphorylated form of STAT3. These data connected aspects of ZIPK biology which have previously been reported in isolation. In addition, this provided further evidence that ZIPK is downstream of the BCR pathway and its activity is inducible. Specifically, the ZIPK:STAT3 S727-P interaction showed the greatest inducibility post-BCR

activation and this interaction was also strongly reduced by ZIPK inhibition. We showed a small decrease in the levels of STAT S727-P when CLL cells are treated with ZIPK inhibitor, but a strong, BCR-dependent, loss of ZIPK:STAT3 interaction and loss of STAT3 S727-P binding at IEG promoters in response to ZIPK inhibition. These data suggest that the ZIPK:STAT3 relationship is not completely S727-P dependent. However, while ZIPK inhibition does not prevent S727 phosphorylation it does impact STAT3:ZIPK interaction and STAT3 S727-P nuclear function. It is possible that there are compensatory STAT3 phosphorylation events which maintain S727-P in the presence of ZIPK inhibition and/or that the ZIPK interaction is not strictly necessary for S727-P. Indeed, it has been suggested that constitutive STAT3 S727-P is maintained in CLL cells by an intrinsic, but unknown, mechanism [116] and it is likely that ZIPK is not required for this step. However, we can hypothesise that without the ZIPK interaction which is lost as a result of DAPK inhibition, STAT3 is unable to effectively target and bind IEG promoters to activate gene transcription.

We have previously discussed ZIPK cellular localisation with regard to DAPK1 and ZIPK T299-P phosphorylation, and can now consider localisation of ZIPK in its relationship with STAT3. Studies on STAT3 phosphorylation in CLL have shown that STAT3 S727-P has both a cytoplasmic and a nuclear fraction [116]. However, the mechanism of serine-phosphorylated STAT3 nuclear translocation in CLL is unknown and the study suggested an unidentified adapter may bind STAT3 to mediate its transport. We, and others, have previously shown that ZIPK is also present in both cellular compartments [278] (data not shown). As discussed, we have observed that DAPK inhibition impacts the ZIPK:STAT3 S727-P interaction and reduces STAT3 S727-P DNA-binding at IEG promoters. These data suggest that ZIPK function, while dispensable for STAT S727 phosphorylation, could be necessary for effective STAT3 nuclear shuttling and IEG promoter targeting.

There is some evidence to suggest ZIPK is also activated in response to CD40L stimulation. We have demonstrated ZIPK inhibition was able to overcome CD40L-mediated IEG expression (Results Figure 4.10) and H3T6/T11 phosphorylation (Results Figure 4.19). The fact that H3T6 and H3T11 phosphorylation was found in IEG loci in response to CD40L stimulation (particularly *DUSP2*) does lend evidence to support that ZIPK can be activated by CD40. If our hypotheses for ZIPK function as a signalling-histone kinase and

transcriptional co-activator are correct, it may well be activated to some degree in response to a variety of stimuli.

Considering the ZIPK:STAT3 interaction was increased following BCR crosslinking, we wanted to assess any potential interactions between ZIPK and NF-kB subunit p65 post CD40L stimulation. We could not confirm with certainty that ZIPK and p65 interacted in CLL or HBL1 cells (data not shown). The fact that ZIPK inhibition could impair CD40L/NF-kB-mediated activation of IEGs despite any interaction with NF-kB proteins suggested that the NF-kB-mediated transcriptional activation of our IEGs functions in a way which does not require ZIPK directly interacting with the transcription factor, as we have observed for STAT3. Interestingly, work has highlighted a previously unreported relationship between NF-κB and STAT3 in CLL which we can consider in this context. The study showed that the high levels of constitutive STAT3 S727-P in CLL also induced high levels of unphosphorylated STAT3 (U-STAT3) which bound to NF-κB dimers p65/p50 in competition with IκB [258, 287]. These U-STAT3/NF-κB complexes could translocate to the nucleus and bind NF-κB target genes to induce their transcription. With this in mind, STAT3 and NF-κB co-regulation has previously been observed in CLL [111, 112] and in our own work we have demonstrated an additive/synergistic effect of combining anti-IgM/CD40L stimulation on IEG expression. Taken together, these data suggest that a complex, STAT3-cooperative, NF-κB activation mechanism exists in CLL.

We hypothesise that the loss of ZIPK:STAT3 interaction and STAT3 S727-P DNA binding may impact NF-κB activation. For example, by disrupting the ZIPK:STAT3 interaction, potential ZIPK-mediated STAT3 nuclear shuttling and STAT3 promoter binding, we may in turn impact NF-κB recruitment and/or activation. Indeed, work has demonstrated the concept of transcription factor assisted loading, and the notion of partner/pioneer transcription factors, whereby one transcription factor binds a specific motif and mediates chromatin modifications to allow the binding of another [288-290]. Specifically, NF-κB can bind and prime enhancers, evidenced by increased H3K27ac, to facilitate STAT3 binding and promote synergistic gene expression [259]. We can only begin to hypothesise on the complex nature of transcription factor loading in CLL with our limited ChIP data for STAT3 and p65. Complete ChIP-seq profiling of these transcription factors in the context of BCR/CD40 activation with and without ZIPK inhibition may provide a clearer picture on how loss of ZIPK function impacts their DNA binding.

6.2.4 ZIPK in the coupling of RNA polymerase II transcription elongation with pre-mRNA processing

We have implicated ZIPK as a signalling histone kinase downstream of the BCR which interacts with RNA pol II and phosphorylates histones to promote IEG expression. As discussed, there are a variety of other histone kinases which have been reported to phosphorylate histones, directly modulate gene expression and also interact with and/or phosphorylate non-histone substrates (see 1.3.3 on signalling kinases) and ZIPK is not the first of this class of enzyme which has been implicated in a relationship with the transcription machinery.

PIM1, JAK2 and IKKα all show chromatin modifying activity linked to transcriptional elongation. PIM1 is recruited by MYC to catalyse H3S10-P at MYC-target genes, and it has been shown that H3S10-P was necessary for subsequent loading of positive transcription elongation factor b (P-TEFb) – a protein complex necessary to release paused RNA pol II into active elongation [170, 291, 292]. Tousled-like kinase (TLK1) has also been shown to stimulate H3S10-P in human epithelial cells and therefore may play a similar histone-kinase role as PIM1 [293]. JAK2 is a well-known signalling kinase which can directly phosphorylate H3T41 to exclude HP1α from chromatin, thus preventing the activation of gene expression programmes [171]. Similarly, IKKα has been reported to be directly recruited to the promoter of NF-kB target genes to phosphorylate H3S10-P for P-TEFb loading and RNA pol II elongation [168]. In addition, IKKα was shown to travel with elongating RNA pol II S2-P and HP1γ during transcription through the gene body [168]. We performed ZIPK ChIP experiments to determine if, and where, ZIPK bound the loci of our model IEGs (data not shown) with the aim of understanding whether or not ZIPK behaved like IKKα. The ZIPK ChIP data was difficult to analyse and the biggest challenge stemmed from the fact that there are no commercially available ChIP grade antibodies raised against ZIPK and we used antibodies validated for co-IP instead. Thus, while we could not confidently say whether ZIPK travels with the RNA pol II molecule, we have shown that they interact, and we observed H3T6-P and H3T11-P in the gene body regions where RNA pol S2-P is actively elongating the nascent transcript. In summary, this class of signalling enzyme mediates gene expression through various methods of facilitating transcription elongation by RNA pol II.

One of our more interesting observations was that ZIPK inhibition could prevent IEG expression in CLL and HBL1 cells despite having seemingly no effect on

RNA pol II recruitment and elongation. This data led us to investigate ZIPKs role in pre-mRNA processing and conclude that ZIPK function was required for the accurate processing of IEG nascent transcripts. Maturation of pre-mRNA precursors often occurs simultaneously with, and mechanically coupled to, transcription by RNA pol II. The co-transcriptional overlap in these two processes enhances the accuracy and efficiency of pre-mRNA processing [263]. Further, these processes occur both on and in the vicinity of the chromatin: which plays a role in coordinating them [203, 294]. One of the first studies to demonstrate co-transcriptional splicing used electron microscopy of chromatin spreads from embryonic *Drosophila melanogaster* to show that intron looping occurred in the presence of RNA pol II-DNA complexes, joined to the elongating transcript, suggesting that splicing takes place prior to transcript release from the RNA pol II complex [295].

In brief, the maturation of most pre-mRNAs requires the attachment of a 7-methylguanosine cap to the 5′ end of the transcript, splicing to excise introns and ligate exons, and formation of a 3′ end site by cleavage and addition of a non-templated poly(A) tail [263]. The co-transcriptional processing of pre-mRNA is mediated by a raft of proteins which interact with the CTD domain of RNA pol II. The CTD domain acts as a platform to recruit and directly interact with a variety of capping, splicing and 3’ end processing factors to the transcription elongation complex [261]. It has been suggested that the CTD phosphorylation occurring during the transcription cycle forms a ‘CTD code’ which guides the numerous processing factors on and off the transcription elongation complex platform as required [264].

Our data suggested that without ZIPK function there is an accumulation of unprocessed pre-mRNA and ZIPK inhibition greatly reduced the ratio of *DUSP2* alternate splice isoforms. Outside of our work, a potential role for H3T6-P and H3T11-P in controlling mRNA processing has not been reported. However, as discussed previously (see 1.4.4.2 on pre-mRNA processing) histone modifications are reported to play a large and well-reported role in pre-mRNA splicing, typically associated with alternative splicing. For example, H3K36me3 is often found enriched in exons while H3K9me2/3 and H3K27me2/3 have been shown to be preferentially excluded from these regions [201, 296]. One study showed that H3K27me3 and H3K36me1 were systemically replaced by H3K36me3 and H3K27me1 during transcription and their levels reflected the expression level of the gene. This study also demonstrated a difference in the

levels of H3K36me3 in alternatively spliced exons, whereby less of the histone modification was found at less-included exons [297]. This work suggested that the histone marks which guide alternative splicing can be actively set during transcription to guide pre-mRNA processing. We observed an impact of ZIPK inhibition on *DUSP2* alternative splicing and it is possible that catalysis of H3T6/T11 phosphorylation is an important priming event for accurate splicing. In light of such data, it would be interesting to assess if ZIPK inhibition could impact H3K36 methylation in exonic regions. In addition, particular *DUSP2* splice isoforms are generated via exon skipping and another study has shown that H3K4me1 as well as H3K36me3 can play a dominant role in skipped exon selection in mammalian development and in the brain [298]

It is worth considering that IEGs show rapid pre-mRNA induction and RNA polymerase recruitment compared to secondary/delayed response genes [173]. IEGs have a distinct genomic architecture and chromatin structure to facilitate their rapid transcription characterised by bivalent promoters poised for rapid activation [191]. Consequently, ZIPK inhibition may be particularly effective against the pre-mRNA processing of this class of gene: but genome-wide expression analysis would be required to confirm this (see 6.3.2 future direction).

Alternatively, it cannot be excluded that ZIPK could directly target non-histone substrates outside of STAT3 and RNA pol II such as proteins of the processing machinery. In addition to ZIPK itself, there is evidence to support the notion that its downstream histone targets, H3T6-P and H3T11-P, can act as a platform for splice factors to bind either directly or via intermediary chromatin-binding proteins which in turn recruit the splice factors. For example, the capping machinery binds both the CTD of RNA pol II and also H3K4me3 found at promoter regions [299]. Similarly, the chromatin remodelling ATPase CDH1 is recruited to active genes by binding H3K4me3 where it interacts with U2 spliceosome components [205]. Additionally, it was shown that HP1γ interacts with H3K9me3 in alternative exons in the *CD44* gene in human cells only when phosphorylated, a process which is controlled upstream by PKC. Interestingly, it was shown that the presence of HP1γ at alternative splice sites not only mediates the inclusion of variable exons but also impacts RNA pol II processivity, which was found to be enriched at HP1γ bound regions [210]. We can hypothesise that ZIPK or H3T6/T11-P may mediate the binding of splicing factors during co-transcriptional pre-mRNA processing, based on our data demonstrating that that loss of ZIPK strongly impacts alternative splicing of *DUSP2* and leads to an accumulation of unprocessed

transcripts. In our data we show that RNA pol II is unaffected in IEG gene bodies following ZIPK inhibition but we cannot accurately infer elongation speed from these experiments. Considering HP1γ-binding demonstrates how chromatin modifying enzymes mediating splicing can impact RNA pol II processivity, elongation rate experiments may be interesting in the context of loss of ZIPK function (see future direction 6.3.3)

We observed that in some cases of dual anti-IgM/CD40L stimulation ibrutinib was able to prevent RNA pol II S2-P recruitment, particularly at *EGR1*, but had little impact on gene expression. In these experiments we sometimes saw RNA pol II accumulation in the 3' end of our model IEGs. These data were confusing and we can only hypothesise on their meaning. As we observed unchanged RNA pol II bound upstream of the TSS at the *EGR1* promoter it is plausible that the IEG elongation kinetics are slightly altered with dual stimulation. This is somewhat evident when comparing IEG expression between anti-IgM alone and dual anti-IgM/CD40L where the peak expression came after 30 and 45 minutes respectively (Results Figure 4.7). These differences may arise from contrasting RNA pol II recruitment dynamics which could be dependent on the signalling pathway and downstream TFs (e.g. CD40L/NF-kB versus BCR/STAT3) at *DUSP2* and *EGR1*. As ibrutinib only inhibited the BCR/STAT3-mediated IEG expression in the context of dual stimulation, we may be observing a specific CD40/NF-kB RNA pol II recruitment signature, typified by slower/less RNA pol II S2-P recruitment and elongation through the gene body. These kind of hypotheses could be examined in future work considering transcription elongation speeds in the context of different pathway activation and inhibitor treatment (see future direction 6.3.3).

We can hypothesise how ZIPK catalysing H3T6 and H3T11 phosphorylation in the gene bodies of IEGs ensures the processing of their pre-mRNA. ZIPK may be recruited by STAT3 and NF-kB to catalyse H3T6-P and H3T11-P at target genes and/or also travel with the elongating RNA pol II like IKKα in order to mediate the recruitment of processing factors to the RNA pol II CTD. Additionally, RNA pol II-associated ZIPK, or H3T6-P/H3T11-P, may directly target the pre-mRNA processing machinery or act as a platform for its recruitment, in a similar fashion to CDH1, HP1γ and H3K4me3 recruiting splicing factors. On the other hand, the presence of ZIPK, H3T6-P and H3T11-P may exclude proteins or histone modifications inhibitory to gene expression from the chromatin around

IEGs, like JAK2. Further work is required to fully understand the mechanism of ZIPK-mediated IEG pre-mRNA processing (see 6.3 future direction).

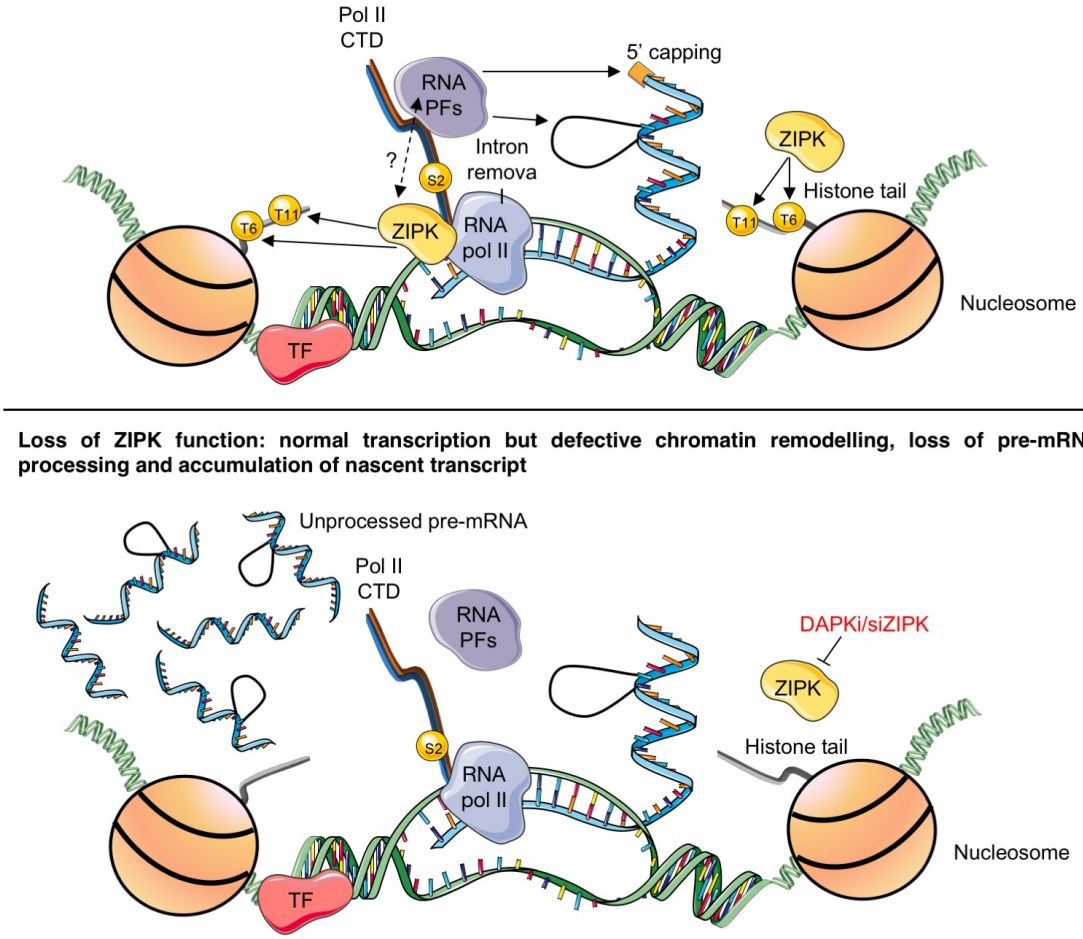

Maturation of pre-mRNAs often occurs simultaneously with their synthesis by RNA polymerase II. The co-transcriptional nature of pre-mRNA processing requires alterations to the chromatin structure by histone-modifying enzymes like ZIPK for the recruitment and action of both the RNA polymerase II itself and a raft of RNA processing factors for splicing, intron removal, 3' end processing and 5' capping.

- ZIPK-mediated phosphorylation of histone H3T6 and H3T11 does not prevent elongating RNA pol II (with which we show it interacts), but is required for the faithful co-transcriptional mRNA processing of key pro-proliferative genes in chronic lymphocytic leukaemia (CLL).
- ZIPK loss of function prevents CLL cell proliferation and promotes apoptosis *in vitro* in a manner comparable to the CLL therapeutic, Ibrutinib.
- ZIPK functions downstream of commonly mutated enzymes in Ibrutinib-resistant CLL and is able to overcome both BCR and CD40-mediated gene expression, while Ibrutinib cannot prevent the latter.

Abbreviations: TF, transcription factor; RNA PFs, RNA processing factors; RNA pol II; RNA polymerase II; Pol II CTD; RNA polymerase II carboxy-terminal domain; S2, serine 2 phosphorylation; T6, threonine 6 phosphorylation; T11, threonine 11 phosphorylation; DAPKi, ZIPK inhibitor. This figure was created using Servier Medical Art templates, which are licensed under a Creative Commons Attribution 3.0 Unported License; https://smart.servier.com.

Figure 6.1: Model summarising the potential involvement of ZIPK in the co-transcriptional recruitment and function of factors coupling transcription & RNA processing.

6.3 Future directions & limitations

Our work has identified a novel role for ZIPK in gene expression through histone phosphorylation-mediated regulation of pre-mRNA processing. The data presented focuses on two IEGs activated downstream of the BCR which are known to play a role in CLL pathogenesis. In order to expand on our work, investigation into the areas described below, which were outside the scope of this project, would help to develop and increase our understanding of ZIPK function and its potential as a therapeutic. Of note, for almost all of the techniques and thoughts described below, the principle caveats for their execution comprise either technical limitations or the expense associated with the experiments.

6.3.1 ZIPK inhibition versus knockdown versus knockout

In our work, we used a commercially available ATP-competitive ZIPK inhibitor (DAPKi) to prevent ZIPK kinase activity. This inhibitor prevented ZIPK function at doses of >25 μM (Results Figure 3.2) and effectively inhibited CLL cell proliferation in a manner comparable with ibrutinib when used at this dose (Thomas et al., forthcoming 2020). The dose of DAPKi we utilised is high when compared with many commercially available targeted inhibitors which we must attribute to its unrefined, non-commercial nature. It is worth noting another ZIPK inhibitor (HS38) was synthesised to examine the involvement of ZIPK in the regulation of smooth muscle contraction [300] and it could be beneficial to compare and contrast this inhibitor with our own.

We also used siRNAs directed against ZIPK to block its expression at the mRNA level, thus preventing its activity, in HBL1 cells (Results Figure 3.12). While sufficient for our work, future experiments could potentially benefit from more efficient ZIPK inhibition. Notably, the use of shRNA directed against ZIPK or CRISPR technology. Like siRNA, shRNA takes advantage of endogenous cellular machinery to silence gene expression. However, shRNA is transfected into the cell via vector-based approaches and can be used to study long-term effects through incorporation into the genome. Considering our siRNA efficiency, use of shRNA-mediated knockdown could allow us to stably prevent ZIPK expression over a longer period of time for further study. In contrast to both, gene knockout approaches like CRISPR [301] lead to complete elimination of gene function. Considering the biological limitations of transient siRNA knock-down, use of CRISPR-cas9-mediated ZIPK gene knockout could provide us with a more complete picture of the effects of loss of ZIPK function. In addition, we used HBL1

cells for our siRNA-mediated ZIPK knockdown to study ZIPK function. From a CLL therapeutic point of view, using any of the above technologies in primary cells would be both beneficial but also technically challenging.

6.3.2 Genome-wide studies

While *EGR1* and *DUSP2* are exemplary model IEGs to study ZIPK molecular mechanisms, next-generation sequencing experiments could increase our understanding of ZIPK function on a genome-wide scale.

RNA-sequencing (RNA-seq) allows the entire transcriptome to be quantified in a high-throughput manner, providing a precise readout of the levels of transcripts and their isoforms present in a cell [302]. For us, there are many advantages in being able to look genome-wide at genes which are downregulated in response to a loss of ZIPK function. Principally, by comparing cells (either HBL1 or CLL) prepared with the technologies described above (DAPKi, si/shRNA, CRISPR) to 'normal' cells we could theoretically assess, genome-wide, the types of genes which are effected by a loss of ZIPK function. This could be particularly interesting when we consider ZIPKs impact on IEGs and ask the question: does ZIPK preferentially effect the processing of short, low exon number, IEGs specifically? RNA-seq would allow us to assess all genes and transcripts effected by a loss of ZIPK function and determine whether slower, secondary response and delayed genes are also affected.

Similarly, ChIP-sequencing (ChIP-seq) comparing cells lacking functioning ZIPK with 'normal' cells would allow us to expand from our model IEGs and assess H3T6 and H3T11 phosphorylation genome-wide. By combining data from RNA-seq and ChIP-seq, in the same way we have combined qPCR and ChIP data, we could identify genes whose activation is marked by H3T6 and H3T11 phosphorylation – and assess whether or not these genes can be downregulated by ZIPK inhibition. These type of experiments would allow us to better understand the characteristics of genes which are regulated by ZIPK and which pathways they are downstream of. Further, ChIP-seq focussing on the transcription factors STAT3 and NF-κB could help us to understand how these proteins work in concert to mediate synergistic gene expression in CLL, a topic we touched upon in this work.

6.3.3 ZIPK in transcription coupled-processing

We have implicated ZIPK as playing a role in the pre-mRNA processing of IEGs downstream of the BCR. We have shown that ZIPK inhibition impacts the effectiveness of pre-mRNA processing through the detection of an accumulation of unprocessed transcripts and impaired alternative splicing. It was however beyond the scope of this project to delve into this mechanism further, and attempt to identify more precisely how ZIPK inhibition prevents faithful co-transcriptional processing of primary transcripts.

RNA-immunoprecipitation (RIP) can be used to map RNA-protein interactions by cross-linking RNA molecules to RNA-binding proteins (RBPs) in a similar way that ChIP assesses DNA-protein interactions [303]. RIP utilises a specific antibody against the protein of interest to pull down RBP and target-RNA complexes and precisely map RBP-binding sites. Any RNA that is associated with this protein complex will also be isolated and can be further analysed by qPCR. There are a raft of proteins involved in the processing of pre-mRNA, but by screening key members of the processing machinery by RIP we could potentially determine whether a loss of ZIPK function prevents their interaction with the pre-mRNA. Similarly, it would be interesting to assess whether or not ZIPK interacts directly with the unprocessed pre-mRNA itself or whether its effect on processing is mediated instead by interactions with members of the processing machinery.

Further concerning the involvement of ZIPK on coupled transcription and mRNA processing, 4sUDRB-seq can measure global transcription elongation speed and the rate of RNA pol II transition into active elongation, and how these factors effect total mRNA production [304]. The technique uses reversible inhibition of transcription elongation with DRB combined with a pulse of 4-thiouridine (4sU) to tag newly transcribed RNA which can be subsequently captured and sequenced. For us, this protocol could allow for the purification of all the nascent pre-mRNA transcripts which persist in the presence of ZIPK inhibition. These kind of experiments would allow us to learn more about ZIPKs mechanism of action with regard to pre-mRNA processing as well as identify the types of genes whose primary transcripts remain unprocessed following ZIPK inhibition.

6.3.4 ZIPK *in-vivo* studies

From a future therapeutic perspective, to understand how ZIPK inhibitors may be used to treat CLL or even other diseases in which DAPK1 is silenced, *in-vivo* models would be a necessary and highly information step. The use of murine models to study the biology of disease is well document and remains essential to understand and improve treatment and therapy [305].

Poor engraftment by CLL cells into mice has limited the utility of xenograft models for the disease [306] but nevertheless there are several mouse models used to study CLL [307]. Of these, the TCL1 transgenic mice [308] and 13q14-deletion models [309] have been comprehensively studied and show close resemblance to the human disease. For us, such mice may require further genetic engineering to prevent DAPK1 expression. Thereafter, survival of CLL-mice treated with or without ZIPK inhibitors could be compared. Further, the efficacy of ZIPK inhibitors in mice modified to present with other unfavourable prognostic markers e.g. p53 mutation, could be considered.

In summary, future work researching the use of ZIPK inhibitors to treat disease, especially ibrutinib resistant CLL with BTK or PLCγ2 mutations, would require the study with *in vivo* mouse models.

6.4 Concluding remarks

In conclusion, our work suggests that ZIPK functions as one of the final downstream enzymes in the transcription cascade of at least the BCR and NF-kB pathways, required for successfully orchestrating the co-transcriptional processing of nascent pre-mRNA transcripts into mature mRNA.

Mechanistically, we implicate ZIPK as a signalling-histone kinase which can directly regulate gene expression through a role in pre-mRNA processing, modify histone H3 at threonine 6 and threonine 11 and also interact with non-histone substrates including STAT3 and RNA polymerase II.

Clinically, we demonstrate that ZIPK inhibition can outperform ibrutinib in blocking pro-proliferative gene expression when the upstream signalling originates from an alternative non-BCR source, such as CD40. As ZIPK seems to function far downstream of both BTK and PLCγ2, and its inhibition is effective against both BCR and CD40-mediated signals, our data suggests that ZIPK inhibition could be an alternative to ibrutinib treatment in CLL and other DAPK1-silenced malignancies.

Chapter 7 References

1. Cooper, M.D., *The early history of B cells.* Nat Rev Immunol, 2015. **15**(3): p. 191-7.
2. Hoffman, W., F.G. Lakkis, and G. Chalasani, *B Cells, Antibodies, and More.* Clin J Am Soc Nephrol, 2016. **11**(1): p. 137-54.
3. Rothenberg, E.V., *Transcriptional control of early T and B cell developmental choices.* Annu Rev Immunol, 2014. **32**: p. 283-321.
4. Wang, L.D. and M.R. Clark, *B-cell antigen-receptor signalling in lymphocyte development.* Immunology, 2003. **110**(4): p. 411-20.
5. Harpaz, Y. and C. Chothia, *Many of the immunoglobulin superfamily domains in cell adhesion molecules and surface receptors belong to a new structural set which is close to that containing variable domains.* J Mol Biol, 1994. **238**(4): p. 528-39.
6. Davies, D.R. and H. Metzger, *Structural basis of antibody function.* Annu Rev Immunol, 1983. **1**: p. 87-117.
7. Williams, A.F. and A.N. Barclay, *The immunoglobulin superfamily--domains for cell surface recognition.* Annu Rev Immunol, 1988. **6**: p. 381-405.
8. D'Angelo, S., et al., *Many Routes to an Antibody Heavy-Chain CDR3: Necessary, Yet Insufficient, for Specific Binding.* Front Immunol, 2018. **9**: p. 395.
9. Schroeder, H.W., Jr. and L. Cavacini, *Structure and function of immunoglobulins.* J Allergy Clin Immunol, 2010. **125**(2 Suppl 2): p. S41-52.
10. Schatz, D.G. and Y. Ji, *Recombination centres and the orchestration of V(D)J recombination.* Nat Rev Immunol, 2011. **11**(4): p. 251-63.
11. Croce, C.M., et al., *Chromosomal location of the genes for human immunoglobulin heavy chains.* Proc Natl Acad Sci U S A, 1979. **76**(7): p. 3416-9.
12. Malcolm, S., et al., *Localization of human immunoglobulin kappa light chain variable region genes to the short arm of chromosome 2 by in situ hybridization.* Proc Natl Acad Sci U S A, 1982. **79**(16): p. 4957-61.
13. Erikson, J., J. Martinis, and C.M. Croce, *Assignment of the genes for human lambda immunoglobulin chains to chromosome 22.* Nature, 1981. **294**(5837): p. 173-5.
14. Jhunjhunwala, S., et al., *The 3D structure of the immunoglobulin heavy-chain locus: implications for long-range genomic interactions.* Cell, 2008. **133**(2): p. 265-79.
15. Gellert, M., *V(D)J recombination: RAG proteins, repair factors, and regulation.* Annu Rev Biochem, 2002. **71**: p. 101-32.
16. Townsend, C.L., et al., *Significant Differences in Physicochemical Properties of Human Immunoglobulin Kappa and Lambda CDR3 Regions.* Front Immunol, 2016. **7**: p. 388.
17. Bassing, C.H., W. Swat, and F.W. Alt, *The mechanism and regulation of chromosomal V(D)J recombination.* Cell, 2002. **109 Suppl**: p. S45-55.
18. Vidarsson, G., G. Dekkers, and T. Rispens, *IgG subclasses and allotypes: from structure to effector functions.* Front Immunol, 2014. **5**: p. 520.

19. Vlasak, J. and R. Ionescu, *Fragmentation of monoclonal antibodies.* MAbs, 2011. **3**(3): p. 253-63.
20. Porter, R.R., *The hydrolysis of rabbit y-globulin and antibodies with crystalline papain.* Biochem J, 1959. **73**: p. 119-26.
21. Nelson, A.L., *Antibody fragments: hope and hype.* MAbs, 2010. **2**(1): p. 77-83.
22. Jones, R.G. and J. Landon, *Enhanced pepsin digestion: a novel process for purifying antibody F(ab')(2) fragments in high yield from serum.* J Immunol Methods, 2002. **263**(1-2): p. 57-74.
23. Morrison, S.J., et al., *Identification of a lineage of multipotent hematopoietic progenitors.* Development, 1997. **124**(10): p. 1929-39.
24. Kondo, M., *Lymphoid and myeloid lineage commitment in multipotent hematopoietic progenitors.* Immunol Rev, 2010. **238**(1): p. 37-46.
25. Matthias, P. and A.G. Rolink, *Transcriptional networks in developing and mature B cells.* Nat Rev Immunol, 2005. **5**(6): p. 497-508.
26. Medina, K.L., et al., *Assembling a gene regulatory network for specification of the B cell fate.* Dev Cell, 2004. **7**(4): p. 607-17.
27. Hesslein, D.G. and D.G. Schatz, *Factors and forces controlling V(D)J recombination.* Adv Immunol, 2001. **78**: p. 169-232.
28. Sanz, E., et al., *Ordering human CD34+CD10-CD19+ pre/pro-B-cell and CD19- common lymphoid progenitor stages in two pro-B-cell development pathways.* Proc Natl Acad Sci U S A, 2010. **107**(13): p. 5925-30.
29. Barnkob, M.S., C. Simon, and L.R. Olsen, *Characterizing the human hematopoietic CDome.* Front Genet, 2014. **5**: p. 331.
30. Engel, P., et al., *CD Nomenclature 2015: Human Leukocyte Differentiation Antigen Workshops as a Driving Force in Immunology.* J Immunol, 2015. **195**(10): p. 4555-63.
31. Tonegawa, S., *Somatic generation of antibody diversity.* Nature, 1983. **302**(5909): p. 575-81.
32. Zhang, M., G. Srivastava, and L. Lu, *The pre-B cell receptor and its function during B cell development.* Cell Mol Immunol, 2004. **1**(2): p. 89-94.
33. Lu, H., K. Schwarz, and M.R. Lieber, *Extent to which hairpin opening by the Artemis:DNA-PKcs complex can contribute to junctional diversity in V(D)J recombination.* Nucleic Acids Res, 2007. **35**(20): p. 6917-23.
34. Repasky, J.A., et al., *Mutational analysis of terminal deoxynucleotidyltransferase-mediated N-nucleotide addition in V(D)J recombination.* J Immunol, 2004. **172**(9): p. 5478-88.
35. Lewis, S.M., *The mechanism of V(D)J joining: lessons from molecular, immunological, and comparative analyses.* Adv Immunol, 1994. **56**: p. 27-150.
36. Jeske, D.J., et al., *Junctional diversity is essential to antibody activity.* J Immunol, 1984. **133**(3): p. 1090-2.
37. Xu, J.L. and M.M. Davis, *Diversity in the CDR3 region of V(H) is sufficient for most antibody specificities.* Immunity, 2000. **13**(1): p. 37-45.
38. Bruce, S.R., R.W. Dingle, and M.L. Peterson, *B-cell and plasma-cell splicing differences: a potential role in regulated immunoglobulin RNA processing.* RNA, 2003. **9**(10): p. 1264-73.
39. Lutz, J., et al., *Pro-B cells sense productive immunoglobulin heavy chain rearrangement irrespective of polypeptide production.* Proc Natl Acad Sci U S A, 2011. **108**(26): p. 10644-9.

40. Vettermann, C. and M.S. Schlissel, *Allelic exclusion of immunoglobulin genes: models and mechanisms.* Immunol Rev, 2010. **237**(1): p. 22-42.
41. Korsmeyer, S.J., et al., *Developmental hierarchy of immunoglobulin gene rearrangements in human leukemic pre-B-cells.* Proc Natl Acad Sci U S A, 1981. **78**(11): p. 7096-100.
42. Martensson, I.L., et al., *The pre-B cell receptor checkpoint.* FEBS Lett, 2010. **584**(12): p. 2572-9.
43. Melchers, F., et al., *The surrogate light chain in B-cell development.* Immunol Today, 1993. **14**(2): p. 60-8.
44. Fuentes-Panana, E.M., et al., *Basal Igalpha/Igbeta signals trigger the coordinated initiation of pre-B cell antigen receptor-dependent processes.* J Immunol, 2004. **173**(2): p. 1000-11.
45. Bannish, G., et al., *Ligand-independent signaling functions for the B lymphocyte antigen receptor and their role in positive selection during B lymphopoiesis.* J Exp Med, 2001. **194**(11): p. 1583-96.
46. Ponte, P.A., et al., *Transcription of immunoglobulin heavy-chain sequences from the excluded allele.* Nature, 1981. **291**(5816): p. 594-6.
47. Reth, M.G., et al., *Regulated progression of a cultured pre-B-cell line to the B-cell stage.* Nature, 1985. **317**(6035): p. 353-5.
48. Brauninger, A., et al., *Regulation of immunoglobulin light chain gene rearrangements during early B cell development in the human.* Eur J Immunol, 2001. **31**(12): p. 3631-7.
49. Sitia, R., M.S. Neuberger, and C. Milstein, *Regulation of membrane IgM expression in secretory B cells: translational and post-translational events.* EMBO J, 1987. **6**(13): p. 3969-77.
50. Geisberger, R., M. Lamers, and G. Achatz, *The riddle of the dual expression of IgM and IgD.* Immunology, 2006. **118**(4): p. 429-37.
51. Gorman, J.R. and F.W. Alt, *Regulation of immunoglobulin light chain isotype expression.* Adv Immunol, 1998. **69**: p. 113-81.
52. Kuo, T.C. and M.S. Schlissel, *Mechanisms controlling expression of the RAG locus during lymphocyte development.* Curr Opin Immunol, 2009. **21**(2): p. 173-8.
53. Luning Prak, E.T., M. Monestier, and R.A. Eisenberg, *B cell receptor editing in tolerance and autoimmunity.* Ann N Y Acad Sci, 2011. **1217**: p. 96-121.
54. Allman, D. and S. Pillai, *Peripheral B cell subsets.* Curr Opin Immunol, 2008. **20**(2): p. 149-57.
55. De Silva, N.S. and U. Klein, *Dynamics of B cells in germinal centres.* Nat Rev Immunol, 2015. **15**(3): p. 137-48.
56. Okada, T., et al., *Antigen-engaged B cells undergo chemotaxis toward the T zone and form motile conjugates with helper T cells.* PLoS Biol, 2005. **3**(6): p. e150.
57. Schwickert, T.A., et al., *A dynamic T cell-limited checkpoint regulates affinity-dependent B cell entry into the germinal center.* J Exp Med, 2011. **208**(6): p. 1243-52.
58. Baumjohann, D., T. Okada, and K.M. Ansel, *Cutting Edge: Distinct waves of BCL6 expression during T follicular helper cell development.* J Immunol, 2011. **187**(5): p. 2089-92.
59. Di Noia, J.M. and M.S. Neuberger, *Molecular mechanisms of antibody somatic hypermutation.* Annu Rev Biochem, 2007. **76**: p. 1-22.

60. Muramatsu, M., et al., *Specific expression of activation-induced cytidine deaminase (AID), a novel member of the RNA-editing deaminase family in germinal center B cells.* J Biol Chem, 1999. **274**(26): p. 18470-6.
61. Victora, G.D., et al., *Germinal center dynamics revealed by multiphoton microscopy with a photoactivatable fluorescent reporter.* Cell, 2010. **143**(4): p. 592-605.
62. Gitlin, A.D., Z. Shulman, and M.C. Nussenzweig, *Clonal selection in the germinal centre by regulated proliferation and hypermutation.* Nature, 2014. **509**(7502): p. 637-40.
63. Manis, J.P., M. Tian, and F.W. Alt, *Mechanism and control of class-switch recombination.* Trends Immunol, 2002. **23**(1): p. 31-9.
64. Chaudhuri, J. and F.W. Alt, *Class-switch recombination: interplay of transcription, DNA deamination and DNA repair.* Nat Rev Immunol, 2004. **4**(7): p. 541-52.
65. Shinkura, R., et al., *The influence of transcriptional orientation on endogenous switch region function.* Nat Immunol, 2003. **4**(5): p. 435-41.
66. Chaudhuri, J., et al., *Transcription-targeted DNA deamination by the AID antibody diversification enzyme.* Nature, 2003. **422**(6933): p. 726-30.
67. Reaban, M.E. and J.A. Griffin, *Induction of RNA-stabilized DNA conformers by transcription of an immunoglobulin switch region.* Nature, 1990. **348**(6299): p. 342-4.
68. Mizuta, R., et al., *Molecular visualization of immunoglobulin switch region RNA/DNA complex by atomic force microscope.* J Biol Chem, 2003. **278**(7): p. 4431-4.
69. Manis, J.P., et al., *Ku70 is required for late B cell development and immunoglobulin heavy chain class switching.* J Exp Med, 1998. **187**(12): p. 2081-9.
70. Boboila, C., et al., *Alternative end-joining catalyzes class switch recombination in the absence of both Ku70 and DNA ligase 4.* J Exp Med, 2010. **207**(2): p. 417-27.
71. Victora, G.D. and M.C. Nussenzweig, *Germinal centers.* Annu Rev Immunol, 2012. **30**: p. 429-57.
72. Suan, D., C. Sundling, and R. Brink, *Plasma cell and memory B cell differentiation from the germinal center.* Curr Opin Immunol, 2017. **45**: p. 97-102.
73. Dorner, T. and A. Radbruch, *Selecting B cells and plasma cells to memory.* J Exp Med, 2005. **201**(4): p. 497-9.
74. Fink, K., *Origin and Function of Circulating Plasmablasts during Acute Viral Infections.* Front Immunol, 2012. **3**: p. 78.
75. Fabbri, G. and R. Dalla-Favera, *The molecular pathogenesis of chronic lymphocytic leukaemia.* Nat Rev Cancer, 2016. **16**(3): p. 145-62.
76. Chiorazzi, N., K.R. Rai, and M. Ferrarini, *Chronic lymphocytic leukemia.* N Engl J Med, 2005. **352**(8): p. 804-15.
77. Rai, K.R., et al., *Clinical staging of chronic lymphocytic leukemia.* Blood, 1975. **46**(2): p. 219-34.
78. Binet, J.L., et al., *A new prognostic classification of chronic lymphocytic leukemia derived from a multivariate survival analysis.* Cancer, 1981. **48**(1): p. 198-206.
79. Zenz, T., et al., *From pathogenesis to treatment of chronic lymphocytic leukaemia.* Nat Rev Cancer, 2010. **10**(1): p. 37-50.
80. Sarfati, M., et al., *Prognostic importance of serum soluble CD23 level in chronic lymphocytic leukemia.* Blood, 1996. **88**(11): p. 4259-64.

81. Damle, R.N., et al., *B-cell chronic lymphocytic leukemia cells express a surface membrane phenotype of activated, antigen-experienced B lymphocytes.* Blood, 2002. **99**(11): p. 4087-93.
82. Damle, R.N., et al., *Ig V gene mutation status and CD38 expression as novel prognostic indicators in chronic lymphocytic leukemia.* Blood, 1999. **94**(6): p. 1840-7.
83. Crespo, M., et al., *ZAP-70 expression as a surrogate for immunoglobulin-variable-region mutations in chronic lymphocytic leukemia.* N Engl J Med, 2003. **348**(18): p. 1764-75.
84. Stilgenbauer, S., P. Lichter, and H. Dohner, *Genetic features of B-cell chronic lymphocytic leukemia.* Rev Clin Exp Hematol, 2000. **4**(1): p. 48-72.
85. Martinez-Trillos, A., et al., *Recurrent gene mutations in CLL.* Adv Exp Med Biol, 2013. **792**: p. 87-107.
86. Landau, D.A., et al., *Mutations driving CLL and their evolution in progression and relapse.* Nature, 2015. **526**(7574): p. 525-30.
87. Beekman, R., et al., *The reference epigenome and regulatory chromatin landscape of chronic lymphocytic leukemia.* Nat Med, 2018. **24**(6): p. 868-880.
88. Gaiti, F., et al., *Epigenetic evolution and lineage histories of chronic lymphocytic leukaemia.* Nature, 2019. **569**(7757): p. 576-580.
89. Pastore, A., et al., *Corrupted coordination of epigenetic modifications leads to diverging chromatin states and transcriptional heterogeneity in CLL.* Nat Commun, 2019. **10**(1): p. 1874.
90. Oakes, C.C., et al., *DNA methylation dynamics during B cell maturation underlie a continuum of disease phenotypes in chronic lymphocytic leukemia.* Nat Genet, 2016. **48**(3): p. 253-64.
91. Raval, A., et al., *Downregulation of death-associated protein kinase 1 (DAPK1) in chronic lymphocytic leukemia.* Cell, 2007. **129**(5): p. 879-90.
92. Kristensen, L.S., et al., *Hypermethylation of DAPK1 is an independent prognostic factor predicting survival in diffuse large B-cell lymphoma.* Oncotarget, 2014. **5**(20): p. 9798-810.
93. Burger, J.A., *Nurture versus nature: the microenvironment in chronic lymphocytic leukemia.* Hematology Am Soc Hematol Educ Program, 2011. **2011**: p. 96-103.
94. Ten Hacken, E. and J.A. Burger, *Microenvironment interactions and B-cell receptor signaling in Chronic Lymphocytic Leukemia: Implications for disease pathogenesis and treatment.* Biochim Biophys Acta, 2016. **1863**(3): p. 401-413.
95. Herishanu, Y., et al., *The lymph node microenvironment promotes B-cell receptor signaling, NF-kappaB activation, and tumor proliferation in chronic lymphocytic leukemia.* Blood, 2011. **117**(2): p. 563-74.
96. Choi, M.Y., M.K. Kashyap, and D. Kumar, *The chronic lymphocytic leukemia microenvironment: Beyond the B-cell receptor.* Best Pract Res Clin Haematol, 2016. **29**(1): p. 40-53.
97. Patten, P.E., et al., *IGHV-unmutated and IGHV-mutated chronic lymphocytic leukemia cells produce activation-induced deaminase protein with a full range of biologic functions.* Blood, 2012. **120**(24): p. 4802-11.
98. Baliakas, P., et al., *Not all IGHV3-21 chronic lymphocytic leukemias are equal: prognostic considerations.* Blood, 2015. **125**(5): p. 856-9.

99. Agathangelidis, A., et al., *Stereotyped B-cell receptors in one-third of chronic lymphocytic leukemia: a molecular classification with implications for targeted therapies.* Blood, 2012. **119**(19): p. 4467-75.
100. Widhopf, G.F., 2nd, et al., *Chronic lymphocytic leukemia B cells of more than 1% of patients express virtually identical immunoglobulins.* Blood, 2004. **104**(8): p. 2499-504.
101. Broker, B.M., et al., *Chronic lymphocytic leukemic (CLL) cells secrete multispecific autoantibodies.* J Autoimmun, 1988. **1**(5): p. 469-81.
102. Sthoeger, Z.M., et al., *Production of autoantibodies by CD5-expressing B lymphocytes from patients with chronic lymphocytic leukemia.* J Exp Med, 1989. **169**(1): p. 255-68.
103. Maity, P.C., et al., *IGLV3-21*01 is an inherited risk factor for CLL through the acquisition of a single-point mutation enabling autonomous BCR signaling.* Proc Natl Acad Sci U S A, 2020. **117**(8): p. 4320-4327.
104. Hayden, M.S. and S. Ghosh, *Shared principles in NF-kappaB signaling.* Cell, 2008. **132**(3): p. 344-62.
105. Zhang, Q., M.J. Lenardo, and D. Baltimore, *30 Years of NF-kappaB: A Blossoming of Relevance to Human Pathobiology.* Cell, 2017. **168**(1-2): p. 37-57.
106. Sun, S.C., *Non-canonical NF-kappaB signaling pathway.* Cell Res, 2011. **21**(1): p. 71-85.
107. Mansouri, L., et al., *NF-kappaB activation in chronic lymphocytic leukemia: A point of convergence of external triggers and intrinsic lesions.* Semin Cancer Biol, 2016. **39**: p. 40-8.
108. Mansouri, L., et al., *Functional loss of IkappaBepsilon leads to NF-kappaB deregulation in aggressive chronic lymphocytic leukemia.* J Exp Med, 2015. **212**(6): p. 833-43.
109. Tuveson, D. and K.R. Rai, *Augmenting NF-kappaB in poor-risk CLL: A general paradigm for other cancers?* J Exp Med, 2015. **212**(6): p. 830-1.
110. Kanduri, M., et al., *Differential genome-wide array-based methylation profiles in prognostic subsets of chronic lymphocytic leukemia.* Blood, 2010. **115**(2): p. 296-305.
111. Rozovski, U., et al., *Activation of the B-cell receptor successively activates NF-kappaB and STAT3 in chronic lymphocytic leukemia cells.* Int J Cancer, 2017. **141**(10): p. 2076-2081.
112. Liu, F.T., et al., *STAT3 and NF-kappaB cooperatively control in vitro spontaneous apoptosis and poor chemo-responsiveness in patients with chronic lymphocytic leukemia.* Oncotarget, 2016. **7**(22): p. 32031-45.
113. Kipps, T.J., et al., *Chronic lymphocytic leukaemia.* Nat Rev Dis Primers, 2017. **3**: p. 17008.
114. Duhren-von Minden, M., et al., *Chronic lymphocytic leukaemia is driven by antigen-independent cell-autonomous signalling.* Nature, 2012. **489**(7415): p. 309-12.
115. Rozovski, U., et al., *Stimulation of the B-cell receptor activates the JAK2/STAT3 signaling pathway in chronic lymphocytic leukemia cells.* Blood, 2014. **123**(24): p. 3797-802.
116. Hazan-Halevy, I., et al., *STAT3 is constitutively phosphorylated on serine 727 residues, binds DNA, and activates transcription in CLL cells.* Blood, 2010. **115**(14): p. 2852-63.
117. Woyach, J.A. and A.J. Johnson, *Targeted therapies in CLL: mechanisms of resistance and strategies for management.* Blood, 2015. **126**(4): p. 471-7.

118. Guo, A., et al., *Heightened BTK-dependent cell proliferation in unmutated chronic lymphocytic leukemia confers increased sensitivity to ibrutinib.* Oncotarget, 2016. **7**(4): p. 4598-610.
119. Packham, G., et al., *The outcome of B-cell receptor signaling in chronic lymphocytic leukemia: proliferation or anergy.* Haematologica, 2014. **99**(7): p. 1138-48.
120. Montillo, M., et al., *Chronic lymphocytic leukemia: novel prognostic factors and their relevance for risk-adapted therapeutic strategies.* Haematologica, 2005. **90**(3): p. 391-9.
121. Fischer, K., et al., *Long-term remissions after FCR chemoimmunotherapy in previously untreated patients with CLL: updated results of the CLL8 trial.* Blood, 2016. **127**(2): p. 208-15.
122. Brown, J.R., et al., *Idelalisib, an inhibitor of phosphatidylinositol 3-kinase p110delta, for relapsed/refractory chronic lymphocytic leukemia.* Blood, 2014. **123**(22): p. 3390-7.
123. Hillmen, P., et al., *Ibrutinib Plus Venetoclax in Relapsed/Refractory Chronic Lymphocytic Leukemia: The CLARITY Study.* J Clin Oncol, 2019. **37**(30): p. 2722-2729.
124. Al-Sawaf, O., et al., *Obinutuzumab in chronic lymphocytic leukemia: design, development and place in therapy.* Drug Des Devel Ther, 2017. **11**: p. 295-304.
125. Moreno, C., et al., *Ibrutinib plus obinutuzumab versus chlorambucil plus obinutuzumab in first-line treatment of chronic lymphocytic leukaemia (iLLUMINATE): a multicentre, randomised, open-label, phase 3 trial.* Lancet Oncol, 2019. **20**(1): p. 43-56.
126. Sharman, J.P., et al., *ELEVATE TN: Phase 3 Study of Acalabrutinib Combined with Obinutuzumab (O) or Alone Vs O Plus Chlorambucil (Clb) in Patients (Pts) with Treatment-Naive Chronic Lymphocytic Leukemia (CLL).* Blood, 2019. **134**(Supplement_1): p. 31.
127. Fischer, K., et al., *Venetoclax and Obinutuzumab in Patients with CLL and Coexisting Conditions.* N Engl J Med, 2019. **380**(23): p. 2225-2236.
128. Burger, J.A., et al., *Ibrutinib as Initial Therapy for Patients with Chronic Lymphocytic Leukemia.* N Engl J Med, 2015. **373**(25): p. 2425-37.
129. Shanafelt, T.D., et al., *Ibrutinib-Rituximab or Chemoimmunotherapy for Chronic Lymphocytic Leukemia.* N Engl J Med, 2019. **381**(5): p. 432-443.
130. Eichhorst, B., et al., *First-line chemoimmunotherapy with bendamustine and rituximab versus fludarabine, cyclophosphamide, and rituximab in patients with advanced chronic lymphocytic leukaemia (CLL10): an international, open-label, randomised, phase 3, non-inferiority trial.* Lancet Oncol, 2016. **17**(7): p. 928-942.
131. Woyach, J.A., et al., *Ibrutinib Regimens versus Chemoimmunotherapy in Older Patients with Untreated CLL.* N Engl J Med, 2018. **379**(26): p. 2517-2528.
132. Byrd, J.C., et al., *Ibrutinib versus ofatumumab in previously treated chronic lymphoid leukemia.* N Engl J Med, 2014. **371**(3): p. 213-23.
133. O'Brien, S., et al., *Single-agent ibrutinib in treatment-naive and relapsed/refractory chronic lymphocytic leukemia: a 5-year experience.* Blood, 2018. **131**(17): p. 1910-1919.
134. Jain, N. and S. O'Brien, *Targeted therapies for CLL: Practical issues with the changing treatment paradigm.* Blood Rev, 2016. **30**(3): p. 233-44.
135. Palma, M., et al., *Ibrutinib induces rapid down-regulation of inflammatory markers and altered transcription of chronic lymphocytic leukaemia-*

related genes in blood and lymph nodes. Br J Haematol, 2018. **183**(2): p. 212-224.
136. Del Papa, B., et al., *Decreased NOTCH1 Activation Correlates with Response to Ibrutinib in Chronic Lymphocytic Leukemia.* Clin Cancer Res, 2019.
137. Holmes, K.B., et al., *Ibrutinib induces chromatin reorganisation of chronic lymphocytic leukaemia cells.* Oncogenesis, 2019. **8**(5): p. 32.
138. Woyach, J.A., et al., *Resistance mechanisms for the Bruton's tyrosine kinase inhibitor ibrutinib.* N Engl J Med, 2014. **370**(24): p. 2286-94.
139. Kaur, V. and A. Swami, *Ibrutinib in CLL: a focus on adverse events, resistance, and novel approaches beyond ibrutinib.* Ann Hematol, 2017. **96**(7): p. 1175-1184.
140. Ahn, I.E., et al., *Clonal evolution leading to ibrutinib resistance in chronic lymphocytic leukemia.* Blood, 2017. **129**(11): p. 1469-1479.
141. Landau, D.A., et al., *The evolutionary landscape of chronic lymphocytic leukemia treated with ibrutinib targeted therapy.* Nat Commun, 2017. **8**(1): p. 2185.
142. Dadashian, E.L., et al., *TLR Signaling Is Activated in Lymph Node-Resident CLL Cells and Is Only Partially Inhibited by Ibrutinib.* Cancer Res, 2019. **79**(2): p. 360-371.
143. Jayappa, K.D., et al., *Microenvironmental agonists generate de novo phenotypic resistance to combined ibrutinib plus venetoclax in CLL and MCL.* Blood Adv, 2017. **1**(14): p. 933-946.
144. Burger, J.A., et al., *Randomized trial of ibrutinib vs ibrutinib plus rituximab in patients with chronic lymphocytic leukemia.* Blood, 2019. **133**(10): p. 1011-1019.
145. Kater, A.P., M.D. Levin, and C.U. Niemann, *Ibrutinib and Venetoclax for First-Line Treatment of CLL.* N Engl J Med, 2019. **381**(8): p. 788-789.
146. Mizuno, T. and T.L. Rothstein, *Cutting edge: CD40 engagement eliminates the need for Bruton's tyrosine kinase in B cell receptor signaling for NF-kappa B.* J Immunol, 2003. **170**(6): p. 2806-10.
147. Mizuno, T. and T.L. Rothstein, *B cell receptor (BCR) cross-talk: CD40 engagement creates an alternate pathway for BCR signaling that activates I kappa B kinase/I kappa B alpha/NF-kappa B without the need for PI3K and phospholipase C gamma.* J Immunol, 2005. **174**(10): p. 6062-70.
148. Bird, A., *DNA methylation patterns and epigenetic memory.* Genes Dev, 2002. **16**(1): p. 6-21.
149. Luger, K., M.L. Dechassa, and D.J. Tremethick, *New insights into nucleosome and chromatin structure: an ordered state or a disordered affair?* Nat Rev Mol Cell Biol, 2012. **13**(7): p. 436-47.
150. Tessarz, P. and T. Kouzarides, *Histone core modifications regulating nucleosome structure and dynamics.* Nat Rev Mol Cell Biol, 2014. **15**(11): p. 703-8.
151. Henneman, B., et al., *Structure and function of archaeal histones.* PLoS Genet, 2018. **14**(9): p. e1007582.
152. Lawrence, M., S. Daujat, and R. Schneider, *Lateral Thinking: How Histone Modifications Regulate Gene Expression.* Trends Genet, 2016. **32**(1): p. 42-56.
153. Greer, E.L. and Y. Shi, *Histone methylation: a dynamic mark in health, disease and inheritance.* Nat Rev Genet, 2012. **13**(5): p. 343-57.

154. Falkenberg, K.J. and R.W. Johnstone, *Histone deacetylases and their inhibitors in cancer, neurological diseases and immune disorders.* Nat Rev Drug Discov, 2014. **13**(9): p. 673-91.
155. Trevino, L.S., Q. Wang, and C.L. Walker, *Phosphorylation of epigenetic "readers, writers and erasers": Implications for developmental reprogramming and the epigenetic basis for health and disease.* Prog Biophys Mol Biol, 2015. **118**(1-2): p. 8-13.
156. Jacobson, R.H., et al., *Structure and function of a human TAFII250 double bromodomain module.* Science, 2000. **288**(5470): p. 1422-5.
157. Yun, M., et al., *Readers of histone modifications.* Cell Res, 2011. **21**(4): p. 564-78.
158. Sudarsanam, P. and F. Winston, *The Swi/Snf family nucleosome-remodeling complexes and transcriptional control.* Trends Genet, 2000. **16**(8): p. 345-51.
159. Saha, A., J. Wittmeyer, and B.R. Cairns, *Chromatin remodelling: the industrial revolution of DNA around histones.* Nat Rev Mol Cell Biol, 2006. **7**(6): p. 437-47.
160. Hyun, K., et al., *Writing, erasing and reading histone lysine methylations.* Exp Mol Med, 2017. **49**(4): p. e324.
161. Black, J.C., C. Van Rechem, and J.R. Whetstine, *Histone lysine methylation dynamics: establishment, regulation, and biological impact.* Mol Cell, 2012. **48**(4): p. 491-507.
162. Vastenhouw, N.L. and A.F. Schier, *Bivalent histone modifications in early embryogenesis.* Curr Opin Cell Biol, 2012. **24**(3): p. 374-86.
163. Bannister, A.J. and T. Kouzarides, *Regulation of chromatin by histone modifications.* Cell Res, 2011. **21**(3): p. 381-95.
164. Carey, M., B. Li, and J.L. Workman, *RSC exploits histone acetylation to abrogate the nucleosomal block to RNA polymerase II elongation.* Mol Cell, 2006. **24**(3): p. 481-7.
165. Rossetto, D., N. Avvakumov, and J. Cote, *Histone phosphorylation: a chromatin modification involved in diverse nuclear events.* Epigenetics, 2012. **7**(10): p. 1098-108.
166. Lau, P.N. and P. Cheung, *Histone code pathway involving H3 S28 phosphorylation and K27 acetylation activates transcription and antagonizes polycomb silencing.* Proc Natl Acad Sci U S A, 2011. **108**(7): p. 2801-6.
167. Baek, S.H., *When signaling kinases meet histones and histone modifiers in the nucleus.* Mol Cell, 2011. **42**(3): p. 274-84.
168. Thorne, J.L., L. Ouboussad, and P.F. Lefevre, *Heterochromatin protein 1 gamma and IkappaB kinase alpha interdependence during tumour necrosis factor gene transcription elongation in activated macrophages.* Nucleic Acids Res, 2012. **40**(16): p. 7676-89.
169. Goodman, R.H. and S. Smolik, *CBP/p300 in cell growth, transformation, and development.* Genes Dev, 2000. **14**(13): p. 1553-77.
170. Zippo, A., et al., *PIM1-dependent phosphorylation of histone H3 at serine 10 is required for MYC-dependent transcriptional activation and oncogenic transformation.* Nat Cell Biol, 2007. **9**(8): p. 932-44.
171. Dawson, M.A., et al., *JAK2 phosphorylates histone H3Y41 and excludes HP1alpha from chromatin.* Nature, 2009. **461**(7265): p. 819-22.
172. Bungard, D., et al., *Signaling kinase AMPK activates stress-promoted transcription via histone H2B phosphorylation.* Science, 2010. **329**(5996): p. 1201-5.

173. Bahrami, S. and F. Drablos, *Gene regulation in the immediate-early response process.* Adv Biol Regul, 2016. **62**: p. 37-49.
174. Greenberg, M.E. and E.B. Ziff, *Stimulation of 3T3 cells induces transcription of the c-fos proto-oncogene.* Nature, 1984. **311**(5985): p. 433-8.
000. Thomas, F., et al., *DAPK3 participates in the mRNA processing of immediate early genes in Chronic Lymphocytic Leukaemia.* Mol Onc, forthcoming 2020.
175. Gomard, T., et al., *Fos family protein degradation by the proteasome.* Biochem Soc Trans, 2008. **36**(Pt 5): p. 858-63.
176. Herschman, H.R., *Primary response genes induced by growth factors and tumor promoters.* Annu Rev Biochem, 1991. **60**: p. 281-319.
177. Healy, S., P. Khan, and J.R. Davie, *Immediate early response genes and cell transformation.* Pharmacol Ther, 2013. **137**(1): p. 64-77.
178. McMahon, S.B. and J.G. Monroe, *The role of early growth response gene 1 (egr-1) in regulation of the immune response.* J Leukoc Biol, 1996. **60**(2): p. 159-66.
179. Vallat, L., et al., *Reverse-engineering the genetic circuitry of a cancer cell with predicted intervention in chronic lymphocytic leukemia.* Proc Natl Acad Sci U S A, 2013. **110**(2): p. 459-64.
180. Gururajan, M., et al., *Early growth response genes regulate B cell development, proliferation, and immune response.* J Immunol, 2008. **181**(7): p. 4590-602.
181. Ke, J., et al., *The role of MAPKs in B cell receptor-induced down-regulation of Egr-1 in immature B lymphoma cells.* J Biol Chem, 2006. **281**(52): p. 39806-18.
182. Dinkel, A., et al., *The transcription factor early growth response 1 (Egr-1) advances differentiation of pre-B and immature B cells.* J Exp Med, 1998. **188**(12): p. 2215-24.
183. Segel, G.B., et al., *Early gene activation in chronic leukemic B lymphocytes induced toward a plasma cell phenotype.* Blood Cells Mol Dis, 2003. **30**(3): p. 277-87.
184. Pede, V., et al., *CLL cells respond to B-Cell receptor stimulation with a microRNA/mRNA signature associated with MYC activation and cell cycle progression.* PLoS One, 2013. **8**(4): p. e60275.
185. Lee, S.L., et al., *Growth and differentiation proceeds normally in cells deficient in the immediate early gene NGFI-A.* J Biol Chem, 1995. **270**(17): p. 9971-7.
186. Young, E., et al., *EGR2 mutations define a new clinically aggressive subgroup of chronic lymphocytic leukemia.* Leukemia, 2017. **31**(7): p. 1547-1554.
187. Lang, R., M. Hammer, and J. Mages, *DUSP meet immunology: dual specificity MAPK phosphatases in control of the inflammatory response.* J Immunol, 2006. **177**(11): p. 7497-504.
188. Jeffrey, K.L., et al., *Positive regulation of immune cell function and inflammatory responses by phosphatase PAC-1.* Nat Immunol, 2006. **7**(3): p. 274-83.
189. Schuhmacher, B., et al., *JUNB, DUSP2, SGK1, SOCS1 and CREBBP are frequently mutated in T-cell/histiocyte-rich large B-cell lymphoma.* Haematologica, 2019. **104**(2): p. 330-337.
190. Jonkers, I. and J.T. Lis, *Getting up to speed with transcription elongation by RNA polymerase II.* Nat Rev Mol Cell Biol, 2015. **16**(3): p. 167-77.

191. Tullai, J.W., et al., *Immediate-early and delayed primary response genes are distinct in function and genomic architecture.* J Biol Chem, 2007. **282**(33): p. 23981-95.
192. Saunders, A., L.J. Core, and J.T. Lis, *Breaking barriers to transcription elongation.* Nat Rev Mol Cell Biol, 2006. **7**(8): p. 557-67.
193. Saha, R.N., et al., *Rapid activity-induced transcription of Arc and other IEGs relies on poised RNA polymerase II.* Nat Neurosci, 2011. **14**(7): p. 848-56.
194. Thomson, S., et al., *The nucleosomal response associated with immediate-early gene induction is mediated via alternative MAP kinase cascades: MSK1 as a potential histone H3/HMG-14 kinase.* EMBO J, 1999. **18**(17): p. 4779-93.
195. Sandoval, J., et al., *Epigenetic Regulation of Early- and Late-Response Genes in Acute Pancreatitis.* J Immunol, 2016. **197**(10): p. 4137-4150.
196. Clayton, A.L., et al., *Phosphoacetylation of histone H3 on c-fos- and c-jun-associated nucleosomes upon gene activation.* EMBO J, 2000. **19**(14): p. 3714-26.
197. Natoli, G., et al., *Interactions of NF-kappaB with chromatin: the art of being at the right place at the right time.* Nat Immunol, 2005. **6**(5): p. 439-45.
198. Saccani, S., S. Pantano, and G. Natoli, *Two waves of nuclear factor kappaB recruitment to target promoters.* J Exp Med, 2001. **193**(12): p. 1351-9.
199. Ramirez-Carrozzi, V.R., et al., *Selective and antagonistic functions of SWI/SNF and Mi-2beta nucleosome remodeling complexes during an inflammatory response.* Genes Dev, 2006. **20**(3): p. 282-96.
200. Rahhal, R. and E. Seto, *Emerging roles of histone modifications and HDACs in RNA splicing.* Nucleic Acids Res, 2019. **47**(10): p. 4911-4926.
201. Schwartz, S., E. Meshorer, and G. Ast, *Chromatin organization marks exon-intron structure.* Nat Struct Mol Biol, 2009. **16**(9): p. 990-5.
202. Tilgner, H., et al., *Nucleosome positioning as a determinant of exon recognition.* Nat Struct Mol Biol, 2009. **16**(9): p. 996-1001.
203. Jimeno-Gonzalez, S. and J.C. Reyes, *Chromatin structure and pre-mRNA processing work together.* Transcription, 2016. **7**(3): p. 63-8.
204. Zhou, H.L., et al., *Regulation of alternative splicing by local histone modifications: potential roles for RNA-guided mechanisms.* Nucleic Acids Res, 2014. **42**(2): p. 701-13.
205. Sims, R.J., 3rd, et al., *Recognition of trimethylated histone H3 lysine 4 facilitates the recruitment of transcription postinitiation factors and pre-mRNA splicing.* Mol Cell, 2007. **28**(4): p. 665-76.
206. Luco, R.F., et al., *Regulation of alternative splicing by histone modifications.* Science, 2010. **327**(5968): p. 996-1000.
207. Vermeulen, M., et al., *Quantitative interaction proteomics and genome-wide profiling of epigenetic histone marks and their readers.* Cell, 2010. **142**(6): p. 967-80.
208. Saksouk, N., E. Simboeck, and J. Dejardin, *Constitutive heterochromatin formation and transcription in mammals.* Epigenetics Chromatin, 2015. **8**: p. 3.
209. Vakoc, C.R., et al., *Histone H3 lysine 9 methylation and HP1gamma are associated with transcription elongation through mammalian chromatin.* Mol Cell, 2005. **19**(3): p. 381-91.

210. Saint-Andre, V., et al., *Histone H3 lysine 9 trimethylation and HP1gamma favor inclusion of alternative exons.* Nat Struct Mol Biol, 2011. **18**(3): p. 337-44.
211. Allo, M., et al., *Control of alternative splicing through siRNA-mediated transcriptional gene silencing.* Nat Struct Mol Biol, 2009. **16**(7): p. 717-24.
212. Sawicka, A. and C. Seiser, *Histone H3 phosphorylation - a versatile chromatin modification for different occasions.* Biochimie, 2012. **94**(11): p. 2193-201.
213. Metzger, E., et al., *Phosphorylation of histone H3T6 by PKCbeta(I) controls demethylation at histone H3K4.* Nature, 2010. **464**(7289): p. 792-6.
214. Metzger, E., et al., *Phosphorylation of histone H3 at threonine 11 establishes a novel chromatin mark for transcriptional regulation.* Nat Cell Biol, 2008. **10**(1): p. 53-60.
215. Kim, J.Y., et al., *A role for WDR5 in integrating threonine 11 phosphorylation to lysine 4 methylation on histone H3 during androgen signaling and in prostate cancer.* Mol Cell, 2014. **54**(4): p. 613-25.
216. Kawai, T., S. Akira, and J.C. Reed, *ZIP kinase triggers apoptosis from nuclear PML oncogenic domains.* Mol Cell Biol, 2003. **23**(17): p. 6174-86.
217. Steinmann, S., et al., *Death-associated protein kinase: A molecule with functional antagonistic duality and a potential role in inflammatory bowel disease (Review).* Int J Oncol, 2015. **47**(1): p. 5-15.
218. Shani, G., et al., *Death-associated protein kinase phosphorylates ZIP kinase, forming a unique kinase hierarchy to activate its cell death functions.* Mol Cell Biol, 2004. **24**(19): p. 8611-26.
219. Nair, S., et al., *Death associated protein kinases: molecular structure and brain injury.* Int J Mol Sci, 2013. **14**(7): p. 13858-72.
220. Leister, P., et al., *ZIP kinase plays a crucial role in androgen receptor-mediated transcription.* Oncogene, 2008. **27**(23): p. 3292-300.
221. Kogel, D., et al., *C-terminal truncation of Dlk/ZIP kinase leads to abrogation of nuclear transport and high apoptotic activity.* Oncogene, 1999. **18**(51): p. 7212-8.
222. Graves, P.R., K.M. Winkfield, and T.A. Haystead, *Regulation of zipper-interacting protein kinase activity in vitro and in vivo by multisite phosphorylation.* J Biol Chem, 2005. **280**(10): p. 9363-74.
223. Sato, N., et al., *Phosphorylation of threonine-265 in Zipper-interacting protein kinase plays an important role in its activity and is induced by IL-6 family cytokines.* Immunol Lett, 2006. **103**(2): p. 127-34.
224. Kogel, D., et al., *Dlk/ZIP kinase-induced apoptosis in human medulloblastoma cells: requirement of the mitochondrial apoptosis pathway.* Br J Cancer, 2001. **85**(11): p. 1801-8.
225. Tang, H.W., et al., *Atg1-mediated myosin II activation regulates autophagosome formation during starvation-induced autophagy.* EMBO J, 2011. **30**(4): p. 636-51.
226. Usui, T., M. Okada, and H. Yamawaki, *Zipper interacting protein kinase (ZIPK): function and signaling.* Apoptosis, 2014. **19**(2): p. 387-91.
227. Murata-Hori, M., et al., *HeLa ZIP kinase induces diphosphorylation of myosin II regulatory light chain and reorganization of actin filaments in nonmuscle cells.* Oncogene, 2001. **20**(57): p. 8175-83.
228. Sato, N., et al., *Physical and functional interactions between STAT3 and ZIP kinase.* Int Immunol, 2005. **17**(12): p. 1543-52.

229. Kogel, D., et al., *Cloning and characterization of Dlk, a novel serine/threonine kinase that is tightly associated with chromatin and phosphorylates core histones.* Oncogene, 1998. **17**(20): p. 2645-54.
230. Preuss, U., G. Landsberg, and K.H. Scheidtmann, *Novel mitosis-specific phosphorylation of histone H3 at Thr11 mediated by Dlk/ZIP kinase.* Nucleic Acids Res, 2003. **31**(3): p. 878-85.
231. Mallipeddi, R., et al., *Reduced expression of insulin-like growth factor-binding protein-3 (IGFBP-3) in Squamous cell carcinoma complicating recessive dystrophic epidermolysis bullosa.* J Invest Dermatol, 2004. **122**(5): p. 1302-9.
232. Bi, J., et al., *Downregulation of ZIP kinase is associated with tumor invasion, metastasis and poor prognosis in gastric cancer.* Int J Cancer, 2009. **124**(7): p. 1587-93.
233. Brognard, J., et al., *Cancer-associated loss-of-function mutations implicate DAPK3 as a tumor-suppressing kinase.* Cancer Res, 2011. **71**(8): p. 3152-61.
234. Li, J., et al., *Zipper-interacting protein kinase promotes epithelial-mesenchymal transition, invasion and metastasis through AKT and NF-kB signaling and is associated with metastasis and poor prognosis in gastric cancer patients.* Oncotarget, 2015. **6**(10): p. 8323-38.
235. Marina, O., et al., *Serologic markers of effective tumor immunity against chronic lymphocytic leukemia include nonmutated B-cell antigens.* Cancer Res, 2010. **70**(4): p. 1344-55.
236. Bojarska-Junak, A., et al., *Assessment of the pathway of apoptosis involving PAR-4, DAXX and ZIPK proteins in CLL patients and its relationship with the principal prognostic factors.* Folia Histochem Cytobiol, 2011. **49**(1): p. 98-103.
237. Bromberg, J.F., et al., *Stat3 as an oncogene.* Cell, 1999. **98**(3): p. 295-303.
238. Rawlings, J.S., K.M. Rosler, and D.A. Harrison, *The JAK/STAT signaling pathway.* J Cell Sci, 2004. **117**(Pt 8): p. 1281-3.
239. Yu, H., et al., *Revisiting STAT3 signalling in cancer: new and unexpected biological functions.* Nat Rev Cancer, 2014. **14**(11): p. 736-46.
240. Redell, M.S., et al., *Stat3 signaling in acute myeloid leukemia: ligand-dependent and -independent activation and induction of apoptosis by a novel small-molecule Stat3 inhibitor.* Blood, 2011. **117**(21): p. 5701-9.
241. Eiring, A.M., et al., *Combined STAT3 and BCR-ABL1 inhibition induces synthetic lethality in therapy-resistant chronic myeloid leukemia.* Leukemia, 2015. **29**(3): p. 586-597.
242. Fasan, A., et al., *STAT3 mutations are highly specific for large granular lymphocytic leukemia.* Leukemia, 2013. **27**(7): p. 1598-600.
243. Antosz, H., et al., *IL-6, IL-10, c-Jun and STAT3 expression in B-CLL.* Blood Cells Mol Dis, 2015. **54**(3): p. 258-65.
244. Harvey, S.E. and C. Cheng, *Methods for Characterization of Alternative RNA Splicing.* Methods Mol Biol, 2016. **1402**: p. 229-241.
245. Honigberg, L.A., et al., *The Bruton tyrosine kinase inhibitor PCI-32765 blocks B-cell activation and is efficacious in models of autoimmune disease and B-cell malignancy.* Proc Natl Acad Sci U S A, 2010. **107**(29): p. 13075-80.
246. Avila-Carino, J., et al., *B-CLL cells with unusual properties.* Int J Cancer, 1997. **70**(1): p. 1-8.

247. Takada, K., K. Yamamoto, and T. Osato, *Analysis of the transformation of human lymphocytes by Epstein-Barr virus. II. Abortive response of leukemic cells to the transforming virus.* Intervirology, 1980. **13**(4): p. 223-31.
248. Walls, E.V., et al., *Activation and immortalization of leukaemic B cells by Epstein-Barr virus.* Int J Cancer, 1989. **44**(5): p. 846-53.
249. Stacchini, A., et al., *MEC1 and MEC2: two new cell lines derived from B-chronic lymphocytic leukaemia in prolymphocytoid transformation.* Leuk Res, 1999. **23**(2): p. 127-36.
250. Wenzl, K., et al., *Loss of TNFAIP3 enhances MYD88L265P-driven signaling in non-Hodgkin lymphoma.* Blood Cancer J, 2018. **8**(10): p. 97.
251. Huynh, J., et al., *Therapeutically exploiting STAT3 activity in cancer - using tissue repair as a road map.* Nat Rev Cancer, 2019. **19**(2): p. 82-96.
252. Rozovski, U., et al., *STAT3 is constitutively acetylated on lysine 685 residues in chronic lymphocytic leukemia cells.* Oncotarget, 2018. **9**(72): p. 33710-33718.
253. Rozovski, U., et al., *Constitutive Phosphorylation of STAT3 by the CK2-BLNK-CD5 Complex.* Mol Cancer Res, 2017. **15**(5): p. 610-618.
254. Yeh, J.E. and D.A. Frank, *STAT3-Interacting Proteins as Modulators of Transcription Factor Function: Implications to Targeted Cancer Therapy.* ChemMedChem, 2016. **11**(8): p. 795-801.
255. Thierry-Mieg, D. and J. Thierry-Mieg, *AceView: a comprehensive cDNA-supported gene and transcripts annotation.* Genome Biol, 2006. **7 Suppl 1**: p. S12 1-14.
256. Cheneby, J., et al., *ReMap 2018: an updated atlas of regulatory regions from an integrative analysis of DNA-binding ChIP-seq experiments.* Nucleic Acids Res, 2018. **46**(D1): p. D267-D275.
257. Jo, B.S. and S.S. Choi, *Introns: The Functional Benefits of Introns in Genomes.* Genomics Inform, 2015. **13**(4): p. 112-8.
258. Liu, Z., et al., *STAT-3 activates NF-kappaB in chronic lymphocytic leukemia cells.* Mol Cancer Res, 2011. **9**(4): p. 507-15.
259. Goldstein, I., et al., *Synergistic gene expression during the acute phase response is characterized by transcription factor assisted loading.* Nat Commun, 2017. **8**(1): p. 1849.
260. Hahn, S., *Structure and mechanism of the RNA polymerase II transcription machinery.* Nat Struct Mol Biol, 2004. **11**(5): p. 394-403.
261. Hsin, J.P. and J.L. Manley, *The RNA polymerase II CTD coordinates transcription and RNA processing.* Genes Dev, 2012. **26**(19): p. 2119-37.
262. Mischo, H.E. and N.J. Proudfoot, *Disengaging polymerase: terminating RNA polymerase II transcription in budding yeast.* Biochim Biophys Acta, 2013. **1829**(1): p. 174-85.
263. Bentley, D.L., *Coupling mRNA processing with transcription in time and space.* Nat Rev Genet, 2014. **15**(3): p. 163-75.
264. Egloff, S., M. Dienstbier, and S. Murphy, *Updating the RNA polymerase CTD code: adding gene-specific layers.* Trends Genet, 2012. **28**(7): p. 333-41.
265. Hnilicova, J., et al., *The C-terminal domain of Brd2 is important for chromatin interaction and regulation of transcription and alternative splicing.* Mol Biol Cell, 2013. **24**(22): p. 3557-68.
266. Okamoto, M., et al., *Identification of death-associated protein kinases inhibitors using structure-based virtual screening.* J Med Chem, 2009. **52**(22): p. 7323-7.

267. Ten Hacken, E., et al., *Functional Differences between IgM and IgD Signaling in Chronic Lymphocytic Leukemia.* J Immunol, 2016. **197**(6): p. 2522-31.
268. Muzio, M., et al., *Constitutive activation of distinct BCR-signaling pathways in a subset of CLL patients: a molecular signature of anergy.* Blood, 2008. **112**(1): p. 188-95.
269. Furman, R.R., et al., *Modulation of NF-kappa B activity and apoptosis in chronic lymphocytic leukemia B cells.* J Immunol, 2000. **164**(4): p. 2200-6.
270. Usui, T., et al., *Death-associated protein kinase 3 mediates vascular inflammation and development of hypertension in spontaneously hypertensive rats.* Hypertension, 2012. **60**(4): p. 1031-9.
271. Mukhopadhyay, R., et al., *DAPK-ZIPK-L13a axis constitutes a negative-feedback module regulating inflammatory gene expression.* Mol Cell, 2008. **32**(3): p. 371-82.
272. Deiss, L.P., et al., *Identification of a novel serine/threonine kinase and a novel 15-kD protein as potential mediators of the gamma interferon-induced cell death.* Genes Dev, 1995. **9**(1): p. 15-30.
273. Singh, P., P. Ravanan, and P. Talwar, *Death Associated Protein Kinase 1 (DAPK1): A Regulator of Apoptosis and Autophagy.* Front Mol Neurosci, 2016. **9**: p. 46.
274. Bialik, S. and A. Kimchi, *The death-associated protein kinases: structure, function, and beyond.* Annu Rev Biochem, 2006. **75**: p. 189-210.
275. Yuan, W., et al., *Correlation of DAPK1 methylation and the risk of gastrointestinal cancer: A systematic review and meta-analysis.* PLoS One, 2017. **12**(9): p. e0184959.
276. Chim, C.S., et al., *Frequent DAP kinase but not p14 or Apaf-1 hypermethylation in B-cell chronic lymphocytic leukemia.* J Hum Genet, 2006. **51**(9): p. 832-8.
277. Lilienthal, N., et al., *A Novel Recombinant Anti-CD22 Immunokinase Delivers Proapoptotic Activity of Death-Associated Protein Kinase (DAPK) and Mediates Cytotoxicity in Neoplastic B Cells.* Mol Cancer Ther, 2016. **15**(5): p. 971-84.
278. Weitzel, D.H., J. Chambers, and T.A. Haystead, *Phosphorylation-dependent control of ZIPK nuclear import is species specific.* Cell Signal, 2011. **23**(1): p. 297-303.
279. Harden, S.V., et al., *Gene promoter hypermethylation in tumors and lymph nodes of stage I lung cancer patients.* Clin Cancer Res, 2003. **9**(4): p. 1370-5.
280. Catto, J.W., et al., *Promoter hypermethylation is associated with tumor location, stage, and subsequent progression in transitional cell carcinoma.* J Clin Oncol, 2005. **23**(13): p. 2903-10.
281. Zhai, J., et al., *Reduced expression levels of the death-associated protein kinase and E-cadherin are correlated with the development of esophageal squamous cell carcinoma.* Exp Ther Med, 2013. **5**(3): p. 972-976.
282. Sanchez-Cespedes, M., et al., *Gene promoter hypermethylation in tumors and serum of head and neck cancer patients.* Cancer Res, 2000. **60**(4): p. 892-5.
283. Hu, S., et al., *Association of aberrant methylation of tumor suppressor genes with tumor aggressiveness and BRAF mutation in papillary thyroid cancer.* Int J Cancer, 2006. **119**(10): p. 2322-9.

284. Gonzalez-Gomez, P., et al., *Frequent death-associated protein-kinase promoter hypermethylation in brain metastases of solid tumors.* Oncol Rep, 2003. **10**(4): p. 1031-3.
285. Lawrence, T., *The nuclear factor NF-kappaB pathway in inflammation.* Cold Spring Harb Perspect Biol, 2009. **1**(6): p. a001651.
286. Inbal, B., et al., *DAP kinase and DRP-1 mediate membrane blebbing and the formation of autophagic vesicles during programmed cell death.* J Cell Biol, 2002. **157**(3): p. 455-68.
287. Yang, J., et al., *Unphosphorylated STAT3 accumulates in response to IL-6 and activates transcription by binding to NFkappaB.* Genes Dev, 2007. **21**(11): p. 1396-408.
288. Goldstein, I., et al., *Transcription factor assisted loading and enhancer dynamics dictate the hepatic fasting response.* Genome Res, 2017. **27**(3): p. 427-439.
289. Voss, T.C., et al., *Dynamic exchange at regulatory elements during chromatin remodeling underlies assisted loading mechanism.* Cell, 2011. **146**(4): p. 544-54.
290. Mayran, A. and J. Drouin, *Pioneer transcription factors shape the epigenetic landscape.* J Biol Chem, 2018. **293**(36): p. 13795-13804.
291. Ivaldi, M.S., C.S. Karam, and V.G. Corces, *Phosphorylation of histone H3 at Ser10 facilitates RNA polymerase II release from promoter-proximal pausing in Drosophila.* Genes Dev, 2007. **21**(21): p. 2818-31.
292. Hartzog, G.A. and J.W. Tamkun, *A new role for histone tail modifications in transcription elongation.* Genes Dev, 2007. **21**(24): p. 3209-13.
293. Sunavala-Dossabhoy, G., et al., *A dominant negative mutant of TLK1 causes chromosome missegregation and aneuploidy in normal breast epithelial cells.* BMC Cell Biol, 2003. **4**: p. 16.
294. Brown, S.J., P. Stoilov, and Y. Xing, *Chromatin and epigenetic regulation of pre-mRNA processing.* Hum Mol Genet, 2012. **21**(R1): p. R90-6.
295. Beyer, A.L., A.H. Bouton, and O.L. Miller, Jr., *Correlation of hnRNP structure and nascent transcript cleavage.* Cell, 1981. **26**(2 Pt 2): p. 155-65.
296. Kolasinska-Zwierz, P., et al., *Differential chromatin marking of introns and expressed exons by H3K36me3.* Nat Genet, 2009. **41**(3): p. 376-81.
297. Dhami, P., et al., *Complex exon-intron marking by histone modifications is not determined solely by nucleosome distribution.* PLoS One, 2010. **5**(8): p. e12339.
298. Hu, Q., et al., *Histone posttranslational modifications predict specific alternative exon subtypes in mammalian brain.* PLoS Comput Biol, 2017. **13**(6): p. e1005602.
299. Perales, R. and D. Bentley, *"Cotranscriptionality": the transcription elongation complex as a nexus for nuclear transactions.* Mol Cell, 2009. **36**(2): p. 178-91.
300. MacDonald, J.A., et al., *A Small Molecule Pyrazolo[3,4-d]Pyrimidinone Inhibitor of Zipper-Interacting Protein Kinase Suppresses Calcium Sensitization of Vascular Smooth Muscle.* Mol Pharmacol, 2016. **89**(1): p. 105-17.
301. Ran, F.A., et al., *Genome engineering using the CRISPR-Cas9 system.* Nat Protoc, 2013. **8**(11): p. 2281-2308.
302. Wang, Z., M. Gerstein, and M. Snyder, *RNA-Seq: a revolutionary tool for transcriptomics.* Nat Rev Genet, 2009. **10**(1): p. 57-63.

303. Gagliardi, M. and M.R. Matarazzo, *RIP: RNA Immunoprecipitation.* Methods Mol Biol, 2016. **1480**: p. 73-86.
304. Fuchs, G., et al., *Simultaneous measurement of genome-wide transcription elongation speeds and rates of RNA polymerase II transition into active elongation with 4sUDRB-seq.* Nat Protoc, 2015. **10**(4): p. 605-18.
305. Vandamme, T.F., *Use of rodents as models of human diseases.* J Pharm Bioallied Sci, 2014. **6**(1): p. 2-9.
306. Kohnken, R., P. Porcu, and A. Mishra, *Overview of the Use of Murine Models in Leukemia and Lymphoma Research.* Front Oncol, 2017. **7**: p. 22.
307. Simonetti, G., et al., *Mouse models in the study of chronic lymphocytic leukemia pathogenesis and therapy.* Blood, 2014. **124**(7): p. 1010-9.
308. Johnson, A.J., et al., *Characterization of the TCL-1 transgenic mouse as a preclinical drug development tool for human chronic lymphocytic leukemia.* Blood, 2006. **108**(4): p. 1334-8.
309. Lia, M., et al., *Functional dissection of the chromosome 13q14 tumor-suppressor locus using transgenic mouse lines.* Blood, 2012. **119**(13): p. 2981-90.

Chapter 8 Appendix

8.1 Appendix 1 – uncropped western blots

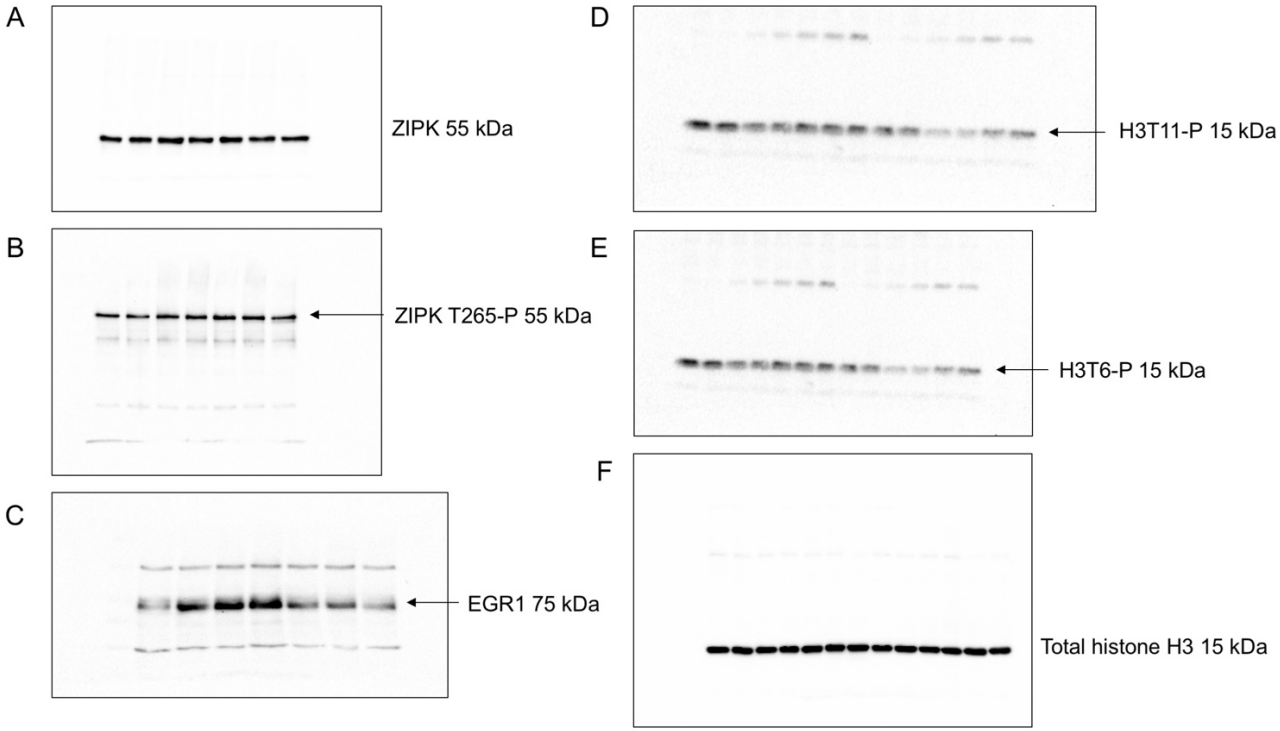

Appendix 1.1: uncropped western blots demonstrating one representative example per antibody for (A) ZIPK (B) ZIPK T265-P (C) EGR1 (D) H3T11-P (E) H3T6-P and (F) histone H3.

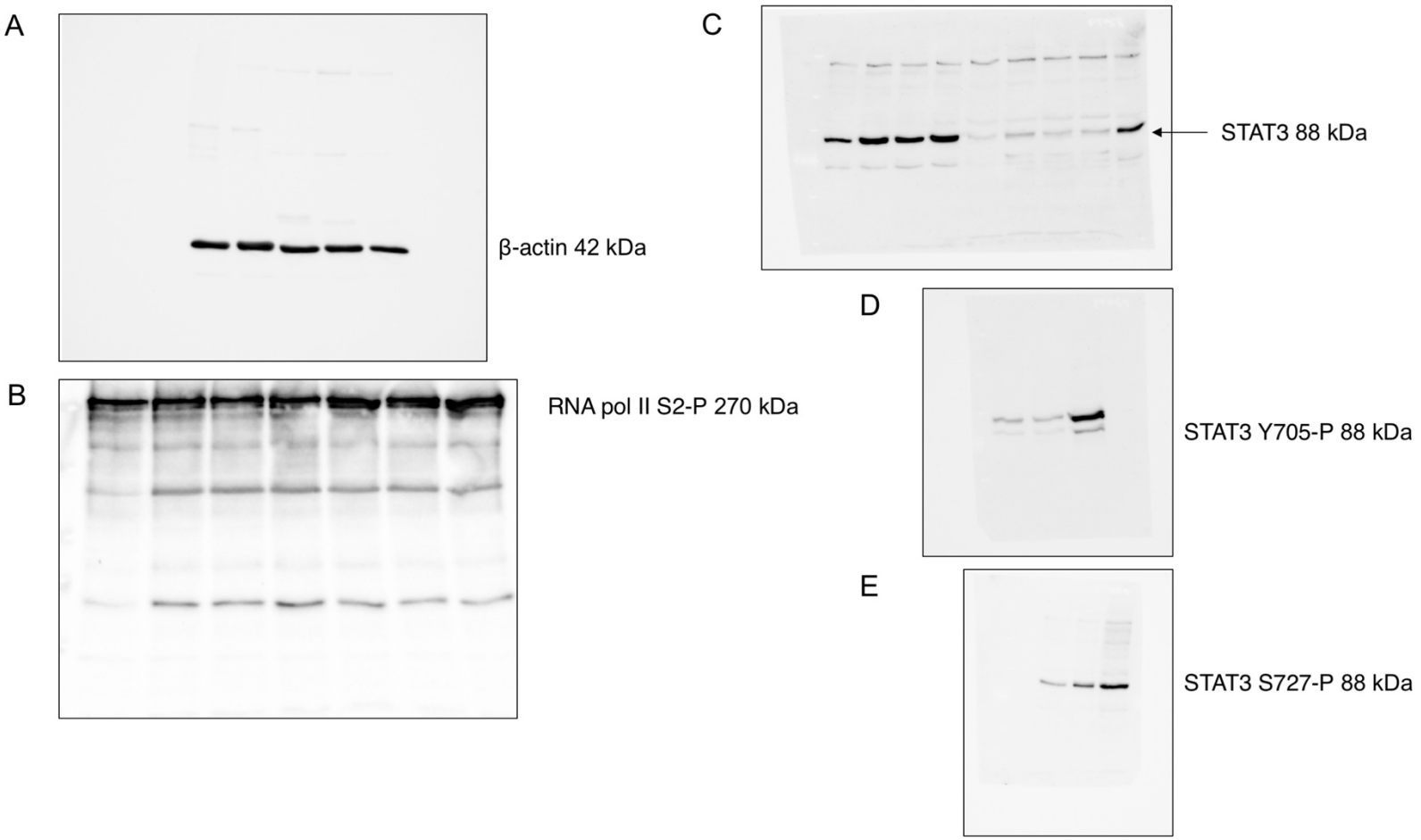

Appendix 1.2: uncropped western blots demonstrating one representative example per antibody for (A) beta-actin (B) RNA pol II S2-P (C) STAT3 (D) STAT3 Y705-P and (E) STAT3 S727-P.

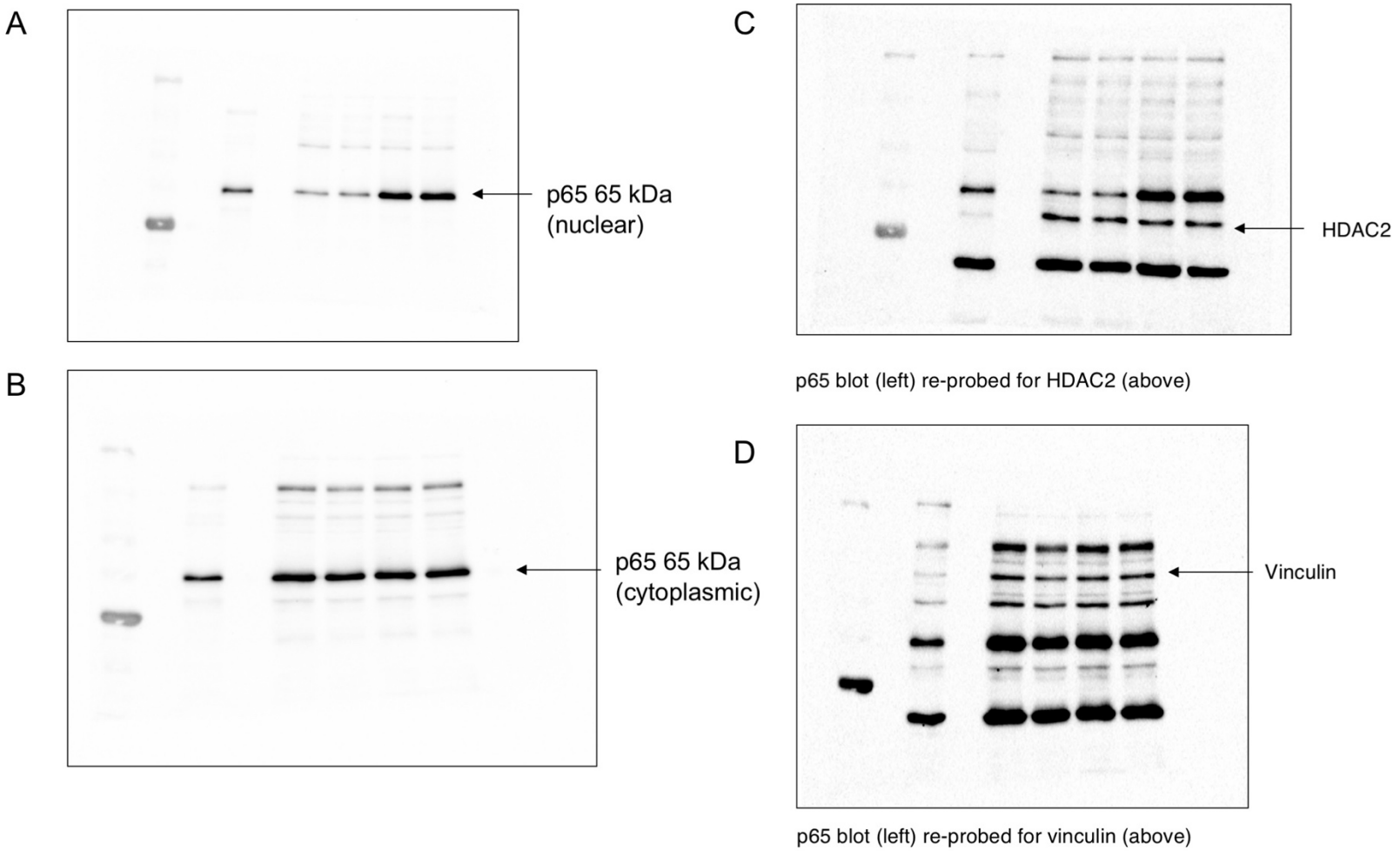

Appendix 1.3: uncropped western blots demonstrating one representative example per antibody for (A) p65 (nuclear) (B) p65 (cytoplasmic) (C) HDAC2 and (D) vinculin.

8.2 Appendix 2 – uncropped co-IPs

Figure 4.2A

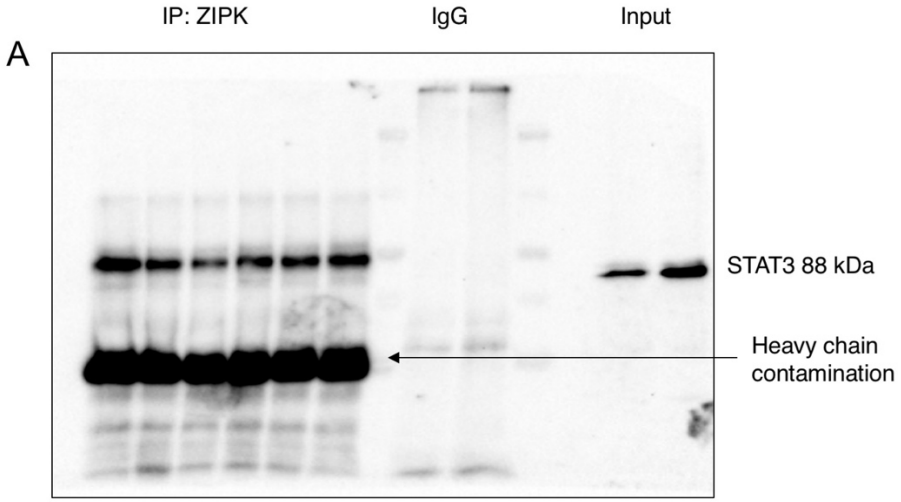

Figure 4.2B

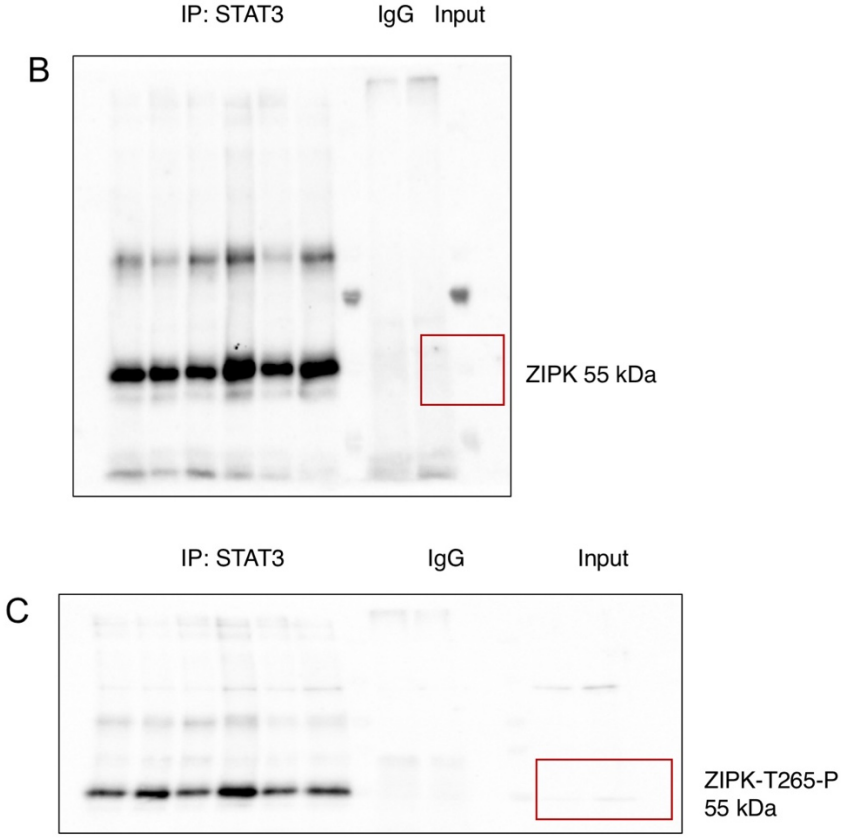

Appendix 2.1: uncropped/uncut co-IPs corresponding to (A) Figure 4.2A and (B) (C) Figure 4.2B. Red boxes indicate faint input samples.

Figure 4.2C

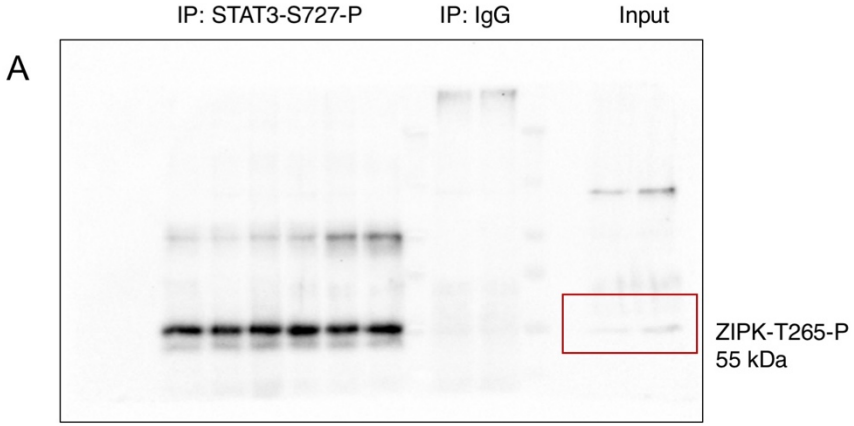

The blot shown in (C) is the same blot shown in (B) with the saturation turned very high to see the faint ZIPK-STAT3 interaction. Even with the high saturation (see the massive oversaturation of the input), the IgG control is still clean.

Figure 4.2D

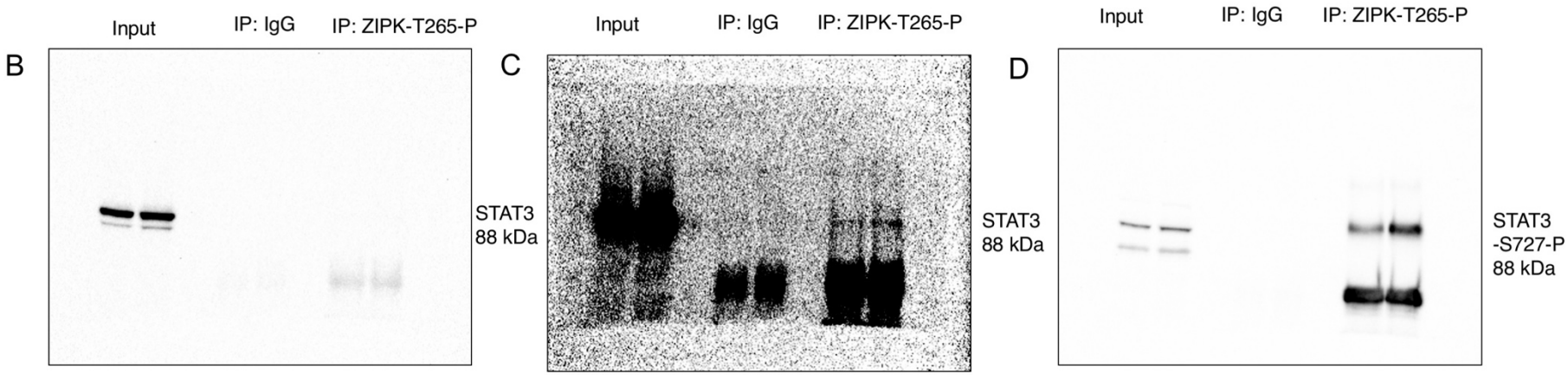

Appendix 2.2: uncropped/uncut co-IPs corresponding to (A) Figure 4.2C and (B) (C) (D) Figure 4.2D. Red boxes indicate faint input samples.

Figure 4.2F

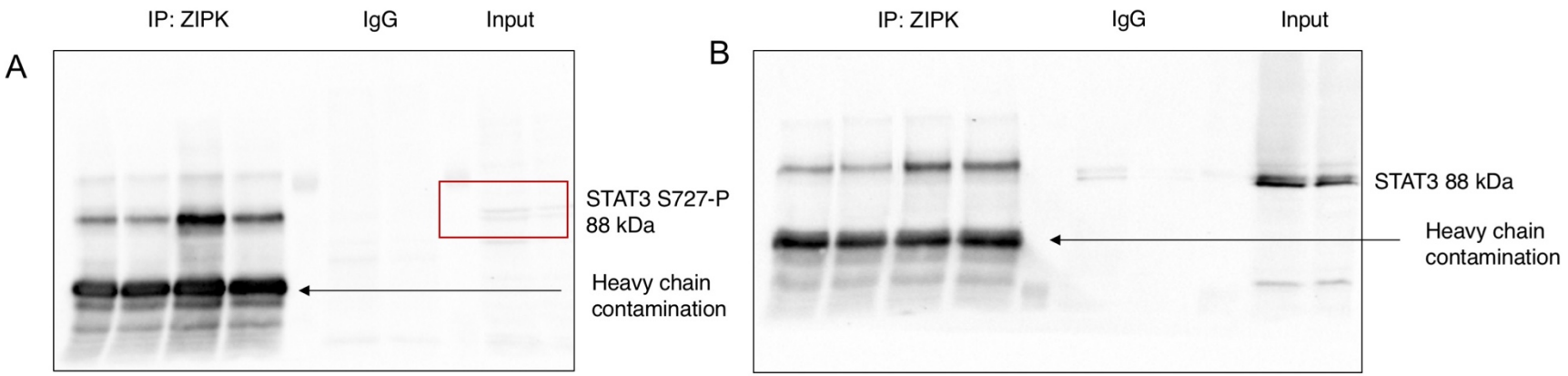

Figure 4.2G

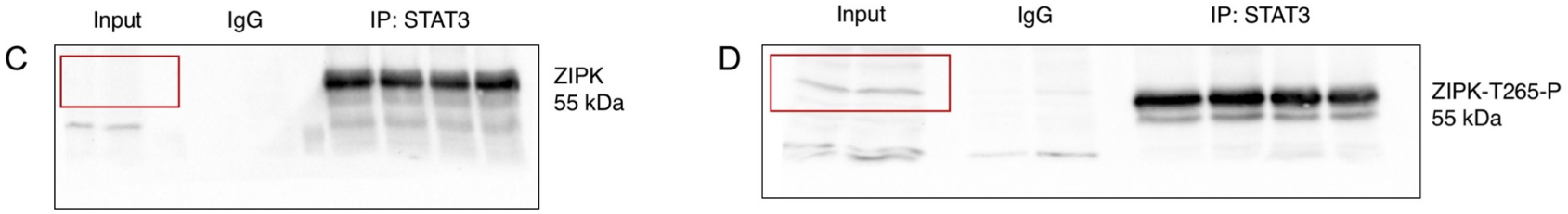

Appendix 2.3: uncropped/uncut co-IPs corresponding to (A) (B) Figure 4.2F and (C) (D) Figure 4.2G. Red boxes indicate faint input samples.

Figure 4.3A

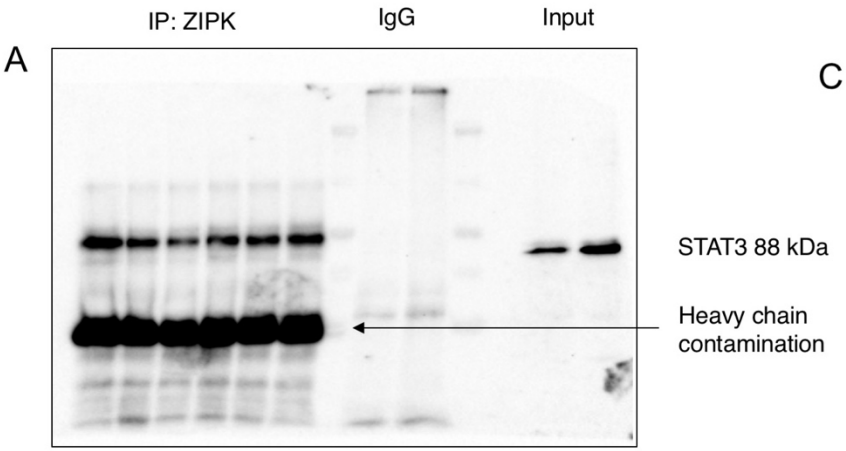

Figure 4.3B IP: STAT3 IgG Input

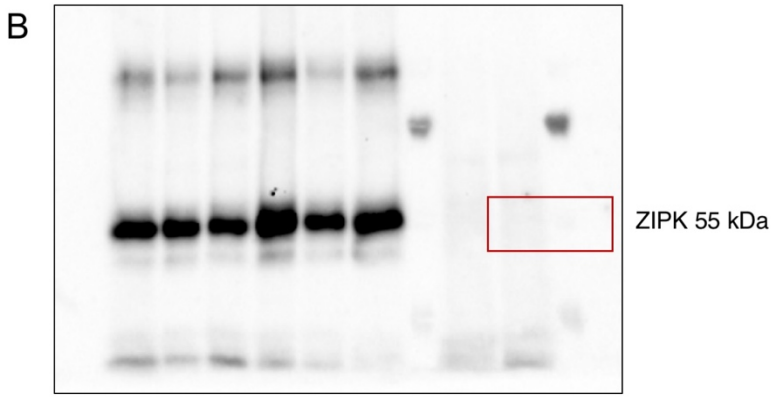

Figure 4.3C

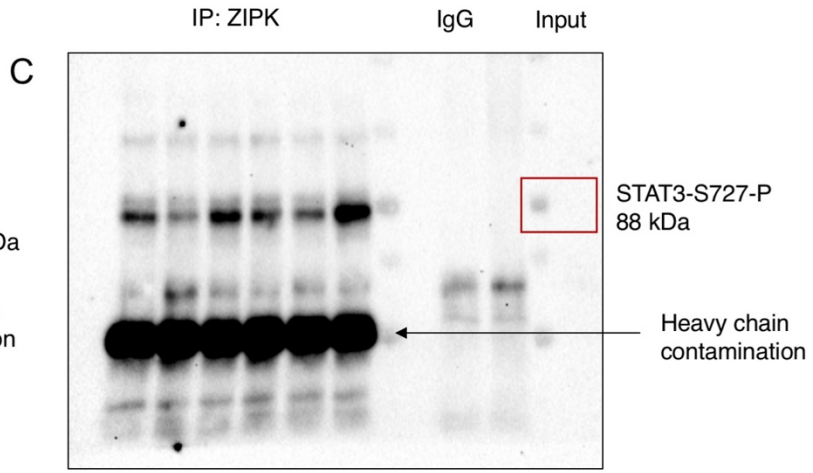

Figure 4.3D IP: ZIPK-T265-P IgG Input

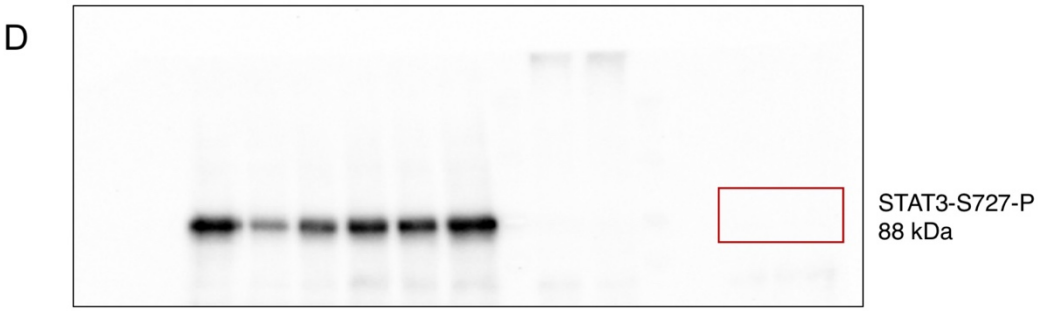

Appendix 2.4: uncropped/uncut co-IPs corresponding to (A) Figure 4.3A (B) Figure 4.3B (C) Figure 4.3C and (D) Figure 4.3D. Red boxes indicate faint input samples.